Genesis of Metasomatic Sapphirine-Corundum-Spinel-bearing Granulites in Sri Lanka

An Integrated Field, Petrological and Geochemical Study

Dissertation
Zur Erlangung des Grades
‘ Doktor der Naturwissenschaften’
am Fachbereich Geowissenschaften
der Johannes Gutenberg-Universität Mainz

G.W.A. Rohan Fernando
aus Matale, Sri Lanka

Mainz 2001

Ich versichere, daß ich die Arbeit selbständig und nur unter Verwendung der angegebenen Quellen und Hilfsmittel verfaßt habe.

Mainz, den 16 .01.2001

ACKNOWLEDGMENTS

It is a great pleasure to think of all those who have contributed to my research work from various aspects. Foremost, I wish to state my deepest appreciation and gratitude to my chief advisor, who is also the head of the petrology research group, for accepting me as his PhD student. He stimulated my work with great interest and taught me the basic fundamentals of phase petrology, fluid- rock interactions and computer modeling. He nurtured me how to resolve research problems independently, especially the problems in high-grade metamorphism and metasomatism. Working with him is a great privilege and I wish to extend my very special thanks to him for his patience, guidance and especially for having the unpleasant task of correcting each version of my manuscript. I am indebted to my co-advisor, without whose help guidance and constant encouragements, this presentation may not have become a success. His advices are invaluable in mineralogical and gemmological aspects of this research work. He generously provided financial support for chemical analyses for the entire project from the Institute of Gemstone Research and also for participating international conferences, which enabled me to strengthen international contacts.

This work was benefited from the scholarship from the German Academic Exchange Service (DAAD) of the Federal Republic of Germany. I would like to thank DAAD for generous financial help during the entire stay in Germany. Travelling and fieldwork were also supported by grants from the DAAD.

Throughout the course of this project I have benefited from fruitful discussions with members of ‘petrology research group’. Thanks to all of them for their encouragement and all enjoyable discussions, which I benefited so much. Many thanks to all of technical staff of the institut für Geowisenschaften, especially the incharge of the electron microprobe and XRF. This presentation greatly benefited from the advanced geological software of ‘Programm Gibbs’ and ‘PerpleX’. Thanks for the providers of the softwares and their lively discussions and written communications through out the study.

In Sri Lanka, I wish to thank the co-ordinator of this academic exchange program and for his comments and English corrections of the first manuscript. Special thanks to the Geological Survey and Mines Bureau (GSMB) and the National Building Research Organization (NBRO) in Sri Lanka for providing me with a preliminary geological report

of the area around Rupaha and to the for allowing me to use their unpublished geological maps.

My mother and all the family members always encouraged me to continue my studies during my entire life. And last but not least, my beloved wife had a tremendous patient, when I was away from her in Germany for more than 3 years or when I had long nights in the University while she accompanied me in Mainz. She also helped me during the field works. She was able to teach me that life does exist outside of geology. It is to all of you I dedicate this thesis.

ZUSAMMENFASSUNG

Ziel der vorliegenden Arbeit war es, die Mechanismen des Massentransfers, die Zusammensetzung und Rolle der Fluide während der krustalen Metasomatose in hochtemperierten metamorphen Gebieten zu verstehen. Für diese Untersuchung bietet sich die Region Rupaha an, ein Gebiet im Hochland-Komplex von Sri Lanka. Es repräsentiert einen Teil des Superkontinentes Gondwana. An 10 Lokalitäten wurden Aufschlüsse ultramafischer Gesteine, eingebettet in Granuliten, beprobt. Die Grenze zwischen Ultramafiten und Granuliten läßt sich mit Hilfe einer ca. 50cm breiten Reaktionszone kartieren. Ausgehend von den Ultramafiten folgen in Richtung der Granulite drei Zonen mit den folgenden, charakteristischen Mineralvergesellschaftungen: (1). Phlogopit + Spinell + Sapphirin, (2). Spinell + Sapphirin + Korund sowie (3). Korund + Biotit + Plagioklas.

Um den Verlauf des P-T-t-Pfades, den Höhepunkt der Metamorphose und die Exhumierungsgeschichte festzustellen, wurden verschiedene Thermobarometer ebenso wie ein Diffusionsmodell für die Zonierung von Granat angewendet. Dabei ergab sich eine maximale Temperatur von 875 ± 20°C (Opx-Cpx-Thermometer) und ein maximaler Druck von 9.0 ± 0.1kbar (Grt-Cpx-Plag-Qz) für die sauren Granulite. Für die Ultramafite ergeben sich für den Höhepunkt Temperaturen von 840 ± 70°C (Opx-Cpx-Thermometer) und ein Druck von 9kbar. Aus koexistierendem Spinell und Sapphirin in der Reaktionszone ergibt sich eine Temperatur von 820 ± 40°C. Dies stimmt mit den Maximaltemperaturen überein, die von den benachbarten Granuliten und Ultramafiten berichtet werden. Die strukturelle Konkordanz der Ultramafite und der sauren, granulitischen Wirtsgesteine stützt die These, daß alle untersuchten Einheiten die gleiche Peakmetamorphose erfahren haben. Die Modellierung der Diffusion in den zonierten Granaten der mafischen Ultramafite führt zu einer dreistufigen Abkühlungsgeschichte. Im initialen Abkühlungstadium wird die maximale Abkühlrate auf 1°C/Ma geschätzt, gefolgt von einer zweiten Abkühlphase mit einer Rate von 30°C/Ma. Die äußeren Granaträander weisen auf eine etwas langsamere Abkühlung mit einer Rate von 10 – 15°C/Ma hin.

Die Abfolge der Mineralzonen, die in den Reaktionszonen, die die Ultramafite von den Si-reichen Gesteinen trennen, verschiedene Al-reiche, Si-untersättigte Minerale enthalten, können mit Hilfe des Diffusionsmodells erklärt werden. Dies bezieht auch die Diffusion von Mg von den Ultramafiten über die verschiedenen Lagen ein, sowie die Diffusion von K und Si in entgegengesetzter Richtung. Die chemischen Potentiale von Mg und Si erzeugten einen kontinuierlichen, monotonen Gradienten, der einen diffusionalen Transport im stabilen Zustand über das Profil ermöglichte. Die starke Al-Anreicherung und der bemerkenswerte Verlust von Si während der Ausbildung der Reaktionsbänder können aus Isoconendiagrammen verdeutlicht werden. Der Si-Verlust und die Al-Zunahme sind sehr wahrscheinlich auf Fluide zurückzuführen, die parallel zu den Grenzbereichen der Gesteineinheiten zirkulierten.

Diese Studie hat nun gezeigt, daß der Massentransport bei verschiedenen geologischen Verhältnissen nicht nur von Druck- und Temperaturbedingungen, sondern ganz besonders auch vom P_{H2O} und der Konzentration von Chlor und Fluor in wässrigen Lösungen kontrolliert wird.

ABSTRACT

The goal of the present study is to understand the mechanism of mass transfer, the composition and the role of fluids during crustal metasomatism in high-temperature metamorphic terranes. A well constrained case study, a locality at Rupaha, Sri Lanka was selected. It is located in the Highland Complex of Sri Lanka, which represents a small, but important fragment of the super-continent Gondwana. Excellent exposures of ultramafic rocks, which are embedded in granulites, were found at 10 localities. These provide a unique background for understanding the metasomatic processes. The boundary between the ultramafic and the granulite rocks are lined with metasomatic reaction zones up to 50cm in width. Progressing from the ultramafics to the granulite host rock, three distinct zones with the following mineral assemblages can be distinguished: (1). phlogopite + spinel + sapphirine, (2). spinel + sapphirine + corundum and (3). corundum + biotite + plagioclase.

In order to assess the P-T-t path, the peak metamorphism and the exhumation history were constrained using different thermobarometers, as well as a diffusion model of garnet zoning. A maximum temperature of 875 ± 20^{o}C (Opx-Cpx thermometer) and at the peak pressure of 9.0 ± 0.1 kbar (Grt-Cpx-Pl-Qtz) was calculated for the silicic granulite. The ultramafic rocks recorded a peak temperature of 840 ± 70^{o}C (Opx-Cpx thermometer) at 9 kbar. Coexisting spinel and sapphirine from the reaction zone yield a temperature of 820 ± 40^{o}C. This is in agreement with the peak-temperatures recorded in the adjacent granulites and ultramafics rocks. The structural concordance of the ultramafic rocks with the siliceous granulite host rock further support the suggestion, that all units have experienced the same peak metamorphism. Diffusion modeling of retrograde zoning in garnets from mafic granulites suggests a three-step cooling history. A maximum cooling rate of 1^{o}C/Ma is estimated during the initial stage of cooling, followed by a cooling rate of ~30^{o}C/Ma. The outermost rims of garnet indicate a slightly slower cooling rate at about 10-15^{o}C/Ma.

The sequences of mineral zones, containing a variety of Al-rich, silica undersaturated minerals in the reaction zones separating the ultramafic rocks from the silica-rich rocks can be explained by a diffusion model. This involves the diffusion of Mg from ultramafic rocks across the layers, and K and Si diffuse in opposite direction. Chemical potential of Mg and Si generated continuous monotonic gradient, allowing steady state diffusional

transport across the profile. The strong enrichment in Al, and the considerable loss of Si, during the formation of reaction bands can be inferred from isocon diagrams. Some Al was probably added to the reaction zones, while Si was lost. This is most likely due to fluids percolating parallel to the zones at the boundary of the rock units.

This study has shown that not only pressure and temperature conditions but most importantly P_{H2O} and the concentration of the chlorine and fluorine in aqueous fluids also control the mass transport in different geological environments.

TABLE OF CONTENTS

Chapter 1

Introduction

GENERAL INTRODUCTION

Crustal fluids have long been recognized as an important driving force in metamorphic systems. Fluids play a potentially major role in the transfer of thermal energy in the crust (Braddy 1988), as a catalyst of metamorphic reactions (Rubie 1986), a driving force for reactions (Ferry 1984) and as a medium for mass transfer (Fyfe et al. 1978). Fluids are required for large-scale metasomatism because they transport solutes by diffusion, and more importantly by infiltration. In such systems, the dissolution and precipitation of minerals by crustal fluids control the location and the size of ore deposits and other metasomatic rocks. The role of fluids, their composition, source and amount during the deep-crustal granulite grade metamorphism and metasomatism remains the subject of lively discussions (e.g. Valley and O'Neil 1984; Newton 1986; Valley et al. 1990; Touret and Hartl 1990).

The theoretical studies in understanding the fundamental physical and chemical parameters that governs the fluid flow and mass transport have advanced significantly (e.g. Frantz and Weisbroad 1974; Frantz and Mao 1976, 1979; Helgeson and Lichtner 1987). Nevertheless, applications are limited to simple idealized systems. A few studies have attempted to quantify diffusion-advection processes in deep crustal environments using, detailed stable isotopic analyses across intact, well-exposed lithological contacts (e.g. Cartwright and Valley 1991).

This study provides constraints on the mechanism of mass transfer, the composition, and the role of fluids in the deep crust, by means of, a well-constrained case study in a previously poorly known terrane of Sri Lanka. I have conducted an integrated field, petrologic and geochemical study of the siliceous granulite-ultramafic rock suite in the Rupaha area. This suite in the Proterozoic basement Sri Lanka contains is one of the best-preserved examples of metasomatic alteration. Metasomatic reaction zones separate the silica-saturated granulites from meta-ultramafic rocks. The most spectacular occurrence in the reaction zone is the presence of colourless sapphirine within the reaction zones. It is the fourth reported occurrence of sapphirine in the Sri Lankan Proterozoic basement (Osanai et al.1989, 1996; Kriegsman 1991a, Kriegsman and Schumacher 2000). Formation of sapphirine in metasomatic zones has so far been reported only in a few instances (Schumacher and Robinson 1987; Dunkley et al. 1999; Hokada et al. 1999).

The latter part of this chapter contains a short summary of the geology of Sri Lanka: recently published data on basement units, lithology, geochronology, large-scale structural trends and its metamorphic history. It also includes a detailed account of the geology of Rupaha, which including a new geological map by the PhD candidate. Chapters 2 to 4 have been written in the form of papers. Hence, there may be some overlapping of the text, especially during the interpretation of geology of Sri Lanka. Mineral abbreviations follow Kretz (1983) throughout the thesis.

Chapter 2 documents the P-T-t path of the granulites at Rupaha. The P-T-t paths characterized by isobaric cooling at deep crustal levels suggest a more prolonged residence in the lower crust. The rocks have experienced slow cooling during this episode and much or all the information needed to construct P-T paths associated with these rocks have erased much of the prograde history. We estimated the cooling history of the area using diffusion modeling of retrograde zoning in garnets from the mafic granulites. A three stage cooling history is proposed.

Chapter 3 gives a detailed account of peak and post-peak metamorphic conditions of the ultramafic rocks at Rupaha. The peak metamorphic assemblages enstatite, diopside, forsterite, spinel and phlogopite are overprinted by retrograde assemblages containing tremolite, talc, dolomite and serpentine. P-T-Phase equilibria, activity-activity diagrams, and temperature-activity diagrams for these assemblages are used to decipher the intricate history of these rocks. They have undergone granulite facies metamorphism, followed by a protracted history of fluid-rock interactions on cooling and exhumation.

The complete petrography, textures, and phase petrology of the metasomatic zones are discussed in **Chapter 4.** The sequence of mineral zones that formed between ultramafic and pelitic units are composed of corundum, sapphirine, spinel, biotite and plagioclase. The P-T conditions of the metasomatic zones were evaluated to ascertain this indicates that: these bands formed during granulite facies conditions. This was achieved through spinel-sapphirine thermometry and T-μ diagrams. The final part of this chapter discusses the mechanism of the mass transport between the ultramafic rocks and the siliceous granulites. Here, chemical potential diagrams, mass balance calculations, biotite chemistry

are used. Mass balance calculations between two rock units show high amounts of mass changes for Si, Mg and some trace elements. Major element chemistry and halogen content of biotite across the rock unit provide insight into the fluid composition.

INTRODUCTION TO THE GEOLOGY OF SRI LANKA

Sri Lanka was a part of East Gondwana, together with fragments of Antarctica, Australia, India, Madagascar, Mozambique and Tanzania (e.g. Powell et al., 1988; Kröner, 1991; Yoshida et al., 1992; Jacobs et al., 1998; Dissanayake and Chandrajith 1999). Sri Lanka acted as a bridge through which Antarctica and East Africa can be correlated. It is thus not surprising that Sri Lanka reveals remarkable geological, geochronological and geotectonic similarities with its neighbouring Gondwana fragments.

Sri Lankan geology has received increasing attention in the last two decades. As a result of this, the nomenclature of rock units, definition of geological boundaries and the timing of major metamorphic and tectonic events have changed substantially. The nomenclature of the basement units, as described in the special issue of the Journal of Precambrian Research - volume 66 on 'Tectonic, metamorphic and isotopic evolution of deep crustal rocks, with special emphasis on Sri Lanka', is used throughout this thesis.

The Proterozoic basement of Sri Lanka exposes substantial parts of the lower continental crust. Four different units were distinguished on the basis of isotopical, geochronological, geochemical and petrological constraints (e.g. Kröner et al., 1991; Cooray 1994; Milisenda et al., 1994)(Fig.1.1).

(1). the Highland Complex (HC);
(2). the Vijayan Complex (VC);
(3). the Wanni Complex (WC) and
(4). the Kadugannawa Complex (KC)

The HC consists mainly of interbeded metapelites, quartzites, marbles, metabasites and charnockites. Calc-silicate gneisses, sapphirine-bearing granulites, cordierite-bearing gneisses and corundum-bearing gneisses are exposed in minor quantities. The VC exposed in eastern Sri Lanka consists of meta-igneous gneisses of tonalitic to leucogranitic

composition. Rocks of the KC are seen in the cores of the six doubly plunging synforms, which were named as *'Arenas'* by Vithanage (1972). The dominant rocks of the KC and WC are hornblende-biotite gneisses, granitic, granodioritic and tonalitic associations. Some granulites are exposed in the southern part of VC near Buttala and Kataragama. They comprise rocks similar to those of HC and are interpreted as tectonic nappes namely: Buttala klippe, Kuda Oya klippe and Kataragama klippe (Fig 1.1).

Isotopic and tectonic history

Isotopic data from HC shows prolonged crustal history. Supracrustal rocks of the central high-grade belt of HC were derived from early Proterozoic to late Archaean source terranes (3.2 - 2.4 Ga) and were probably deposited some ~2 - 2.4 Ga ago in a Proterozoic basement, which is now believed to be the host for the present day stratigraphic succession (Table 1.1, see also Crowford 1969; Crowford and Oliver 1969; Hölzl et al. 1994; Kröner et al. 1987; Milisenda et al. 1988). The rocks from VC, WC and KC, which are predominantly of granitoids, yield relatively younger deposition ages at ~1.1Ga ago (Milisenda et al. 1988). This implies that igneous activity had occurred after the deposition of supracrustal rocks of HC, but prior to fabric-forming events since their tectonic layering is parallel to that of supracrustal rocks (Table 1.1. see also Hölzl et al. 1991, 1994; Kröner and Jaeckel 1994).

The HC and WC were separated from each other until at least 750 Ma ago. They must have come together, perhaps during WC thrusting over HC, prior to peak granulite facies metamorphism (Kröner and Jaeckel 1994). The boundary between HC and WC is an isotopic boundary based on large-scale sample grids and, as such, not recognizable in the field (Milisenda et al. 1988; Milisenda 1991). The absence of field evidence at the boundary of WC and HC provided that high-grade fabric-forming events may have been destroyed the possible pre-peak metamorphic tectonism (Kröner et al. 1991). The source terrane for the Wanni supracrustal association remains controversial and is unlikely to be present in Sri Lanka.

Although HC and WC are characterized by different primary sedimentary and magmatic ages, it appears that both segments have been affected by a common peak metamorphism of Pan-African age. The timing of peak metamorphism was estimated to be ~610-~550 Ma

old. No significant Pb loss occurred in the time record between 1900 Ma (the end of the deposition of supracrustal rocks of HC) and 600 Ma ago (Bauer, et al., 1991; Hölzl et al., 1991, 1994; Kröner et al., 1991; Kröner and Williams, 1993). Taking into account similarities in geology, geotectonics and geochronology in the other Gondwana fragments, the rocks of the HC show a link to the Pan-African Mozambique belt (Kriegsman 1991b; Kröner et al.1991; Powell et al. 1998; Dissanayake and Chandrajith 1999). The HC and WC were together thrust over the VC with a top to the eastward vergence at about 580-550 Ma under upper amphibolite facies conditions (Kleinschrodt 1994). The rocks of WC have been subjected to upper amphibolite to granulite facies metamorphism. Further exhumation of the lower crustal rocks was not accompanied by tectonic events as all deformation fabrics were preserved during subsequent slow cooling.

During the Jurassic time, the Sri Lankan basement experienced crustal extension (Table 1.1 see also Powell et al., 1988). The Jurassic sediments on the top of the crystalline basement are preserved at three isolated occurrences (Tabbowa, Andigama and Pallama) in northwestern Sri Lanka (Cooray, 1984; Vithanage, 1985) (Fig 1.1.). After the initial break-up of Gondwana, Sri Lanka has moved together with India. In the Miocene period, the Cauvery basin, which separates India and Sri Lanka, was created. It was filled by a thick cover of limestone, which is now resting on the northwestern coastal strip of Sri Lanka and the southeastern India (Vithanage, 1985). Table.1.1 summarizes the geochronological and tectonic events identified so far in the basement of Sri Lanka.

Structural history

The structural evolution presented here is based on the detailed studies of Berger and Jayasinghe (1976), Voll and Kleinschrodt (1991), Kriegsman (1993) and Kehelpannala (1997). At least three major phases of structural events (D_1, D_2 and D_3) have been recognized. Some workers have identified locally up to 6 deformation events (e.g. Kehelpannala, 1997). Nevertheless, they can be broadly categorised into three major phases (Fig 1.2).

D_{1a} – *Early extenson and low P/high T metamorphism*

The growth of fibrolitic sillimanite suggest the low P/high T metamorphism prior to crustal thickening occurred at the earliest deformation.

D_{1b} – *Crustal thickening*

The crustal thickening is demarcated by crenulated sillimanite inclusions in garnet and the formation of granitic layering, which now appear as parallel to the early foliation planes (S_1). Crustal thickening was followed by peak granulite metamorphism at 9kbar at the deepest levels of Highland Complex (Schumacher et al. 1990; Kriegsmann 1993).

D_2 – *Extensional collapse*

D_2 deformation event is dominant in many places. The large-scale isoclinal and recumbent folds, boudinage of metabasite and calc-silicate rocks in the metapelites matrix and the nappe tectonics are ascribed to the D_2 events. D_2 affected close to the peak metamorphic conditions as evidenced from L-S tectonic fabric with N-S stretching lineation, present in many rock types.

D_3 – *Late folding and thrusting*

The last major deformation (D_3) took place with the development of N-S trending upright folds within HC, thrusting of HC over VC, local development of biotite lineation with E-W azimuth, E-verging asymmetric inclined folds near HC/VC contact cut by eastward direct thrusts, N-S trending upright folds and steep shear zones.

Metamorphic history

Peak P-T conditions of crystalline rocks of Sri Lanka have been estimated using numerous thermobarometers and different mineral paragenesis. Schumacher and Faulhaber (1994) estimated the P-T condition of the Eastern, North-Eastern and South-Eastern parts of the HC at 760-830^{o}C (Grt-Opx thermometer of Harley, 1984) and 9-10kbar (Grt-Cpx-Pl-Qtz barometer of Newton and Perkins, 1982). Sandiford et al. (1988), using Grt-Cpx and Grt-Opx thermometry, estimated that the minimum temperature of peak metamorphism was 670-730^{o}C. Kriegsman (1993) obtained the peak equilibrium temperatures of sapphirine-bearing granulites in HC at 830^{o}C and 9 kbar with a petrogenetic grid. Schenk et al. (1988) (two-pyroxene thermometry) obtained a maximum temperature of 900^{o}C for the HC. Voll et al. (1994) derived peak temperatures of metamorphism at 850-900^{o}C using two-feldspar thermometry.

It is now evident that the ion-exchange thermometries, all of which assemblages include garnet, show peak temperatures and pressures at lower values relative to two-pyroxene and two-feldspar thermometries. It can be speculated that all thermometries, which have garnet as an exchange mineral, show lower values due to retrograde resetting of garnet during slow cooling. Therefore, it seems that most of the granulites in HC experienced a maximum temperature of around 850-900^{o}C as revealed by two-pyroxene and two-feldspar thermometries.

A field pressure gradient in the HC has been proposed from the central and eastern part to the southwestern regions. The maximum pressures at 9-10 kbar in the central and eastern parts of HC decrease to about 5-6 kbar in the western part of HC (Hapuarachchi, 1975; Newton and Hansen, 1986; Schenk et al, 1991; Schumacher et al., 1990; Faulhaber and Raith, 1991; Schumacher and Faulhaber, 1994), though this was questioned by Perera (1984) and Mathavan and Fernando (1991).

The retrograde path of the HC is controversial. The cooling and decompression paths obtained from meta-igneous rocks are different from those obtained from metasedimentary rocks, although they are part of the same supracrustal succession. Sandiford et al. (1988) obtained a early decompression path for the orthogneisses followed by a isobaric cooling path. An early isobaric cooling path prior to the decompression event was recognised in the metabasite and Fe-rich charnockites (Schumacher et al. 1990; Prame 1991). The isobaric cooling subsequent to the decompression event was previously thought to confine only to the meta-igneous rocks of the HC. These events are now also reported in metasediments in the Buttala klippe (Mathavan and Fernando*, in press*).

A clockwise P-T path of the whole HC is indicated by the presence of early kyanite inclusions in garnets, following peak metamorphic sillimanite and the retrograde andalusite in metapelitic rocks (Hiroi et al. 1987; Raase and Schenk 1994). Kriegsman (1993) reviewed the available P-T and structural data, and, combined with his own data from sapphirine-bearing granulites, proposed a clockwise P-T-t path for the Sri Lankan lower crust. This would imply a crustal thickening event, which was followed by heating and unroofing (Fig. 1.2).

The temperatures in the WC, VC and KC are identical to each other. They record considerably lower temperatures than the rocks from HC. Hornblende-plagioclase thermometry of amphibolites yields a temperature of 700 ± 75 ^{o}C. The overall pressure was estimated at 6.9 kbar (Burton and O'Nions 1990; Schumacher et al. 1990).

GEOLOGY OF THE RUPAHA AREA

The area around Rupaha is part of a hilly to mountainous terrain that also forms the majority of the central highlands of Sri Lanka. The whole area is crossed by a northeasterly flowing trellis drainage system. Much of the drainage follows fractures, joints and distinct shear zones. In general terms, it seems that there is a close match between topography and the geological framework of the area. The rocks with a high percentage of quartz (e.g. quartzite, charnockite) are responsible for most of the ridges of the area, while easily weathered carbonate-bearing rocks and biotite-feldspar-rich rocks form valleys. A noteworthy feature is that numerous peaks protrude as high as 2,000 metres above sea level.

The geological and structural framework of this area is largely based on a provisional geological map (1:100 000) of the Geological survey and Mines Bureau of Sri Lanka (GSMB). A detailed mapping on 1:10,000 scale was needed for very thin bands of different rock units, which could not be identified in large-scale maps (Fig. 1.3). The rocks strike generally N-S, a dip of 25-40° towards the west. Apart from this, the northwestern part of the area is characterized by a doubly plunging synform with an axial trace of NNW-SSE.

Two principal rock units were identified and are broadly categorized as orthogneisses and paragneisses. Orthogneisses are largely composed of charnockites, charnockite gneisses and biotite gneisses. The latter are grey gneisses, but usually lack orthopyroxene. The orthogneisses in the area are of granodioritic to quartz monzonitic composition. They contain mafic minerals of orthopyroxene, clinopyroxene, hornblende and a few biotites. Some quartz grains are up to few centimetres long and mark an intensely flattened and stretched texture.

Granulite grade, multiply deformed metasediments are exposed within a synform in the NW, as well as in thin bands in the rest of the mapping area. These paragneisses consist mainly of quartzites, quartzofeldspathic gneisses, a few scattered occurrences of marbles and semi pelitic gneisses, including garnet-biotite gneisses, corundum-biotite gneisses and garnet-sillimanite-graphite gneisses, with large porphyroblastic garnets formerly termed as '*khondalites*'. Streaky, banded khondalite layers act as stratigraphic markers in the area. The pelitic paragneisses are extensively weathered, probably due to the presence of high feldspar content. A few outcrops of marbles occur throughout. Accessory minerals include apatite, zircon, ilmenite and rutile. Outcrops of garnet-biotite gneisses have been partly migmatized. The migmatized patches are essentially leucocratic, distinctly layered medium-grained quartzo-feldspathic gneisses, intercalated at places with charnockitic gneisses.

Ultramafic complexes have been found to the west of the Rupaha village. They were interpreted earlier as intrusive bodies, which cut through older basement rocks. Coomaraswamy (1904) provided the first report of a serpentinite deposit from Rupaha and termed it a 'serpentine marble' mainly due to its pale green colour and the differences in mineralogy from those of other marbles. Soyza (1986) has provided an account of the economic importance of the body. Siriwardena (1988) has carried out a preliminary study of this 'serpentine marble' deposit. He described two corundum-bearing locations near the ultramafic body. Corundum-bearing rocks described here are from one of 11 reported *in-situ* occurrences in Sri Lanka referred by Coomaraswamy (1903), Cooray and Kumarapeli (1960), Coates (1935), Wells (1956), Silva and Siriwardena (1988) and Rupasinghe and Dissanayake (1987). Recent work by Fernando et al. (1995) interpreted the ultramafic body as a part of the supracrustal succession, which has been subjected to intense high-grade metamorphism and deformation events.

Despite the fact that there is a considerable wealth of information on the economic importance of the serpentinite body, no attempts were made to present a mechanism for the formation of silica-undersaturated corundum bearing rocks at the contact of this serpentinite body. The present study focuses on the serpentinite body and its contact rock units, which are well exposed along the tributary of the main river Halgran Oya, named *'Garandu Kandura'* (Fig. 1.4).

GEOLOGY OF THE STUDY AREA

The geology around the deposit was described by Siriwardena (1988). The exposure around serpentinite body contains three mineralogically and the petrologically different rock units; (1). granulite zone; (2). ultramafic zone; (3). reaction zone. The granulite zone preserves the original metamorphic textures and minerals typical of granulites in the area. The reaction zone has been recognized in between these two rock units. This succession is roughly repeated in at least ten locations within 300m distances before the rocks are covered by thick soil overburden (Fig. 1.4).

Granulite zone

The rocks from the Granulite zone are described in the preceding section as garnet-biotite gneisses and charnockites. But in particular, Garnet-biotite gneisses and charnockites display thin compositional banding with development of lineated quartz and mica flakes. The thin bands of impure marble (calc-silicate gneisses) and sillimanite-biotite gneisses are intercalated with charnockites and garnet-biotite gneisses in the vicinity of the ultramafic rocks (Fig. 1.4).

Ultramafic zone

Ultramafic rocks form as several lens shaped bodies with a maximum width of 100 metres and extensions along strikes of 50 metres or more. The Rupaha exposure consists predominantly of medium-grained, dark brown and greenish-grey serpentinites, with carbonate veins and are intensely sheared. At places, the serpentinites contain white coloured, fresh, medium-grained orthopyroxenes. Pale green ultramafic rock is characterized by numerous cross cutting veinlets in irregular fashion. The dark green ultramafic variety is less altered; nevertheless some purplish coloured clusters of spinel are embedded at places. The textural features demonstrated that the ultramafic body has been subjected to high-grade metamorphism with other regional granulitic rocks. The phlogopite is found at the interface of ultramafic-siliceous granulite.

Reaction zone

The reaction zone is composed of four distinct mineral assemblages. The zone adjacent to siliceous gneisses consists of syenitic-looking Crn(5%)-Bt-Pl-bearing gneisses. This zone is generally up to 3m thick at places. The randomly arranged porphyroblastic corundum

crystals are embedded in this feldspar matrix in the quartz undersaturated rock. The rest of the zone consists of thin bands of Crn(30%) + Pl + Bt-bearing gneisses, Crn + Spr + Spinel-bearing gneisses and Phl + Spr + Spl-bearing gneisses. The zone boundaries are very sharp, which are roughly aligned parallel to the regional foliation.

REFERENCES

Bauer N, Kröner A, Todt W, Liew TC, Hofmann AW (1991). U-Pb isotopic systematics of zircons from prograde and retrograde transition zones in high-grade orthogneisses, Sri Lanka. J. Geol. 99: 527-545

Berger AR, Jayasinghe NR (1976). Precambrian structure and chronology in the Highland Series of Sri Lanka. Precam. Res. 3: 559-576

Braddy JB (1988) The role of volatiles in the thermal history of metamorphic terranes. J. Petrol. 29: 1187-1213

Burton KW, O'Nions RK (1990). The timescale and mechanism of granulite formation at Kurunegala, Sri Lanka. Contrib. Mineral. Petrol. 106: 66-89

Cartwright I, Valley JW (1991). Steep oxygen-isotope gradients at marble-metagranite contacts in the northwest Adirondack Mountains. New York USA: products of fluid hosted diffusion. Earth Planet. Sci. Lett. 107: 148-163

Coates JS (1935). The Geology of Ceylon, Cey. J. Sci. 19: 101-191

Coomaraswamy AK (1903). Occurrences of corundum insitu near Kandy, Ceylon. Geol. Mag. 21: 348-350

Coomaraswamy AK (1904) Administrative report. Mineral. Surv. Ceylon.

Cooray PG, Kumarapeli PS (1960). Corundum in biotite-sillimanite gneiss from near Polgahawela, Ceylon. Geol. Mag. 47: 480-487

Cooray PG (1984). An introduction to the geology of Sri Lanka. National Museums of Sri Lanka, (second ed), pp340

*Cooray PG (*1994) The Precambrian of Sri Lanka: a historic review. Precam. Res. 66: 3-18

Crowford AR (1969). India, Ceylon and Pakistan: near age data and comparisons with Australia. Nature 223: 380-384

Crowford AR, Oliver RL (1969). Precambrian chronology of Ceylon. Geol. Soc. Australia Sp. Publ 2: 283-316

Dissanayake CB, Chandrajith R (1999). Sri Lanka-Madagaskar Gondwana Linkage: evidence for a Pan-African Mineral belt. J. Geol. 107: 223-235

Dunkley DJ, Clarke GL, Harley SL (1999). Diffusion metasomatism in silica-undersaturated sapphirine-bearing granulite from Rumdoole Peak, Framnes Mountains, east Antartica. Contrib. Mineral. Petrol. 134: 264-276

Faulhaber S, Raith M (1991). Geothermometry of high-grade rocks: a case study on garnet-pyroxene granulites in southern Sri Lanka. Mineral Mag. 55: 33-56

Fernando GWAR, Dissanayake CB, Rupasinghe MS (1995). Corundum mineralization of Sri Lanka and its relationships to Gondwana tectonics, (abs), Proceed. Intern. Symp. On "India and Antarctica during the Precambrian and granulite and crustal processes in East Antarctica",Vishakapatnam, India, 18

Ferry JM (1984). A biotite isograd in south central Maine, USA: mineral reactions, fluid transfer and heat transfer. J. Petrol. 25: 871-893

Frantz JD, Mao HK (1976). Bimetasomatism resulting from intergranular diffusion: I. A theoretical model for monomineralic reaction zone sequences. Am. J. Sci. 276: 817-840

Frantz JD, Mao HK (1976). Bimetasomatism resulting from intergranular diffusion: II. Prediction of multimineralic zone sequences Am. J. Sci. 279: 302-323

Frantz JD, and Weisbraod A (1974). Infiltration metasomatism in the system K_2O-SiO_2-Al_2O_3-H_2O-HCl. In: Geochemical transport and kinetics (*Hofmann AW; Giletti BJ; Yoder HSJ; Yund RA* eds). Carnegie Institute Washington DC, 261-271

Fyfe WS, Price NJ, Thompson AB (1978). Fluids in the earth's crust: Elsevier Publ., Amsterdam, pp583

Geological Survey and Mines Bureau (1996). Geological Map of Kandy and Hanguranketha, provisional map series, Sheet 14

Hapuarachchi DJAC (1975). The granulite facies in Sri Lanka. Geol. Surv. Dept. Sri Lanka, Prof. Pap. 4: pp29

Harley SL (1984). An Experimental study of the partitioning of Fe and Mg between garnet and orthopyroxene. Contrib. Mineral. Petrol. 86: 359-373

Helgeson HC, Lichtner PC (1987). Fluid flow and mineral reactions at high temperatures and pressures. J. Geol. Soc. London 144: 313-326

Hiroi Y, Yoshida Y, Vithanage PW (1987). Relict kyanite in the Highland and Southwest gneisses in Sri Lanka: evidence of prograde metamorphism and a characteristic in common with the Lützom-Holm Complex in East Antarctica. Geol. Soc. Sri Lanka Sp. Publ. 3: pp28

Hokada T, Osanai Y, Toyoshima T, Owada M. Tsunogae T, Crowe WA (1999). Petrology and metamorphism of sapphirine-bearing aluminous gneisses from Tonagh Island in the Napier Complex, East Antarctica, Polar Geosci. 12: 49-70

Hölzl S, Hofmann AW, Todt W, Köhler H (1994). U-Pb geochronology of the Sri Lanka basement. Precam. Res. 66: 123-149

Hölzl S, Köhler H, Kröner A, Jaeckel P, Liew TC (1991). Geochronology of Sri Lankan basement. In: The crystalline crust of Sri Lanka, Part 1, Summary of the research of the German-Sri Lankan Consortium (*Kröner A* ed). Geol. Surv. Dept. Sri Lanka Prof. Pap. 5: 237-257

Jaeckel P, Kröner A, Williams IS (1991). U/Pb isotopic systematics in single zircons from lower crustal rocks in Sri Lanka as revealed by ion microprobe and evaporation analysis. Terra Abstracts 3: 490

Jacobs J, Fanning CM, Henjes-Kunst F, Olesch M, Paech HJ (1998). Continuation of Mozambique Belt into East Antarctica: Grenville age metamorphism and polyphase Pan-African high-grade events in Central Dronning Maud Land. J. Geol. 106: 385-406

Kehelpannala KVW (1997). Deformation of high-grade Gondwana fragment, Sri Lanka. Gondwana Res. 1: 47-68

Kleinschrodt R (1994). Large-scale thrusting in the lower crustal basement of Sri Lanka. Precam. Res. 66: 39-57

Kretz R (1983) Symbols for rock forming minerals. Am. Mineral. 68: 277-279

Kriegsman LM (1991a). Sapphirine-bearing granulite from central Sri Lanka-outcrop description and mineral chemistry. In: (*Kröner A* ed) the crystalline crust of Sri Lanka, part 1, summary of research of Sri Lankan-German Consortium (*Kröner A* ed). Geol. Surv. Dept. of Sri Lanka, Prof. Pap. 5: 178-187

Kriegsman LM (1991b). Structural geology of the Sri Lankan basement. In: The crystalline crust of Sri Lanka, Part 1, Summary of the research of the German-Sri Lankan Consortium (*Kröner A* ed). Geol. Surv. Dept. Sri Lanka Prof. Pap 5: 52-68

Kriegsman LM (1993). Geodymamic evolution of the Pan-African lower crust in Sri Lanka-Structural and petrological investigations into a high-grade gneiss terrain. PhD thesis, University of Utrecht, The Netherlands, pp207

Kriegsman LM, Schumacher JC (2000). Petrology of sapphirine-bearing and associated granulites from central Sri Lanka. J. Petrol. 40: 1211-1239

Kröner A (1991). African linkage of Precambrian Sri Lanka. Geol. Rundschau 80: 429-440

Kröner A, Jaeckel P (1994). Zircon ages from rocks of the Wanni Complex: a crustal unit distinct from the Highland Complex. J. Geol. Soc. Sri Lanka 5: 21-36

Kröner A, Williams AS (1993). Age of metamorphism of high-grade rocks of Sri Lanka. J. Geol. 101: 521-531

Kröner A, Cooray PG, Vitanage PW (1991). Lithotectonic subdivision of the Precambrian basement in Sri Lanka. In: The crystalline crust of Sri Lanka, Part 1. Summary of research of the German-Sri Lankan Consortium (*Kröner A* ed). Geol. Surv. Dept. Sri Lanka Prof. Pap. 5: 5-21

Kröner A, Williams IS, Compston W, Baur N, Vitanage PW, Perera LRK (1987). Zircon Ion Microprobe dating of High-grade rocks in Sri Lanka. J. Geol. 95: 775-791

Liew TC, Milisenda CC, Hofmann AW (1991). Isotopic characterization of the high-grade basement rocks in Sri Lanka In: The crystalline crust of Sri Lanka, Part 1. Summary of research of the German-Sri Lankan Consortium (*Kröner A* ed). Geol. Surv. Dept. Sri Lanka Prof. Pap. 5: 258-266

Mathavan V, Fernando GWAR (1991) Partial melting in cordierite-sillimanite gneiss from Dombawela, Matale, Sri Lanka. (abs), Proceed. 49 th Ann Sess Sri Lanka Assoc. Adv. Sci. (SLAAS), 94

Mathavan V, Fernando GWAR (*in press*). Mineral Chemistry and Reaction Textures in Calc-Silicate Granulites from the Highland Complex of Sri Lanka: Evidence for Isobaric Cooling and Decompression Paths in the Metasediments (*Lithos*)

Milisenda CC (1991). Development of continental crust: a study of the high-grade terrain of Sri Lanka, Ph D thesis, University of Mainz, Germany, pp138

Milisenda CC, Liew TC, Hoffman AW, Kröner A (1988) Isotopic mapping of age provinces in Precambrian high-grade terrains: Sri Lanka. J. Geol. 96: 608-615

Milisenda CC, Liew TC, Hoffman AW, Köhler H (1994). Nd isotopic mapping of the Sri Lanka basement: update and additional constrains from Sr isotopes. Precam. Res. 66: 95-110

Newton RC (1986). Fluids of the granulite facies metamorphism. In: Fluid-rock interactions during metamorphism. (*Walther JV, Woods BJ* eds). Advances in physical geochemistry 5, Springer Verlag, New York, 36-59

Newton RC, Hansen EC (1986). The south India-Sri Lanka high-grade terrain as a possible deep crust section. In: The nature of the lower continental crust : (*Dawson DB, Carswell DA, Hall J, Wedepohl* eds). Geol. Soc. Sp. Publ. 24: 297-307

Newton RC, Perkins D III (1982). Thermodynamic calibration of geobarometers based on the assemblages garnet-plagioclase-orthopyroxene (clinopyroxene)-quartz. Am. Mineral. 67: 203-222

Osanai Y (1989). A preliminary report on sapphirine-kornerupine granulite from Highland Series, Sri Lanka (extended abstract), Seminar on recent advances in Precambrian geology in Sri Lanka

Osanai Y, Owada M, Kagami H, Hamamoto T, Hensen J (1996). Sapphirine granulite and related high-P-T metamorphic rocks from Highland Complex, Sri Lanka, In: Gondwana Research Group Misc. Publ. 4, (*Santosh M, Yoshida M* eds), 107-108

Perera LRK (1984). Co-existing cordierite-almandine – a key to the metamorphic history of Sri Lanka. Precam. Res. 25: 349-364

Powell C Mac, Roosts SR, Veevers JJ (1988). Pre-breakup continental extension in East Gondwanaland and the early opening of eastern Indian Ocean. Tectonophysics 155: 261-283

Prame WKBN (1991). Petrology of the Kataragama Complex, Sri Lanka: evidence for high P-T granulite facies metamorphism and subsequent isobaric cooling. In: The crystalline crust of Sri Lanka, Part 1. Summary of research of the German-Sri Lankan Consortium (*Kröner A* ed). Geol. Surv. Dept. Sri Lanka Prof. Pap. 5: 200-224

Raase P, Schenk V (1994). Petrology of granulite-facies metapelites of the Highland Complex, Sri Lanka: implications for the metamorphic zonation and the P-T path. Precam. Res. 66: 265-294

Rubie DC (1986). The catalysis of mineral reactions by water and restrictions on the presence of aqueous fluids during metamorphism, Mineral. Mag. 50: 399-415

Rupasinghe MS, Dissanayake CB (1987). New in-situ corundum deposits in Sri Lanka. J. Gemmol. Assoc. Sri Lanka 4: 2-5

Sandiford M, Powell R, Martin SF, Perera LRK (1988). Thermal and baric evolution of garnet granulites from Sri Lanka. J. Metamorphic Geol. 6: 351-364

Schenk V, Raase P, Schumacher R (1988). Very high temperatures and isobaric cooling before tectonic uplift in the Highland Series. Terra Cognita 8: 265

Schenk V, Raase P, Schumacher R (1991). Metamorphic zonation and P-T history of the Highland Complex in Sri Lanka. In: The crystalline crust of Sri Lanka Part 1. Summary of research in German-Sri Lankan Consortium (*Kröner A* ed). Geol. Surv. Dept. Sri Lanka Prof. Pap. 5: 150-163

Schumacher JC, Robinson P (1987). Mineral chemistry and metasomatic growth of alumineous enclaves in gedrite-cordierite-gneiss from southwestern New Hampshire, USA. J. Petrol. 28: 1033-1073

Schumacher R, Schenk V, Raase P, Vithanage PW (1990). Granulite facies metamorphism of metabasic and intermediate rocks in the Highland Series of Sri Lanka. In: High-grade metamorphism and crustal anatexis, (*Ashwarth JR, Brown M* eds), Unwin Hymann Ltd., London, 235-271

Schumacher R, Faulhaber S (1994). Summary and discussion of P-T estimates from garnet-pyroxene-plagioclase-quartz-bearing granulite- facies rocks from Sri Lanka. Precam. Res. 66: 295-308

*Silva KKMW, Siriwardena CHER (*1988). Geology and the origin of the corundum-bearing skarn at Bakamuna, Sri Lanka. Mineral. Deposita 23: 186-190

Sriwardena CHER (1988). Preliminary report of the survey of Rupaha serpentine deposit, Geol. Surv. Dept. (unpublished) pp15

Soyza EG (1986). An account of serpentine deposit of Rupaha, Sri Lanka. J. Gemmol. Ass. Sri Lanka 3: 30-34

Touret JLR, Hartl THD (1990). Syn-metamorphic fluid inclusions in granulites. In: Granulites and crustal evolution. (*Vielauf D, Vidal P* eds). NATO ASI Series C 311, Kluwer Publishers, Dordrecht, 397-417

Valley JW, O'Neil JR (1984). Fluid heterogeneity during granulite facies metamorphism in the Adirondacks: Stable isotope evidence. Contrib. Mineral. Petrol. 85: 158

Valley JW, Bohlen SR, Essene EJ, Lamb W (1990). Metamorphism in Adirondacks: II The role of fluids. J. Petrol. 31: 555-596

Vithanage PW (1972). Post-Precambrian uplifts and regional neotectonic movements in Ceylon. 24th IGC Montreal, Canada, 3: 642-654

Vithanage PW (1985). Tectonics and mineralization in Sri Lanka. Geol. Soc. Finland Bull. 57: 157-168

Voll G, Kleinschrodt R (1991). Sri Lanka: structural, magmatic and metamorphic development of Gondwana fragment. In: The crystalline crust of Sri Lanka, Part -1. Summary of research of the German-Sri Lankan Consortium (*Kröner A* ed). Geol. Surv. Dept. Sri Lanka Prof. Pap. 5: 22-51

Voll G, Evangelakakis C, Kroll H (1994). Revised two-feldspar geothermometry applied to Sri Lankan feldspars. Precam. Res. 66: 351-377

Wells AJ (1956). Corundum from Ceylon. Geol. Mag. 42: 25-31

Yoshida M, Funaki M, Vithanage PW (1992). Proterozoic to Mesozoic East Gondwana: the juxtaposition of India, Sri Lanka and Antarctica, Tectonics. 11: 381-391

Table 1.1 Geochronological and tectonic events of crystalline and non-crystalline rocks of Sri Lanka

Age (Ma)	WC	HC	VC	Major Tectonics
~3200-2400 *(SHRIMP U-Pb detrital zircon)*		Age of supracrustals (9)		
~ 2287 ± 108 *(whole rock Rb-Sr, K-Ar)*		Age of supracrustals (3,4)		
~2350-2000 *(Sm-Nd model ages, U-Pb zircon fraction upper intercept)*		Deposition of supracrustals in the Proterozoic basement (5, 6, 11, 12, 16, 17)		
~1942-1850 *(U-Pb zircon fraction upper intercept)*		Intrusion of granitoid rocks (1, 5, 6, 11,12, 16, 17)		
~1100 *(Sm-Nd model ages)*	Deposition of supracrustal rocks (5, 6, 12, 14, 16, 17)		Deposition of supracrustal rocks (11, 12, 16, 17)	
~1100-1000 *(SHRIMP U-Pb detrital zircon)*	Intrusion of granitoid rocks (6, 7, 8, 15)		Intrusion of granitoid rocks (5)	
~750 *(U-Pb zircon)*				Amalgamation of HC and WC (15)
~610-550 *(U-Pb zircon fraction lower intercept, U-Pb monazite)*	Regional granulite facies metamorphism, (1, 7, 12)	Regional granulite facies metamorphism (1, 5, 6)		Pan-African orogeny (collision between East- and West-Gondwana) (9, 10, 12, 18)
~580-550				Thrusting of HC-WC over VC (8)
~591-456 *(U-Pb zircon fraction lower intercept)*			Regional amphibolite facies metamorphism (5, 6, 11)	
~160-200	Deposition of Jurassic sediments on the crystalline rocks (2)			Crustal extension of East Gondwana (12,18, 20)
~26	Deposition of carbonates sediments in the Cauvery basin (2)			Separation of Sri Lanka from India (19)

(1). Bauer et al. (1991) (2). Cooray (1984) (3). Crowford (1969)
(4). Crowford and Oliver (1969) (5). Hölzl et al. (1991) (6). Hölzl et al. (1994)
(7). Jaeckel et al. (1991) (8). Kleinschrodt (1994). (9). Kriegsman (1991b)
(10). Kriegsman (1993) (11). Kröner et al. (1987) (12). Kröner (1991)
(13). Kröner et al. (1991) (14). Kröner et al. (1994) (15). Kröner and Jaeckel (1994)
(16). Liew et al. (1991) (17). Milisenda et al. (1988) (18). Powell et al. (1988)
(19). Vithanage (1985) (20). Yoshida et al. (1992)

FIGURE CAPTIONS

Fig. 1.1 Simplified geological map of the Sri Lanka showing all major litho-tectonic units (after Cooray 1994). The area outlined by the box is the studied area (Rupaha area), which is shown in greater detail in Fig. 1.3.

Fig. 1.2 P-T-t-D path for the granulites of the Highland Complex in Sri Lanka (after Kreigsman 1993). The prograde path is characterized by crustal thickening, and subsequent heating, while the retrograde path shows early isothermal decompression, followed by isobaric cooling.

Fig. 1.3 Geological map of the area around Rupaha. The Proterozoic rocks are composed of charnockites, charnockitic gneisses, quartzites, garnet-sillimanite-graphite gneisses (khondalites), garnet-biotite gneisses, and scattered marbles. The study concerns the metamorphosed ultramafic rocks, which are exposed at *'Garandu Kandura'* and their adjoining rocks. Geological map modified after Siriwardena (1988) and Geological Survey & Mines Bureau (1996). The study area given by the shaded box is shown in detail in Fig 1.4.

Fig. 1.4 Detailed geological and location map of the area around the main serpentinite body exposed at the *'Garandu Kandura'*, Rupaha, Sri Lanka.

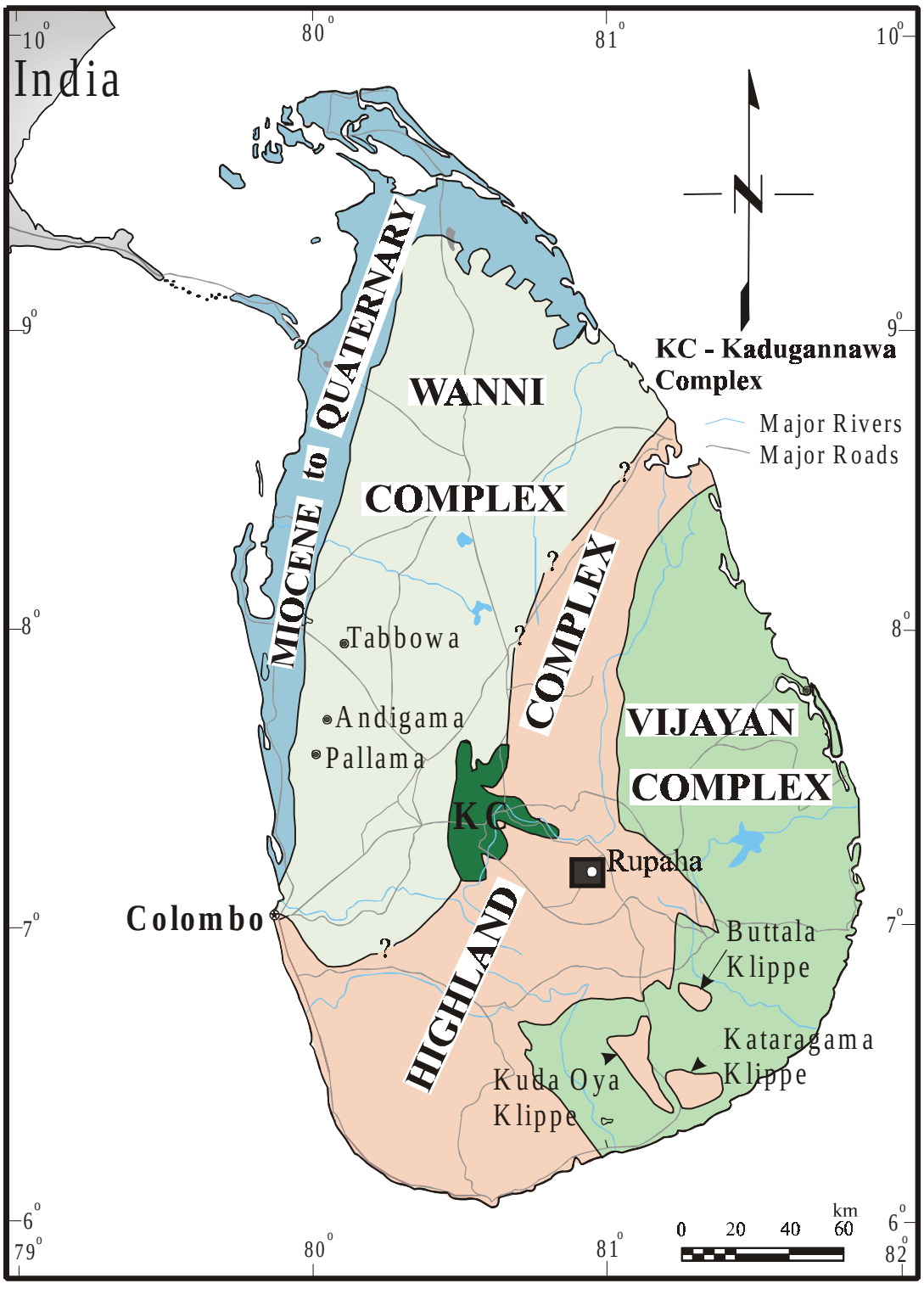
India
10°
80°
81°
10°
9°
9°
8°
8°
7°
7°
6°
79°
80°
81°
82°
MIOCENE to QUATERNARY
WANNI
COMPLEX
KC - Kadugannawa Complex
Major Rivers
Major Roads
Tabbowa
Andigama
Pallama
KC
COMPLEX
VIJAYAN
COMPLEX
Rupaha
Colombo
HIGHLAND
Buttala Klippe
Kataragama Klippe
Kuda Oya Klippe
0 20 40 60 km

Fig 1.1

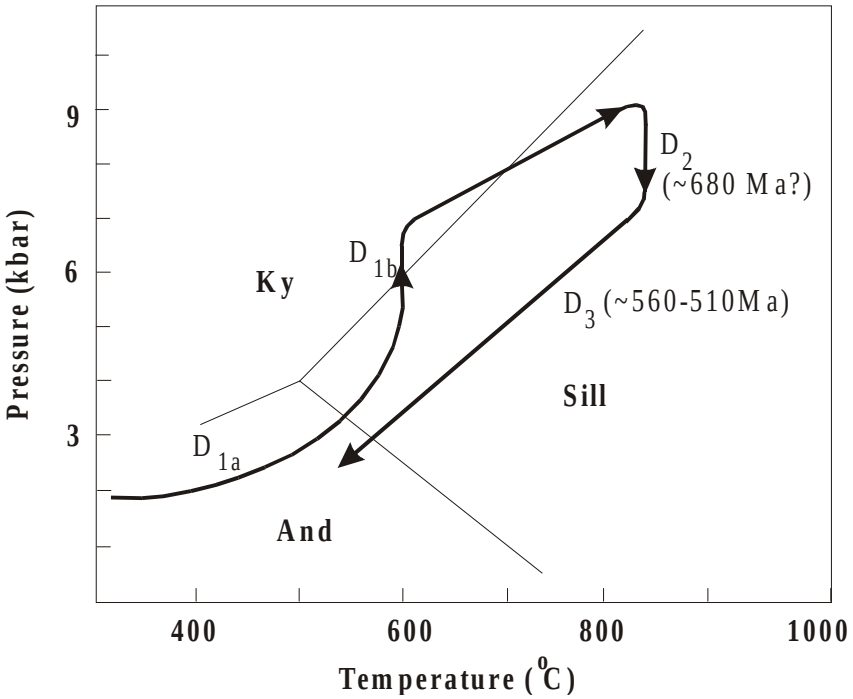

D_{1a}	Early extension and lowP /High-T metamorphism
D_{1b}	Crustal thickening
D_2	Extensional collapse- main deformation
D_3	Late folding and thrusting

Fig.1.2

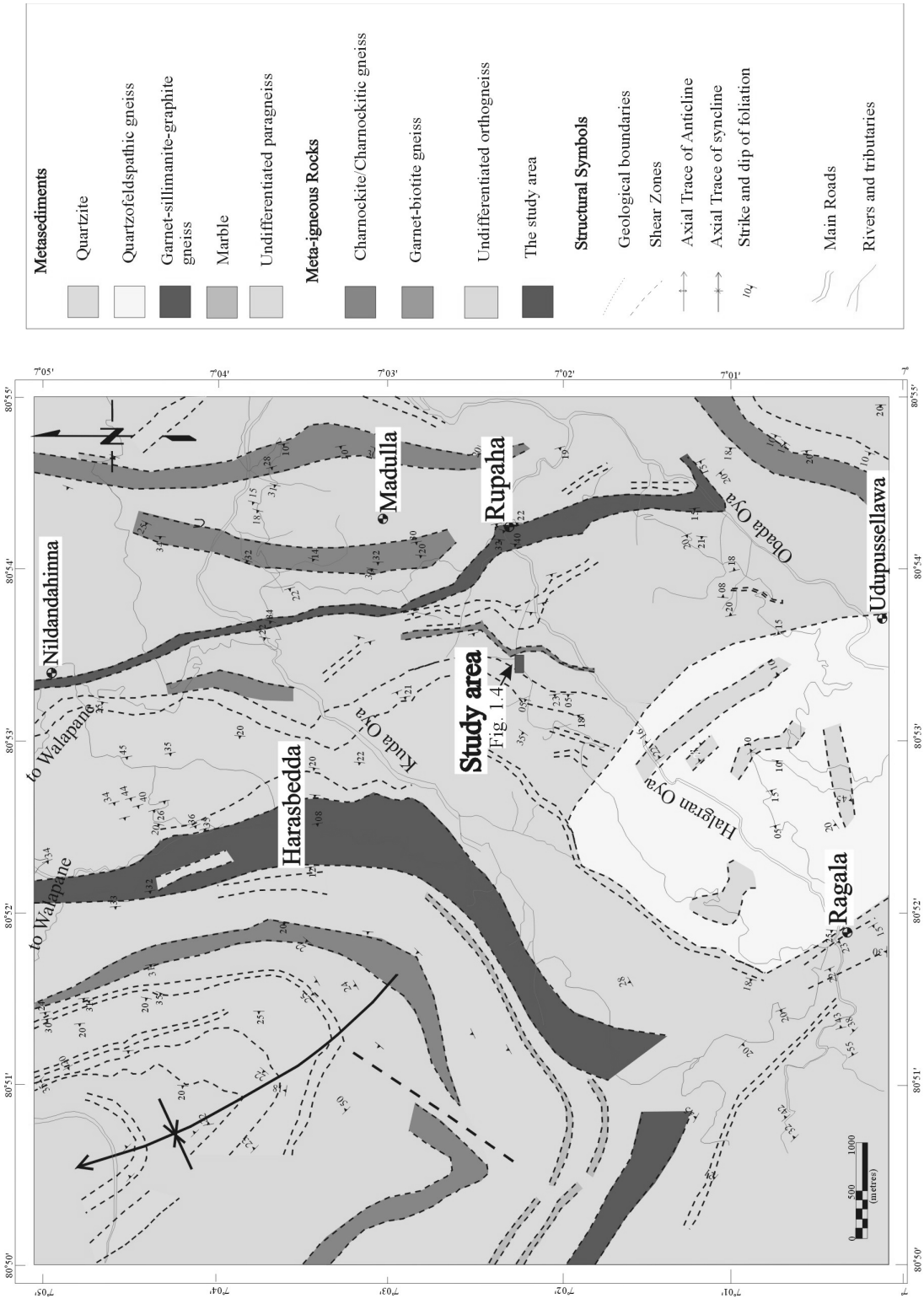
Metasediments
Quartzite
Quartzofeldspathic gneiss
Garnet-sillimanite-graphite gneiss
Marble
Undifferentiated paragneiss
Meta-igneous Rocks
Charnockite/Charnockitic gneiss
Garnet-biotite gneiss
Undifferentiated orthogneiss
The study area
Structural Symbols
Geological boundaries
Shear Zones
Axial Trace of Anticline
Axial Trace of syncline
Strike and dip of foliation
Main Roads
Rivers and tributaries
Nildandahinna
Madulla
Rupaha
Udupussellawa
Harasbedda
Study area
Fig. 1.4
Kuda Oya
Obada Oya
Halgran Oya
Ragala
to Walapane
to Walapane
7°05'
7°04'
7°03'
7°02'
7°01'
80°55'
80°54'
80°53'
80°52'
80°51'
80°50'
0
500
1000
(metres)

Fig. 1.3

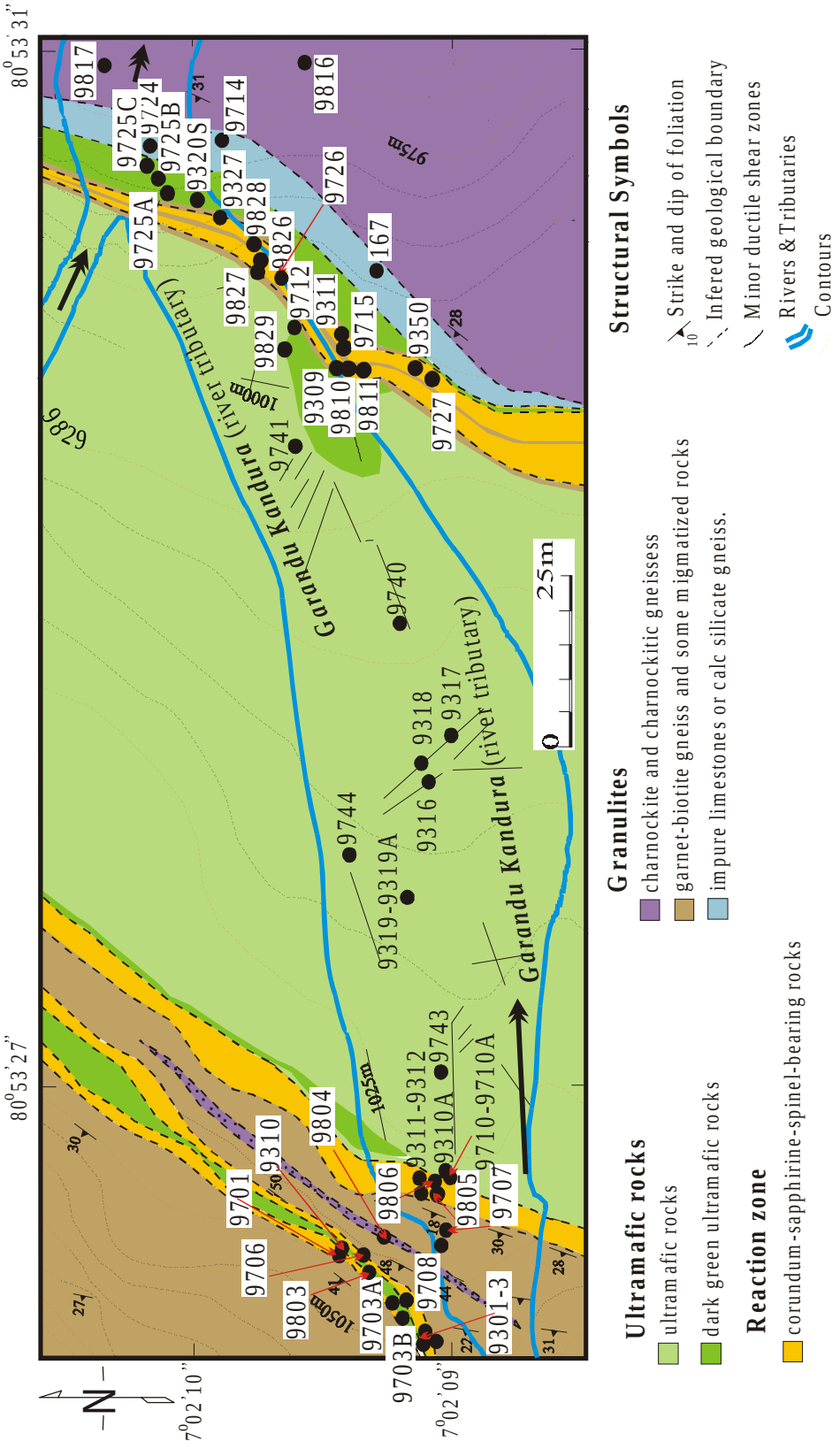
80°53'31"
80°53'27"
7°02'10"
7°02'09"
N
9817
9725C
9724
9725B
9320S
9714
9725A
9828
9826
9816
9726
9827
9712
9311
167
9829
9715
9350
9309
9810
9811
9727
9741
9740
9744
9319-9319A
9316
9318
9317
9743
9311-9312
9310A
9710-9710A
9804
9310
9701
9806
9805
9707
9706
9803
9703A
9708
9703B
9301-3
Garandu Kandura (river tributary)
Garandu Kandura (river tributary)
1000m
1025m
1050m
975m
0
25m
Structural Symbols
Strike and dip of foliation
Infered geological boundary
Minor ductile shear zones
Rivers & Tributaries
Contours
Granulites
charnockite and charnockitic gneisess
garnet-biotite gneiss and some migmatized rocks
impure limestones or calc silicate gneiss.
Ultramafic rocks
ultramafic rocks
dark green ultramafic rocks
Reaction zone
corundum-sapphirine-spinel-bearing rocks

Fig.1.4

Chapter 2

Retrograde diffusion zoning in garnet: Implications for three-stage cooling history of mafic granulites in the Highland Complex of Sri Lanka

ABSTRACT

Diffusion modeling of retrograded garnet rims from mafic granulites is used to estimate the cooling rates in the Proterozoic basement of Sri Lanka, which represents a small, but important fragment of the super-continent Gondwana. Metamorphic peak temperatures and pressures estimated with two-pyroxene thermometry and garnet-clinopyroxene-plagioclase-quartz (GADS) barometry, yield 875 ± 4°C and 8.7 ± 0.4 kbar, which is significantly higher than garnet-biotite Fe-Mg exchange thermometry of 820 ± 20°C. Garnet rims exhibit narrow but regular retrograde zoning in terms of Fe and Mg exchange between garnets touching biotite and give temperature of 685°C.

The observed garnet zoning requires a three-step cooling history. Equilibrium was achieved along grain boundaries during the first cooling step. During the subsequent faster cooling, only local exchange between garnet and biotite occurs. A maximum cooling rate of 1°C/Ma is estimated during the initial stage of cooling followed by a cooling rate of ~30°C/Ma. The outermost rims of garnet indicate that cooling slowed down at or near the blocking temperature of garnet to about 10-15°C/Ma. The three-stage temperature-time history is not in agreement with the cooling history inferred from mineral radiogenic ages in the literature. The difference in cooling rates between our calculations and using thermochronology is mainly due to the lack of larger reliable set of geochronological results of different minerals and radiogenic isotope systems.

INTRODUCTION

One of the common features of granulite facies rocks is the textural and chemical equilibration during high-grade metamorphic conditions. Compositional zoning in minerals, if formed during the prograde path, is generally completely homogenized during granulite facies metamorphism. Existing mineral zoning in granulites is typically due to prolonged cooling and exhumation (e.g. Lasaga et al. 1977; Lasaga 1983; Giletti 1986; Essene 1989). Thus, mineral zoning in granulite terranes is critical for understanding the exhumation and uplift history of the specific terrane. This can be done by accurate determination of the pressure-temperature-time evolution path. If the compositions of mineral phases record and preserve peak equilibrium conditions, the time-temperature path (T-t) can be correctly pinpointed. But, if cores of zoned minerals do not represent the actual thermal peak, utilizing core compositions for geothermometry leads to meaningless results. On the other hand, if one can evaluate and estimate the correct peak compositions of minerals, the actual T-t history of the rocks can be tentatively estimated. Interpretation of the cooling history in granulites from Sri Lanka using garnet zoning and recovered peak compositions of garnets illustrate a well-constrained three-stage cooling history of the rocks.

Cooling rates of rocks are usually determined by three different ways; using closure temperature of minerals for radiogenic isotopes (e.g. Mezger et al. 1992) or for stable isotopes (e.g. Giletti 1986; Eiler et al. 1992, 1995) or diffusive zoning in metamorphic minerals (e.g. Dodson 1973; Lasaga 1983; Spear 1991; Lindström et al. 1991; Spear and Florence 1992; Florence and Spear 1995; Spear and Parrish 1996; Weyer et al. 1999).

To quantify the cooling history of rocks, many workers have discussed the use of garnet diffusion zoning patterns. Some have used the assumption of a large amount of (infinite) biotite, which implies a fixed biotite composition that is unaffected by diffusional exchange with the garnet (e.g. Dodson 1973). This assumption is correct for some granulites, where biotite makes up the bulk of the rock, and diffusion of grain boundaries is fast (e.g. Weyer et al. 1999). The other extreme is to balance the diffusional fluxes of the elements between touching biotite and garnet grains (e.g. Lasaga 1983; Spear and Florence 1992; Lindström et al. 1991; Florence and Spear 1995; Spear and Parrish 1996). The

diffusional gain or loss of garnet is balanced by the compositional change of its coexisting biotite.

The Fe-Mg inter-diffusion of more than two minerals in a rock like that exchange between garnet, biotite and clinopyroxene, for example, requires that all fluxes between these minerals are balanced in a closed system. Hence, the knowledge of interdiffusion coefficients of all individual phases, modal abundances and surface areas of these phases are required (see Eiler et al. 1992 for more details).

Lower crustal granulites are exposed in many places in Gondwana fragments, such as the small fragment of Sri Lanka. Granulites of Sri Lanka often have significant amounts of ferro-magnesian rocks, which are commonly interpreted as metamorphosed basic igneous rocks. These granulites, which show consistent isobaric cooling in the area around Rupaha within the Highland Complex (Fig.2.1), are used to evaluate its P-T and cooling history. Up to now only a few studies have presented cooling rates for Sri Lankan granulites (Hölzl et al. 1991; Burton and O'Nions 1990). There has been renewed interest to evaluate the internal consistency of cooling rates of Sri Lankan granulites because cooling and uplift history of Sri Lankan basement has been poorly defined by both methods.

We use garnet diffusion to determine the cooling rates. The interpretation is based on: (1) recovering of peak composition of garnets; (2) application of diffusion models to estimate the cooling rates using numerical zoning patterns. The results are combined with geochronology from the literature to describe the complete exhumation history of the granulites.

GEOLOGICAL SETTING

The Proterozoic basement of Sri Lanka exposes substantial parts of lower continental crust in which four different units were distinguished on the basis of isotopical, geochronological, geochemical and petrological constraints (Cooray 1994; Kröner et al. 1991; Milisenda et al. 1994)(Fig 2.1.): (1) the Highland Complex (HC); (2) the Vijayan Complex (VC); (3) the Wanni Complex (WC) and (4) the Kadugannawa Complex (KC). The WC consists mainly of metabasites and charnockites while the HC is comprised of

interbedded metapelites, quartzites and marbles in addition to rocks from WC. The VC is exposed in eastern Sri Lanka, consisting of meta-igneous gneisses of tonalitic to leucogranitic composition. The HC rocks yield relatively old crustal residence Sm-Nd model ages (2-3 Ga. Milisenda et al. 1994), while rocks from the other units give significantly younger residence times of 1-2 Ga. Metamorphic grade reaches granulite facies throughout the HC, the WC and the KC, albeit locally retrogressed to amphibolite facies, while the VC has amphibolite facies assemblages. The timing of peak metamorphism was estimated between ~550-~610 Ma (Hölzl et al. 1991,1994; Kröner et al. 1991; Kröner and Williams 1993).

The area of this study is located in the central part of Sri Lanka, at Rupaha, within the central Granulite belt of the HC (Fig.2.1). It consists mainly of meta-igneous rocks (orthogneisses and charnockitic gneisses), which are intercalated with metasediments (quartzite, garnet-sillimanite-graphite gneisses, garnet-biotite gneisses, corundum-biotite gneisses and minor calc-silicates, marbles and ultramafics). The small-scale structures and geological units in the study area are illustrated in Fig. 2.1.

PETROGRAPHY

Two rock-types of mafic granulites, differing in mineral paragenesis and model proportions can be distinguished. Garnet-biotite-clinopyroxene-bearing gneisses (sample location No. 9708 in Fig. 2.1) are coarse-grained, dark and show a strong schistosity. Assemblages are typically Grt + Bt + Pl ± Ilm; Grt + Bt + Cpx + Pl ± Qtz ± Ilm; Grt + Cpx + Pl ± Qtz ± Ilm (for abbreviations see Kretz 1982). Garnet contains inclusions of plagioclase and biotite. Some parts of the rock are migmatized. Charnockites (sample location No. 9817 in Fig. 2.1) in the area are characterized by the mineral paragenesis Opx +Kfs +Pl +Qtz ± Ilm ± Ap; Hbl + Opx + Pl + Kfs + Qtz ± Ilm ± Ap; Opx + Cpx +Pl + Qtz ± Ilm ± Ap ± Grt. The quartz content varies in these rocks from a few volume percent up to about 10%. In garnet-clinopyroxene-biotite-bearing gneisses, no reaction textures are observed. Garnet-quartz grain boundaries are absent suggesting that the reaction garnet + quartz to Cpx + plagioclase + ilmenite has occurred. Biotite and garnet are in equilibrium in many places (Fig.2.2a). Both pyroxenes in charnockites are generally devoid of inclusions, though some small rounded grains of hornblende and plagioclase may be

present. Large elongated crystals of hornblende in the matrix have irregular shaped edges (Fig. 2.2b). A few grains of biotite are present in some samples of the two-pyroxene-hornblende-bearing assemblages. Some late stage chlorites replaced hornblende. The primary metamorphic mineral assemblages selected for thermobarometric study are Opx-Cpx-Pl-Hbl-Qtz and Grt-Bt-Cpx-Pl-Qtz along with minor amounts of magnetite, ilmenite, apatite, rutile and zircon.

ANALYTICAL TECHNIQUES

Thin sections from the two rock types showing the primary mineral assemblages with no or minor retrogression were selected for thermobarometry. After detailed optical inspection of polished thin sections, mineral analyses were performed on carbon-coated thin sections at the University of Mainz, Germany, using the JEOL microprobe (JEOL JXA 8900 RL) with operating conditions of 15keV accelerating voltage, 12nA beam current and 2µm beam diameter. Elements were calibrated against synthetic and natural standards. Online ZAF corrections were performed (Amstrong 1988, 1989). Mineral compositions of coexisting garnet-biotite, garnet-clinopyroxene, and garnet-clinopyroxene-plagioclase-quartz from garnet biotite gneisses and coexisting two-pyroxenes from charnockites were analyzed. Garnets were analyzed for both rim and core compositions, that physically contact with either biotite or clinopyroxene. Thermobarometric pairs were selected from adjacent grains in the view of separate thermobarometric calculations. Some representative garnets, adjacent to biotite were investigated for a probable zoning pattern by running microprobe line profile across the grain at 3µm spacing for Fe, Mg, Ca and Mn. A two-dimensional compositional map of Mg- distribution in garnet, which is in mutual contact with biotite, plagioclase and other garnet, was obtained with the automated JEOL microprobe using a wavelength dispersive spectrometer (WDS)(15kV, 30nA and 1µm probe diameter). All iron was assumed to be Fe^{2+} on recalculation.

MINERAL CHEMISTRY

Chemistry of mineral assemblages in one dataset used for thermobarometry of Rupaha granulites are presented in Table 2.1. The comprehensive analytical data set is attached in the Appendices C1-C4.

Garnets are mainly almandine-pyrope-grossular solid solutions, with average almandine content just about 50%. The pyrope content is around 21% while grossular and spessartine content are 16% and 13% respectively. They are typical about 700µm diameter on average. Fig.2.3a is a back-scattered image and Fig. 2.3b, a microprobe line profile of the same grain (Complete chemical data is attached in Appendix C5). Flat zoning of garnet is observed throughout most grains except in the vicinity of adjacent biotite, where X_{Mg} decreases and X_{Fe} increases slightly towards the garnet rim. The rims are approximately 20µm wide (Fig. 2.4). Garnet is typically unzoned towards non-Fe-Mg minerals (e.g. plagioclase) or other garnet. Garnet is not zoned with respect to Ca. Modal abundance of biotite is approximately half of the modal abundance of garnet. Biotite inclusions are preserved in some garnet grains. No zoning was found in clinopyroxene and there is no compositional zoning in contrast to the marked Fe/(Fe+Mg) gradient in garnet. Fe/(Fe+Mg) in clinopyroxene varies from 0.28-0.30 in biotite gneisses while it is between 0.51-0.53 in charnockitic rock. X_{Al} values range from 0.05-0.07. Orthopyroxene in charnockite is of homogeneous composition and has a Fe/(Fe+Mg) value of 0.64-0.67.

PRESSURE-TEMPERATURE ESTIMATES AND FLUID COMPOSITION

Results of ion exchange thermometry (Table 2.2) are based on the garnet-biotite (Dasgupta et al. 1991), the garnet-clinopyroxene (Sengupta et al. 1989) and the orthopyroxene-clinopyroxene (Brey and Köhler 1990) equilibria. The pressures were determined from the calibration of garnet-clinopyroxene-plagioclase-quartz (Eckert et al. 1991) assemblages. Temperature and pressure were calculated by simultaneous solving of the barometric and temperature equations, where applicable (Fig. 2.5). The highest P-T estimates were obtained for Opx-Cpx thermometry together with GADS barometer. Temperatures range from 870-882^{o}C, with pressures of 8.6-9.1 kbar. All three calibrations (Lindsley et al.1981; Kretz 1982; Brey and Köhler 1990) yield identical results within the variation of mineral chemistry. Mineral equilibrium temperatures of 775-840^{o}C at this locality were obtained from Grt-Bt/GADS, using garnet cores, at pressures of 7.6 – 8.3 kbar. These are significantly lower than the Opx-Cpx/GADS thermobarometer values presented above. Pressure-temperature estimates obtained from garnet rim and adjacent biotite compositions with GADS barometer range from 685-795^{o}C and 6.7-7.8 kbar. Pressure-temperature estimates for Grt (rim)-Cpx (rim)/GADS are significantly lower (between 706-738^{o}C and

6.9-7.2 kbar). More than six calibrations (e.g. Ferry and Spear 1978; Hodges and Spear 1982; Perchuk and Lavent'eva 1983; Ganguly and Saxena 1984; Indares and Martignole 1985; Bhattacharya et al. 1992; Kleeman and Reinhardt 1994) were used to Grt(core)-Bt temperatures. While considerable scatter was observed (710-840^{o}C), none of the calibrations indicates peak temperatures close to that of the Opx-Cpx thermometers.

Furthermore, no significant difference of the Grt-Cpx thermometer between the calibrations of Ellis and Green (1979) and Sengupta et al. (1989) was observed. The wide array of computed garnet-biotite temperatures is a function of the cooling history of the sample.

Fluid composition of charnockites can be calculated from the model buffering reactions of 2Tr = 4Di +3En + 2Qtz +2H_2O and 2Ann + 6Qtz = 3Fs + 3San + 2H_2O (Lamb and Valley 1988). The thermodynamic database of Holland and Powell (1998) was used together with activity model for a_{Tr} in Ca-amphiboles of Holland and Blundy (1994). The activity of anorthite was calculated after Holland and Powell (1992), while a_{San} in K-feldspar and a_{En} and a_{Fs} in Opx was obtained following Holland and Powell (1996). The calculated a_{H2O} is in the range of 0.05-0.09. These values indicate a low activity of water during peak metamorphism.

CONSTRUCTION OF FLUID SATURATED P-T GRIDS

An activity-corrected petrogenetic grid was calculated for the chemical system CaO-K_2O-FeO-MgO-Al_2O_3-SiO_2-H_2O (CKFMASH), using the phases Grt, Pl, Kfs, Cpx, Opx, Bt, Hbl and Qtz (Fig.2.6)(see abbreviations for mineral activities). They were calculated using the PeRpLeX software of Connolly (1990). The diagram was constructed using the X_{H2O} = 0.1, which corresponds to the calculated water activity of 0.05-0.09 (Holland and Powell 1991, 1998).

All possible reactions occurring in garnet-biotite-clinopyroxene gneiss and charnockites are shown here with the aim of unraveling the PT conditions of the area. On the basis of observed textural relationships in the rocks, a PT estimate of around 850-910^{o}C and 7.5-9-0 kbars can be calculated (shaded area). The melting curve of the system Qtz-Ab-Or-H_2O-

CO_2 for X_{H2O} = 0.1 was added to the diagram according to the experiments of Ebadi and Johannes (1991) and Johannes and Holtz (1996). The estimated PT conditions from the petrogenetic grid are in agreement with PT estimates from the Cpx-Opx/GADS ion-exchange thermobarometry.

The results of thermobarometry of our study compare well with the PT estimates of other areas of the HC. Schumacher and Faulhaber (1994) estimated the P-T condition of the Eastern, North-eastern and South-eastern part of the HC at 760-830^{o}C and 9-10 kbar. Sandiford et al. (1988) used Gt-Cpx and Gt-Opx thermometry to illustrate the minimum temperature of metamorphism to be 670-730^{o}C. They noted that the actual peak metamorphism could easily be much higher. Kriegsman (1993) obtained peak equilibrium temperatures for sapphirine-bearing granulites in HC at 830^{o}C and 9 kbar using petrogenetic grids. Schenk et al. (1988) derived from two-pyroxene thermometry in the HC a maximum temperature of 900^{o}C. Voll et al. (1994) estimated the peak temperatures of metamorphism between 850-900^{o}C by using revised two-feldspar thermometry.

INTERDIFFUSION OF ELEMENTS DURING SLOW COOLING

The recent acquisition of diffusion coefficients for interdiffusion of Fe-Mg in garnet, biotite and pyroxene permits to quantify the effect of diffusion during slow cooling of rocks. A number of experimental values for interdiffusion of Fe and Mg in garnet have been published so far (e.g. Cygan and Lasaga 1985; Chakraborthi and Ganguly 1992 Ganguly et al. 1998). Diffusion coefficients determined from the most recent experiments by Ganguly et al. (1998) are consistent with high-temperature systems and were used in our calculations.

The Fe-Mg interdiffusion rates of biotite, pyroxene and garnet are quite different. The diffusion coefficients of pyroxene, garnet and biotite differ by three orders of magnitude at 850^{o}C, and the diffusion of Ca and Mg in pyroxene is even slower by over 2 orders of magnitude (Fig. 2.7). Similar inter-diffusion rates of Fe and Mg have been observed in pyroxenes and garnets (Ganguly and Tazzoli 1994; Ghose and Ganguly 1982), while biotite has much faster Fe-Mg interdiffusion. Minerals with relatively fast diffusion coefficients, like biotite, and to some degree, garnet and Cpx, will partially re-equilibrate

during cooling from granulite and amphibolite conditions. Therefore, one cannot expect to obtain the peak temperature from both garnet-clinopyroxene and garnet-biotite thermometry in granulite terranes. Hence, not surprisingly, these thermometers (e.g. Ellis and Green 1979; Sengupta et al. 1989; Dasgupta et al. 1991), yield temperatures that are 50-150^{o}C lower than two-pyroxene thermometer for Rupaha granulites. These reset temperatures are '*apparent temperatures*' (Spear 1991; Spear and Florence 1992; Spear and Parrish 1996), since they correspond to neither closure temperature nor equilibrium peak temperature. Similar observation has been reported from the ultra-high temperature (UHT) terranes (~950-1000^{o}C) of Enderby Land, which show the Grt-Cpx temperature of only 720^{o}C (Ellis and Green 1985).

In summary, the two-pyroxene thermometer most likely records peak or near peak temperatures at Rupaha (875 ± 4^{o}C), while garnet (core)-biotite (820 ± 20^{o}C), Grt (rim)-Bt (776 ± 40^{o}C) and Grt (rim)-Cpx (734 ± 10^{o}C) documents slow cooling of the terrane. In the following chapters, we will retrieve information for the cooling history based on the Fe-Mg profiles in garnet.

COOLING RATES FROM GARNET PROFILES

The peculiarity of the Fe-Mg profile in garnet is that it is homogeneously reset throughout most of the crystal, with minor Fe increases and Mg decreases at the rim (Fig. 2.3b). This indicates a complete resetting of the garnet during an initial protracted cooling event, which was followed by a faster cooling, which resulted in the small Fe-Mg zoning at the rim.

The composition of the Fe-Mg minerals at peak pressure and temperature has to be calculated from thermodynamic and mass balance equations, since the garnet as well as biotite and clinopyroxene in the matrix changed their Fe/Mg composition throughout in the first cooling step. This was accomplished by using the modal abundances of garnet, biotite and clinopyroxene to calculate the bulk Fe-Mg of the rock. The equilibrium equations between the garnet, biotite and clinopyroxene were solved for Fe-Mg using this bulk composition at 875^{o}C and 9kbar. This was achieved by simultaneously solving the mass balance equation for Fe and Mg and the mass action equations describing Fe-Mg

exchange. For these calculations it was assumed that no net transfer reaction occurred during cooling. This assumption is supported by fact that no retrograde growth of any high temperature phases can be observed in the studied sample. Modal mineralogy of the rock and the calculated Fe and Mg values of garnet at 875^{o}C and 9 kbar are given in Table 2.3 and Table 2.4, respectively.

The diffusion model was set up based on the observed mineral zoning. During the first stage of cooling garnets are homogeneously changed, while during the second stage only garnet adjacent to biotite show appreciable zoning. Hence the first cooling step was modeled using 'bulk' diffusion model, assuming grain boundary diffusion is fast compared to that of volume diffusion in garnet (e.g. Joesten 1991; Eiler et al. 1992, 1995). In that case, diffusional fluxes should be balanced in representative volumetric elements, which are large compared to individual grains. Nevertheless, clinopyroxene occurs only in small quantities, therefore the diffusive fluxes have been balanced only between garnet and biotite. During the second cooling period diffusion along grain boundaries was limited, so that garnet zoning only developed where biotite contacted and shared grain boundaries. For this case we assume a model, which has a binary interdiffusion between garnet and adjacent biotite grains. For a further discussion of diffusive exchange modeling and the mathematical treatments see Dodson 1973; Lasaga 1983; Lindström et al. 1991; Eiler et al. 1992; Spear and Florence 1992; Florence and Spear 1995; Spear and Parrish 1996 and Weyer et al. 1999. We used the program Gibbs (Spear and Peacock 1990; Spear and Florence 1992; Florence and Spear 1995) to solve the resulting differential equations, mass action and flux balance equations.

The diameter of garnet used here is 668 μm. Both garnet and biotite are assumed to be homogeneous at starting temperatures (875^{o}C). Significant zoning is predicted for garnets for cooling rates in excess of 1^{o}C/Ma. Hence a maximum cooling of 1^{o}C/Ma is estimated in the first step. During the second step, we have calculated the zoning profiles for linear cooling rates of 100, 50, 30, 20, 15, and 1^{o}C/Ma for the starting temperature of 820^{o}C. The starting temperature is obtained from apparent garnet (core)-biotite geothermometry. The zoning patterns calculated for the constant cooling rates is shown for these five cooling rates in Fig 2.8, along with the microprobe data. The calculated zoning profile for a cooling rate of 30^{o}C/Ma is in excellent agreement with measured zoning profiles of garnet

at Rupaha. A consistent cooling rate is obtained over the temperature interval from 820^{o}C to 500^{o}C. However, X_{Mg} profile developed at the outermost rim (7-10 μm), indicated that the cooling rate has decreased, slightly probably at the temperatures below 650^{o}C. The resulting cooling rate can be estimated around 15^{o}C/Ma (Fig. 2.8).

DISCUSSION AND CONCLUSIONS

Ca-Fe-Mg exchange thermobarometry of co-existing Opx-Cpx and Grt-Cpx-Pl.Qtz is consistent with calculated PT phase diagrams for the rocks of the Rupaha area. They indicated that peak metamorphism occurred at 875 ± 20^{o}C and pressures of 9.0 ± 0.1 kbar. Water activity is low <0.1, as inferred from the charnockites. Fe-Mg exchange thermometry of Grt(core)-Bt resulted in 820 ± 20^{o}C. The garnet-biotite exchange temperatures are interpreted to represent apparent temperatures due to slow cooling.

The experimental studies on Opx-Cpx thermometry are primarily designed on the transfer of Ca-Mg components between co-existing Opx and Cpx (Lindsley et al. 1981; Kretz 1982 Carlson and Lindsley 1988). Brey and Köhler (1990) later used the Opx-Cpx thermometry in the account of Ca-Fe-Mg exchange. The results of Opx-Cpx geothermometry from all three methods were nearly identical to each other. The Ca-Mg interdiffusion of pyroxene is several orders lower than that of Fe-Mg diffusion in either garnet or pyroxenes (Fig. 2.7). Hence, one can speculate that the effect on Fe-Mg exchange is negligible when compared to the Ca-Mg exchange on pyroxene thermometry calculations. This is further supported by the observation that no retrograde zoning is present in pyroxene or garnet with respect to Ca. Therefore, we propose that the thermometer most likely to preserve peak metamorphic temperature is the Opx-Cpx thermometer.

Our insight for recovering of near-peak cooling history is very useful, since it is possible to refine the initial cooling of granulites from the Fe/Mg diffusion, which is an especially sensitive monitor of initial cooling at high temperatures. Results of diffusion modeling of Fe-Mg exchange between garnet, clinopyroxene and biotite suggest that the HC of Sri Lanka has undergone at least three cooling stages. The U-Pb dating from metamorphic zircons from syntectonic granitoids yields an age of 608 ± 3Ma, which is interpreted as the period of peak metamorphic event. The first cooling had occurred at a maximum cooling

rate of 1°C/Ma in the first 55 Ma starting at 875°C and 9kbar. The slow cooling rate is probably due to a prolonged crustal residence time at the beginning of cooling until the temperature of 820°C. In the second step, cooling continues much faster at a rate of ~30°C/Ma until the temperature decreases below the 600-650°C. This may be related to rapid tectonic uplift of neighbouring Gondwana fragments during the Ordovician period. However, the third cooling rate can also be accounted because the measured zoning profile shows the slight deviation from the calculated zoning profile for 30°C/Ma at the outermost garnet rim (Fig 2.8). This can be tentatively assumed to be around 15°C/Ma, which may perhaps continue until the garnet-biotite Fe-Mg exchange closed. The Rb-Sr biotite ages of 439 ± 10 Ma (Hölzl et al. 1991), which is believed to record the time at temperatures around 300 ± 30°C (Spear 1993), indicates the final cooling during the uplift of the basement.

Some radiometric data available for Sri Lankan crystalline rocks provide a useful comparison with our results (Fig. 2.9). Hölzl et al. (1991) have tentatively constructed a two stage cooling history from Sm-Nd garnet ages and Rb-Sr/whole rock biotite ages from the rocks of the HC. The cooling rate of 2 to 3°C/Ma was determined from the garnet dating followed by a significantly higher rate of around 10 to 25°C/Ma from biotite ages. These results are not in agreement with the conclusions of our results, especially the first step of cooling. This discrepancy has occurred probably because they derived the cooling rates assuming the blocking temperature of garnet at 800°C. Mezger et al. (1992) reported that the closure temperature for Sm-Nd exchange in garnet would be about 600°C, which is well below the temperature (~800°C) used to calculate the cooling rates by Hölzl et al. (1991). This suggests that the first stage of cooling inferred from Sm-Nd garnet ages is misleading. The second step in the cooling history is in relatively good agreement with our findings. However, taking into account the few radiogenic ages and larger errors, cooling rates determined from geochronology may not be correctly representing the cooling history of the Sri Lankan granulites.

REFERENCES

Amstrong JT (1988) Quantitative analyses of silicate and oxide minerals: comparisions of Monte Carlo, ZAF and Phi-rho-z procedures. In: Microbeam analysis-1988 (*Newbury DE* ed). San Francisco Press, San Francisco, 239-246

Amstrong JT (1989). CITZAF: combined ZAF and phi-rho (Z) electron beam correction programs. California Institute of Technology, Pasadena, CA

Bhattacharya A, Mohanty L, Maji A, Sen SK, Raith M (1992) Non-ideal mixing in the phlogopite-annite binary: Constraints from experimental data on Mg-Fe partitioning and a reformulation of the garnet-biotite geothermometer. Contrib. Mineral. Petrol. 111: 87-93

Brady JB, McCallister RH (1983) Diffusion data for clinopyroxenes from homogenisation and self-diffusion experiments. Am. Mineral. 68: 95-105

Brey GP, Köhler T (1990) Geothermobarometry in four-phase Lherzolites II. New thermobarometers and practical assessment of existing thermobarometers. J. Petrol. 31: 1353-1378

Burton KW, O'Nions RK (1990) The timescale and mechanism of granulite formation at Kurunegala, Sri Lanka. Contrib. Mineral. Petrol. 106: 66-89

Carlson WD, Lindsley DH (1988) Thermometry of pyroxenes on the join $Mg_2Si_2O_6$-$CaMgSi_2O_6$. Am. Mineral. 73: 242-252

Chakraborthi S, Ganguly J (1992) Cation diffusion in aluminosilicate garnets: experimental determination in spessartine-almandine diffusion couples, evaluation of effective binary diffusion coefficients, and applications. Contrib. Mineral. Petrol. 111: 74-86

Connolly JAD (1990) Multivariate phase diagrams: an algorithm based on generalized thermodynamics. Am. J. Sci. 290: 666-718

*Cooray PG (*1994) The Precambrian of Sri Lanka: a historic review. Precam. Res. 66: 3-18

Cyan RT, Lasaga AC (1985) Self-diffusion of magnesium in garnet at 750-900^{o}C. Am. J. Sci. 285: 328-350

Dasgupta S, Sengupta Pulak, Guha D, Fukuoka M (1991) A refined garnet-biotite Fe-Mg exchange geothermometer and its application in amphibolites and granulites. Contrib. Mineral. Petrol. 109: 130-137

*Dodson MH (*1973) Closure temperature in cooling geochronological and petrological systems. Contrib. Mineral. Petrol. 40: 259-274

Ebadi A, Johannes W (1991) Beginning of melting and composition of first melts in the system Qtz-Ab-Or-H_2O-CO_2. Contrib. Mineral. Petrol. 106: 286-295

Eckert JOJ, Newton RC, Kleppa OJ (1991) The ΔH of reaction and recalibration of garnet-pyroxene-plagioclase-quartz geobarometers in the CMAS system by solution calorimetry. Am. Mineral. 76:148-160

Eiler JM, Baumgartner LP, Valley JW (1992) Intercrystalline stable isotope diffusion: a fast grain boundary model. Contrib. Mineral. Petrol. 112: 534-557

Eiler JM, Valley JW, Graham CM, Baumgartner LP (1995) The oxygen isotope anatomy of a slowly cooled metamorphic rock. Am. Mineral. 80: 757-764

Ellis DJ, Green EH (1979) An experimental study of the effect of Ca upon garnet-clinopyroxene Fe-Mg Exchange equilibria. Contrib. Mineral. Petrol. 71:13-22

Ellis DJ, Green EH (1985) Garnet-forming reactions in mafic granulites from Enderby Land, Antarctica-implication for geothermometry and geobarometry. J. Petrol. 26: 633-662

Essene EJ (1989). The current status of thermobarometry in metamorphic rocks In evolution of metamorphic belts. (*Daly JS, Cliff RA, Yardley BWD eds).* Geol. Soc. London. Sp. Publ. 43: 1-44

Ferry JM, Spear FS (1978) Experimental calibration of the partitioning of Fe and Mg between biotite and garnet. Contrib. Mineral. Petrol. 66:113-117

Florence FP, Spear FS (1995) Intergranuler diffusion kinetics of Fe and Mg during retrograde metamorphism of a pelitic gneiss from the Adirondack Mountains Earth Planet Sci. Lett. 134: 329-340

Ganguly J, Saxena SK (1984). Mixing properties of aluminosilicate garnets: constraints from natural and experimental data, and applications to geothermobarometry, Am. Mineral. 69: 88-97

Ganguly J, Tazzoli V (1994) Fe^{2+}-Mg interdiffusion in orthopyroxene: Retrieval from the data on intracrystalline exchange reaction. Am. Mineral. 79: 930-937

*Ganguly J, Cheng W, Chakraborthi S (*1998) Cation diffusion in aluminosilicate garnets: experimental determination in pyrope-almandine diffusion couples. Contrib. Mineral. Petrol. 131:171-180

*Ghose S, Ganguly J (*1982) Mg-Fe order disorder in ferromagnesian silicates. In: Advances in physical geochemistry 2 *(Saxena SK* ed), Springer Verlag New York, 3-100

Giletti BJ (1986) Diffusion effects on oxygen isotope temperatures of slowly cooled igneous and metamorphic rocks Earth Planet Sci. Lett. 77: 218-228

Hodges KV, Spear FS (1982). Geothermometry, geobarometry and Al_2SiO_5 triple point at Mt. Moosilauke, New Hampshire. Am. Mineral. 67: 1118-1134

Holland TJB, Blundy J (1994) Non-ideal interactions in calcic amphiboles and their bearing on amphibole-plagioclase thermometry. Contrib. Mineral. Petrol. 116: 433-447

Holland TJB, Powell R (1991). A compensated-Redlich-Kwong (CORK) euation for volumes and fugacities of CO_2 and H_2O in the Range 1 bar to 50Kbar and 100-1600^oC. Contrib. Mineral. Petrol. 109: 265-273

Holland TJB, Powell R (1992) Plagioclase feldspars: activity-composition relations based upon Darken's quadratic formalism and Landau theory. Am. Mineral. 77: 53-61

Holland TJB, Powell R (1996) Thermodynamics of order-disorder in minerals:II. Symmetric formalism applied to solid solutions. Am. Mineral. 81:1425-1437

*Holland TJB, Powell R (*1998) An internally consistent thermodynamic data set for phases of petrological interest. J. metamorphic Geol. 16: 309-343

*Hölzl S, Köhler H, Kröner A, Jaeckel P, Liew TC (*1991) Chronology of Sri Lankan basement. In: The Crystalline crust of Sri Lanka, Part 1, summary of research of the German-Sri Lankan consortium, Part 1 (*Kröner A* ed). Geol. Surv. Dep. Prof. Pap. 5: 237-257

Hölzl S, Hofmann AW, Todt W, Köhler (1994).U-Pb geochronology of the Sri Lankan basement. Precam. Res. 66: 123-149

Inderas A, Martignole J (1985). Biotite-garnet geothermometry in the granulite facies: the influence of Ti and Al in biotite. Am. Mineral. 70: 272-278

Joesten R (1991) Grain boundary diffusion boundary kinetics in silicate and oxide minerals. In: Diffusion, atomic ordering and mass transport; selected topics in geochemistry (*Ganguly J* ed) Adv. Phys. Geochem. 8, Springer Verlag, 345-395

Johannes W, Holtz F (1996) Petrogenesis and experimental petrology of granitic rocks, Springer Verlag, Heidelberg, pp337

Kleeman U, Reinhardt J (1994). Garnet-biotite thermometry revisited: The effect of Al^{VI} and Ti in biotite. Eu. J. Mineral 6: 925-941

Kretz R (1982). Transfer and exchange equilibria in a portion of the pyroxene quadrilateral as deduced from natural and experimental data. Geochim. Cosmochim. Acta 46: 411-421

Kretz R (1983) Symbols for rock forming minerals. Am Mineral 68: 277-279

Kriegsman LM (1993) Geodynamic evolution of the Pan-African lower crust in Sri Lanka, PhD Thesis, University of Utrecht, The Nederlands, pp207

Kröner A (1991) African linkage of Precambrian Sri Lanka, Geol. Rundschau 80: 429-440

Kröner A, Cooray PG, Vithanage PW (1991) Lithotectonic sub divisions of Precambrian basement of Sri Lanka, In: The Crystalline crust of Sri Lanka, Summary of research of the German-Sri Lankan consortium, Part 1 (*Kröner A* ed). Geol. Surv. Dep. Prof. Pap. 5: 5-21

Kröner A, Williams AS (1993) Age of metamorphism of high-grade rocks of Sri Lanka, J. Geol. 101: 521-531

Lamb WM, Valley JW (1988) Granulite facies amphibole and biotite equilibria, and calculated peak-metamorphic water activities. Contrib. Mineral. Petrol. 100: 349-360

Lasaga AC (1983) Geospeedometry: An extension of geothermometry. In: Kinetics and equilibrium in mineral reactions (*Saxena SK ed*). Adv. Phy. Geochem. 3, Springer Verlag, 243-284

Lasaga AC, Richardson SM, Holland HD (1977). The mathematics of cation diffusion and exchange between silicate minerals during retrograde metamorphism, In: Energetics of geological process (*Saxena SK, Bhattacharji S eds*), New York, Springer Verlag, 81-114

Lindsley DH, Grover JE, Davidson PM (1981) The thermodynamics of the $Mg_2Si_2O_6$-$CaMgSi_2O_6$ join: A review and an improved model. In: Thermodynamics of minerals and melts. (*Newton RC, Novrotsky A, Wood BJ* eds) Adv. Phy. Geochem.1 Springer Verlag, 149-175

Lindström R, Viitanen M, Juhanoja J (1991) Geospeedometry of metamorphic rocks: examples in the Rantasalmi-Sulkava and Kiuruvesi areas, eastern Findland. Biotite-garnet diffusion couples. J. Metamorphic Geol. 9: 181-190

Mezger K, Essene EJ, Halliday AN (1992) Closure tempterature of the Sm-Nd system in metamorphic garnets Earth Planet. Sci. Lett. 113: 397-409

Milicenda CC, Liew TC, Hofmann AW (1994) Nd isotopic mapping of the Sri Lanka basement: update and additional constraints from Sr isotopes. Precam. Res. 66: 95-110

Pattison DRM (1994) Are reversed Fe-Mg exchange and solid solution experiments really reversed? Am. Mineral. 79: 938-950

Perchuk LL, Lavrent'eva IV (1983). Experimental investigation of exchange equilibria in the system cordierite-garnet-biotite. In: Kinetics and equilibrium in mineral reactions (*Saxena SK* ed). Adv. Phys. Geochem. 3, Springer Verlag, 199-239

Sandiford M, Powell R, Martin SF, Perera LRK (1988). Thermal and baric evolution of garnet granulites from Sri Lanka. J, Metamorphic Geol. 6: 351-364

Schenk V, Raase P, Schumacher R (1988) Very high temperatures and isobaric cooling before tectonic uplift in the Highland Series. Terra Cognita 8: 265

Schumacher R, Faulhaber S (1994) Summary and discussion of P-T estimates from garnet-pyroxene-plagioclase-quartz-bearing granulite- facies rocks from Sri Lanka. Precam. Res. 66: 295-308

Sengupta Pulak, Dasgupta S, Bhattacharya PK, Hariya Y (1989) Mixing behaviour in quaternary garnet solid solution and an extended Ellis and Green garnet-clinopyroxene geothermometer. Contrib. Mineral. Petrol. 103: 223-227

Spear FS (1991) On the interpretations of peak metamorphic temperatures in light of garnet diffusion during cooling. J. Metamorphic Geol. 9: 379-388

Spear FS (1993) Metamorphic phase equilibria and pressure-temperature-time paths Monograph series, Mineral. Soc. Am, Washinton D.C., pp799

Spear FS, Florence FP (1992) Thermobarometry in granulites: pitfalls and new approaches. Precam. Res. 55: 209-241

*Spear FS, Parrish RR (*1996) Petrology and cooling rates of the Valhalla Complex, British Columbia, Canada. J. Petrol. 37:733-765

Spear FS, Peacock SM (1990) Metamorphic P-T-t paths: Program manual and computer exercises for the calculation of metamorphic phase equilibria, pressure-temperature-time paths and thermal evolution of orogenic belts. Geol. Soc. Am. Short Course, Dallas, Texas, pp188

Voll G, Evangelakakis C, Kroll H (1994) Revised two-feldspar geothermometry applied to Sri Lankan feldspars. Precam. Res. 66: 351-377

Weyer S, Jarick J, Mezger K (1999) Quantitative-temperature-time information from retrograde diffusion zoning in garnet: constraints for the P-T-t history of the central Black Forest, Germany. J. Metamorphic Geol. 17: 449-461

Table 1.1 Chemistry of mineral assemblages used to calculate the thermobarometry at Rupaha

Assemblage	Grt-Bt assemblages				Grt-Cpx assemblages		Opx-Cpx assemblages		Grt-Cpx-Pl-Qtz assemblages		
Sample no.	RU 9708				RU 9708		RU 9817		RU 9708A		
Mineral	Grt	Grt	Bt at	Bt	Grt	Cpx	Opx	Cpx	Grt	Pl	Cpx
	rim	core	Grt contact	matrix	rim	rim	core	core	core	matrix	core
No. of Oxygens	12	12	11	11	12	6	6	6	12	8	6
SiO_2	38.24	37.95	37.18	38.07	38.65	52.19	48.33	50.65	38.52	61.45	52.04
TiO_2	0.06	0.08	5.67	5.26	0.08	0.11	0.08	0.09	0.04	0.00	0.22
Al_2O_3	21.43	21.21	13.18	12.89	21.15	1.57	0.68	1.22	21.32	23.80	2.00
Cr_2O_3	0.05	0.06	0.10	0.00	0.10	0.00	0.05	0.05	0.05	0.05	0.06
FeO	23.61	22.98	14.63	14.35	23.30	9.52	38.03	18.44	23.50	0.05	10.20
MnO	5.91	5.81	0.05	0.14	6.25	1.00	0.89	0.38	6.27	0.00	1.23
MgO	5.48	5.66	14.12	13.55	5.44	13.54	10.66	8.45	5.59	0.02	13.14
CaO	5.92	5.96	0.21	0.16	6.05	21.39	0.87	20.75	5.99	5.57	21.09
Na_2O	0.07	0.11	0.21	0.22	0.19	0.34	0.01	0.51	0.01	8.40	0.52
BaO	nd	nd	0.31	0.24	0.00	0.00	nd	nd	nd	0.00	nd
K2O	nd	nd	9.08	8.65	0.00	0.02	nd	nd	nd	0.48	0.02
F	0.00	0.09	1.63	1.55	0.13	0.00	nd	nd	0.00	nd	nd
Cl	0.01	0.03	0.31	0.35	0.08	0.00	nd	nd	0.02	nd	nd
Total	100.78	99.94	96.66	95.43	101.43	99.68	99.61	100.55	101.30	99.83	100.51
Cations											
Si	2.97	2.97	2.66	2.73	2.99	1.96	1.97	1.96	2.98	2.74	1.95
Al	1.96	1.96	1.11	1.09	1.93	0.07	0.03	0.06	1.94	1.25	0.09
Ti	0.00	0.01	0.31	0.28	0	0.00	0	0	0	0	0.01
Cr	0	0	0.01	0	0.01	0.00	0	0	0	0	0
Fe	1.53	1.50	0.88	0.86	1.51	0.30	1.29	0.60	1.52	0	0.32
Mg	0.64	0.66	1.51	1.45	0.63	0.76	0.65	0.49	0.64	0	0.73
Mn	0.39	0.39	0.01	0.01	0.41	0.03	0.03	0.01	0.41	0	0.04
Ba	0	0	0.01	0.01	0	0.00	0	0	0	0	0
Ca	0.49	0.50	0	0.01	0.50	0.86	0.04	0.86	0.50	0.27	0.85
Na	0.01	0.02	0.03	0.03	0.03	0.03	0	0.04	0	0.73	0.04
K	0	0	0.83	0.79	0	0.00	0	0	0	0.03	0
Total Cations	8	8	7.36	7.25	8	4	4.02	4.02	8	5.01	4.02
F	0	0.02	0.37	0.35	0.03	0	0	0	0	0	0
Cl	0	0	0.04	0.04	0.01	0	0	0	0	0	0
$X_{almandine}$	0.50	0.49			0.49				0.49		
X_{pyrope}	0.21	0.22			0.21				0.21		
$X_{grossular}$	0.16	0.16			0.16				0.16		
$X_{spessartine}$	0.13	0.13			0.13				0.13		
Fe/(Fe+Mg)			0.37	0.37		0.28	0.67	0.55			0.30

Table 2.2 Results of thermobarometry estimates for granulites from the Rupaha, Sri Lanka

		Temperature (^{o}C)	Pressure (kbar)
Grt-Bt / GADS			
Dasgupta et al. (1992) and Eckert et al. (1991)			
	garnet core	774-840	7.6-8.3
		(820 ± 20	8.1 ± 0.2)
	garnet rim	685-821	6.2-8.1
		(780 ± 40	7.6 ± 0.6)
Grt-Cpx / GADS			
Sengupta et al. (1989) and Eckert et al. (1991)			
		706-738	6.9-7.2
		(724 ± 10	7.1 ± 0.1)
Opx-Cpx / GADS			
Brey and Köhler (1990) and Eckert et al. (1991)			
		870-882	8.6-9.1
		(874 ± 4	8.7 ± 0.4)

Table 2.3 Modal mineralogy of Rupaha mafic granulites

Mineral		**Modal Percentage** **Radius/half length (µm) of mineral grains**
Garnet	47.8	300
Biotite	27.2	300
Plagioclase	14.6	300
Cpx	7.4	200
Quartz	3.0	300
Total	100.00	

Table 2.4 Calculated peak compositions of garnet, biotite and clinopyroxene

	Peak temperature	Apparent temperature	Reset temperature
	calculated	core	rim
	875°C	**820°C**	**685°C**
garnet			
Fe	1.503	1.528	1.605
Mg	0.670	0.645	0.479
Fe/(Fe+Mg)	0.692	0.703	0.770
Mg/(Fe+Mg)	0.308	0.297	0.230
biotite			
Fe	0.967	0.928	0.928
Mg	1.551	1.590	1.590
Fe/(Fe+Mg)	0.384	0.369	0.369
Mg/(Fe+Mg)	0.616	0.631	0.631
Cpx			
Fe	0.341	0.311	0.311
Mg	0.697	0.727	0.727
Fe/(Fe+Mg)	0.329	0.300	0.300
Mg/(Fe+Mg)	0.671	0.700	0.700

FIGURE CAPTIONS

Fig. 2.1 Simplified geological map of the area around Rupaha, Sri Lanka (after Cooray 1994; Kröner et al. 1991)

Fig. 2.2 (a). Photomicrograph showing relationship of model garnet to the rock and other phases in the sample. Inclusions of biotite in garnets evidence for early phase of biotite. (b). Photomicrograph illustrates small hornblende inclusions in orthopyroxene in two-pyroxene-bearing gneiss. Note the co-existing Opx-Cpx assemblage in the upper right corner.

Fig. 2.3 (a). Backscattered electron image of co-existing garnet-biotite in granulites at Rupaha, Sri Lanka. A chemical composition profile was run across the garnet along the drawn line A-B. (b). Profiles are showing mole fractions of almandine, pyrope, grossular and spessartine along the line depicted in Fig 2.3a. Profiles were assembled from 174 closely spaced quantitative spot analyses of garnet. Note that X_{Mg} decreases and X_{Fe} and X_{Mn} increases at the biotite contacts while no significant X_{Ca} change is observed.

Fig. 2.4 (a). Compositional map showing the Mg distribution of garnet contacting biotite, plagioclase and garnet with a resolution of 1µm (the area is as indicated in the box in Fig. 2.3a). Note that Mg decreases of Mg at the rims of garnet touching biotite.

Fig. 2.5 Summary of the results of combined ion-exchange thermobarometries of granulites at Rupaha, Sri Lanka.

Fig. 2.6 Schreinemakers grid (CKFMASH) calculated at X_{H2O}= 0.1 using the thermodynamic database of Holland and Powell (1998) (shaded area is representative of Rupaha granulites). The following reactions represent the respective numbers in the diagram: Note that reaction equations are written such at the high temperature assemblage is on the right of the ‘ = ’ sign

2 Di + En =2 Hed +En;

2 Tr = 2 Qtz + 4 Di + 3 En + $2H_2O$;

2 Ann + 6 Qtz + Grs = Alm + 3 Hed + 2 San + 2 H_2O;

San + Tr + 3 Hed + H_2O = 4 Qtz + 5 Di + 4 Ann;

3 Ann + 2An + 6 Qtz = Alm + 3 San + 2 Hed + 3 H_2O

The experimentally determined solidus curve of the system Qtz-Ab-Or-H_2O-CO_2 at X_{H2O} = 0.1 is from (Ebadi and Johannes 1991; Johannes and Holtz 1996). Abbreviations as in Kretz (1992) [Calculated activities used: *orthopyroxene*: a_{En} = 0.11, a_{Fs} = 0.39; *clinopyroxene*: a_{Di} = 0.40, a_{Hed} = 0.44; *biotite*: a_{Ann} = 0.013, a_{Phl} = 0.16; *feldspar*: a_{An} = 0.28, a_{Ab} = 0.75, a_{San} = 0.82; *garnet*: a_{Prp} = 0.017, a_{Grs} = 0.007, a_{Alm} = 0.089; *hornblende*: a_{Tr} = 0.005].

Fig. 2.7 Arrhenius plots of Fe-Mg and Ca-Mg interdiffusion coefficients used in this study: garnet (Ganguly et al. 1998), biotite (Pattison, 1994), orthopyroxene and clinopyroxene (Fe-Mg: Ganguly and Tazzoli 1994; Ghost and Ganguly 1982), clinopyroxene (Ca-Mg: Brady and McCallister 1983).

Fig. 2.8 Comparisons of geospeedometry simulations of Diff-Gibbs profiles with different cooling rates and measured Mg/(Fe+Mg) of garnets in granulites at Rupaha. The best-fit model assumed at the cooling rate of 30^{o}C/Ma (see text for more details).

Fig. 2.9 Calculated cooling paths of granulites from Sri Lanka from this study compares with the geochronological cooling rates from Hölzl et al. 1991. Peak metamorphism was estimated from U-Pb zircon ages (608 ± 3Ma) (Hölzl et al. 1991, 1994). The geochronlogical cooling paths are inferred from: (1) blocking temperatures of garnet from Sm-Nd garnet ages (561±12Ma) (Hölzl et al. 1991), (2) blocking temperatures of biotites from Rb-Sr ages (439 ± 10Ma) (Hölzl et al. 1991), (3) Rb-Sr blocking temperature of biotite (300 ± 30^{o}C) from Spear (1993).

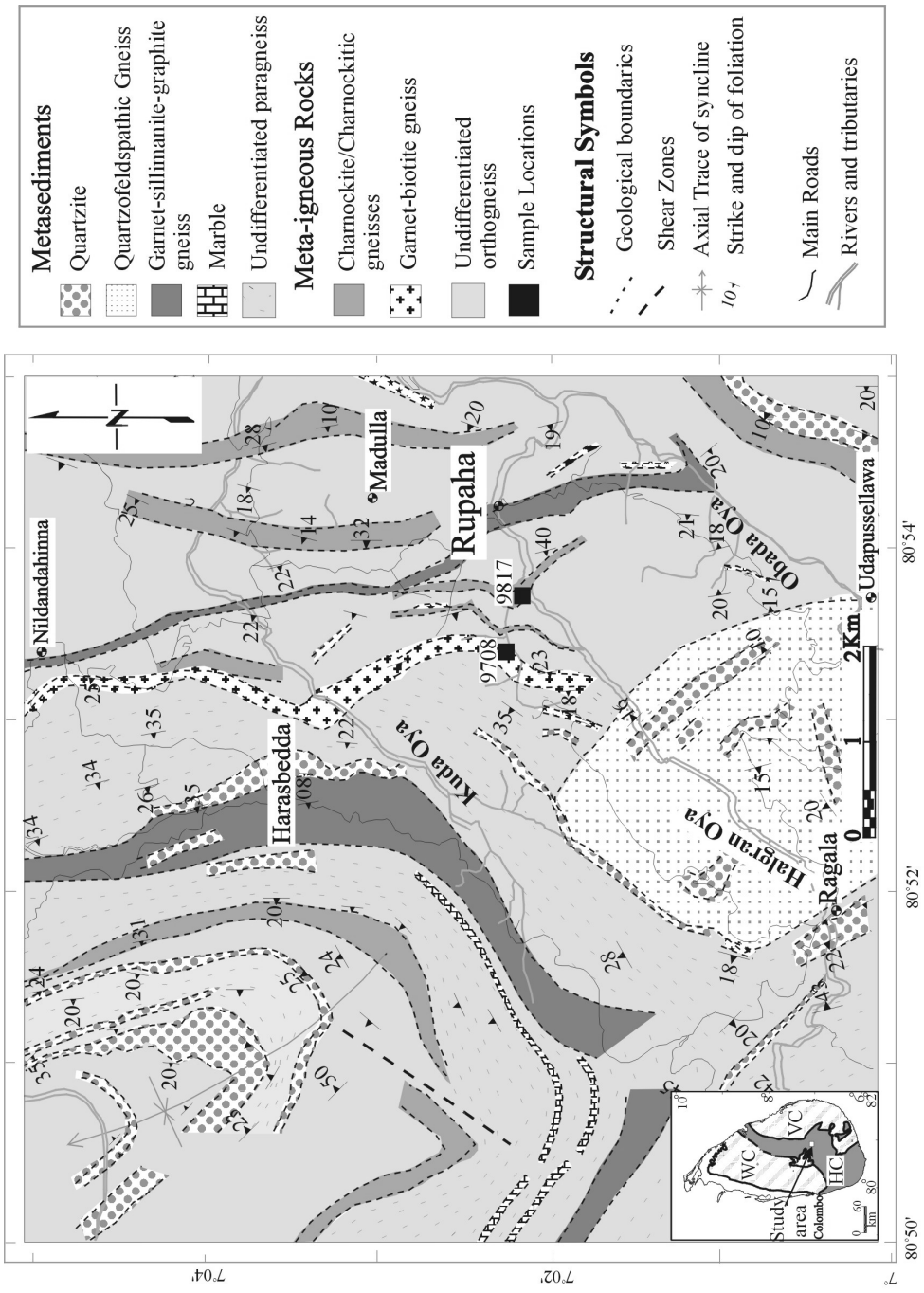
Metasediments
Quartzite
Quartzofeldspathic Gneiss
Garnet-sillimanite-graphite gneiss
Marble
Undifferentiated paragneiss
Meta-igneous Rocks
Charnockite/Charnockitic gneisses
Garnet-biotite gneiss
Undifferentiated orthogneiss
Sample Locations
Structural Symbols
Geological boundaries
Shear Zones
Axial Trace of syncline
Strike and dip of foliation
Main Roads
Rivers and tributaries
N
Nildandahinna
Madulla
Rupaha
Udapussellawa
Harasbedda
Kuda Oya
Obada Oya
Halgran Oya
Ragala
9817
9708
2Km
0
1
WC
VC
HC
Study area
Colombo
7°04'
7°02'
7°
80°50'
80°52'
80°54'

Fig. 2.1

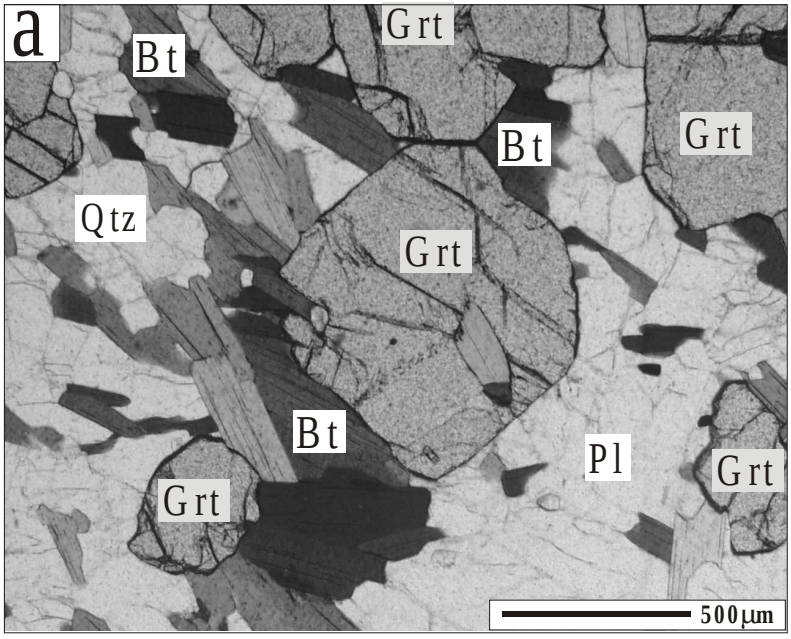
a
Grt
Bt
Bt
Grt
Qtz
Grt
Bt
Pl
Grt
Grt
500μm

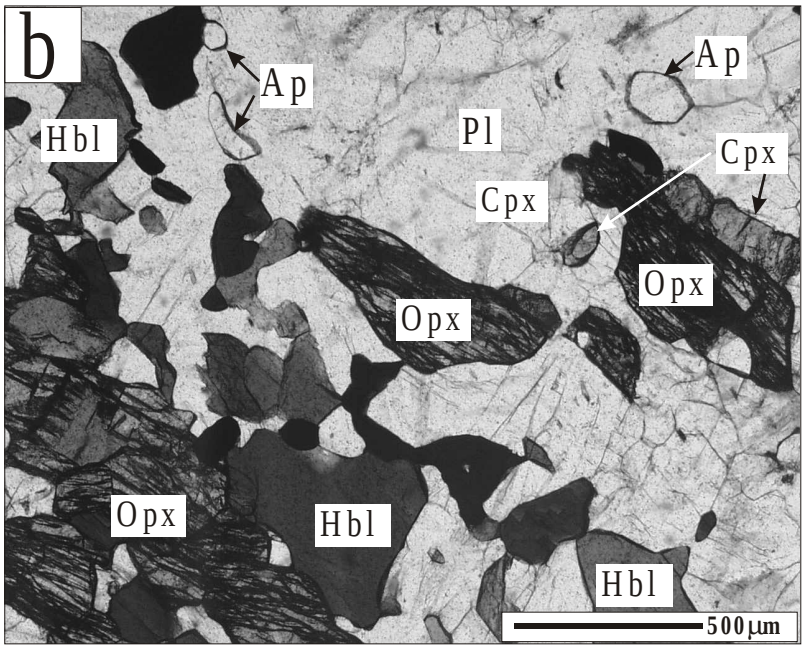
b
Ap
Ap
Hbl
Pl
Cpx
Cpx
Opx
Opx
Opx
Hbl
Hbl
500μm

Fig. 2.2

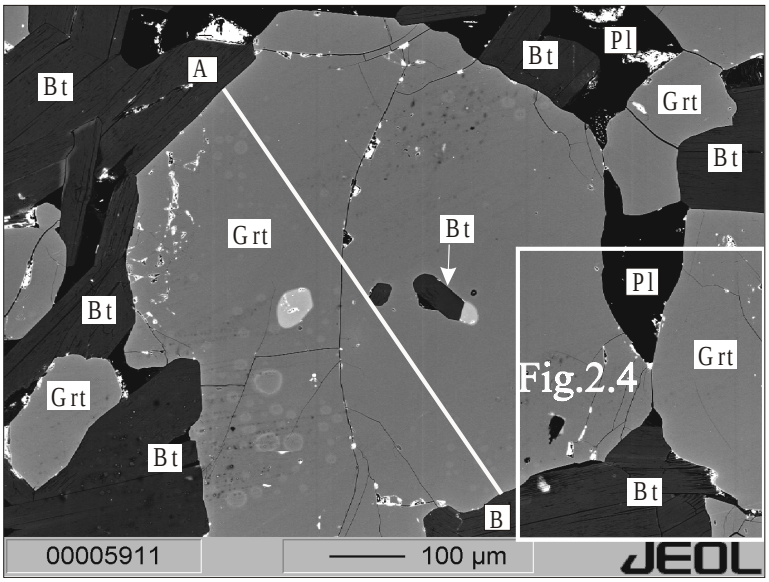

Fig.2.3a

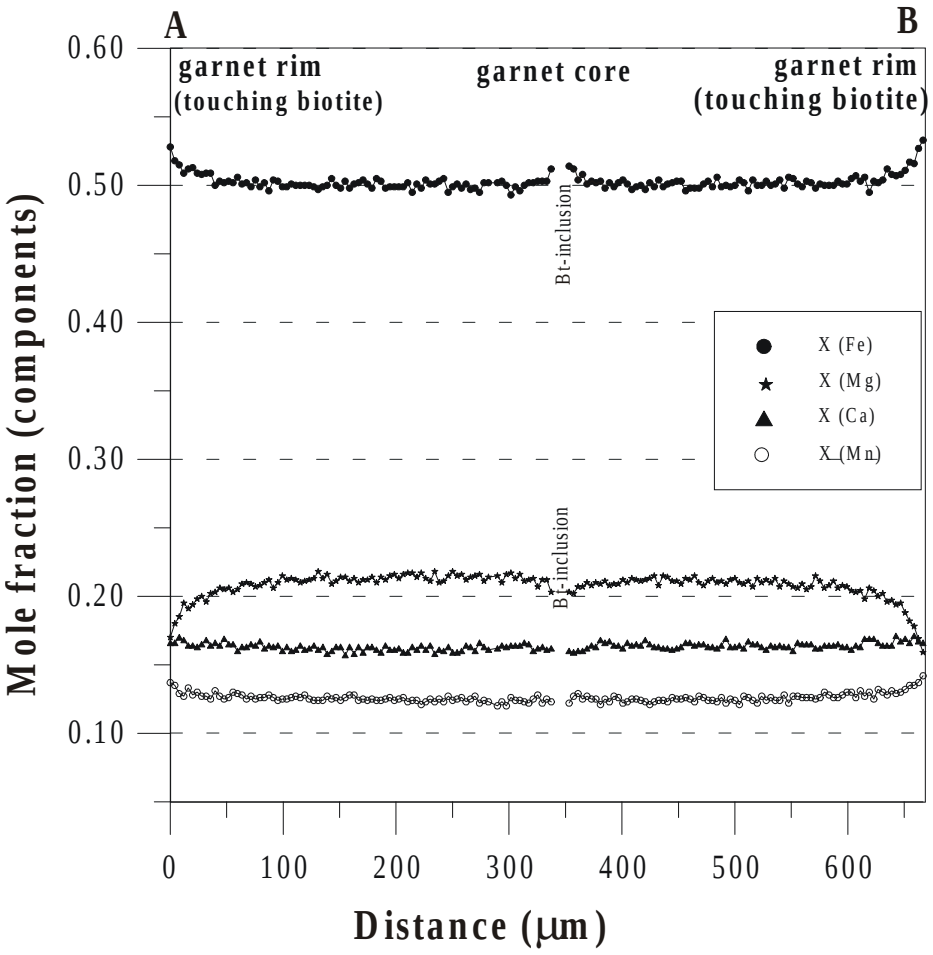

Fig. 2.3b

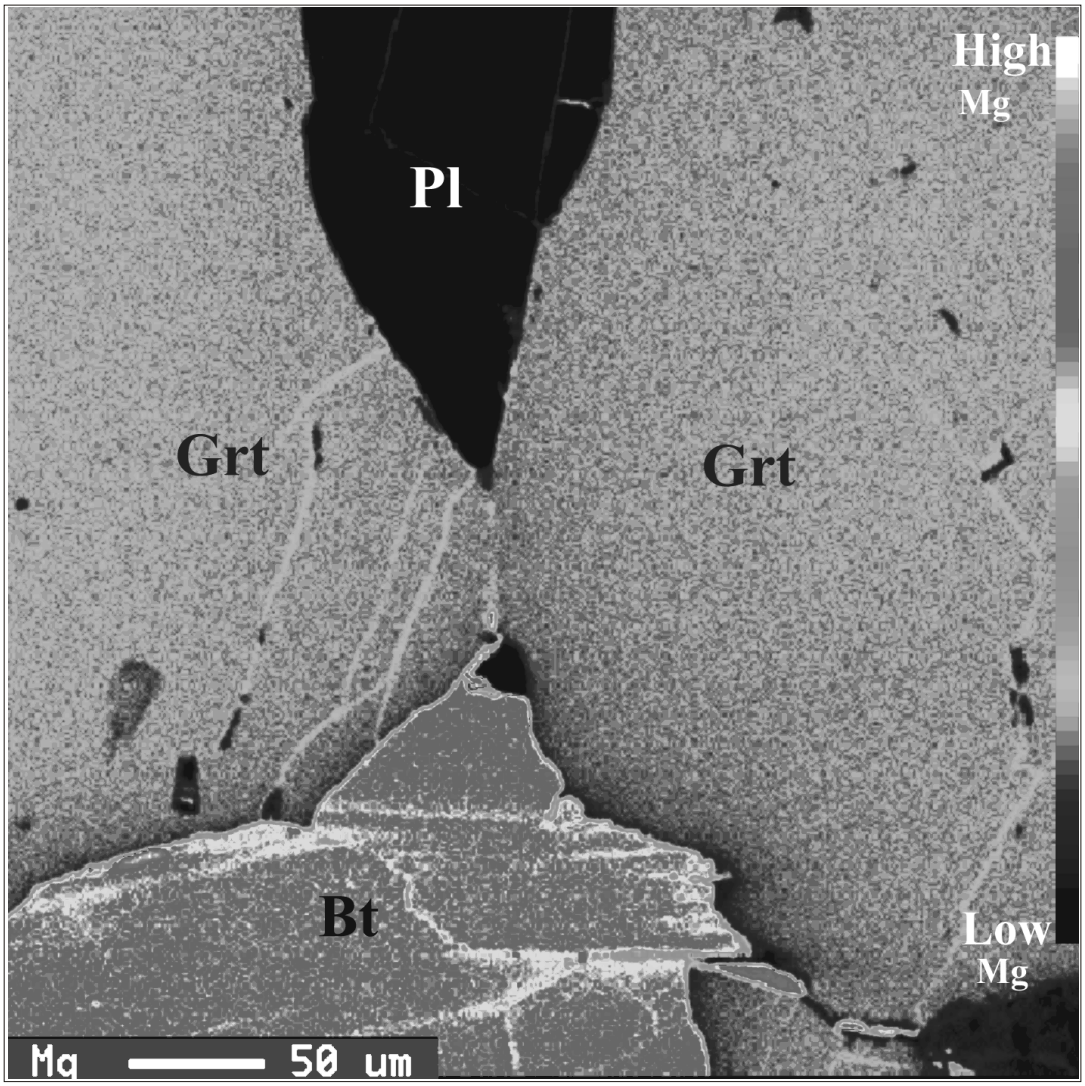

Fig. 2.4

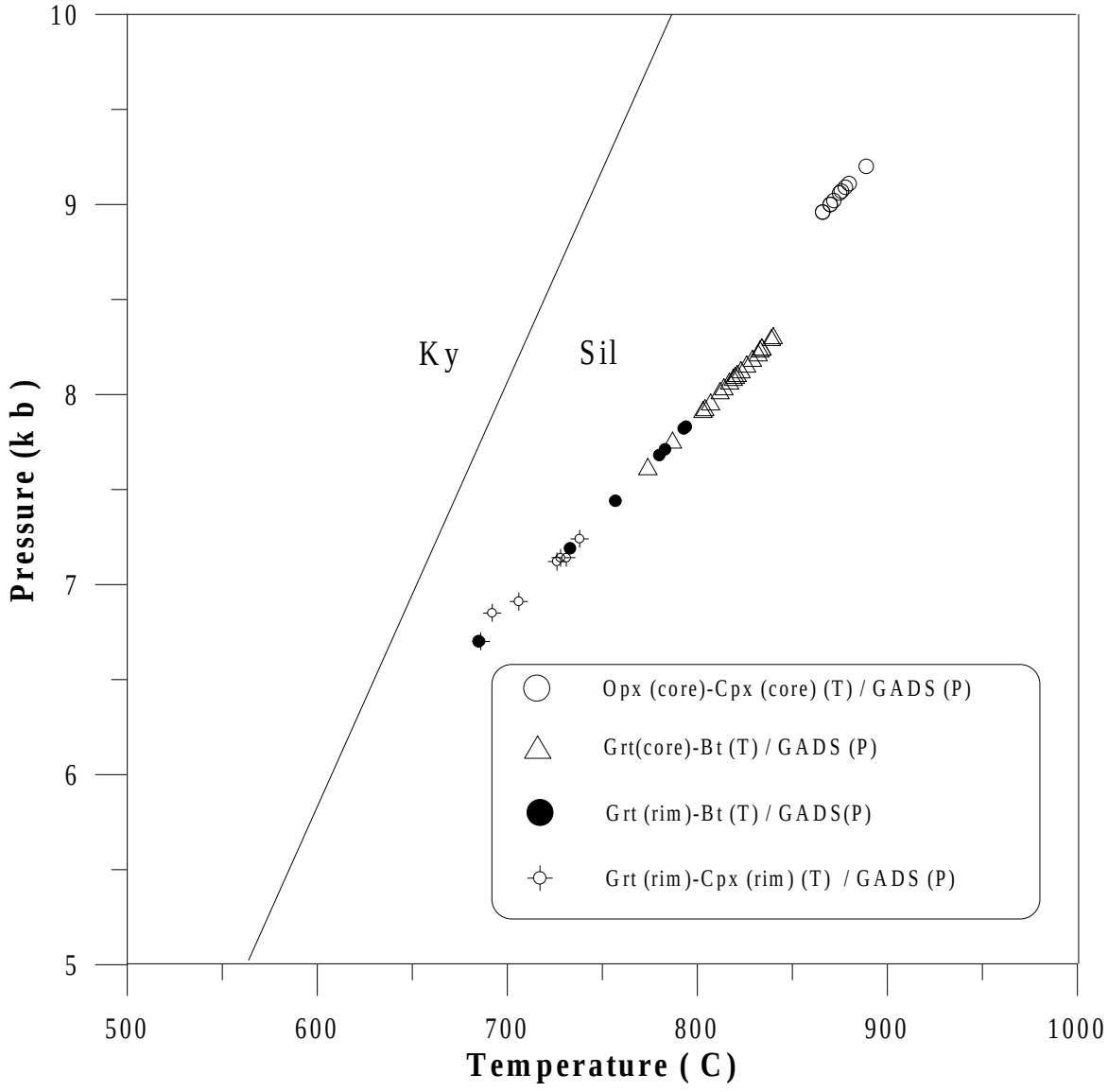
10
9
8
7
6
5
Pressure (k b)
Ky
Sil
500
600
700
800
900
1000
Temperature (C)
Opx (core)-Cpx (core) (T) / GADS (P)
Grt(core)-Bt (T) / GADS (P)
Grt (rim)-Bt (T) / GADS(P)
Grt (rim)-Cpx (rim) (T) / GADS (P)

Fig. 2.5

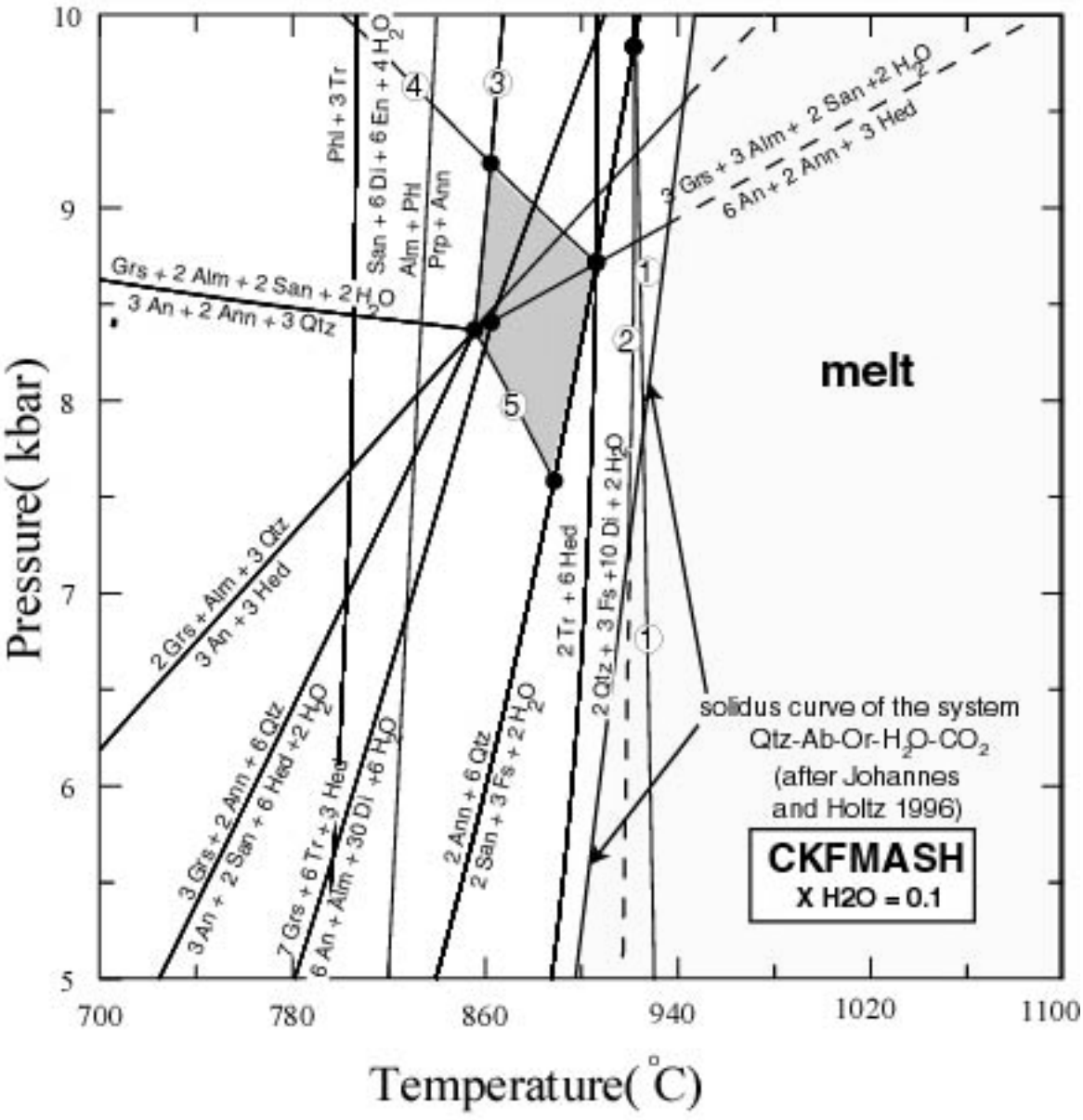
Pressure(kbar)
Temperature(°C)
10
9
8
7
6
5
700
780
860
940
1020
1100
melt
solidus curve of the system
Qtz-Ab-Or-H2O-CO2
(after Johannes
and Holtz 1996)
CKFMASH
X H2O = 0.1
Phl + 3 Tr
San + 6 Di + 6 En + 4 H2O
Alm + Phl
Prp + Ann
3 Grs + 3 Alm + 2 San +2 H2O
6 An + 2 Ann + 3 Hed
Grs + 2 Alm + 2 San + 2 H2O
3 An + 2 Ann + 3 Qtz
2 Grs + Alm + 3 Qtz
3 An + 3 Hed
3 Grs + 2 Ann + 6 Qtz
3 An + 2 San + 6 Hed +2 H2O
7 Grs + 6 Tr + 3 Hed
6 An + Alm + 30 Di +6 H2O
2 Ann + 6 Qtz
2 San + 3 Fs + 2 H2O
2 Tr + 6 Hed
2 Qtz + 3 Fs +10 Di + 2 H2O
1
2
3
4
5

Fig 2.6

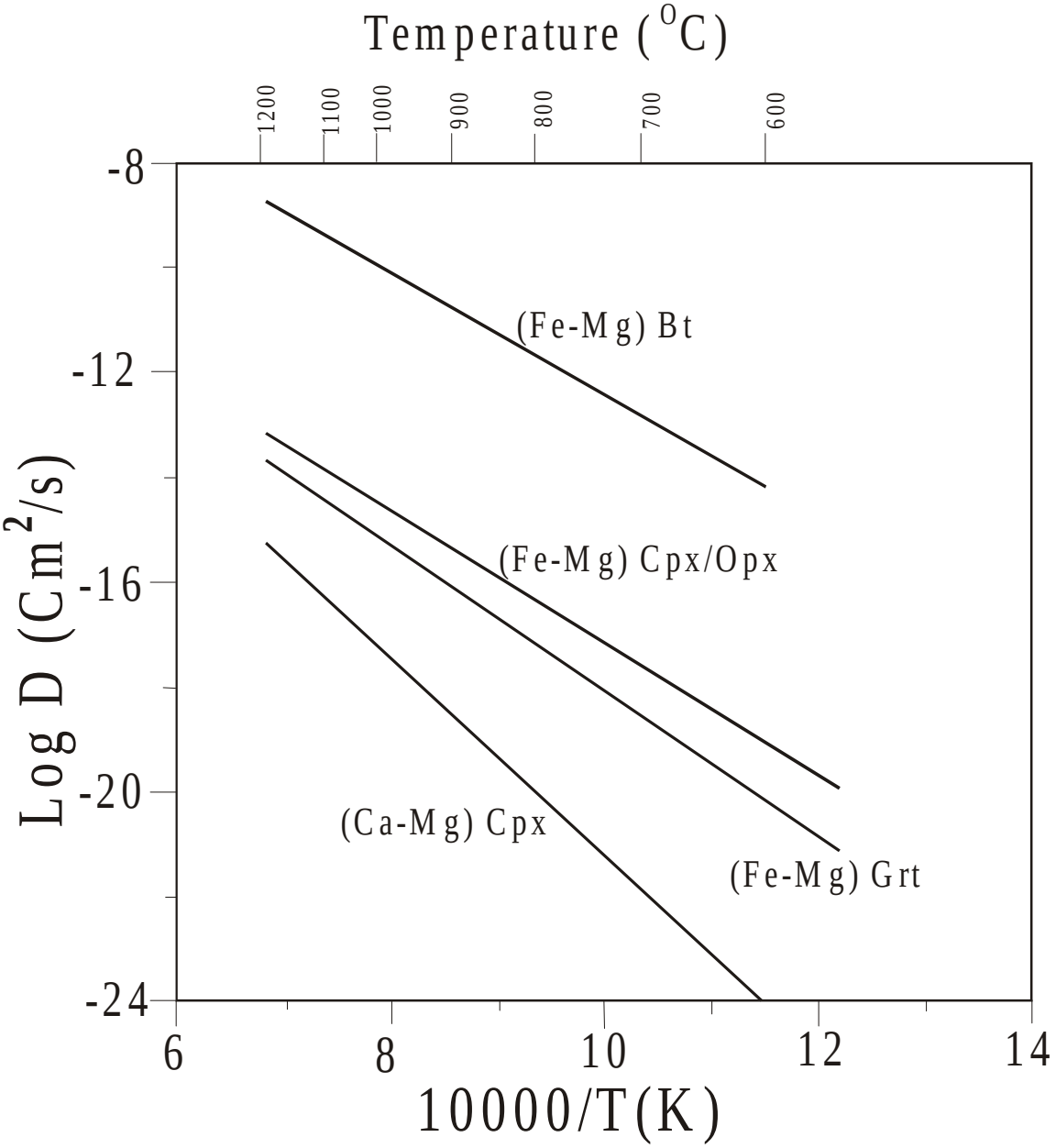
Temperature (°C)
1200
1100
1000
900
800
700
600
-8
-12
-16
-20
-24
Log D (Cm²/s)
(Fe-Mg) Bt
(Fe-Mg) Cpx/Opx
(Ca-Mg) Cpx
(Fe-Mg) Grt
6
8
10
12
14
10000/T(K)

Fig. 2.7

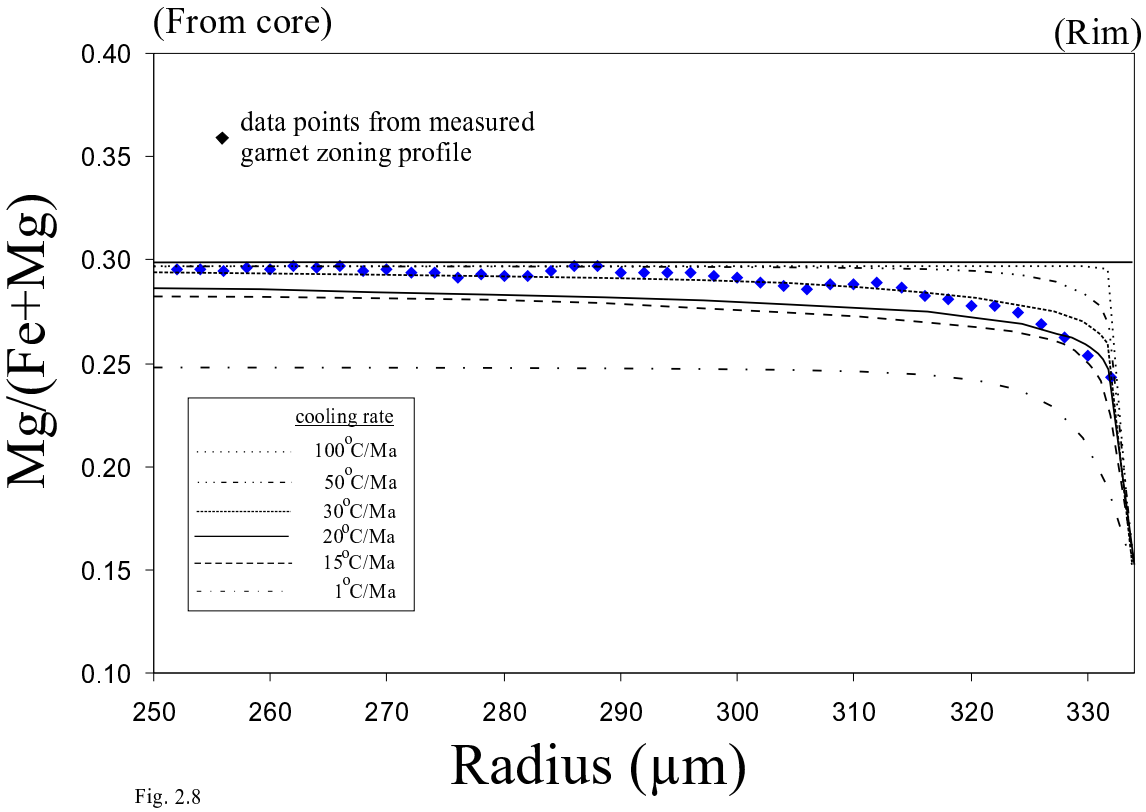
(From core)
(Rim)
data points from measured
garnet zoning profile
cooling rate
100°C/Ma
50°C/Ma
30°C/Ma
20°C/Ma
15°C/Ma
1°C/Ma
Mg/(Fe+Mg)
0.40
0.35
0.30
0.25
0.20
0.15
0.10
250
260
270
280
290
300
310
320
330
Radius (μm)

Fig. 2.8

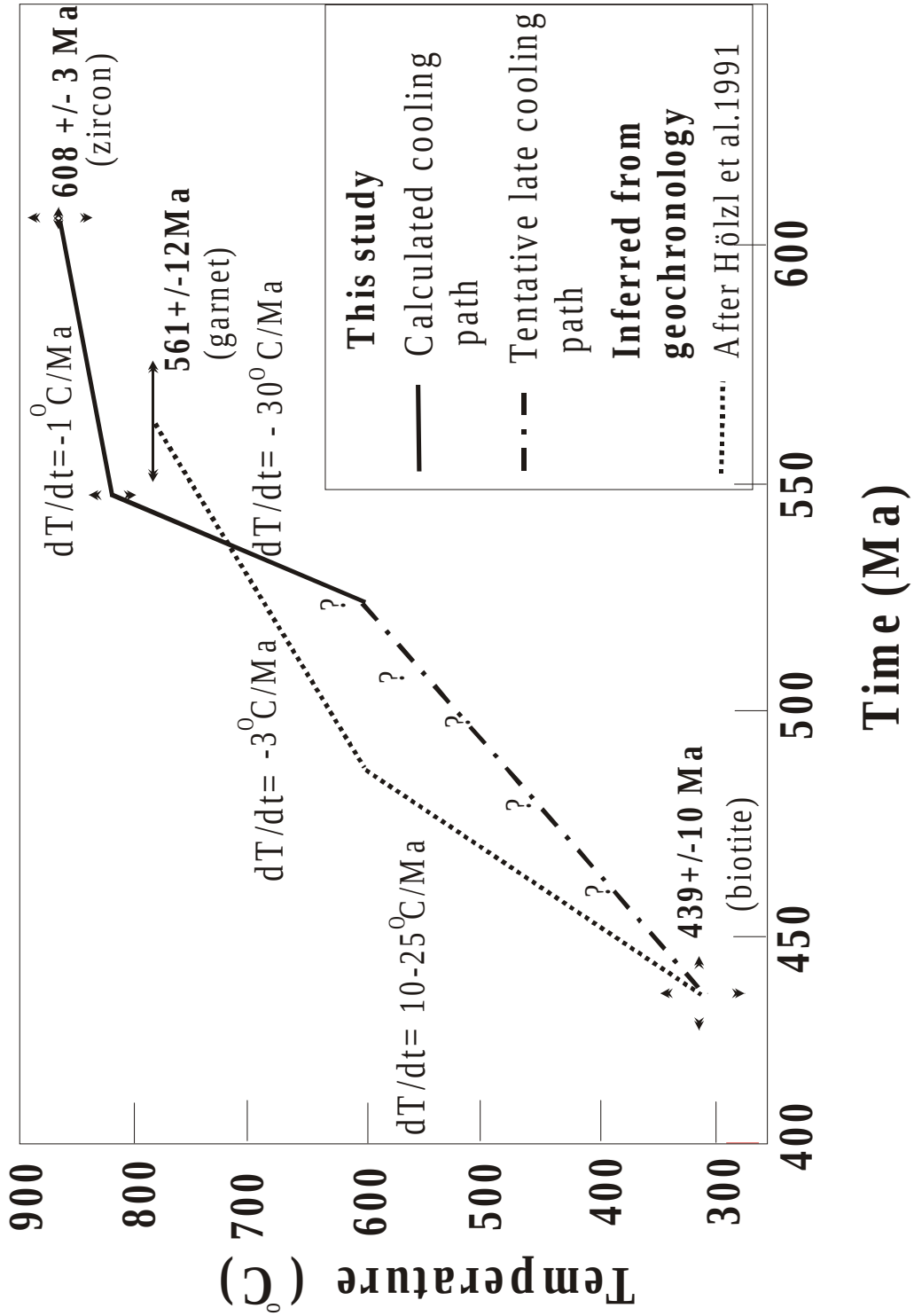
Temperature (°C)
900
800
700
600
500
400
300
400
450
500
550
600
Time (Ma)
608 +/- 3 Ma
(zircon)
561+/-12Ma
(garnet)
439+/-10 Ma
(biotite)
dT/dt=-1°C/Ma
dT/dt= - 30°C/Ma
dT/dt= -3°C/Ma
dT/dt= 10-25°C/Ma
?
?
?
?
This study
Calculated cooling path
Tentative late cooling path
Inferred from geochronology
After Hölzl et al.1991

Fig.2.9

Chapter 3

High-temperature metasomatism and retrogression of granulite facies ultramafics from the Highland Complex of Sri Lanka: Field relationships, phase equilibria and fluid fluxes

ABSTRACT

The ultramafic rocks at Rupaha, Sri Lanka were emplaced early into the Proterozoic basement and subjected to deformation and granulite facies metamorphism at 850^{o}C at 9 kbar. The results of two-pyroxene thermometry are consistent with geothermobarometric results obtained from the surrounding granulites. Structures, textures and the mineralogy of the blackwall suggest that the K-Si-metasomatism took place contemporaneous to the granulite facies metamorphism. Fluid circulating at the deep crust would result in several types of metasomatic processes. The metasomatic reaction was started by infiltration of K_2O and SiO_2 along the lithological contacts between ultramafic rocks and surrounding granulites or diffusion of these components from the surrounding granulites. As the ultramafic rock cooled together with surrounding granulites, the retrograde overprints and the carbonation and hydration textures are produced. These textures involve a partially retrogression of enstatite and forsterite to tremolite and dolomite, which formed through introduction of CaO and CO_2. The stability of tremolite + dolomite at 730–640^{o}C and 9kbar condition records a $0.40 \geq X_{CO2} \geq 0.15$ for the fluid phase.

INTRODUCTION

Ultramafic rocks found in metamorphic terranes are frequently exposed as suites of small bodies but are of special petrological interest. They may loose their original mineralogical, structural, textural and bulk chemical properties on their way to the surface with advancing metamorphism. Nevertheless, the understanding of the relationship of pressure, temperature, fluid history, mineral transformation and reaction textures of ultramafic rocks can provide many clues to its original nature. Ultramafics are often intercalated with host gneisses in granulite terranes, which have chemistry different from those of ultramafics. The contrast in chemistry between two adjacent rocks in such a terrane could often lead to metasomatism. Significant advances in understanding the process of such metamorphic ultramafic rocks have come from several previous studies (e.g. Evans and Trommsdorf 1970; Trommsdorf and Evans 1974; Springer 1974; Pinsent and Hirst 1977; Evans 1977; Desmarais 1981; Kimball et al. 1985; Peretti et al. 1992; Kassoli-Fournaraki et al. 1995; Dasgupta et al., 1997).

Until recently, attention has been focused on pressure and temperature conditions of the rocks as a major cause of metamorphism. The finding of fluid inclusions in minerals (see reviews by Roedder 1984; Crawford and Hollister 1986) and recent discussions on the role of fluids in regional metamorphic and contact metamorphic environments (e.g. Rice and Ferry 1982; see also reviews by Barton et al. 1991 and Ferry 1991) reveal that fluids play an important role in these environments. The study of fluid–rock ratio of rocks and the nature of fluid flow during metamorphism has been discussed extensively in recent times (e.g. Walther and Wood 1986; Rumble 1989; Baumgartner and Ferry 1991; Newton et al. 1998). Mineral assemblages and the stable isotopic compositions of metamorphic rocks are routinely used as a monitor of metamorphic fluid flow. In particular, most mineralogical investigations are focussed on the role of fluid flow in driving prograde reactions (e.g. Labotka et al. 1988; Bickle and Barker 1990; Baumgartner and Ferry 1991; Nabelek 1991; Cartwright and Buick 1995). However, the role of retrograde fluid flow, which usually involves hydration and carbonation, following peak conditions, has not received much attention (but Ferry 1996; Roselle 1997). The goal of this study is to discuss field relationships, petrology and geochemistry of ultramafic enclaves that characterize the pressure-temperature and fluid compositions at Rupaha, Sri Lanka. Using this data, we will

present evidences for the high temperature and retrograde fluid-rock interactions of ultramafic rocks.

The ultramafic rocks in the Rupaha area are generally massive. They crop out as a series of discontinuous lenses and pods enveloped by surrounding granulites (Fig. 3.1). Peak metamorphic assemblages (e.g. enstatite-forsterite-diopside) are observed only in few places. These rocks often show evidences for retrograde overprints in which peak metamorphic assemblages are replaced by tremolite, dolomite and talc in many places. Therefore, the path of retrograde fluid flow can be evaluated on the basis of retrograde mineral assemblages of the ultramafic rocks at Rupaha.

GEOLOGICAL SETTING AROUND RUPAHA ULTRAMAFIC BODY

The Proterozoic basement of Sri Lanka consists mostly of granulite to amphibolite facies rocks. Sm-Nd model ages, determined for a variety of lithology, define three distinct crustal units: the Highland Complex (HC); the Wanni Complex (WC); and the Vijayan Complex (VC) (Fig.3.1) (Milisenda et al. 1988, 1994; Cooray 1994). The rocks of the area around Rupaha lie within the HC of Sri Lanka. The principle rock units in the area are ortho- and para-gneisses. The meta-sediments and the meta-igneous charnockitic rocks are intimately intercalated in the field on all scales (from metre to kilometre). The meta-sediments include quartzites, marbles, pelitic gneisses and calc-silicate granulites. Ortho-gneisses are present as charnockites, charnockite gneisses and biotite gneisses. At least three major phases of structural events (D_1, D_2 and D_3) have been recognized (Berger and Jayasinghe 1976; Kriegsman 1993). The D_1 event is believed to predate peak metamorphic conditions, while the D_2 event is contemporaneous with it. D_3 is believed to form during the early retrogression.

Field mapping in the area of Rupaha showed, that the ultramafic bodies are exposed discontinuously as elongated belts along most of the western part of Rupaha. Its length is about 2 km, with a thickness ranging from a few metres (northern part of the body) to several hundred metres (in the river tributary *'Garandu Kandura'*) where it is best exposed (Fig. 3.1). Apparently the ultramafic rocks acted as a competent unit during deformation of the area. The planes of foliation and the direction of dips within the ultramafic rocks are

difficult to identify. But when it is visible, the foliation is similar to the regional striking trend, approximately N-S. Metasomatic mineral reaction zones are observed at contacts between ultramafic rocks and siliceous granulites. Similar contact relations are repeated in at least six places, all within the main exposure at *'Garandu Kandura'*. Further north of the river basement, ultramafic rocks can again be traced discontinuously in four places. Here, morphological, physical and textural features of all rock types are similar to those at *Garandu Kandura*.

The ultramafic rocks at Rupaha are composed primarily of the metamorphic equivalent of dunites and peridotites. Based on their physical and textural appearance, and mineral paragenesis, four rock types have been divided (Fig. 3.1): (1). Pale green coloured ultramafic rocks (PG) (e.g. sample numbers 9740, 9744 in Fig 3.1), (2). Dark green coloured ultramafics (DG) (e.g. sample numbers 9320S, 9703 in Fig 3.1), (3). Phlogopite dominate ultramafic rocks at the physical contacts of the surrounding granulites known as *blackwall zone* (BW) (e.g. sample numbers 9710A, 9712 in Fig 3.1), (4). Late carbonatized and brecciated veins (CV) (e.g. sample numbers 9316, 9317, 9318 in Fig 3.1).

Olivine is the main constituent in all rock types, except the late carbonatized and brecciated veins, where serpentine is the dominant constituent. Colourless, porphyroblastic orthopyroxenes are present in most fresh PG rocks (Fig 3.2a). The DG rocks include accessory Fe-oxides, some phlogopites and scanty relicts of spinel. The colour of spinel varies from dark blue to purple. The spinel occurs as subhedral crystals, smoothly bounded clots and frequently as clusters of grains of 1 to 2 mm size. Clots are elongated resulting in micro-scale pinch and swell structures (e.g. sample No. 9320S in Fig 3.1). Although two different ultramafic rocks have been observed, there does not seem to be any spatial relationship or distribution of the different types.

The blackwall rocks (BW) often exhibit a planar fabric and are confined to the physical contacts of the ultramafic body with the surrounding granulites (e.g. 9710A in Fig 3.1). These rocks occur as thin lenses about 10-50 cm wide, they are also composed of predominantly olivine with lesser amounts of phlogopite, and traces of clinopyroxene and spinel, but significantly porphyroblastic orthopyroxene is absent here. Pronounced changes in modal abundances of minerals occur as phlogopite increases progressively within this

zone, and clinopyroxene and olivine decrease. With further deformation, elongated phlogopite crystals lie along grain boundaries defining a distinct fabric. Both field relationships and textures suggest that phlogopite formed during the blackwall alteration (cf. Dubińka and Wiewióra 1999).

Carbonate-serpentine veins (CV) dissect the ultramafic rocks (Fig. 3.1). The carbonate-dominated veins are a few millimetres to several centimetres thick. In addition to these veins, blackish-green, frequently brecciated sheet-like bodies are well developed along brittle fractures and shear zones (Fig. 3.2b). The orientations of these sheet-like bodies are random. Shearing in the rocks is confined only to the PG part of the rock (e.g. 9316, 9317, 9318 in Fig. 3.1). The extensive occurrences of late carbonate veins in pale green ultramafic rocks perhaps lead earlier workers to describe this unit as 'serpentine marble' (e.g. Coomaraswamy 1904; Soyza 1986; Rupasinghe and Dissanayake 1987; Siriwardena 1988).

METHOD OF INVESTIGATION

The Rupaha ultramafic body was surveyed on aerial photographs, mapped in detail in the field. The geological mapping was carried out on the scale of 1:500 near the ultramafic unit during the course of this study. As far as possible, all ultramafic units, not only from the main exposure but also from other isolated locations were identified and mapped. Twenty-five samples representing every ultramafic unit were collected from 18 locations in the ultramafic rocks, exposed at *'Garandu Kandura'* (Fig. 3.1). At each outcrop care was taken to collect the least altered, freshest samples. Mineral parageneses of each sample were identified by petrographic observations and microprobe measurements. Modes of every representative rock types were measured by counting 2000 points in thin section. The major and trace element analyses of whole rocks were determined by X-ray Fluorescence spectroscopy (Philips-PW1404) at the University of Mainz, Germany. Mineral compositions were measured with a JEOL microprobe (JEOL JXA 8900 RL) at the University of Mainz, Germany with analytical operating conditions of 15 keV accelerating voltage, 12nA beam current and 2μm beam diameter. Synthetic and natural standards were used. Halides were calibrated with tugtupite, $Na_4AlBeSi_4O_{12}$(Cl, S) (7.58

wt % Cl) and F-phlogopite (9.20 wt % F). An online ZAF correction was used for data processing (Amstrong 1988, 1989).

WHOLE ROCK CHEMISTRY

The all whole rock major and trace element compositions are listed in Table 3.1. All the samples examined are silica poor, with SiO_2 composition ranging from 37-45%. High amounts of total Fe are characteristic for dark-green ultramafics, in which secondary magnetite is responsible for this high Fe content. Fig. 3.3 illustrates the compositional variability of different zones in ultramafics. A marked increase in K_2O, TiO_2, Al_2O_3, and volatiles along with a decrease in MgO is observed for samples close to the border of the ultramafic rocks (blackwall zone). This is reflected by the increased modal abundance of phlogopite, and a decrease in the modal abundance of olivine, orthopyroxene and clinopyroxene (Table 3.1). Samples from late carbonatized and brecciated veins (CV) have low Mg and high volatile concentrations (Fig. 3.3a, b). Table 3.1 also includes some lithophile trace element data for Rupaha ultramafic samples. Concentrations of fluid immobile trace elements are below detection limit in many of our samples. Ni and Cr concentrations, which are compatible with olivine and spinel, show a large increase in the dark coloured ultramafics (Table 3.1) while Ba and Rb significantly increase towards the blackwall zone of the ultramafic rocks. The high Ni and Cr of the DG rocks suggest that original protoliths environment of the ultramafic would be earth's upper mantle (see also review from Evans 1977), but now have been completely metamorphosed.

MINERAL CHEMISTRY

Compositions of the minerals found in the ultramafics are listed in Table 3.4. *Olivine* composition in pale green rocks is $Fo_{(98-99)}$, while dark green rocks have $Fo_{(95-96)}$(Table 3.4a). *Orthopyroxene* is enstatite with $En_{(98-99),}$ while *clinopyroxene* consist of 99% of diopside component.

Spinel belongs close to the spinel end member of the spinel-hercynite solid solution with X_{Mg} = 0.91-0.92 (Table 3.4a). It has very low Cr contentas [(Cr/(Cr + Al) = 0.001] and (recalculated) Fe^{3+} (0.003-0.021) contents. These values are comparable with the spinels from the high-grade meta-peridotite bodies of Ruby Range Montana (Desmarais 1981;

X_{Mg} = 0.48- 0.63 and [Cr/(Cr + Al) = 0.02-0.15], but differ from the primary igneous spinels found in the low grade metamorphic terranes of British Columbia (Pinsent and Hirst 1977; X_{Mg} = 0.05-0.62 and Cr/(Cr + Al) = 0.58-0.76). The same chemistry of spinel in igneous rocks was observed by Basu and MacGresor (1974), Evans and Frost (1974), Sack and Ghiorso (1991) and Clynne and Borg (1997).

Phlogopites in the BW and PC are high in Mg (X_{Mg} = 0.985-0.995), compared with phlogopite in the DG, which are poorer in Mg (X_{Mg} = 0.970-0.978). No significant difference between the two groups has been observed with respect to Cl (0.04-0.08 pfu) (Table 3.4b). Phlogopite in DG rocks has a much higher Al content (2.50-2.85 pfu) compared to that of PG and BW variety (2.00–2.45 pfu). Fe content is also significantly high in the dark green rock (Table 3.4b). A remarkably high F content is observed in some phlogopites. Phlogopite found at the BW rocks shows the highest values of F, ranging from 0.813 - 0.899 pfu. This indicates high F/ F+OH in the fluids (Table 3.4b). High F increases the stability of biotite towards higher temperatures (Hensen and Osanai 1994).

Amphibole is a nearly pure tremolite with a formula of $Ca_{1.94}Mg_{4.90}Si_{7.90}O_{22}(OH_{1.93}F_{0.06}Cl_{0.01})$. *Talc* is low in Al and Fe and, has a X_{Mg} of 0.98-0.99. Talc is too fine-grained to obtain proper analyses in the shear zone. Antigorite, which is a high temperature and pressure form of *serpentine,* is perhaps the major serpentine mineral present within the assemblages.

PETROGRAPHY

Mineral assemblages

Mineral associations in different lithologies and the textural evidence for mineralogical equilibrium and disequilibrium are discussed in the next sections. Mineral associations of four different lithologies are listed in Table 3.2 and illustrated in Fig 3.4 in the composition map of $MgO\text{-}SiO_2\text{-}CaO\text{-}(H_2O\text{-}CO_2)$. The mineral association does not only include presumed primary minerals, but also late-stage minerals appearing in the reaction textures. Modes of eight samples in four different units of ultramafic rocks are listed in Table 3.3. The peak-metamorphic minerals and secondary minerals have been identified from textures, where secondary minerals commonly overprint peak-metamorphic minerals.

Pale green ultramafic rocks (PG)

Pale green ultramafic rocks are distinguished by the presence of forsterite, diopside, enstatite and also tremolite and dolomite. The observed mineral associations are; Fo + Di + En, Fo + Tr + Dol, and En + Tr + Dol. Mineral abbreviations are those of Kretz (1983). Textural evidences suggest that forsterite; enstatite and diopside are from early metamorphic phases (Fig. 3.4a) while tremolite and dolomite overprint the former (Fig.3.4d).

Dark green ultramafic rocks (DG)

Mineralogy of DG zone differs from PG zone by the appearance of spinel and phlogopite (Table 3.2). Where DG rocks consist of phlogopite, this is always confined to the BW zone (e.g. 920S). The occurrence of orthopyroxene has been observed in DG rocks few places (e.g. 9824), but at the PG zone. Mode of phlogopite increases up to ~6% due to replacement of many early metamorphic minerals. The DG consists the assemblages of Fo + Phl, Spl + Phl, Spl + Di + Phl, Fo + Di + Phl, Fo + Di + Dol and Fo + Phl + Dol, where phlogopite and dolomite appear as late overprints. This zone is the least altered zone among all ultramafic lithologies showing an average mode of secondary minerals of about 6%.

Phlogopite-bearing blackwall rocks (BW)

The phlogopite-bearing blackwall rocks, in general, are medium- to coarse-grained, and composed predominantly of olivine (~60%) with lesser phlogopite (~12%). The main changes occur within BW zone, they are summarized in the Table 3.3. Mineral associations of this zone are almost identical with the DG zone, but differ significantly with the modes of phlogopite and olivine and the state of alterations (Table 3.2). The formation of coarse-grained phlogopite is quite advanced in this zone at the expense of forsterite and spinel. Oriented phlogopites are well interlocked with olivine. The marked increase of hydrated minerals at the physical contact indicates a flux of fluid, accompanied by potassium and silicon.

Late carbonatized and brecciated veins (CV)

These veins contain variety of mineral assemblages that are interpreted as having formed during retrogression. The observed mineral assemblages in the late veins are Dol + Tlc +

Srp and Tlc + Tre + Dol. Ninety percent of forsterite has been completely altered to serpentine within this zone.

Textural relations

From structural and textural relationships it is clear that the Rupaha ultramafic body has been completely transferred to new phases under high-grade metamorphic conditions. Crystallization outlasted penetrative D_2 deformation, which is the major fabric-forming event in the region. The following evidences pointed to this conclusion; No typical igneous textures and structures have been observed through out the ultramafic body; minerals have irregular anhedral habits; absence of mineral relicts; no mineral zoning; and the presence of micro-scale pinch and swell structures in spinel and lineated phlogopite in the BW zone, which follow the D_2 deformation of the region.

Peak and near-peak metamorphic assemblages

The earliest, high temperature assemblages are forsterite-enstatite-diopside, and forsterite-spinel (Fig. 3.5a, b). They are preserved in the less altered portions of the body. Both assemblages can be stable at granulite facies temperatures and pressures. Olivine is variably serpentinized, whereas some olivine grains are altered into the serpentine minerals along cleavage fractures and borders. The other high-temperature assemblages in ultramafic rocks are phlogopite-bearing assemblages, which are apparently restricted to BW zone of ultramafic rocks (Fig.3.5c). These are mostly developed within a metre of the body contact. In places, phlogopite commonly replaced spinel and forsterite, forming thin coronas separating them (Fig 3.5b). The phlogopite is aligned with regional foliation, interpreted to be D_2. The D_2 deformation fabric has been shown to be near-peak metamorphism. Hence, phlogopite formed in ultramafics close to, or at, Peak PT. The formation of phlogopite at the physical contacts of the body indicates that mass transport between ultramafics and host granulites occurred during granulite facies metamorphism.

Retrograde metamorphic assemblages

Several retrograde reaction textures overprint peak mineral assemblages within the pale green ultramafics (PG). The stable mineral assemblages are illustrated in Fig. 3.4 The most common is the replacement of enstatite by tremolite and dolomite (Fig. 3.5d). Tremolite also occurs as well-formed prismatic crystals, which grow within the forsterite matrix as

well. Tremolite overprints has been observed at the forsterite-forsterite grain boundaries as well (Fig. 3.5e). These textures provide an unequivocal sense of tremolite formed either from enstatite or from forsterite or both ways with infiltration of Ca-rich fluids.

Talc quite often replaces tremolite in late carbonatized veins (CV) (Fig 3.5f). Here talc formed through the infiltration of H_2O and CO_2-bearing fluids. The source of these fluids is external to the ultramafics. The last prominent retrograde alterations are veins of serpentine minerals. In general, the abundance of serpentine is greatest in samples that have abundant late veins (Table.3.3). Here forsterites are altered to serpentine completely in almost every sample. Nevertheless, the degree of alteration is less in zone of DG lithology.

CONDITION OF METAMORPHISM

Peak metamorphic temperature

Unaltered portions of the rocks, together with mineral fabrics discussed indicate that the earliest assemblage was orthopyroxene + clinopyroxene + olivine ± spinel. Peak metamorphic temperatures were estimated using the two-pyroxene geothermometry of Kretz (1982) and Brey and Köhler (1990). Thirteen pyroxene pairs were chosen for thermometry. Selected data used for Opx-Cpx calculations are given in the Table 3.4a (mineral pairs 30-46, 32-48, 34-53). The calibration of Brey and Köhler (1990) yields temperatures of 750 ± 41^{o}C while Kretz's (1982) calibration gives higher values of 842 ± 68^{o}C at 9kbar conditions. A pressure estimate of 9kbar was used, based on the surrounding granulites (see chapter 2). The temperature estimates of the ultramafic rocks are consistent with those of the surrounding granulites. This supports the view, which is based on field and petrological observations that ultramafic rocks have equilibrated under granulite facies conditions.

Evolution of the mineral paragenesis and mineral fluid-reactions

Mineralogical changes and reaction textures observed in the ultramafic rocks have several important implications in response to change in temperature, fluid and bulk composition. The growth of phlogopite in the ultramafic rocks was investigated by comparing phlogopite assemblages with phase equilibria for the simplified system MgO-SiO_2-K_2O-

Al_2O_3-H_2O-CO_2. We used the μSiO_2-μK_2O diagram and T-μK_2O diagram to illustrate the peak metamorphic conditions, including the effect of fluids during the formation of phlogopite. The fluid induced retrograde metamorphic conditions are illustrated from μCO2-μCaO and T-μCaO diagrams. All diagrams were calculated with the PerPleX software (Connolly 1990). Reduced activities were used for diopside, enstatite, forsterite, talc, spinel, phlogopite, and tremolite that measurably deviated from pure substances while talc, dolomite, brucite, K-feldspar, plagioclase and periclase were considered as pure phases. The thermodynamic data of Holland and Powell (1998) were used together with the following activity models; The a_{Tr} in Ca-amphiboles was calculated after Holland and Blundy (1994) while a_{En} and a_{Fs} in enstatite were computed after Holland and Powell (1996). Activity models for diopside, talc, spinel and olivine are from Holland and Powell (1998). Fluids were considered CO_2-H_2O solutions that obey the equation of state given by Holland and Powell (1991, 1998). We used the 'ionic solution model' [$a_{Phl} = (X_{Mg})^3 * (X_{OH})^2$] to calculate the activity of phlogopite because of the high F content that is measured in phlogopites.

Peak metamorphic conditions

The mineral assemblages of forsterite-enstatite-diopside are recognized as the peak assemblage in the rock and may represent the metamorphic episode that took place during the highest temperature attained by the rock (Fig. 3.5a). These mineral assemblages are also graphically presented in the H_2O saturated CaO-MgO-SiO_2 ternary diagram (Fig 3.4a).

The reaction texture of a phlogopite corona around spinel suggests a reaction involving forsterite + spinel to form phlogopite (Fig. 3.5b). A model explaining the formation of phlogopite from forsterite and spinel is shown in the μSiO2-μK_2O diagram in the Fig. 3.6. It relates the formation of phlogopite in an open system. The influx of K_2O and also SiO_2 is required to produce phlogopite. Therefore, the reaction (1) could be the most reasonable explanation for phlogopite formation at the given PT condition.

$$2\ Spl + 5\ Fo + 4\ H_2O + 7\ SiO_2 + 2\ K_2O \text{ ----------} \rightarrow 4\ Phl \qquad (1)$$

The geometry of blackwall zones and mineral assemblages also suggests a localized fluid flow along the physical contacts. The Si and K must have been added from outside to the system during the reaction in order to form phlogopite. The influx of H_2O-rich fluid, which was probably saturated in SiO_2, triggered the reaction leading to the formation of phlogopite.

The possible temperature conditions involving hydration and the activity of K_2O, projecting from SiO_2, is shown by the T-μK_2O diagram (Fig 3.7), which was calculated for 9kbar. This diagram illustrates that the formation of phlogopite requires at least a temperature of 800^oC. This is close to the peak metamorphic conditions of the ultramafic rocks. This result is consistent with the temperature calculations of two-pyroxene thermometry of ultramafics.

The phases of muscovite, sanidine, anorthite, clinochlore, brucite and periclase were included to highlight the conditions under which these minerals would not be expected.

Retrograde metamorphic conditions

Phase relations of retrograde mineral assemblages are plotted in the fluid saturated (H_2O-CO_2) ternary diagrams of CaO-MgO-SiO_2 (Figs 3.4b and 3.4c), This illustrates the typical phase relations of retrograde minerals in the zones of PG and CV. Retrograde minerals like tremolite, dolomite, talc and antigorite from enstatite, forsterite and diopside have formed in these zones.

Abundance of hydrated minerals like phlogopite at the rocks from BW suggests water must have been present in the pore fluids in the high-temperature conditions. And also, the evidence for CO_2 + H_2O in fluids during retrogression is indicated by the overprints of tremolite + dolomites over enstatite (Fig. 3.5d) and the formation of tremolite in the forsterite-forsterite grain boundaries (Fig. 3.5e). The reaction producing tremolite either from forsterite of from enstatite requires Ca^{2+}. For tremolite and dolomite, such a reactions may be simplified to;

$8\ Fo + H_2O + 13\ CaO + 22\ CO_2 \text{ ---------}\rightarrow\ Tr + 3\ Dol$ (2)

$4\ En + H_2O + 5\ CaO + 6\ CO_2 \text{ ----------}\rightarrow\ Tr + 3\ Dol$ (3)

Significantly, diopside is absent in any of tremolite-bearing samples (see also Table 3.2). Hence, the transition of tremolite and dolomite additionally involved the Ca and CO_2 in the reactions. The calculation of the chemical potential diagram of CO_2 Vs CaO, shown in Fig. 3.8, illustrates the stability of Tr-Dol-Fo-Tlc-Di-En-Qtz in a system CaO-MgO-SiO_2-H_2O at 750^oC and 9kbars. Diagrams were calculated with measured mineral compositions converted to activities. The resulting diagram reproduces mineral reactions, which are very similar to the observed products of retrograde reactions. For example, the influx of CO_2 and CaO is required to form Tr + Dol from En or Fo.

Further evolution is governed by constant MgO activity and progressively decreasing activity of CO_2 and CaO while passing the Tr + Dol, finally arriving at the Tlc + Dol zone (as shown in the dark line in Fig. 3.8). This path attributed to form Tlc from Tr in the late veins. The activity change of CaO and CO_2 indicates the strong gradient in chemical potential. These calculations, support interference from the arguments detailed above, are obviously the factors controlling the retrograde overprints of the ultramafic rocks.

The activity corrected T-μCaO diagram is calculated for the system MgO-SiO_2-H_2O-CO_2 at 9kbar conditions, using the thermodynamic database of Holland and Powell (1998) (Fig. 3.9). The shaded area marks the stability fields of En + Tr + Dol, Fo + Tr + Dol and Tr + Dol + Tlc. Fig. 3.9 was calculated for X_{CO2} [=CO_2/(CO_2+H_2O)] = 0.30. The univariant point A overlapped with univariant point B for X_{CO2} of 0.40, indicating forsterite is unstable, when $X_{CO2} > 0.40$. Insomuch, the univariant point A overlapped with the univariant point C, when $X_{CO2} < 0.15$. No enstatite can be formed with $X_{CO2} < 0.15$ at the given pressure conditions. Hence, it can be concluded that the stability fields of En + Tr + Dol and Fo + Tr + Dol occur together at the fluid condition of $0.40 \geq X_{CO2} \geq 0.15$ at 9kbar conditions. Therefore, T-μCaO diagram provides a reasonable estimate of 640-750^oC for En + Tr + Dol and Fo + Tr + Dol assemblages of ultramafic rocks at 9 kbar conditions during the granulite-amphibolite retrograde condition.

When summarising the retrograde history of ultramafic rocks, it can be pointed out that with the progressing of retrograde reactions (2) to (3), the pervasive CO_2 fluid flow ($0.52 \geq X_{CO2} \geq 0.21$) accompanied with the influx of Ca^{2+} to the ultramafic rocks may have been retrogressed at temperatures between 730 and 640^{o}C. The equilibrium assemblages should contain talc instead of tremolite at lower temperatures. The stability of talc rather than tremolite in the low-grade assemblages at Rupaha shows evidence for the presence of water-rich fluid conditions. The first appearance of antigorite marks a pervasive hydration event in later stages. The antigorite event therefore reflects infiltration of H_2O into host rock at temperatures below 640^{o}C through the brittle fractures.

SUMMARY AND DISCUSSION

Metamorphism

Although mineralogically complex, the metamorphosed ultramafic rocks at Rupaha are compositionally simple, permitting a relatively straightforward interpretation of their metamorphic evolution. Such rocks are commonly mantle-derived silica-undersaturated rocks. The low concentrations of Cr, Ni and Fe in spinel, olivine and diopside indicate that their protoliths have been completely transformed into a metamorphic rock during granulite facies. They formed as alpine type peridotites in the metamorphic terranes (Evans 1977).

K-Si-metasomatism

There are several lines of chemical evidences for a high temperature metasomatism at the out side most part of the body. The direction of the planer structural elements suggests that the phlogopite growth took place contemporaneous with the major deformation episode (D_2), which in turn is believed to be syn-peak metamorphic (Berger and Jayasinghe 1976; Kriegsman 1993). The formation of phlogopite during deformation requires infiltration of potassium and silica. Similar circumstances have been discussed by many other workers (e.g. Harker 1932; Beach 1973, 1976; Gresens 1966; Kerrich et al. 1977; Brodie 1980). The enrichment of K, Ti, Al, Rb and Ba measured for whole rocks also supports this hypothesis (see also Fig. 3.3).

Application of μSiO_2-μK_2O and T-μK_2O diagrams illustrate the near-peak K-Si-metasomatism in the ultramafic rocks at the physical contacts from potassium-rich granulites. The reaction was started by K_2O, SiO_2 and H_2O infiltration along the granulite-ultramafic contact or diffusion of these elements from the surrounding granulites The stability field of phlogopite, as illustrated in T-μK_2O, suggest the K-metasomatism may have occurred contemporaneous to the granulite facies metamorphism.

Fluid flow during retrogression

The replacement of enstatite and forsterite by tremolite and dolomite confirms the presence of CO_2-rich infiltrating fluids ($0.40 \geq X_{CO2} \geq 0.15$) at elevated temperatures (730-640^oC) at 9kbar. The retrogression can be modelled assuming the chemical potential gradients in Ca and CO_2, which may possibly have served to modify the peak metamorphic mineral assemblages. The second, but widespread hydration occurred at much lower temperatures and is marked by the formation of serpentine from forsterite.

Field evidences and textures of the formation of retrograde minerals like, tremolite, dolomite and talc within the ultramafic rocks suggests that the formation was, in general, not localized by fault-controlled influx. Retrograde metamorphism simply corresponds to a progressive opening of the system, whenever fluid circulation introduces H_2O and CO_2 to more permeable zones. However, it is clear that he massive brecciation and carbonation allowed fluid interaction with large volumes of rocks, as opposed to the retrogression, where minor brecciation occurred and fluid flowed mainly along the grain boundaries.

Mechanism of the emplacement

Any model for the mechanism of emplacement of the ultramafics should account for the sequence of metamorphism, metasomatism as well as retrograde events. The ultramafic rocks at Rupaha are the only locality so far found in the entire Highland Complex of Sri Lanka, in which they have been metamorphosed at granulite facies. One possible explanation for the observations is that a piece of the mantle was faulted up to the lower crust (cf. Dick 1979). The fluid circulating at the deep crust would result in several types of metasomatic processes. As the ultramafic rock cooled together with surrounding granulites, the retrograde overprints and the carbonation and hydration textures are produced.

REFERENCES

*Amstrong JT (*1988). Quantitative analyses of silicate and oxide minerals: comparisions of Monte Carlo, ZAF and Phi-rho-z procedures. In: (*Newbury DE* eds). Microbeam analysis-1988, San Francisco Press, San Francisco, 239-246

Amstrong JT (1989). CITZAF: combined ZAF and phi-rho (Z) electron beam correction programs. California Institute of Technology, Pasadena, CA

Barton MD, Ilchik RP, Marikos MA (1991) Metasomatism. In: Contact metamorphism, Reviews in Mineralogy (*Kerrik M* ed), Mineral. Soc. Am. 26: 321-345

Basu AR, MacGregor ID (1975). Chromite spinels from ultramafic xenoliths. Geochim. Cosmochim. Acta 39: 937-945

Baumgartner LP, Ferry JM (1991). A model for coupled-fluid flow and mixed-volatile mineral reactions with applications to regional metamorphism. Contrib. Mineral. Petrol. 106: 273-285

Beach A (1973). The mineralogy of high temperature shear zones at Scourie, N.W. Scotland. J. Petrol. 14: 231-248

Beach A (1976). The interrelations of fluid transport, deformation, geochemistry and heat flow in the early Proterozoic shear zones in the Lewisian Complex. Phil. Trans. R. Soc. A280: 569-604

Berger AR, Jayasinghe NR (1976). Precambrian structure and chronology in the Highland Series of Sri Lanka. Precam. Res. 3: 559-576

Bickle MJ, Barker J (1990). Advective-diffusive transport of isotopic fronts: an example from Naxos, Greece. Earth Planet. Sci. Lett. 97:78-93

Brey GP, Köhler T (1990) Geothermobarometry in four-phase Lherzolites II. New thermobarometers and practical assessment of existing thermobarometers. J. Petrol. 31: 1353-1378

*Brodie KH (*1980). Variation in mineral chemistry across a shear zone in phlogopite peridotite. J. Structural Geol. 2: 265-272

Cartwright I, Buick IS (1995). Formation of wollastonite-bearing marbles during regional metamorphic channelled fluid flow in the Upper Calc-silicate unit of the Reynolds Range Group, central Australia. J. Metamorphic Geol. 13: 397-413

Clynne MA, Borg LE (1997). Olivine and chromian spinel in primitive calc-alkaline and theolitic lavas from the southernmost Cascade range, California: a reflection of relative fertility of the source. Canadian Mineral. 35: 453-472

Coomaraswamy AK (1904) Administrative report. Mineral. Surv. Ceylon

Cooray PG (1994) The Precambrian of Sri Lanka: a historic review. Precam. Res. 66: 1-18

Connolly JAD (1990). Multivariate phase diagrams: an algorithm based on generalized thermodynamics. Am. J. Sci. 290: 666-718

Crawford ML, Hollister LS (1986). Metamorphis fluids: The evidence from fluid inclusions. In: Fluid-rock interactions during metamorphism In: Advances in physical geochemistry 5 (*Walther JV, Wood BJ* eds), Springer Verlag, 1-35

Dasgupta S, Ehl J, Raith M, Sengupta Pranesh, Sengupta Pulak (1997). Mid-crustal contact metamorphism around the Chimakurthy mafic-ultramafic Complex, eastern Ghats, India. Contrib. Mineral. Petrol. 129: 182-197

Desmarais NR (1981). Metamorphosed Precambrian ultramafic rocks in the Ruby range, Montana. Precam. Res. 16: 67-101

Dick HJB (1979). Alteration and metamorphism of peridotite at Islas Orcardes Fracture zone (abs) EOS Trans, Am. Geophys. Un. 60: 973

Dubińska E, Wiewióra A (1999). Layer silicates from a rodingite and its blackwall from Przemiłów (Lower Silesia, Poland): mineralogical record of metasomatic processes during serpentinization and serpentinite Recrystallization. Mineral. Petrol. 67: 223-237

Evans BW (1977). Metamorphism of alpine peridotite and serpentinite. Ann. Rev. Earth. Planet. Sci. 5: 397-447

Evans BW, Frost BR (1974). Chrome-spinel in progressive metamorphism - a preliminary analysis. Geochim. Cosmochim. Acta 39: 959-972

Evans BW, Trommsdorf V (1970). Regional metamorphism of ultramafic rocks in the central Alps: Paragenesis in the system CaO-MgO-SiO_2-H_2O. Schweiz. Min. Petrol. Mitt. 50: 481-492

Ferry JM (1991) Dehydration and decarbonation reactions as a record of fluid infiltration. Metasomatism. In: Contact metamorphism, Reviews in Mineralogy (*Kerrik M* ed), Mineral. Soc. Am. 26: 351-391

Ferry JM (1996). Prograde and retrograde fluid flow during contact metamorphism of siliceous carbonate rocks from the Ballachulish aureole, Scotland. Contrib. Mineral. Petrol. 124: 235-254

Gresens RL (1966). The effect of structurally produced pressure gradients on diffusion in rocks. J. Geol. 74: 307-321

Harker A (1932). Metamorphism, Chapman and Hall, London, pp362

Hensen BJ and Osanai Y (1994). Experimental studies in dehydration melting of F-bearing biotite in model pelite compositions. Mineral. Mag. 58A: 410-411

Holland TJB, Blundy J (1994) Non-ideal interactions in calcic amphiboles and their bearing on amphibole-plagioclase thermometry. Contrib. Mineral. Petrol. 116: 433-447

Holland TJB, Powell R (1991). A compensated-Redlich-Kwong (CORK) equation for volumes and fugacities of CO_2 and H_2O in the Range 1bar to 50 Kbar and 100-1600^oC. Contrib. Mineral. Petrol. 109: 265-273

Holland TJB, Powell R (1996) Thermodynamics of order-disorder in minerals:II. Symmetric formalism applied to solid solutions. Am. Mineral. 81:1425-1437

*Holland TJB, Powell R (*1998) An internally consistent thermodynamic data set for phases of petrological interest. J. metamorphic Geol. 16: 309-343

Kassoli-Fournaraki A, Filippidis A, Kolcheva K, Hatzipanayotou K, Koepke J, Dimadis E (1995). Multi-stage alteration of the Gorgona Ultramafic body, central Rhodope massif, Greece. Chem. Erde 55: 331-344

Kerrich R, Fyfe WS, Gorman BE, Allison I (1977). Local modification of rock chemistry by deformation. Contrib. Mineral. Petrol. 65: 183-190

Kimball KL, Spear FS, Dick HJB (1985). High temperature alteration of Abyssal ultramafics from the Islas Orcadas Fracture zone, South Atlantic. Contrib. Mineral. Petrol. 91: 307-320

Kretz R (1982). Transfer and exchange equilibria in a portion of the pyroxene quadrilateral as deduced from natural and experimental data. Geochim. Cosmochim. Acta 46: 411-421

Kretz R (1983) Symbols for rock forming minerals. Am. Mineral. 68: 277-279

Kriegsman LM (1993). Geodymamic evolution of the Pan-African lower crust in Sri Lanka-Structural and petrological investigations into a high-grade gneiss terrain. PhD thesis, University of Utrecht, The Netherlands, pp207

Labotka TC, Nabelek PI, Papike JJ (1988). Fluid infiltration through the Big Horse limestone member in the North Peak contact aureole, Utah. Am. Mineral. 73:1302-1324

Milisenda CC, Liew TC, Hofmann AW, Kröner A (1988) Isotopic mapping of age provinces in Precambrian high-grade terrains: Sri Lanka. J. Geol. 96: 608-615

Milisenda CC, Liew TC, Hofmann AW (1994) Nd isotopic mapping of the Sri Lanka basement: update and additional constraints from Sr isotopes. Precam. Res. 66: 95-110

*Nabelek PI (*1991). Stable isotope monitors. In: Contact metamorphism. Reviews in Mineralogy, 26 (*Kerrick D* ed), Mineral. Soc. Am. Washington DC, 395-436

Newton RC, Aranovich L Ya, Hansen EC, Vandenheuvel BA (1998). Hypersaline fluids in Precambrian deep-crustal metamorphism. Precam. Res. 91: 41-63

Peretti A, Dubessy J, Mullis J, Frost R, Trommsdorf V (1992). Highly reducing conditions during Alpine metamorphism of Malenco peridotite (Sandrio, northern Italy) indicated by mineral paragenesis and H2 in fluid inclusions. Contrib. Mineral. Petrol. 112: 329-340

Pinsent RH, Hirst DM (1977). The metamorphism of Blue River Ultramafic Body, Cassiar, British Columbia, Canada. J. Petrol. 18: 567-594

Roedder E (1984). Fluid inclusions, Reviews in Mineralogy 12, (*Ribbe Paul H* ed), Mineral. Soc. Am. Washington DC, pp646

Roselle GT (1997). Integrated petrologic, stable isotopic and statistical study of fluid-flow in carbonates of the Ubehebe Peak contact aureole, Death Valley National Park, California, PhD dissertation, University of Wiscosin-Madison, pp239

Rice JM, Ferry JM (1982). Buffering, infiltration and the control of intensive variables during metamorphism, In: Characterization of metamorphism through mineral equilibria, Reviews in Mineralogy 10, (*Ferry JM* ed). Mineral. Soc. Am. Washington DC, 263-326

Rumble D III (1989). Evidences of fluid flow during regional metamorphism. Eu. J. Mineral. 1: 731-737

Rupasinghe MS, Dissanayake CB (1987*).* New in-situ corundum deposits in Sri Lanka. J. Gemmol. Assoc. Sri Lanka 4: 2-5

Sack RO, Ghiorso MS (1991). Chromian spinel as petrogenetic indicators: Thermodynamics and petrological applications. Am. Mineral. 76: 827-847

Sriwardena CHER (1988). Preliminary report of the survey of Rupaha serpentine deposit, Geol Surv Dept (unpublished) pp.15

Soyza EG (1986). An account of serpentine deposit of Rupaha, Sri Lanka, J. Gemmol. Ass. Sri Lanka 3: 30-34

Springer RK (1974). Contact metamorphosed ultramafic rocks in the western Sierra Nevada foothills, California. J. Petrol. 15: 160-195

Trommsdorf V, Evans BW (1974). Alpine metamorphism of ultramafic rocks. Schweiz. Min. Petrol. Mitt. 54: 333-352

*Walther JV, Wood BJ (*eds) (1986). Fluid-rock interactions during metamorphism, Advances in physical geochemistry 5, Springer Verlag, 1-35

Table 3.1. Major and trace element abundance of typical ultramafic rock types

	pale green rocks (PG)						dark green rocks (DG)			blackwall rocks (BW)				late carbonatized veins (CV)			
	9740	9741	9744	9743	9710.00	9829	9320	9703	9320A	9710A	9710B	9712	9712A	9316	9317	9318	9318
SiO_2 %	38.78	37.74	37.13	37.31	39.15	39.17	37.60	40.61	36.90	38.76	37.92	38.63	38.45	44.37	40.96	42.17	45.23
Al_2O_3 %	0.17	0.16	0.15	0.14	0.16	0.10	0.06	0.15	0.19	2.32	2.41	2.30	2.45	0.42	0.41	0.52	0.55
Fe_2O_3 %	1.32	1.47	1.50	1.42	1.42	1.62	4.69	5.56	4.30	1.37	1.39	1.40	1.54	0.82	0.98	0.98	0.91
MnO %	0.04	0.04	0.04	0.04	0.04	0.04	0.09	0.10	0.10	0.04	0.04	0.05	0.05	0.07	0.06	0.04	0.08
MgO %	50.19	49.01	49.25	50.24	52.70	50.85	49.07	48.78	49.22	45.69	46.02	46.08	46.23	35.92	41.32	42.78	38.79
CaO %	0.64	0.70	0.66	0.32	0.38	0.34	0.08	0.08	0.04	0.41	0.40	0.40	0.39	3.22	1.36	0.50	1.23
Na_2O %	0.01	0.01	0.01	0.01	0.01	0.22	0.36	0.13	0.18	0.00	0.00	0.01	0.01	0.23	0.19	0.25	0.23
K_2O %	0.01	0.01	0.00	0.00	0.01	0.02	0.02	0.07	0.02	1.43	1.33	1.28	1.32	0.03	0.03	0.04	0.04
TiO_2 %	0.01	0.01	0.01	0.01	0.01	0.01	0.01	0.01	0.02	0.07	0.07	0.07	0.06	0.02	0.03	0.03	0.03
P_2O_5 %	0.02	0.01	0.02	0.02	0.02	0.02	0.02	0.02	0.02	0.02	0.02	0.02	0.02	0.02	0.01	0.02	0.01
LOI %	10.34	10.53	10.40	11.21	7.79	8.58	9.41	5.17	9.56	9.98	10.01	9.62	9.22	15.42	14.91	14.26	13.93
Total %	101.53	99.69	99.17	100.72	101.69	100.97	101.41	100.68	100.56	100.09	99.61	99.86	99.74	100.53	100.25	101.59	101.04
Cr	3	5	2	3	bdl	bdl	233	364	230	1	2	2	1	nd	nd	nd	nd
Ni	4	4	2	3	3	3	13	11	14	2	2	2	2	nd	nd	nd	nd
Zn	30	31	31	30	32	30	54	78	52	34	36	30	32	nd	nd	nd	nd
Rb	bdl	bdl	bdl	bdl	bdl	bdl	bdl	4	bdl	112	120	100	108	nd	nd	nd	nd
Ba	15	12	12	12	18	17	16	25	17	212	189	198	208	nd	nd	nd	nd

nd-not detected; bdl-below detection limit; all iron as Fe_2O_3

Uncertainties for major oxides (%): Si = 0.13, Al = 0.25, Fe = 0.11, Mn = 0.88, Mg = 0.23, Ca = 0.16, Na = 0.61, K = 0.45, Ti = 0.16, P = 0.48

Uncertainties for trace elements (%): Cr = 1.2, Ni = 0.8, Zn = 1.3, Rb = 2.4, Ba = 0.6

Detection limits of trace elements (ppm): Cr = 2.1, Ni = 1.1, Zn = 1.8, Rb = 1.3, Ba = 6.6

Table 3.2 Mineral associations in ultramafic rocks

Sample No.	Fo	En	Di	Spl	Phl	Tr	Dol	Tlc	Mag
pale green ultramafics (PG)									
9744	X	X	X						
9710		X				X^r	X^r		
9710	X					X^r	X^r		
9740	X	X					X^r		
9825	X	X				X^r	X^r	X^r	
dark green ultramafics (DG)									
9320S			X	X	X				
9320S	X		X		X				X
9703	X				X		X		X
9320S	X		X				X		
9824	X	X							
blackwall rocks (BW)									
9710A			X	X	X				
9710A	X		X		X				
9710B	X				X		X		
carbonatized veins (CV)									
9316							X	X	
9317						X	X	X	
9318	X						X		

X- occurs as matrix assemblages

X^r- early retrograde phase

X^a- occurs as alterations

Table 3.3. Modes of selected samples of metamorphosed ultramafic rock

(PG-pale green, DG-dark green, BW-blackwall, CV-carbonatized veins)

	9710	9311	9720S	9703A	9712	9310A	9316	9318
rock type	PG	PG	DG	DG	BW	BW	CV	CV
olivine	63.6	68.2	72.6	78.8	56.2	64.2	4.0	4.6
opx	1.9	1.6	0.0	0.0	0.0	0.0	0.0	0.0
cpx	0	0.3	0.0	1.3	0.5	0.3	0.0	0.0
spinel	0	0.0	13.4	8.2	0.5	0.2	0.0	0.0
phlogopite	0.1	0.1	5.8	7.0	14.5	10.1	0.0	0.0
tremolite[a]	1.1	2.7	0.0	0.0	0.0	0.0	5.2	5.8
dolomite[a]	5.2	4.3	1.2	0.1	2.3	0.2	8.4	7.6
serpentine[a]	28.1	22.8	6.8	4.2	26.0	25.0	55.2	54.2
Fe-oxide[a]	0	0	0.2	0.4	0.0	0.0	0.0	0.0
talc[a]	0	0	0.0	0.0	0.0	0.0	27.2	27.8

[a] Secondary phases

Table 3.4a Some selected orthopyroxene, clinopyroxene, olivine and spinel analyses of different zones in the ultramafic rock (PG-pale green, DG-dark green, BW-blackwall, CV-carbonatized veins)

	olivine				Opx			Cpx					spinel			
rock type	PG	DG	BW	CV	PG	PG	PG	PG	PG	PG	BW	BW	DG	DG	BW	BW
sample No.	9710	9320S	9710A	9318	9740	9743	9744	9740	9743	9744	9710A	9710A	9320S	9320S	9710A	9710A
analyses No	10	113	76	21	30	32	34	46	48	53	62	65	107	108	92	93
SiO_2	42.28	41.64	42.05	42.05	59.42	59.25	59.72	54.85	55.54	55.12	55.89	54.38	0.15	0	0.031	0.01
TiO_2	0	0	0	0.042	0.05	0	0.03	0.061	0	0.012	0	0.033	0.00	0.013	0	0.05
Al_2O_3	0.043	0.01	0	0.01	0.45	0.42	0.488	0.196	0.284	0.42	0.897	0.864	67.01	68.71	68.13	68.33
Cr_2O_3	0	0	0	0	0.02	0.03	0.011	0.068	0.036	0.017	0.046	0	0.08	0.043	0.034	0.07
Fe_2O_3	-	-	-	-	-	-	-	-	-	-	-	-	1.1	0.88	0.16	0
FeO	1.41	4.23	1.68	1.281	0.97	0.99	0.966	0.327	0.302	0.298	0.291	0.284	3.06	3.43	3.9	4.14
MnO	0.044	0.149	0.052	0.031	0.04	0.09	0.039	0.054	0	0.067	0.01	0.031	0.11	0.034	0.059	0.06
MgO	56.31	53.98	56.47	56.15	39.11	39.03	39.03	18.89	19.12	18.89	18.92	18.54	24.86	25.23	24.61	24.41
CaO	0	0.041	0.032	0	0.16	0.21	0.331	24.98	24.43	24.76	24.93	24.6	0.04	0	0	0.00
Na_2O	0.019	0.013	0.048	0.032	0.00	0.02	0.055	0.147	0.157	0.156	0.218	0.36	0.07	0.041	0.051	0.07
K_2O	0.012	0.01	0.056	0.027	0.01	0.03	0.036	0.029	0	0.032	0.016	0.429	0.04	0.053	0.019	0.05
Total	100.12	100.07	100.39	99.62	100.24	100.06	100.71	99.60	99.87	99.77	101.22	99.52	96.52	98.34	96.98	97.19
	formula for 4 oxygens				formula for 6 oxygens				formula for 6 oxygens					formula for 4 oxygens		
Si	0.996	0.994	0.990	0.995	1.991	1.990	1.993	1.987	1.999	1.990	1.986	1.975	0.004	0.000	0.001	0.000
Al	0.001	0.000	0.000	0.000	0.018	0.016	0.019	0.008	0.012	0.018	0.038	0.037	1.975	1.986	1.998	2.001
Cr	0.000	0.000	0.000	0.000	0.001	0.001	0.000	0.002	0.001	0.000	0.001	0.000	0.002	0.001	0.001	0.001
Fe^3	-	-	-	-	-	-	-	-	-	-	-	-	0.021	0.016	0.003	0.000
Ti	0.000	0.000	0.000	0.001	0.001	0.000	0.001	0.002	0.000	0.000	0.000	0.001	0.000	0.000	0.000	0.001
Fe^2	0.028	0.084	0.033	0.025	0.027	0.028	0.027	0.010	0.009	0.009	0.009	0.009	0.064	0.070	0.081	0.086
Mg	1.977	1.922	1.982	1.980	1.954	1.954	1.941	1.020	1.026	1.017	1.003	1.004	0.926	0.922	0.912	0.904
Mn	0.001	0.003	0.001	0.001	0.001	0.003	0.001	0.002	0.000	0.002	0.000	0.001	0.002	0.001	0.001	0.001
Ca	0.000	0.001	0.001	0.000	0.006	0.007	0.012	0.970	0.942	0.958	0.949	0.957	0.001	0.000	0.000	0.000
Na	0.001	0.001	0.002	0.001	0.000	0.001	0.004	0.010	0.011	0.011	0.015	0.025	0.004	0.002	0.002	0.003
K	0.000	0.000	0.002	0.001	0.000	0.001	0.002	0.001	0.000	0.001	0.001	0.020	0.001	0.002	0.001	0.002
Sum-Cat	3.004	3.005	3.011	3.004	3.999	4.001	4.000	4.012	4.000	4.006	4.002	4.029	3.000	3.000	3.000	2.999
En	-	-	-	-	98.64	98.59	98.63	-	-	-			-			-
Fs	-	-	-	-	1.36	1.41	1.37	-	-	-			-			-
Di	-	-	-	-	-	-	-	99.03	99.13	99.12	99.11	99.11	-			-
Hed	-	-	-	-	-	-	-	0.97	0.87	0.88	0.89	0.89	-			-
Fa	1.40	4.19	1.64	1.25	-	-	-	-	-	-			-			-
Fo	98.60	95.81	98.36	98.75	-	-	-	-	-	-			-			-
X_{Mg}	-	-	-	-	-	-	-	-	-	-			0.94	0.93	0.92	0.91
Cr/(Cr+Al)	-	-	-	-	-	-	-	-	-	-			0.001	0.001	0.001	0.000

all iron as FeO except spinel

Table 3.4b Some selected phlogopite, tremolite, talc and serpentine analyses of different zones in the ultramafic rock (PG-pale green, DG-dark green, BW-blackwall, CV-carbonatized veins)

mineral			phlogopite					tremolite		talc			serpentine			carbonate			
rock type	PG	PG	DG	DG	BW	BW	PG	PG	PG	CV	CV	CV	CV	CV	PG	PG	PG	PG	CV
sample No.	9710	9710	9320S	9320S	9710A	9710A	9710	9710	9710	9318	9317	9318	9318	9318	9710	9710	9710	9318
analyses No.	33	73	111	117	66	72	5	6	8	12	14	27	28	29	1	2	3	20
SiO_2	41.95	40.98	39.22	39.79	41.33	41.23	58.83	57.81	57.05	59.91	57.79	40.82	40.62	42.06	nd	nd	nd	nd
TiO_2	0.43	0.35	0.48	1.46	0.43	0.34	0.00	0.03	0.02	0.06	0.00	0.00	0.02	0.00	nd	nd	nd	nd
Al_2O_3	12.70	14.82	17.41	15.74	15.34	14.71	0.57	1.29	1.56	0.58	0.57	0.04	0.34	0.35	0.00	0.26	0.00	0.00
FeO	0.45	0.46	1.10	1.14	0.40	0.52	0.48	0.56	0.34	0.46	0.65	1.31	0.78	0.34	0.27	0.00	0.20	0.27
Cr_2O_3	0.07	0.00	0.03	0.04	0.00	0.02	0.09	0.03	0.06	0.03	0.01	0.01	0.06	0.00	0.00	0.06	0.00	0.00
MnO	0.04	0.02	0.02	0.00	0.02	0.00	0.04	0.01	0.00	0.01	0.00	0.06	0.04	0.03	0.03	0.06	0.06	0.04
MgO	28.94	27.58	25.69	25.96	27.33	27.57	24.47	24.18	23.82	31.51	31.82	42.38	41.75	42.01	22.78	22.62	22.25	23.25
CaO	0.00	0.00	0.00	0.00	0.00	0.00	13.38	13.38	14.34	0.07	0.08	0.04	0.02	0.05	32.88	32.64	32.67	32.40
Na_2O	0.12	0.84	0.29	0.46	0.53	0.53	0.12	0.26	0.45	0.27	0.24	0.03	0.10	0.06	0.00	0.01	0.08	0.00
K_2O	9.14	10.07	9.82	9.31	9.81	9.92	0.01	0.06	0.11	0.06	0.00	0.01	0.09	0.05	0.01	0.00	0.00	0.00
BaO	0.08	0.07	0.38	0.47	0.35	0.25	0.00	0.00	0.00	0.00	0.00	0.00	0.00	0.08	0.04	0.09	0.00	0.00
SrO	nd	nd	nd	nd	nd	nd	nd	nd	nd	nd	nd	nd	nd	nd	0.10	0.10	0.09	0.05
F	1.21	1.76	1.37	1.41	1.89	2.08	0.13	0.20	0.31	nd	nd	0.00	0.00	0.00	nd	nd	nd	nd
Cl	0.28	0.66	0.20	0.20	0.26	0.33	0.03	0.04	0.08	nd	nd	0.19	0.08	0.17	nd	nd	nd	nd
CO_2	nd	nd	nd	nd	nd	nd	nd	nd	nd	nd	nd	nd	nd	nd	43.89	44.23	44.65	43.98
Total	95.42	97.59	95.99	95.96	97.70	97.50	98.155	97.843	98.141	92.951	91.163	84.89	83.89	85.19	100.00	100.00	100.00	100.00
			formula for 22 oxygens				formula for 23 oxygens			formula for 22 oxygens		formula for 18 oxygens			formula based on (Ca+Mg+Fe+Mn)=1			
Si	5.813	5.607	5.453	5.532	5.625	5.633	7.952	7.862	7.782	7.837	7.734	3.912	3.922	3.982	0	0	0	0
Ti	0.044	0.036	0.050	0.152	0.044	0.035	0.000	0.003	0.002	0.006	0.000	0.000	0.002	0.000	0	0	0	0
Al	2.074	2.390	2.853	2.579	2.460	2.368	0.091	0.206	0.250	0.089	0.089	0.004	0.038	0.040	0	0	0	0
Cr	0.008	0.000	0.003	0.004	0.000	0.002	0.010	0.003	0.007	0.004	0.001	0.000	0.004	0.000	0	0	0	0
Mg	5.978	5.626	5.325	5.380	5.545	5.615	4.931	4.902	4.844	6.145	6.348	6.054	6.008	5.930	0.489	0.490	0.485	0.498
Fe	0.052	0.052	0.128	0.132	0.046	0.060	0.054	0.063	0.039	0.050	0.073	0.104	0.062	0.026	0.003	0.000	0.003	0.003
Mn	0.005	0.002	0.003	0.000	0.003	0.000	0.005	0.001	0.000	0.001	0.000	0.004	0.004	0.002	0.004	0.001	0.001	0.000
Ca	0.000	0.000	0.000	0.000	0.000	0.000	1.938	1.950	2.096	0.009	0.012	0.004	0.002	0.004	0.507	0.508	0.511	0.499
Na	0.033	0.221	0.078	0.123	0.141	0.140	0.032	0.069	0.118	0.069	0.063	0.006	0.018	0.012	0	0	0	0
K	1.616	1.758	1.742	1.651	1.703	1.729	0.002	0.011	0.020	0.010	0.000	0.002	0.010	0.006	0	0	0	0
Ba	0.004	0.004	0.020	0.025	0.019	0.013	0.000	0.000	0.000	0.000	0.000	0.000	0.000	0.002	0	0	0	0
sum-cat	15.628	15.695	15.655	15.579	15.586	15.594	15.015	15.070	15.158	14.220	14.320	10.094	10.072	10.006	1.003	0.999	1.000	1.000
F	0.530	0.761	0.601	0.619	0.813	0.899	0.055	0.086	0.136	-	-	-	-	-				
Cl	0.066	0.152	0.046	0.047	0.060	0.076	0.008	0.009	0.019	-	-	0.062	0.026	0.054				
OH	1.404	3.086	1.353	1.334	1.126	1.026	1.938	1.906	1.846	-	-	3.984	3.993	3.987				
X_{Fe}	0.009	0.009	0.023	0.024	0.008	0.010	0.011	0.013	0.008	-	-							
F/(F+OH)	0.274	0.198	0.308	0.317	0.419	0.467	-	-	-	-	-							
X_{Mg}	0.991	0.991	0.977	0.976	0.992	0.990	0.989	0.987	0.992	0.992	0.989							

OH was calculated by stoichiometry

n.d. not detected

FIGURE CAPTIONS

Fig. 3.1 Geological and Structural map of the area around Rupaha. The Proterozoic rocks are composed of charnockites, charnockitic gneisses, quartzites, garnet-sillimanite-graphite gneisses (khondalites), garnet-biotite gneisses, and little scattered marbles.

Fig. 3.2 (a). Photograph of the pale green coloured fresh-looking ultramafic rock has coarse-grained colourless porphyroblast orthopyroxene in its fresh-looking samples; (b). Photograph of dark blue to back coloured massive late-veins cross cutting the ultramafic body.

Fig. 3. 3 Whole rock analyses of different zones plotted against: (a). MgO vs SiO_2, (b). LOI vs SiO_2.

Fig. 3.4 Chemographic diagrams for the CaO-MgO-SiO_2 system projected from H_2O and CO_2. These diagrams illustrate the different mineral assemblages found in different zones in the ultramafic rock.

Fig. 3.5 Photomicrographs of ultramafic rocks showing different prograde and retrograde disequilibrium mineral textures: (a). The appearance of olivine-forsterite-enstatite in the same thin section (as relicts phase?) marks the early peak metamorphic history of the rock, (b). Phlogopite corona around spinel marks the possible reaction between forsterite and spinel to form phlogopite, (c). Aligned phlogopite at the blackwall zone marks the major deformation fabric of the blackwall rock, (d). Poikiloblastic enstatite has numerous inclusions. Enstatite has commonly retrograde to tremolite, (e). Formation of retrograde tremolite along forsterite-forsterite grain boundaries. Also note the occurrences of late stage carbonate veins, (f). Reaction textures of talc after tremolite marks the fluid present retrogression of the rock.

Fig. 3.6 μK_2O-μSiO_2 diagrams at 850^oC/9kbar. The arrows indicate possible infiltration pathway of phlogopite formation at the blackwall zone. The diagram was calculated from PerPleX software (Connolly, 1990) using the thermodynamic database of Holland and Powell (1998).

Fig. 3.7 T-μK_2O diagrams at 9kbar. Activity corrected diagram suggest that phlogopite is stable in the temperatures above 800^oC, which corresponds to peak metamorphism of ultramafic rocks.

Fig. 3.8 Chemical potential diagram of μCaO vs μCO_2 showing a gradient of CaO and CO_2 at 750^oC/9kbar. The dark line indicates the existence of a chemical potential gradient during the formation of retrograde mineral assemblages (shaded area). The diagram was calculated from PerPleX software (Connolly, 1990) using the thermodynamic database of Holland and Powell (1998).

Fig. 3.9 T-μCaO diagram for the system CaO-MgO-SiO_2-H_2O-CO_2 calculated at 9 kbar. The retrograde assemblages of tremolite, dolomite and talc document the stability limit of 640-730^oC at X_{CO2} of 0.30. See text for more details.

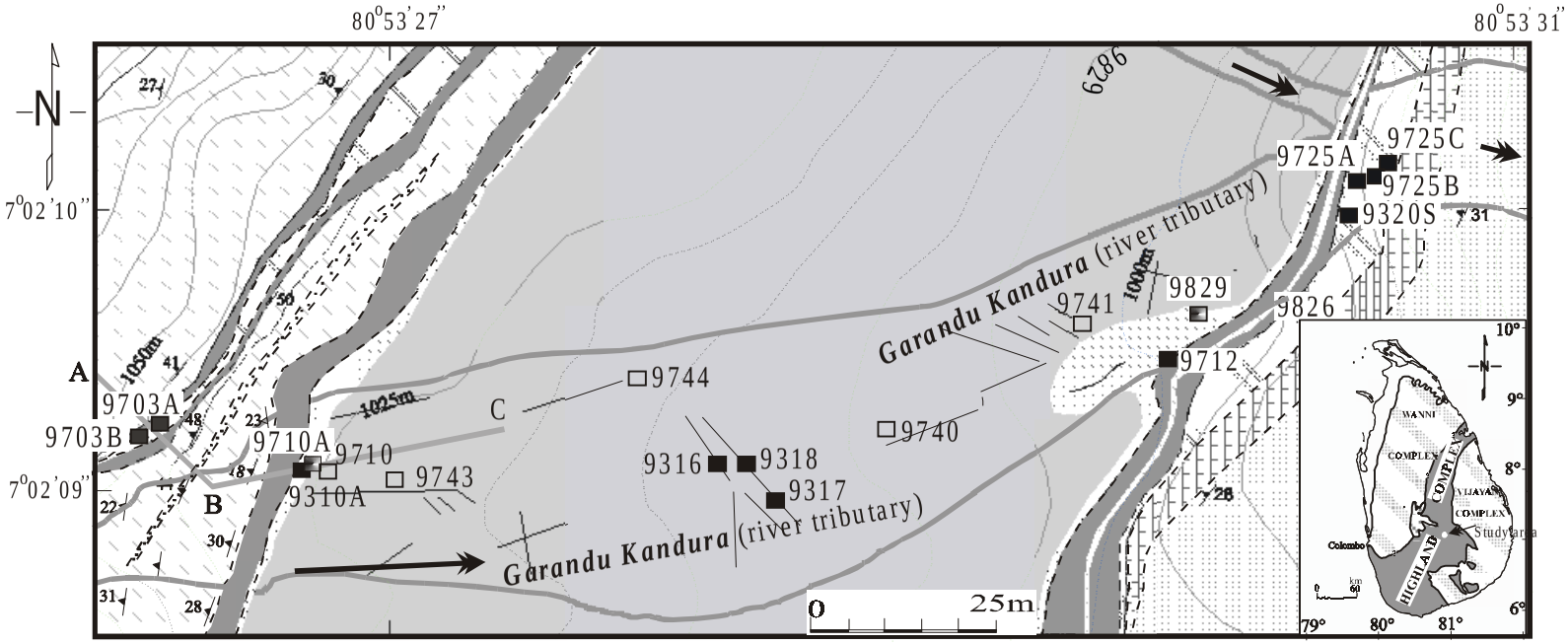

Ultramafic rocks

- Pale green rock (PG) with many late veinlets (CV)
- dark green rock (DG)
- phlogopite dominated rock (PC)

Reaction zone

- corundum-sapphirine-spinel-bearing rocks

Granulites

- charnockite and charnockitic gneisses
- garnet-biotite gneiss and some migmatized rocks
- impure limestones or calc silicate gneiss.

Structural Symbols

- Strike and dip of foliation
- Infered geological boundary
- Minor ductile shear zones
- Rivers & Tributaries
- Contours

Observed mineral assemblages

- Fo + Di + En + Tr + Atg + Dol (PG)
- Fo + Di + Phl + Spl + Fe-Oxd (DG)
- Fo + Di + Phl + Spl + Atg + Dol (BW)
- Fo + Tre + Tlc + Atg + Dol (CV)

Fig.3.1

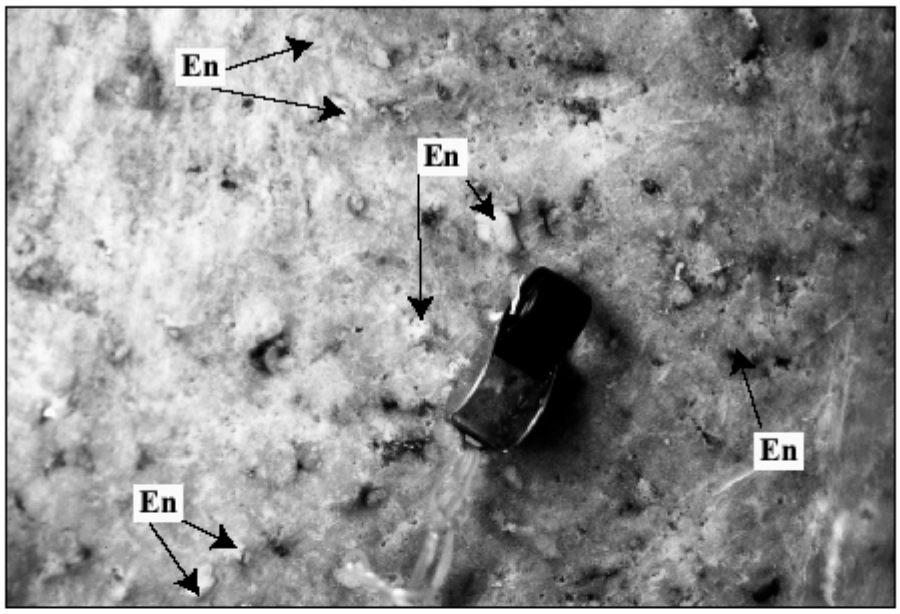

Fig. 3.2a

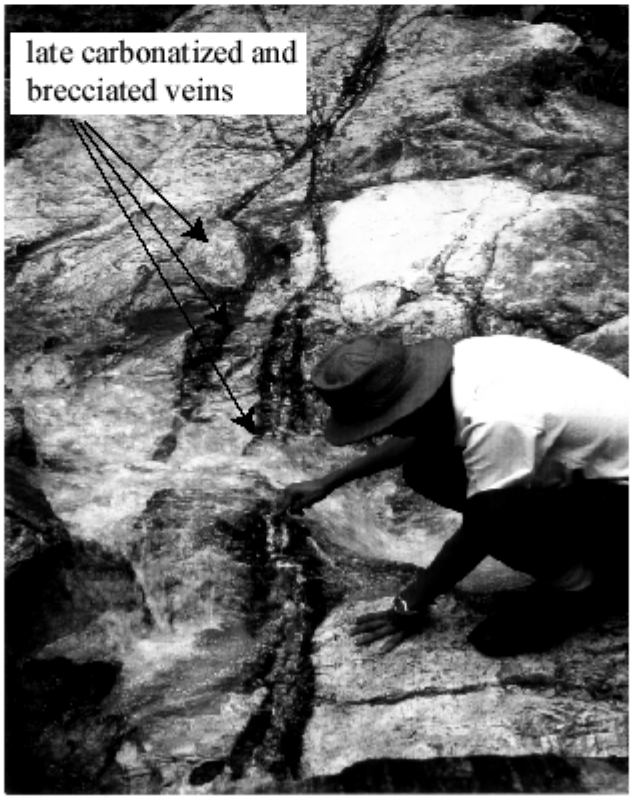

Fig. 3.2b

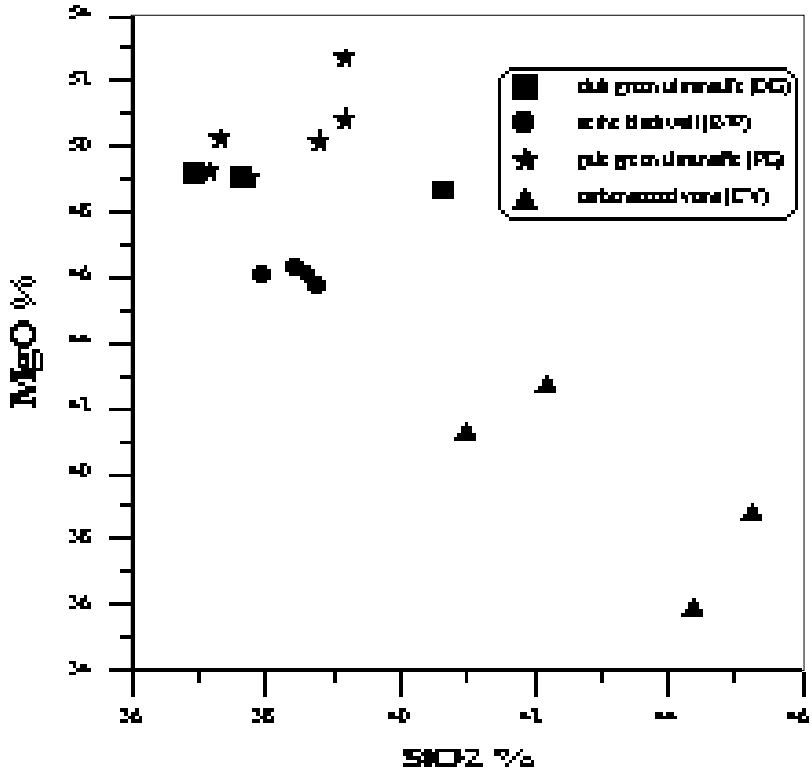

Fig.3.3a

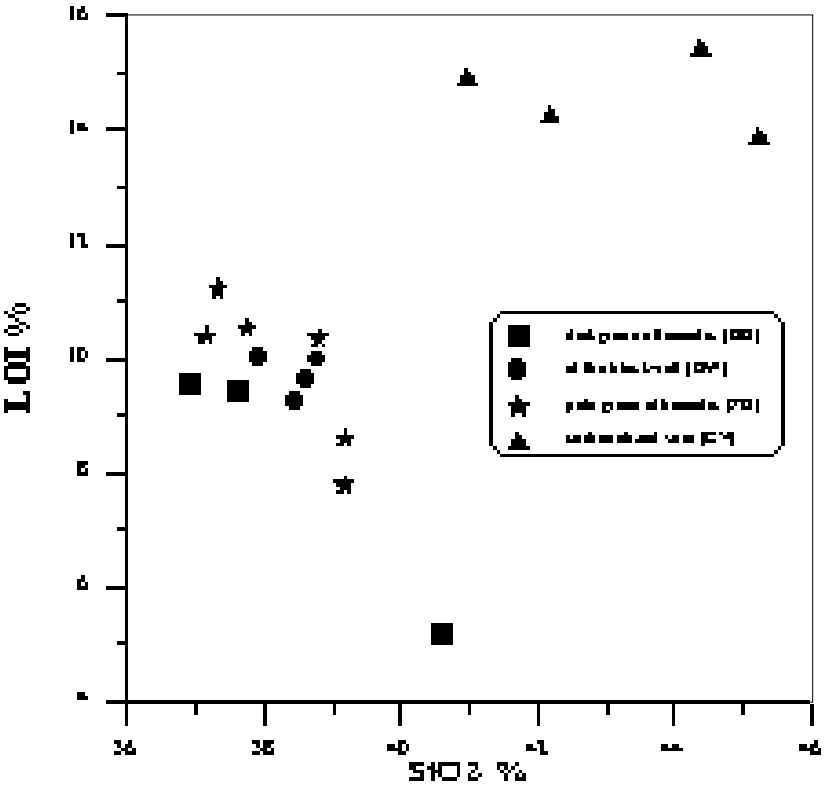

Fig.3.3b

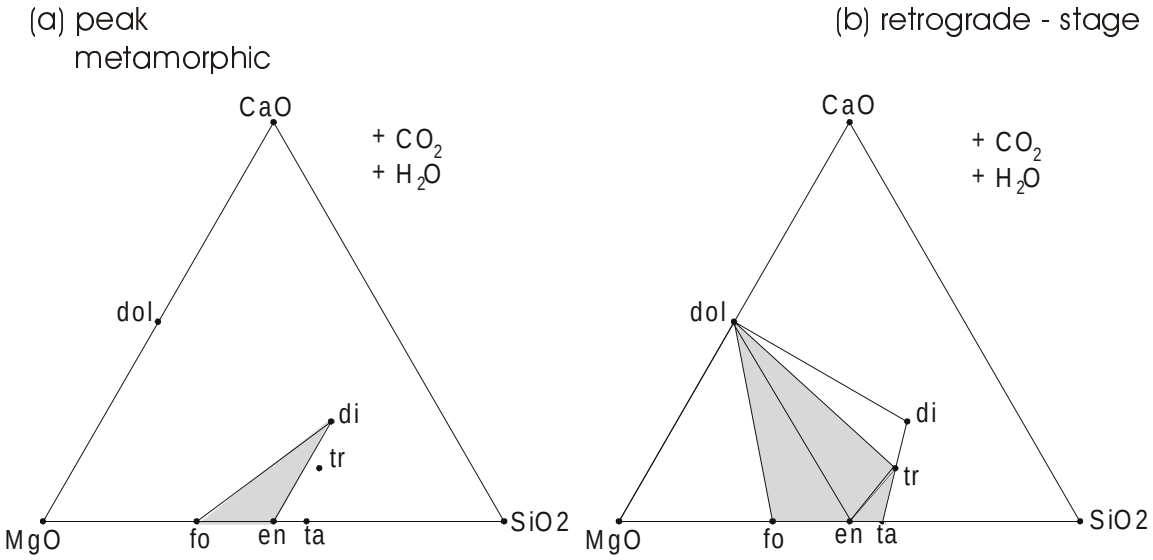
(a) peak
metamorphic
CaO
+ CO2
+ H2O
dol
di
tr
MgO
fo
en
ta
SiO2
(b) retrograde - stage 1
CaO
+ CO2
+ H2O
dol
di
tr
MgO
fo
en
ta
SiO2

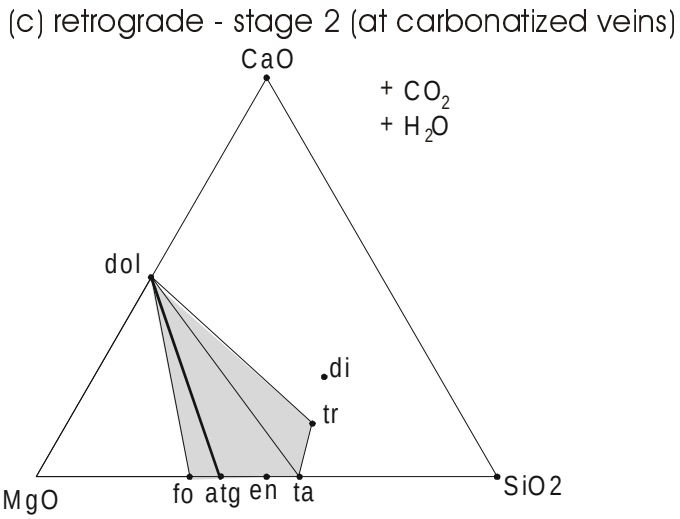
(c) retrograde - stage 2 (at carbonatized veins)
CaO
+ CO2
+ H2O
dol
di
tr
MgO
fo
atg
en
ta
SiO2

Fig. 3.4

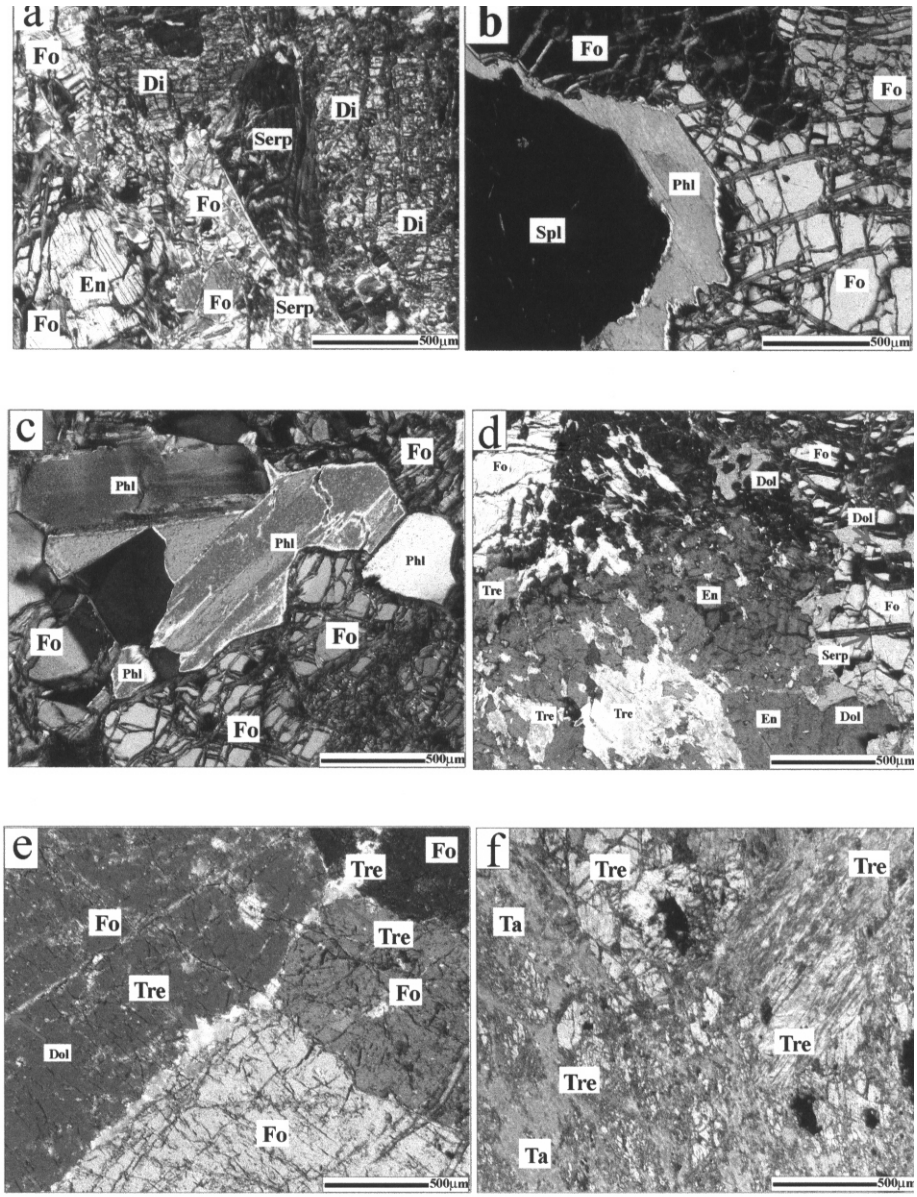
a
Fo
Di
Di
Serp
Fo
Di
En
Fo
Serp
Fo
500µm
b
Fo
Fo
Phl
Spl
Fo
500µm
c
Fo
Phl
Phl
Phl
Fo
Fo
Phl
Fo
500µm
d
Fo
Fo
Dol
Dol
Tre
En
Fo
Serp
Tre
Tre
En
Dol
500µm
e
Fo
Tre
Fo
Tre
Tre
Fo
Dol
Fo
500µm
f
Tre
Tre
Ta
Tre
Tre
Ta
500µm

Fig. 3.5

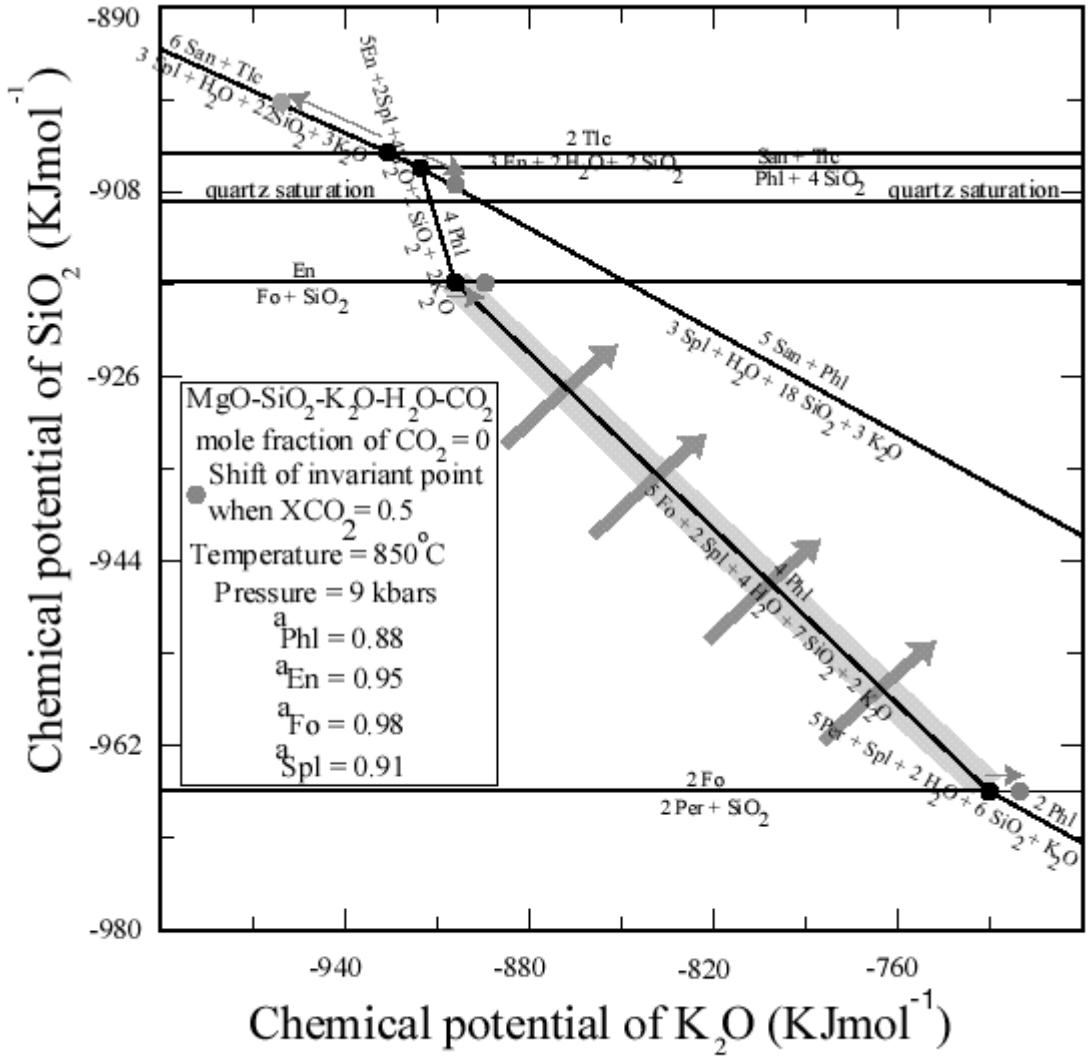
-890
-908
-926
-944
-962
-980
-940
-880
-820
-760
Chemical potential of SiO_2 (KJmol^{-1})
Chemical potential of K_2O (KJmol^{-1})
6 San + Tlc
3 Spl + H_2O + 22 SiO_2 + 3 K_2O
5En + 2Spl + H_2O + SiO_2 + K_2O
2 Tlc
3 En + H_2O + SiO_2
San + Tlc
Phl + 4 SiO_2
quartz saturation
quartz saturation
4 Phl
En
Fo + SiO_2
3 Spl + H_2O + 18 SiO_2 + 3 K_2O
5 San + Phl
MgO-SiO_2-K_2O-H_2O-CO_2
mole fraction of CO_2 = 0
Shift of invariant point
when XCO_2 = 0.5
Temperature = 850°C
Pressure = 9 kbars
a_{Phl} = 0.88
a_{En} = 0.95
a_{Fo} = 0.98
a_{Spl} = 0.91
5 Fo + 2 Spl + 4 H_2O + 7 SiO_2 + 2 K_2O
4 Phl
5 Per + Spl + 2 H_2O + 6 SiO_2 + K_2O
2 Fo
2 Per + SiO_2
2 Phl

Fig. 3.6

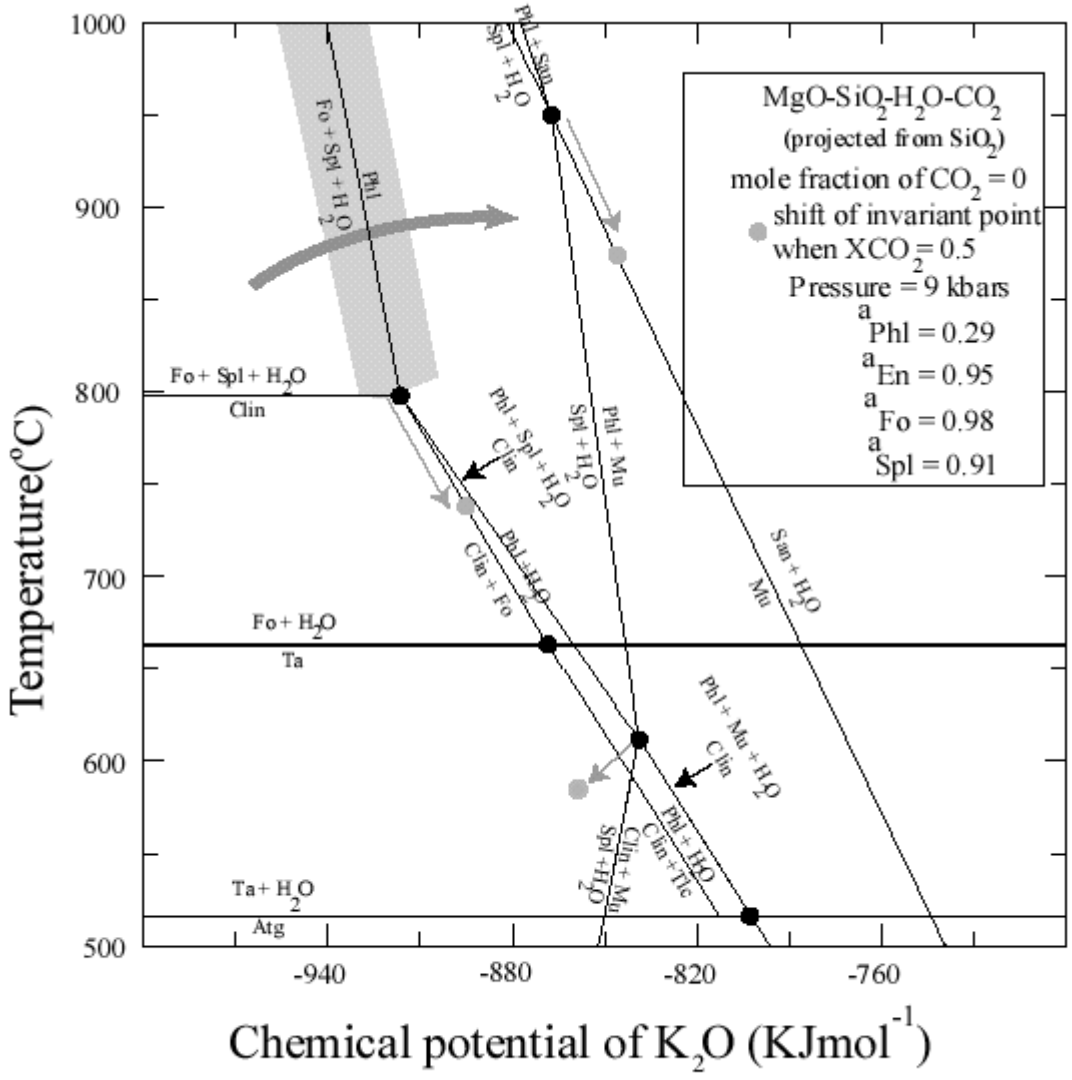
MgO-SiO2-H2O-CO2
(projected from SiO2)
mole fraction of CO2 = 0
shift of invariant point
when XCO2 = 0.5
Pressure = 9 kbars
aPhl = 0.29
aEn = 0.95
aFo = 0.98
aSpl = 0.91
Fo + Spl + H2O
Clin
Fo + H2O
Ta
Ta + H2O
Atg
Phl
Fo + Spl + H2O
Phl + San
Spl + H2O
Phl + Spl + H2O
Clin
Clin + Fo
Phl + H2O
Phl + Mu
Spl + H2O
San + H2O
Mu
Phl + Mu + H2O
Clin
Phl + H2O
Clin + Tlc
Clin + Mu
Spl + H2O
1000
900
800
700
600
500
-940
-880
-820
-760
Temperature(°C)
Chemical potential of K2O (KJmol-1)

Fig. 3.7

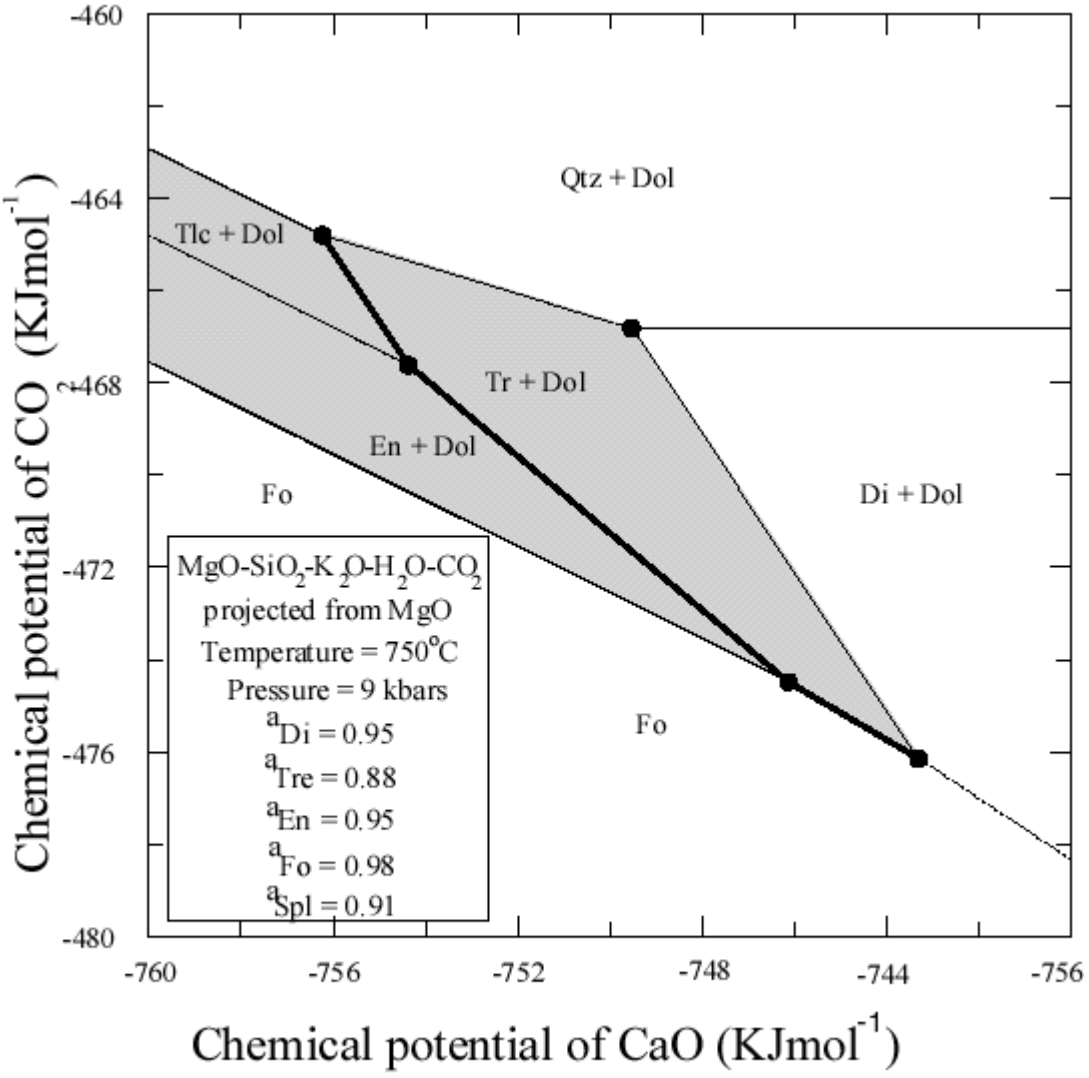
-460
-464
-468
-472
-476
-480
-760
-756
-752
-748
-744
-756
Chemical potential of CO (KJmol-1)
Chemical potential of CaO (KJmol-1)
Qtz + Dol
Tlc + Dol
Tr + Dol
En + Dol
Fo
Di + Dol
Fo
MgO-SiO2-K2O-H2O-CO2
projected from MgO
Temperature = 750°C
Pressure = 9 kbars
aDi = 0.95
aTre = 0.88
aEn = 0.95
aFo = 0.98
aSpl = 0.91

Fig. 3.8

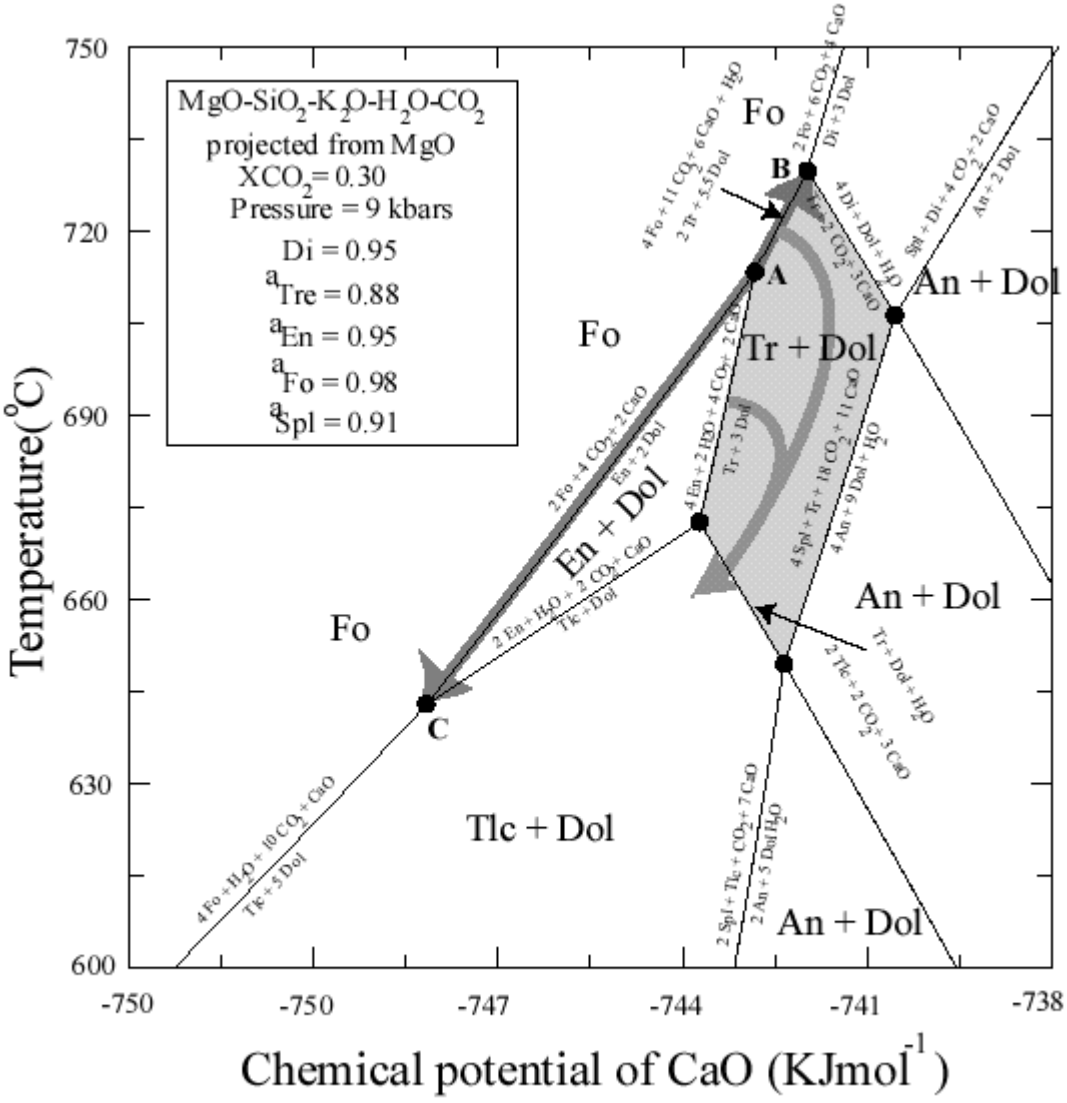
MgO-SiO2-K2O-H2O-CO2
projected from MgO
XCO2= 0.30
Pressure = 9 kbars
Di = 0.95
aTre = 0.88
aEn = 0.95
aFo = 0.98
aSpl = 0.91
Fo
Fo
Fo
En + Dol
Tr + Dol
An + Dol
An + Dol
An + Dol
Tlc + Dol
A
B
C
Temperature(°C)
Chemical potential of CaO (KJmol-1)
750
720
690
660
630
600
-750
-750
-747
-744
-741
-738

Fig. 3.9

Chapter 4

Genesis of silica-undersaturated sapphirine-corundum-spinel-bearing reaction zones from Rupaha, Sri Lanka

ABSTRACT

Field and petrological observations of ultramafic enclaves in granulites from 10 localities at Rupaha in the Highland Complex of Sri Lanka, place critical constraints on mass transfer mechanisms in the lower crust. Mineral reaction zones are observed at contacts between ultramafic rocks and siliceous granulites. The reaction zones developed between these units from ultramafic to siliceous granulites are: phlogopite + spinel + sapphirine, spinel + sapphirine + corundum and corundum + biotite + plagioclase. Spinel-sapphirine thermometry yields a temperature of 820 ± 40^{o}C, which is in agreement with the peak-temperatures recorded in the adjacent crustal granulites and ultramafics rocks.

The sequences of mineral zones, containing a variety of Al-rich, silica undersaturated minerals in the reaction zones separating the ultramafic rocks from the silica-rich rocks can be explained by a diffusion model. This involves the diffusion of Mg from ultramafic rocks across the layers, and K and Si diffuse in opposite direction. Chemical potential of Mg generated continuous monotonic gradient, allowing steady state diffusional transport across the profile. The strong enrichment in Al, and the considerable loss of Si, during the formation of reaction bands can be inferred from isocon diagrams. Some Al was probably added to the reaction zones, while Si was lost. This is most likely due to fluids percolating parallel to the zones at the boundary of the rock units. High temperature supercritical fluids, especially Chlorine and Fluorine, present in the pore spaces are also responsible for the transport of U and Th to- and LIL elements from the reaction zones.

INTRODUCTION

Studies of metasomatism during high-grade regional metamorphism have focussed attention on the mechanism of the mass transfer in the lower crust. Metamorphic fluids may act as a medium for mass transport (see also Fyfe et al. 1978; Ferry and Dipple 1991). The most striking example for metasomatism is the developing of distinct reaction zones (e.g. Korzhinskii 1970; Braddy 1977; Frisch and Helgeson 1984). The present paper discusses the constraints on the mechanism of mass transfer between enclaves of ultramafic rocks interbedded within thick layers of siliceous granulites at Rupaha, Sri Lanka. Several silica-undersaturated mineral assemblages containing spinel, sapphirine and corundum separate the ultramafic from granulites. Here, the fourth occurrences of sapphirine in the Sri Lankan Proterozoic basement is reported (Osanai 1989; Kriegsman 1991, Osanai et al. 1996; Kriegsman and Schumacher 2000). Formation of sapphirine in metasomatic zones has been reported in a few instances (Schumacher and Robinson 1987; Dunkley et al. 1999; Hokada et al. 1999).

Understanding of mass transfer for metasomatic processes for geologic systems requires information about mineral paragenesis, spatial distribution of minerals, relative abundances, and chemical composition of minerals and fluids. Here, we report data on the formation of reaction zones from field observations, lateral changes in mineral chemistry, chemical potential diagrams and mass balance. Variations of biotite chemistry and halogen contents in biotites in closely spaced samples of a complete profile (cross-section of ultramafic rocks, reaction zones and siliceous granulites) provide insight into fluid composition. These data permit calculation of the extent to which chemical components have been introduced, removed, and/or redistributed during metasomatism. The results suggest that reaction bands were formed during high-temperature and pressure. Diffusion most likely was the dominant mechanism of transport across layers, whereas significant Si leakage is proposed parallel to the layers.

REGIONAL GEOLOGY AND P-T EVOLUTION

The study area (Fig. 4.1) is located in the central part of the Highland Complex, which is also the part of Proterozoic belt in the Sri Lankan lower crust (Cooray 1994). The other important metamorphic units of Sri Lankan basements are the Wanni Complex and the Vijayan Complex. The Highland Complex shows a prolonged crustal history (~3.2 - 2.4 Ga). It consists of granulite facies rocks, as does the younger rocks from the Vanni Complex (~1.1 Ga) (Kröner et al. 1991; Milisenda et al. 1994). Evidence from the U-Pb system dates granulite facies metamorphism at ~610-550Ma (Bauer et al. 1991; Hölzl et al. 1994). The Vijayan Complex shows Amphibolite facies assemblages. Three major phases of structural events have been recognized (Berger and Jayasinghe 1976; Kriegsman 1993). The first event (D_{1a} and D_{1b}) are believed to predate peak metamorphic conditions, while the D_2 event is contemporaneous with peak PT. The D_3 is believed to form during the early retrogression.

Supracrustal sequences, consisting of marbles, garnet-sillimanite-graphite gneisses and qurartzites constitute about 50% of the HC terrane. The remainder of the terrane is composed of orthogneisses. Peak temperature was estimated to be between 760-830^{o}C at a pressure of 9-10kbar in the east and southeast part. Lower temperatures around ~700^{o}C/5-6kbar are indicated in the northwest (e.g. Faulhaber and Raith 1991; Schumacher and Faulhaber 1994). Schenk et al. (1988) and Voll et al. (1994) derived a maximum temperature of 900^{o}C for granulite assemblages from two-pyroxene and two-feldspar thermometry respectively. Metamorphic peak temperatures and pressures estimated from the rocks at Rupaha with two-pyroxene thermometry and garnet-clinopyroxene-plagioclase-quartz barometry, yield temperatures of 875 ± 20^{o}C and pressures of 9.0 ± 0.1 kbar respectively (chapter 2).

This study focuses on the region of ultramafic rocks that crop out as a series of discontinuous lenses and pods, enveloped by surrounding granulites at Rupaha. Lithological layering strikes 030-040^{o} and dips 20-40^{o} to west (Fig 4.1). In all mapped exposures, the strike is broadly parallel to regional foliation. The present orientation of lithological layering was that attained at the peak of the metamorphic event. Metasomatic reaction zones separate granulite rocks from those of ultramafic enclaves. Reaction zone sequences are repeated at least in 10 places in the area. The sequence is best exposed at the

river tributary named *Garandu Kandura* (Fig. 4.2). The thickness of reaction zones varies significantly from locations to location (10-150cm). The mineral assemblages and textural characteristics of the reaction zones are described in the following paragraph.

ANALYTICAL METHODS

The chemical composition of the various parts of the reaction zones relative to their original protoliths was used to evaluate the gain and losses of materials that occurred. Rock samples were taken from a traverse across the sampling points of 9805-9806 (Fig. 4.2 and Fig. 4.3), where the least altered samples can be found. Rock slabs were cut roughly perpendicular to main foliation from each sample. Thin sections were cut, so that profiles covering the entire samples were obtained. Nine samples from siliceous granulites, six from corundum gneisses and three each from the reaction zones were analysed for 34 elements and loss of ignition (LOI) at the XRF laboratory at the University of Mainz, Germany, using a PHILIPS PW 1404 spectrometer. Mineral analyses were performed with a JEOL microprobe (JEOL JXA 8900 RL) with 15kV voltage and a 12nA beam current with a beam diameter of 2μm. Elements were calibrated against synthetic and natural standards. Fluorine and chlorine were calibrated with Tugtupite, $Na_4AlBeSi_4O_{12}$(Cl, S) (7.58 wt % Cl) and F-phlogopite (9.20 wt% F). Online ZAF corrections were performed using the technique of Amstrong (1988, 1989).

PETROGRAPHY OF THE RUPAHA SPINEL-SAPPHIRINE-CORUNDUM OCCURRENCES

Two complete profiles of relatively fresh samples (profile 9805-9806, profile 9715-9311) were selected for petrographic study. A schematic diagram of profile 9805-9806 and a photograph of hand specimen of the reaction zone are shown in Figs. 4.3a and b. Different mineral zones were identified on the basis of mineral assemblages and textures. These zones depicted in the Fig 4.3a are shown in the insets labelled A, B, C and D. In each case, progressing from ultramafic to siliceous granulites the following mineral assemblages sequences occur:

(1)	En	Fo	Di	-	-	-	-	-	-	-	-	-	-	(*ultramafic rocks*)
(2)	-	Fo	Di	Phl	Spl	-	-	-	-	-	-	-	-	(*ultramafic rocks*)
(3)	-	-	-	Phl	Spl	Spr	-	-	-	-	-	-	-	(*zone A*)
(4)	-	-	-	Phl	Spl	Spr	Crn	-	-	-	-	-	-	(*zone B*)
(5)	-	-	-	-	-	-	Crn	Pl	Bt	-	-	-	-	(*Crn ~30%)(zone C*)
(6)	-	-	-	-	-	-	Crn	Pl	Bt	-	-	-	-	(*Crn ~ 5%)(zone D*)
(7)	-	-	-	-	-	-	-	Pl	Bt	Qtz	Kfs	-	Sil	(*siliceous granulites*)
(8)	-	-	-	-	-	-	-	Pl	Bt	Qtz	Kfs	Cpx	Grt	(*siliceous granulites*)

(for abbreviations see: Kretz 1983)

Ultramafic rocks

The peak metamorphic mineral assemblages in the ultramafic rocks is presented by forsterite + diopside + enstatite (Fig. 4.4a). Olivine is the dominant phase, which contains about 65% of mode (without alteration). Many of olivine grains have been altered to serpentine. Thin bands of ultramafic rock neighbouring the reaction zone contain a significant amount of phlogopite, which often exhibit a planar fabric (e.g. RU 9310A in Fig 4.1). The width of this zone is about 10-50 cm. These rocks are composed of predominantly olivine with about ~12% of phlogopite modal, and traces of spinel and diopside (<1%)(Fig 4.4b).

Phlogopite- spinel-sapphirine zone (zone A)

The contact between the ultramafic country rock and the Phl + Spl + Spr bearing zone A is sharp but lobate. Aligned phlogopites are interlocked with spinel and sapphirine (Fig. 4.4c). Sapphirine replaces phlogopite in this zone.

Spinel-sapphirine-corundum zone (zone B)

Corundum + spinel + sapphirine mineral assemblages are common in zone B. First appearance of corundum marks this zone. Corundum coexists with spinel and sapphirine. Sapphirine grains are colourless, and anhedral (Fig. 4.4d). Phlogopite occurs in this zone only as rounded grains or as relicts in sapphirine. In contrast to the neighbouring zone, the

rocks occurring in the zone B are usually massive and lack any preferred mineral orientation.

Corundum- biotite-plagioclase zone (zone C)

Zone c is characterized by an abundance of samples containing plagioclase + corundum + biotite (Fig. 4.4e). Sapphirine is absent within this zone. Biotite is iron rich because biotite is in dark coloured in hand specimen. Plagioclase is commonly twinned. Biotite, corundum and plagioclase have subequal modes (~30% each).

Corundum- gneiss zone (zone D)

Zone D is the same as zone C in terms of the mineral assemblages, but the mineral modes and the degree of alteration is quite different. Plagioclase is volumetrically dominant over corundum and biotite (mode Pl ~80%, Crn ~5%, Bt ~10%). The zone is usually wider than other mineralogical zones and characterized by barrel-shaped corundum crystals (2mm-1cm), embedded in white coloured plagioclase matrix. Corundum crystals are not of gem quality. They are often surrounded by biotite flakes. Secondary chlorite is present as fine-grained, un-oriented crystals, as well as intergrowths with fine-grained muscovite, which appears to replace corundum. Here, diaspore occurs as vein fillings in corundum. Fibrolitization of biotite is advanced in many specimens within the zone D.

Siliceous granulites

Garnet-biotite-clinopyroxene-bearing gneisses (sample No.9708 in Fig. 4.1) are coarse-grained, dark coloured and display a strong schistosity (see Fig. 2.2a in chapter 2). Assemblages are typically Grt + Bt + Pl ± Ilm; Grt + Bt + Cpx + Pl ± Qtz ± Ilm; Grt + Cpx + Pl ± Qtz ± Ilm. Sillimanite-biotite gneisses in this zone are intercalated in thin bands (Fig. 4.4e). See chapter 1 for more details.

MINERAL CHEMISTRY

Compositions of the minerals in the reaction bands are presented in Table 4.1. The site distribution of cations in sapphirine, spinel, corundum, plagioclase and biotite was calculated assuming perfect stoichiometry.

Sapphirine

Sapphirines are fairly rich in X_{Mg} [=Mg/(Mg+Fe)] content, ranging 0.978-0.986. Along the traverse, X_{Mg} content is slightly higher in zone A than zone B. The colourless nature of sapphirine is due to high Mg content. Along the traverse from zone A to zone B, the Al content increases slightly (Table 4.1a). In general, actual sapphirines are more aluminous than the theoretical end-member $Mg_4Al_8Si_2O_{20}$ (2:2:1), due to $Si^{[4]}Mg^{[6]} = Al^{[6]}Al^{[4]}$ substitution. This substitution allows the composition of $Mg_7Al_{18}Si_3O_{40}$ (7:9:3) for sapphirine at Rupaha.

Spinel

The analysed spinel composition belongs to spinel-hercynite solid solution with X_{Mg} varying from 0.962-0.965 (Fig.4.1.a). Al content in spinel is always high, which ranges from 15.95-16.07pfu. No systematic variation in elements was observed across the reaction zones.

Corundum

Corundum is found in zone B, C and D are nearly pure phases, but contain few amounts of Fe (0.0015-0.0025 pfu) (Table 4.1b). Ti and Cr contents are insignificant in all zones.

Plagioclase

Plagioclase in zone C is more anorthitic (An_{86-91}) than that of zone D (An_{31-37}) (Table 4.1c). Si and Al contents of plagioclase have reciprocal variations between both zones because the high Al and low Si content were measured from zone C.

GROWTH OF THE MINERAL ZONES

Forsterite + spinel in the ultramafic zone, together with the presence of sapphirine + spinel in the neighbouring zone A suggest that forsterite is replaced by sapphirine, which was in turn replaced by corundum in zones B and C. Formation of sapphirine from ultramafic rocks obviously requires the addition of SiO_2 and the removal of MgO. The relative decreases of Mg-bearing minerals from ultramafic-bearing rocks to siliceous granulites through zone A to D mark the lateral variation of bulk chemistry across the reaction zones.

Several textural features of the reaction zones examined give evidence for metasomatic transport. Among those that place constraints on metasomatic development are, the sharp contacts that exist between mineral zones and the presence of relatively few mineral phases in each zone (e.g. Thompson 1959; Korzhinskii 1970; Fischer 1973, 1977; Braddy 1977; Joesten 1977).

The purpose of the following part is to present the physical conditions, the nature of metasomatism and its quantitative estimate of mass transfer. Quantitative chemical potential diagrams illustrate differences in chemical potential between siliceous granulites and ultramafic rocks. Quantitative mass transfer of elements is calculated from mass balances using isocon technique. The variation of some elements in biotites including halogens from siliceous granulites to ultramafic rocks across the reaction zones were studied in order to find further constraints of fluids composition. The biotite chemistry can also be used as monitors of fluid composition during metasomatic processes.

PHYSICAL CONDITIONS OF METASOMATISM -TEMPERATURE ESTIMATES

The empirically derived Fe-Mg exchange thermometer for co-existing spinel-sapphirine assemblages (Owen and Greenough 1991) was used to evaluate the temperatures during the formation of reaction bands. The geothermometer yields a temperature of 820 ± 40^{o}C, assuming a pressure of 9kbar. This pressure corresponds to the peak pressure recorded by the Grt-Cpx-Pl-Qtz barometry in the surrounding granulites (Chapter 2). The temperature obtained agrees well with the maximum temperature recorded in these granulites of 875 ± 20^{o}C (Chapter 2). Ultramafic rocks yielded a temperature of 842 ± 68^{o}C (Chapter 3). The mineral chemistry data used for the temperature estimates are presented in Table 4.1a.

The stability field of sapphirine-spinel-corundum assemblages is shown in a chemical potential diagram of MgO (μMgO)(Fig. 4.5). The activity corrected T-μMgO diagram is calculated for the system MgO-Al_2O_3-SiO_2-H_2O-CO_2 at 9kbar condition and assuming X_{CO2} = 0, using the thermodynamic database of Holland and Powell (1998). The activity models for spinel and sapphirine are those of Holland and Powell (1998). The shaded area marks the stability field of sapphirine. The assemblage spinel-sapphirine-corundum occurs together at temperatures above 780^{o}C. The grey area in Fig.4.5 was calculated for the X_{CO2} = 0.5. The stability field of sapphirine extends towards the lower temperatures (725^{o}C).

Nevertheless, the phase petrology agrees with reaction bands forming at high temperatures close to peak, granulite facies conditions.

Thermometry and T-μMgO diagrams provide a reasonable estimate of 850^{o}C for co-existing spinel-sapphirine-corundum assemblages at reaction zones. The pressure estimates of 9kbar in the surrounding siliceous granulite are taken as the reference pressure for the following calculations.

CHEMICAL POTENTIAL DIAGRAMS

Equilibrium phase relations among pertinent minerals are shown in the Fig. 4.6 for the system Al_2O_3-SiO_2-MgO-H_2O at 850^{o}C, 9kbar fluid and solid pressure, and a_{H2O} of 1. The univariant boundaries and saturation limits were calculated with the thermodynamic database of Holland and Powell (1998). The activities of sapphirine and spinel were also calculated from the same database.

It can be seen in Fig 4.6 that spinel and forsterite are stable at high potential of MgO at low SiO_2 potential. Note that the enstatite-spinel stability field terminates against the spinel-sapphirine with increasing SiO_2 potential. The further increase in potential of SiO_2 is marked by the appearance of corundum and sapphirine. Sillimanite and quartz occupy a relatively high SiO_2 potential with low MgO potential. This latter assemblage is seen in the siliceous granulites. It is obvious from the Fig 4.6 that the two contrasting rock types show strong chemical potential gradients in MgO and SiO_2. The components MgO and SiO_2 will start migrating to eliminate these gradients. As a result, the new minerals corundum and sapphirine are formed in the intermediate zones. The gradient of the chemical potential of MgO and SiO_2 changes abruptly at the boundaries of all the mineral zones. The dark line was drawn in the Fig. 4.6 to approximately a steady-state diffusional transfer of material to and from the parent rocks. The mass transfer of components across lithological boundaries at Rupaha can be accomplished through diffusion (Korzhinskii 1970; Braddy 1977; Rumble 1982).

MASS BALANCE CALCULATIONS

Methods and assumptions

The extent to which components were added to, or removed from a zone during the formation of the metasomatic zones can be assessed with the aid of mass balance calculations (Gresens 1967; Grant 1986; Baumgartner and Olsen 1995). The interpretation of mass balance calculations has been a major problem in many recent studies (e.g. Grant 1986; Baumgartner and Olsen 1995). Possible reference frames have to be assumed, e.g. one can assume constant volume or one can assume immobility of one (or more) components. The isocon method (Grant 1986) is a graphical representation of Gresens' method (1967), which was originally developed to determine the mobility of elements in the metasomatized rocks. Grant (1986) expressed the composition–volume equation as a linear relationship. Hence, for immobile components, the ratio of the concentrations in the original to altered rock concentration is constant, yielding a straight line, the isocon line. Baumgartner and Olsen (1995) introduced a statistically more rigorous least-square approach to the isocon method. An algorithm was presented to identify the immobile elements, with uncertainties, as does in our calculations. For a further discussion of the mathematical treatments and problems of mass balances see Gresens (1967), Grant (1986) and Baumgartner and Olsen (1995).

Elements with low-solubility are typically assumed to be immobile during an alteration process (Ague 1991; 1994; MacLean and Barrett 1993; Roser and Nathan 1997). This argument is based on experimental determination of solubility of such elements (Baumgartner and Eugster 1988; Ayers and Watson 1991, 1993). For summary see Eugster and Baumgartner (1987). Elements commonly assumed to have low mobility in rocks during the alteration and deformations include Al, Ti and high field strength elements (HFSE) such as Y, Zr, Nb, Hf and Ta (Grant 1986; Kerrich et al. 1987; Glazner and Bartley 1991; Marquer and Burkhard 1992). Although Al and Ti are widely believed to be relatively immobile in many geologic environments, there are many cases where one or both were mobile in the tectonic environments (Yardley 1977; Kerrick 1988; O'Hara 1989; Gieré 1990a, 1990b; Selverstone et al. 1991). The proven mobility of these elements under the appropriate fluid composition and PT conditions show that no element can be considered as immobile. Nevertheless, if several elements considered being immobile define on isocon line, this lends support for their respective immobility. The composition

of original protoliths is also a problem, because the true protolith no longer exists. However, the petrologic and field evidence presented earlier suggests that the siliceous granulite were the protolith for the reaction zones. Mass balance calculations have been done for alteration of this parent to; (a) corundum gneiss (5% Crn) (zone D), (b) corundum-biotite gneiss (30% Crn) (zone C) and (c). spinel-sapphirine-phlogopite gneiss (zone A). The compositional data in Tables 4.2a, b, c and d were used to evaluate mass transfer. A one-sigma confidence interval was chosen to account for a reasonable uncertainty in the element concentrations. By identifying all combinations of overlapping cone areas in the isocon plot, all possible compatible element combinations were obtained with the Program 'ISOCON 4.2' (Baumgartner and Olsen, 1995). At this point, geochemical considerations are introduced for the modelling. The mobility of Al and Ti deserves special attention when selecting the best-fit immobile element combination. It should be noted that neither Al nor Ti would fit into the same isocon in any of three alterations. This indicates either Ti or Al is mobile during the formation of reaction bands. The isocon combination that includes Al has more elements immobile. The light rare earth elements (LREE) of La, Ce, Pr, Sm and Nd are also colinear with Al in many combinations. On the other hand, the LREE results are less systematic than those for major and minor elements. The wide variations of LREE are probably due to analytical uncertainties due to limited sample size.

We selected isocon (65), which includes the elements Al, Nb, Hf, Ta, Pr, Nd and Sm, all considered to be relatively immobile (Table 4.3a). Isocons in Figs. 4.7b and c are mainly based on Ti, Zr and Hf, which show excellent linear arrays (Tables 4.3b, c). Lanthanum, Ce and Sm are also considered to be as immobile. Similar immobility of the combination of Ti, Zr and Hf in theses environments has also been suggested by Kerrich et al. 1987. Therefore, the element combination (61) would be the best-fit isocons for the alteration to zone C and zone A. (Tables 4.3b, c). It is interesting to note that all isocon diagrams show similar geochemical trends in Si, Mg, LREE, U, and Th, reflecting systematic element mobility of these elements (Figs. 4.7a, b, c).

Mass balance- interpretation

The geochemical trend for the mass transfer of major and minor elements is illustrated in Fig. 4.8a and 4.8b. Mass losses, particularly the depletion in Si, LIL elements (Ba, Na, K,

Rb, Pb etc.) are inferred. In each of the zone, the materials gained gneisses include Mg, Al, U, Th and volatiles. In particular, a substantial loss of Si during the formation of reaction promoted the formation of silica-undersaturated minerals like corundum and spinel. Zones that consist corundum are characterized by absolute gains of 30 to 50 weight percent of Al (Fig. 4.8a). The mass gain of Al in the zone A is comparatively lower than those of zone C. This is because of the presence of sapphirine and spinel in the expense of corundum in zone A. The enrichment of Mg in the Zone A and C correlates with the presence of Mg-bearing minerals such as spinel and sapphirine. The fact, that elements like U, Pb are extremely enriched during the alteration, could be due to enrichments of some accessory minerals like monazite or alternatively, since these minerals have very low concentrations, this might reflect the sample volumes. The alteration to zone D from gneisses is accounted for a weight loss of 27 ± 7% while alteration to zone C and A have minor overall mass changes (~5-10%).

In summary, all rocks were metasomatically altered under conditions of volume reduction. The increase of Al requires introduction of aluminum from outside the system, since ultramafic rocks cannot provide it. Such additions may have occurred by local redistribution from neighbouring lithologies and/or introduction as a hydrothermal solute.

HALIDE COMPOSITION OF FLUIDS

Fluorine and chlorine are ubiquitous in fluids from all crustal levels, because they are incorporated into main common rock forming minerals such as amphiboles, micas or apatite. The presence of halogen-bearing fluids can easily be monitored and their abundance in metamorphic fluids can quantitatively be estimated (see also Munoz and Ludington 1974; Munoz and Swenson 1981; Munoz 1984; Zhu and Sverjenski 1991, 1992; Finch 1995; Finch et al. 1995; Markl and Bucher 1998). As fluids are involved in most magmatic and metamorphic events, the halogens are rendered powerful tools for the understanding of fluid evolution (Boudreau and McCallum 1989; Kullerud 1995, 1996; Markl and Schumacher 1996). Mineral-fluid equilibria used for models of any crustal processes depend on the composition of co-existing fluid. Results of the various studies show that (e.g. Touret 1985; Mora and Valley 1989), in some high-grade metamorphic terranes chlorine species should be taken into account in addition to typically modelling

H_2O-CO_2 binary mixture. Chlorine species have a profound effect on the H_2O activity. Hence, detailed knowledge of the abundance of the chlorine in fluids is necessary to allow precise modeling and it can help to decipher the progress of metamorphic reactions as well as the sources of fluids encountered in regionally metamorphosed terranes.

The fluid evaluation from the composition of halogen-bearing minerals in high-temperature metasomatic systems is less well studied. This part reports chemical analyses of F and Cl-bearing biotites in the reaction zones at Rupaha with its neighbouring siliceous granulites and ultramafic rocks. The focus of this part is placed on the changes of composition of biotite and the effect of halides in fluids contemporaneous with the high-temperature metasomatism.

Samples were chosen to provide a representative selection of each zone. Approximately 170 biotite grains, ranging along the profile ultramafic rocks, through the reaction zones to the siliceous granulites were analysed. Nearly all biotite grains show no alteration to chlorite. Error bars for biotite analyses, which represent the 1σ standard deviations, are presented for each analytical point. The chemical compositions of biotites from the siliceous granulites to ultramafic rocks studied are given in Table 4.4. The biotite formula was calculated on the basis of 22 oxygens. The chemistry of biotite was plotted against the distance from the rock in order to demonstrate the variation with the different rock types (Fig 4.9). Average values (given as stars in Fig.4.9) and 1σ standard deviation are given for each set of analysis from a section or zone. The chemical compositions of biotites are given in Tables C6 to C11 in Appendix. Biotite formulas were calculated on the basis of 22 oxygens, excluding H_2O.

Element variations in biotite

The element variation pattern in the tetrahedral position of biotite from siliceous granulites shows a trend of decreasing of Si towards the reaction zones, and subsequently increasing towards the ultramafic rocks (Fig 4.9a). Aluminum replaces it there, showing reciprocal relationship with Si (Fig. 4.9b). Note that biotites in the silica undersaturated reaction zones have excess Al to put into octahedral position while no excess Al is observed either in siliceous granulites or ultramafic rocks (Appendices C6-C11). (The site allocation method assumes complete filling of tetrahedral site by Si, then Al - theoretically 8 atoms

per 22 oxygens- The rest of Al atoms are assigned to octahedral positions). The dashed lines in each diagram denote the polynomial fits for chemistry of the particular elements.

The Mg and Fe concentrations in mica are a strong function of location. Biotites in ultramafic rocks are nearly pure phlogopites. X_{Mg} systematically decreases towards the siliceous granulites (Fig. 4.9c). The majority of the variation in biotite in the octahedral position comes from differences on the Fe and Mg contents (Fig .4.9d). Ti decreases, while Mg increases (Fig .4.9e). The evaluation of the biotite stoichiometry indicates that the substitutions preferably take place by the Tschermaks or Ti- Tschermaks substitution (Guidotti et al. 1977; Dymek 1983; Spear 1993).

The F-content of biotite first decreases and then increases towards the ultramafic rocks (Fig. 4.9f). In all cases, except siliceous granulites, biotite shows strong Fe-F avoidance. The extremely high F content at the ultramafic-reaction band interface is due to characteristic heterogeneous F- activity in fluids. The thin section evidences also support the idea for the formation of biotites from forsterite and spinel at the contacts with sufficient fluid activity (Fig. 4.4e see also Chapter 3). This suggests that the F contents of biotites of the present study have two controls: (1) strong structural control which is responsible for Fe-F avoidance, and (2). The activity of F in the fluid with, which the biotite last equilibrated.

The chlorine content of biotite is low and insignificant when compared to Fluorine. However, the high chlorine content is observed in the granulites (Fig. 4.9f). It ranges from 0.08-0.12 atoms pfu in the granulites while 0.03-0.06 atoms pfu is measured in the ultramafics.

Estimate of chloride content in fluid

The chlorine content of biotite can be used to calculate the composition of the chlorine content of the fluid phase, if assumed, that it is in local equilibrium with the aqueous fluids (e.g. Munoz 1984; Zhu and Sverjensky 1991; Robert et al. 1993; Kullerud 1995, 1996). Experimental studies on the partitioning of halogens between mica and fluids show that the amount of Cl in biotite is a strong function of fluid composition, temperature and pressure and Fe, Mg concentrations (e.g. Munoz and Ludington 1974; Munoz and Swenson 1981;

Munoz 1984; Aksyuk and Zhukovskaya 1994). Zhu and Sverjensky (1991, 1992) developed a method to calculate the activity of HCl^o in aqueous fluids. Assuming unit activity of water in the system, one can calculate the activity of HCl^o of the fluids during biotite crystallization. Once the HCl^o concentration of aqueous fluids is known, the speciation and metal ion concentration of the supercritical fluids can be calculated at the temperature and pressure of interest (Wolery 1979, 1983; Eugster and Baumgartner 1987).

The Gibbs free energy for the reaction involving a partitioning of OH-biotite to Cl-biotite were calculated using thermodynamic properties for OH end member components from Berman (1988, 1990) with adjustment of free energies according to Sverjenski et al. (1991), and for Cl end member components from Zhu and Sverjenski (1991). Heat capacities, molar volume and entropy are taken from Zhu and Sverjenski (1991) and references therein (Table 4.4). The thermodynamic database are said to be internally consistent and therefore used for our calculations (for more details see Zhu and Sverjenski 1992).

The total of 21 analyses of biotite from siliceous gneisses and 58 from ultramafic equivalents was used for calculations (Appendix Tables C6, C11). The number of cations in the biotite formula was calculated on the basis of 22 oxygens. We assumed ideal mixing of F, Cl and OH in the hydroxyl site in mole fraction calculations.

Zhu and Sverjensky (1992) used experimental results of previous studies to calculate the slopes of the reaction (1) for different temperatures.

$$\log\left(\frac{X_{Cl}}{X_{OH}}\right)=\frac{1}{2}\left(\frac{\Delta G_R^o}{2.303RT}\right)X_{Mg}+\frac{1}{2}\log K-\log\left(\frac{a_{H2O}}{a_{HCl}}\right) \qquad (1)$$

The calculated average slope of -0.46 at 850°C for the Rupaha rocks matches well with the predicted value of Zhu and Sverjensky (1992) at 850°C (see Fig.10b of Zhu and Sverjensky 1992). The plot of $\log(X_{Cl}/X_{OH})$ against the X_{Mg} from biotites at Rupaha is shown in Fig. 4.10. The dotted lines denote the slope of –0.46, which is calculated at 850°C. The diagram shows that the fluid compositions at the grain boundaries of the reaction zones are in equilibrium with the neighbouring precursor rocks. For example, biotites at the boundary of zone D record fluid compositions similar to that of the siliceous

granulites while boundary of zone A is similar to that of ultramafic rocks. The average $\log(X_{Cl}/X_{OH})$ and X_{Mg} values of biotites from pelitic and ultramafic equivalents are provided in Table 4.5. The logarithms of the activity of HCl for the siliceous granulite are calculated as –3.6 while an activity of a_{HCl} of –3.5 was calculated for the ultramafic rocks. It shows that the HCl activities in fluids in the two rock types are equal within the error of determination.

SUMMARY AND CONCLUSIONS

Conditions of metamorphism and metasomatism

The field and petrologic observations suggest that the reaction bands associated with siliceous granulites and ultramafic rocks at Rupaha formed by diffusional transport between the two chemically different rock types. The reaction bands are comprised of silica undersaturated corundum, sapphirine and spinel assemblages. The ion-exchange thermometry provides an estimate of 820 ± 40^{o}C for coexisting spinel and sapphirine at 9 kbar. This observation, together with T-μMgO diagrams suggest that reaction bands too are formed during high temperature granulite facies metamorphism. Mg contents and low X_{Fe}, together with low SiO_2 and high Al_2O_3, in the Rupaha reaction zones provide appropriate geochemical conditions for sapphirine formation.

Mechanism of metasomatism

The zoned sequence can be well illustrated by an activity diagram of SiO_2 vs MgO. The reaction bands formed primarily due to Mg and Si metasomatism. Chemical potential of Mg generated continuous monotonic gradient across the profile, allowing steady state diffusion. This agrees with a dominant transport by diffusion.

Major and trace element concentrations provide quantitative constraints on element mobility. Mass gains, particularly the enrichment in Al, and the considerable loss of Si, during the formation of reaction bands are inferred from isocon diagrams. Ti, Zr and Hf behaved isochemically in most zones. The diffusional transport of elements over more than centimetre distances is permitted with the presence of fluids in the system. It is most likely that a fluid phase pervaded the grain boundaries sufficiently to provide an interconnected network through which diffusion could occur. The concentration of the fluids in the system

is known from the biotite chemistry. High temperature supercritical fluids are responsible for carrying U and Th to and LIL elements from the rocks. The absence of a pervasive fluid flux during the formation of reaction bands was probably the most important condition for development of these textures and geometry, allowing them to be controlled by diffusive transport. The idea is also supported by the presence of element variation in biotite across the profile. The reciprocal relationship of Si and Al in the reaction zones are illustrated. The gain of Al and losses of Si at the reaction zones do not fit with the simple bi-metasomatic process. It is most likely that the introduction of Al-rich fluids into these rocks and leaking of Si along sub parallel channels, most likely along the foliation planes, while Mg is diffused across the layers resulted, in metasomatic reactions bands.

This study uses the reaction zones formed in the granulite-ultramafic contact at Rupaha to derive information about mass transport in high-grade granulites. These reaction zones are formed by diffusion-controlled reaction mechanisms that develop during peak metamorphism. This study has shown that not only pressure and temperature conditions but most importantly P_{H2O} and the concentration of the aqueous fluids also control the diffusion of the elements in different geological environments. Therefore, nature and reaction kinetics of supercritical fluids during the high-temperature metasomatism should take into account in mass transfer calculations.

REFERENCES

Ague JJ (1991). Evidence for major mass transfer and volume strain during regional metamorphism of pelites. Geol. 19: 855-858

Ague JJ (1994). Mass transfer during Barrovian metamorphism of pelites, south-central Connecticut. I: Evidence for changes in composition and volume. Am. J. Sci. 294: 989-1057

Aksyuk AM, Zhukovskaya TN (1994). Experimental calibration of the phlogopite fluorimeter at 500-700^{o}C and 1-4 kbar, and estimated HF concentrations of fluids associated with marbles: some examples. Geochim. Cosmochim. Acta. 58: 4305-4315

Armstrong JT (1988). Quantitative analyses of silicate and oxide minerals: comparisons of Monte Carlo, ZAF and Phi-rho-z procedures. In: Microbeam analysis (*Newbury DE* ed). -1988, San Francisco Press, San Francisco, 239-246

Amstrong JT (1989). CITZAF: combined ZAF and phi-rho (Z) electron beam correction programs. California Institute of Technology, Pasadena, CA

Ayers JC, Watson EB (1991). Solubility of apatite, monazite, zircon and rutile in supercritical aqueous fluids with implications for subduction zone geochemistry. Royal Soc. (Lond) Phil. Trans. 335: 365-375

Ayers JC, Watson EB (1993). Rutile solubility and mobility in supercritical aqueous fluids. Contrib. Mineral. Petrol. 114: 321-330

Bauer N, Kröner A, Todt W, Liew TC, Hofmann AW (1991). U-Pb isotope systematics of zircons from prograde and retrograde transition zones in high-grade orthogneisses, Sri Lanka. J. Geol. 99: 527-545

Baumgartner LP, Eugster HP (1988): Experimental determination of corundum solubility and Al-speciation in supercritical H_2O-H solutions [abs.]. Geol. Soc. Am. Abs. with Prog. 20:191

Baumgartner LP, Olsen SN (1995). A Least-Squares approach to mass transport calculations using the Isocon method. Econ. Geol. 90: 1261-1270

Berger AR, Jayasinghe NR (1976). Precambrian structure and chronology in the Highland Series of Sri Lanka. Precam. Res. 3: 559-576

Berman, RG (1988). Internally consistence thermodynamic data for minerals in system Na_2O - K_2O – CaO – MgO – FeO - Fe_2O_3 - Al_2O_3 - SiO_2 – TiO_2 -H_2O - CO_2: representation, estimation, and high temperature extrapolation, J. Petrol. 29: 445-522

Berman RG (1990). Mixing properties of Ca-Mg-Fe-Mn in garnets. Am. Mineral. 75: 328-344

Boudreau AE, McCallum IS (1989). Investigations of the Stillwater complex V. Apatites as indicators of evolving fluid composition. Contrib. Mineral. Petrol. 102: 138-153

Braddy JB (1977). Metasomatic zoning in metamorphic rocks. Geochem. Cosmochim. Acta 41: 113-125

*Cooray PG (*1994) The Precambrian of Sri Lanka: a historic review. Precam. Res. 66: 3-18

Dunkley DJ, Clarke GL, Harley SL (1999). Diffusion metasomatism in silica-undersaturated sapphirine-bearing granulite from Rumdoole Peak, Framnes Mountains, East Antartica. Contrib. Mineral. Petrol. 134: 264-276

Dymek RF (1983). Titanium, aluminium and interlayer cation substitutions in biotite from high-grade gneisses, west Greenland. Am. Mineral. 68: 880-899

Eugster HP, Baumgartner LP (1987). Mineral solubilities and speciation in supercritical metamorphic fluids. In: (*Carmichael ISE, Eugster HP* eds), Thermodynamic modeling of geological materials: minerals, fluids and melts. Mineral. Soc. Am., Reviews of Mineral. 17: 367-403

Faulhaber S, Raith M (1991).Geothermometry and geobarometry of high-grade rocks: a case study on garnet-pyroxene granulites in southern Sri Lanka, Min. Mag. 55: 17-40

Ferry JM, Dipple GM (1991). Fluid flow, mineral reactions and metasomatism. Geol. 19: 211-214

Finch A (1995). Metasomatic overprinting by juvenile igneous fluids, Igdlerfigsalik, South Grrenland, Contrib. Mineral. Petrol. 122: 11-24

Finch A, Parsons I, Mingard SC (1995). Biotites as indicators of fluorine fugacities in late-stage magmatic fluids: the Garder Province of South Greenland. J. Petrol. 36: 1701-1728

Fischer GW (1973). Non-equilibrium thermodynamics as a model for diffusion controlled metamorphic processes. Am. J. Sci. 273: 897-924

Fischer GW (1977). Non-equilibrium thermodynamics in metamorphism. In: Thermodynamic in Geology. (*Fraser DG* ed). Reidel Publ Co, Boston, 381-403

Frisch CJ, Helgeson HC (1984). Metasomatic phase relations in dolomites of the Adamello Alps. Am. J. Sci. 284: 121-185

Fyfe WS, Price NJ, Thompson AB (1978). Fluids in the earth's crust: Elsevier Publ, Amsterdam, pp383

Gieré R (1990a). Quantification of element mobility at a tonalite/dolomite contact. PhD dissertation, University of Zürich, Switzerland, pp92

Gieré R (1990b). Hydrothermal mobility of Ti, Zr and REE; examples from the Bergell and Adamello contact aureoles (Italy). Terra Nova 2: 60-67

*Glazner AF, Bartley JM (*1991) Volume loss, fluid flow and state of strain in extensional mylonites from central Mojave Desert, California. J. Structural Geol. 13:587-594

Grant JA (1986) The isocon diagram-a simple solution to Gresens equation to metasomatic alteration. Econ. Geol. 81: 1976-1982

Gresens RL (1967) Composition-volume relationships of metasomatism. Chem. Geol. 2: 47-55

Guidotti, CV (1984). Micas in metamorphic rock. In: Micas. (*Bailey SW* ed), Mineral. Soc. Am., Reviews in Mineral. 13: 357-456

Guidotti, CV, Cheney JT, Guggenheim S (1977). Distribution of Ti betweencoexisting muscovite and biotite in pelitic schists from northwestern Maine. Am. Mineral. 62: 438-448

Hokada T, Osanai Y, Toyoshima T, Owada M. Tsunogae T, Crowe WA (1999). Petrology and metamorphism of sapphirine-bearing aluminous gneisses from Tonagh Island in the Napier Complex, East Antarctica, Polar Geosci. 12: 49-70

*Holland TJB, Powell R (*1998) An internally consistent thermodynamic data set for phases of petrological interest. J. metamorphic Geol. 16: 309-343

Hölzl S, Hofmann AW, Todt W, Köhler H (1994). U-Pb geochronology of the Sri Lankan basement, Precam. Res. 66: 123-149

Joesten R (1977). Evolution of mineral assemblage zoning in diffusion metasomatism. Geochem. Cosmochim. Acta 41: 649-670

Kerrich R, Fyfe WS, Barnett RL, Blair BB, Willmore LM (1987). Corundum, Cr-muscovite rocks at O,Briens, Zimbawe: the conjunctions of hydrothermal desilicification and LIL-element enrichment- geochemical and isotope evidences. Contrib. Mineral. Petrol. 95: 481-498

Kerrick DM (1988): Al_2O_5-bearing segregations in the Lepontine Alps, Switzerland; aluminium mobility in metapelites. Geol. 16: 636-640

Korzhinskii DS (1970). Theory of metasomatic zoning. Clareanden Press, Oxford, 111-146

Kretz R (1983) Symbols for rock forming minerals. Am. Mineral. 68: 277-279

Kriegsman LM (1991). Sapphirine-bearing granulite from central Sri Lanka-outcrop description and mineral chemistry. In: the crystalline crust of Sri Lanka, part 1, summary of research of Sri Lankan-German Consortium (*Kröner A* ed), Geol. Surv. Dept. of Sri Lanka, Prof Pap 5: 178-187

Kriegsman LM (1993). Geodymamic evolution of the Pan-African lower crust in Sri Lanka-Structural and petrological investigations into a high-grade gneiss terrain. PhD thesis, University of Utrecht, The Nederlands, pp207

Kriesman LM, Schumacher JC (2000). Petrology of sapphirine-bearing and associated granulites from central Sri Lanka. J. Petrol. 40: 1211-1239

*Kröner A, Cooray PG, Vitanage PW (*1991). Lithotectonic subdivision of the Precambrian basement in Sri Lanka. In: The crystalline crust of Sri Lanka, Part -1. Summary of research of the German-Sri Lankan Consortium *Kröner A* (Ed), Geol. Surv. Dept. Sri Lanka, Prof. Pap. 5: 5-21

Kullerud K (1995). Chlorine, titanium and barium-rich biotites: factors controlling biotite composition and implication for garnet-biotite geothermometry, Contrib. Mineral. Petrol. 120: 42-59

Kullerud K (1996). Chlorine-rich amphiboles: interplay between amphibole composition and evolving fluid, Eu. J. Mineral. 8: 355-370

MacLean WH, Barrett TJ (1993). Lithogeochemical techniques using immobile elements. J. Geochem. Explor. 48: 109-133

Markl G, Bucher K (1998). Metamorphic salt in granulite; implications for the presence and composition of fluid in the Lower crust. Nature, 391: 781-783

Markl G, Schumacher JC (1996). Spatial variations in temperature and composition of greisen-forming fluids: an example from the Variscan Triberg granite complex, Germany. Econ. Geol. 91: 576-589

Marquer D, Burkhard M (1992) Fluid circulation, progressive deformation and mass transfer processes in the upper crust: the example of basement-cover relationships in the External Crystalline Massifs, Switzerlands. J. Structural Geol. 14: 1047-1057

Milicenda CC, Liew TC, Hofmann AW (1994) Nd isotopic mapping of the Sri Lanka basement: update and additional constraints from Sr isotopes. Precam. Res. 66: 95-110

Mora C, Valley JW (1989). Halogen-rich scapolite and biotite: implications for metamorphic fluid-rock interaction. Am. Mineral. 74: 721-737

Munoz JL (1984). F-OH and Cl-OH exchange in micas with applications to hydrothermal ore deposits. In: Micas. (*Bailey SW* ed), Mineral. Soc. Am., Reviews in Mineral. 13: 469-494

Munoz JL, Ludington S (1974). Fluoride-hydroxyl exchange in biotite. Am. J. Sci. 274: 396-413

Munoz JL, Swenzen A (1981). Chloride-hydroxyl exchange in biotite and estimation of relative HCl/HF activities in hydrothermal fluids. Econ. Geol. 76: 2212-2221

O'Hara K, Blackburn WH (1989) Volume loss model for trace elements enrichments in mylonites. Geol. 17: 524-527

Osanai Y (1989). A preliminary report on sapphirine/kornerupine granulite from Highland Series, Sri Lanka (extended abstract), Seminar on recent advances in Precambrian geology in Sri Lanka

Osanai Y, Owada M, Kagami H, Hamamoto T, Hensen J (1996). Sapphirine granulite and related high-P-T metamorphic rocks from Highland Complex, Sri Lanka, Gondwana Research Group Misc. Publ. No. 4, (*Santosh M, Yoshida M* eds), 107-108

Owen VJ, Greenough JD (1991). An empirical sapphirine-spinel Fe-Mg exchange thermometer and its application to high-grade xenoliths in the Popes Harbour dyke, Nova Scotia, Canada. Lithos 26:317-322

Robert JL, Beny JM, Della Ventura J, Hardy M (1993). Fluorine in micas: crystal chemical control of OH-F distribution between trioctahedral and dioctaheral sites. Eu. J. Mineral. 5: 7-18

Roser BP, Nathan S (1997). An evaluation of elemental mobility during metamorphism of a turbidite sequence (Greenland Group, New Zealand). Geol. Mag. 134: 219-234

Rumble D III (1982). The role of perfectly mobile components metamorphism. Ann. Rev. Earth. Planet. Sci. 10: 221-233.

Schenk V, Raase P, Schumacher R (1988) Very high temperatures and isobaric cooling before tectonic uplift in the Highland Series. Terra Cognita 8: 265

Schumacher JC, Robinson P (1987). Mineral chemistry and metasomatic growth of alumineous enclaves in gedrite-cordierite-gneiss from southwestern New Hampshire, USA. J. Petrol. 28: 1033-1073

Schumacher R, Faulhaber S (1994). Summary and discussion of P-T estimates from garnet-pyroxene-plagioclase-quartz-bearing granulite- facies rocks from Sri Lanka. Precam. Res. 66: 295-308

Selverstone J, Morteani G, Staude JM (1991) Fluid channelling during ductile shearing transformation of granodiorite into aluminous schist in the Tauren Window, eastern Alps. J. Metamorphic Geol. 9: 419-431

Spear FS (1993) Metamorphic phase equilibria and pressure-temperature-time paths Monograph series, Mineral. Soc. Am., Washinton D.C., pp799

Thompson JB (1959). Local equilibrium in metasomatic processes. In: Researches in geochemistry (*Abelson, PH ed*), John Willey & Sons, New York, 437-457

Touret JLR (1985). Fluid regime in southern Norway: the record of fluid inclusions. In: The deep Proterozoic crust in the North Atlantic Provinces (*Tobi AC, Touret JLR* eds). Reidel, Dordrecht, 517-550

Voll G, Evangelakakis C, Kroll H (1994) Revised two-feldspar geothermometry applied to Sri Lankan feldspars. Precam. Res. 66: 351-377

Wolery TJ (1979). Calculation of chemical equilibria between aqueous solutions and minerals: the EQ3/6 software package. Lawrence Livermore National Laboratory, URCL-52658

*Wolrey TJ, Sherwood DJ, Jackson KJ, Delany JM, Puigdomenech I (*1983). EQ3/6: Status and applications, Lawrence Livermore National Lab, Livermore, CA, UCRL-91884, pp.12

Yardley BWD (1977). The nature and significance of the mechanism of suillimanite growth in the Conemara schist, Ireland. Contrib. Mineral. Petrol. 65: 53-58

Zhu C, Sverjensky DA (1991). Partitioning of F-Cl-OH between minerals and hydrothermal fluids. Geochim. Cosmochim. Acta 55: 1837-1858

Zhu C, Sverjensky DA (1992). F-Cl-OH partitioning between biotite and apatite. Geochim. Cosmochim. Acta 56: 3435-3467

Table 4.1a Sapphirine and spinel compositions of reaction zones (respective pairs were used for Spr-Spl ion exchange thermometr

Location	9806	9806	9806	9806	9806	9806	9806	9806	9806	9806	9806	9806
analyses	65	73	77	79	81	85	68	74	78	80	82	86
Mineral pair	Spr 1	Spr 2	Spr 3	Spr 4	Spr 5	Spr 6	Spl 1	Spl 2	Spl 3	Spl 4	Spl 5	Spl 6
Zone	A	A	A	B	B	B	A	A	A	B	B	B
SiO_2	12.82	12.88	12.06	11.46	11.85	12.43	0.02	0.02	0.00	0.01	0.04	0.01
TiO_2	0.07	0.05	0.03	0.06	0.07	0.05	0.00	0.01	0.01	0.00	0.00	0.01
Al_2O_3	64.49	65.63	67.30	67.45	67.06	64.43	69.27	68.87	69.72	70.28	69.96	70.11
FeO	0.57	0.51	0.55	0.61	0.76	0.69	1.72	1.68	1.89	1.83	1.86	1.71
Cr_2O_3	0.01	0.00	0.00	0.05	0.03	0.02	0.00	0.03	0.02	0.02	0.02	0.01
MnO	0.03	0.00	0.01	0.03	0.02	0.06	0.06	0.05	0.00	0.03	0.02	0.07
MgO	20.12	20.24	19.66	19.38	19.34	20.09	26.55	25.82	26.93	26.71	26.59	26.62
CaO	0.02	0.04	0.03	0.03	0.05	0.03	0.01	0.03	0.01	0.02	0.00	0.00
Na_2O	0.04	0.02	0.00	0.02	0.05	0.02	0.03	0.08	0.03	0.00	0.04	0.01
K_2O	0.04	0.00	0.00	0.01	0.01	0.03	0.01	0.07	0.00	0.02	0.01	0.02
Total	98.21	99.36	99.64	99.10	99.23	97.84	97.66	96.64	98.61	98.92	98.55	98.58
		formula on the basis of 20 oxygens							formula on the basis of 32 oxygens			
Si	1.505	1.493	1.394	1.334	1.378	1.466	0.004	0.003	0.000	0.002	0.007	0.002
Ti	0.006	0.004	0.003	0.005	0.006	0.005	0.000	0.001	0.001	0.000	0.000	0.002
Al	8.915	8.959	9.164	9.246	9.183	8.952	15.953	16.027	15.915	15.981	15.972	15.990
Fe	0.056	0.049	0.053	0.060	0.074	0.068	0.281	0.278	0.306	0.296	0.302	0.277
Cr	0.001	0.000	0.000	0.005	0.003	0.001	0.000	0.004	0.003	0.004	0.004	0.002
Mn	0.003	0.000	0.001	0.003	0.001	0.006	0.009	0.008	0.000	0.005	0.003	0.011
Mg	3.521	3.498	3.389	3.363	3.352	3.533	7.740	7.606	7.782	7.688	7.684	7.686
Ca	0.003	0.005	0.003	0.004	0.006	0.003	0.002	0.006	0.003	0.005	0.000	0.000
Na	0.009	0.004	0.000	0.004	0.012	0.005	0.009	0.030	0.010	0.000	0.017	0.003
K	0.005	0.000	0.000	0.001	0.001	0.004	0.003	0.017	0.000	0.004	0.003	0.006
Cations	14.024	14.012	14.007	14.025	14.016	14.043	24.001	23.980	24.020	23.985	23.992	23.979
X_{Mg}	0.984	0.986	0.985	0.982	0.978	0.981	0.965	0.965	0.962	0.963	0.962	0.965

all iron as FeO

X_{Mg}= Mg/(Fe+Mg)

Table 4.1b Corundum composition of reaction zones

Location	9805	9805	9805	9805	9805	9806
analyses	89	90	92	93	94	58
Zone	D	D	D	C	C	B
SiO_2	0.03	0.04	0.03	0.03	0.03	0.05
TiO_2	0.05	0.04	0.03	0.13	0.05	0.02
Al_2O_3	98.88	99.19	99.75	99.71	99.17	98.83
FeO	0.14	0.12	0.23	0.18	0.12	0.10
Cr_2O_3	0.01	0.00	0.01	0.00	0.02	0.01
MnO	0.00	0.01	0.01	0.00	0.01	0.00
MgO	0.02	0.02	0.01	0.02	0.02	0.01
CaO	0.00	0.00	0.00	0.00	0.01	0.01
GeO_2	0.00	0.01	0.00	0.01	0.01	0.00
Sc_2O_3	0.00	0.00	0.00	0.00	0.00	0.00
V_2O_3	0.00	0.00	0.00	0.00	0.00	0.00
Ga_2O_3	0.02	0.01	0.02	0.01	0.01	0.00
Total	99.15	99.45	100.08	100.09	99.44	99.04
Si	0.0005	0.0007	0.0005	0.0006	0.0005	0.0008
Ti	0.0006	0.0005	0.0003	0.0016	0.0006	0.0003
Al	1.9945	1.9944	1.9941	1.9928	1.9944	1.9950
Fe	0.0020	0.0018	0.0032	0.0025	0.0017	0.0015
Cr	0.0001	0.0000	0.0001	0.0000	0.0002	0.0001
Mn	0.0000	0.0001	0.0001	0.0000	0.0002	0.0000
Mg	0.0006	0.0006	0.0003	0.0004	0.0005	0.0003
Ca	0.0000	0.0000	0.0000	0.0000	0.0002	0.0002
Ge	0.0000	0.0001	0.0000	0.0001	0.0001	0.0000
Sc	0.0000	0.0000	0.0000	0.0000	0.0000	0.0000
V	0.0000	0.0000	0.0000	0.0000	0.0000	0.0000
Ga	0.0002	0.0001	0.0002	0.0001	0.0001	0.0000
Cations	1.9985	1.9983	1.9988	1.9981	1.9985	1.9982

all iron as FeO

Table 4.1c Representative plagioclase composition of reaction zones

Sample	9805	9805	9806	9806
analyses	124	126	68	69
zone	D	D	C	C
SiO_2	59.34	59.90	45.36	44.68
TiO_2	0.00	0.00	0.01	0.01
Al_2O_3	25.21	24.79	34.48	34.87
FeO	0.09	0.00	0.00	0.02
Cr_2O_3	0.00	0.05	0.00	0.01
MnO	0.06	0.01	0.00	0.03
MgO	0.09	0.00	0.00	0.00
CaO	6.35	6.46	18.29	18.55
Na_2O	7.57	7.94	1.16	1.04
K_2O	0.58	0.26	0.03	0.00
BaO	0.09	0.02	0.00	0.00
F	0.14	0.00	0.12	0.05
Cl	0.01	0.00	0.00	0.01
Total	99.52	99.42	99.45	99.27
Si	10.652	10.740	8.409	8.311
Ti	0.000	0.000	0.001	0.001
Al	5.333	5.238	7.533	7.644
Fe	0.013	0.000	0.000	0.003
Cr	0.000	0.007	0.000	0.002
Mn	0.009	0.002	0.000	0.005
Mg	0.023	0.000	0.000	0.000
Ca	1.221	1.241	3.633	3.696
Na	2.634	2.760	0.415	0.376
K	0.132	0.059	0.008	0.000
Ba	0.007	0.001	0.000	0.000
F	0.079	0.000	0.070	0.029
Cl	0.003	0.000	0.000	0.002
X_{An}	0.31	0.31	0.90	0.91
An	30.63	30.57	89.57	90.76
Ab	66.07	67.99	10.24	9.24
Or	3.30	1.45	0.20	0.00

Xan = [(Ca/(Ca+Na+K)]

Table 4.2a Whole rock analyses of siliceous granulites (parent rock)

Sample No.	RU 9708 L	RU 9708 M	RU 9708 N	RU 9707 L	RU 9707 M	RU 9707 N	RU 9804	RU 9708 A *	RU 9708 B*	Average	1s
SiO_2 %	61.77	61.72	62.14	58.84	59.33	58.84	63.80	65.57	64.82	61.871	2.526
Al_2O_3 %	18.92	19.03	19.28	19.22	18.68	19.36	18.80	16.71	18.11	18.679	0.830
Fe_2O_3 %	2.29	2.25	2.13	5.56	5.58	5.21	4.48	4.59	2.35	3.827	1.536
MnO %	0.14	0.14	0.12	0.05	0.05	0.05	0.02	0.03	0.03	0.071	0.050
MgO %	0.89	0.84	0.80	0.98	0.87	0.85	0.44	0.45	0.85	0.775	0.195
CaO %	2.05	2.13	2.11	4.53	4.55	4.80	2.65	2.59	2.85	3.139	1.150
Na_2O %	3.96	4.04	4.01	4.77	4.80	5.02	4.86	5.03	2.48	4.331	0.820
K_2O %	8.17	8.26	7.85	3.69	3.67	3.50	3.51	3.47	7.03	5.460	2.274
TiO_2 %	0.31	0.19	0.22	0.50	0.54	0.60	0.36	0.26	0.31	0.365	0.149
P_2O_5 %	0.05	0.04	0.05	0.06	0.05	0.04	0.05	0.08	0.01	0.048	0.019
LOI %	1.06	0.97	0.91	1.45	1.51	1.36	0.72	0.88	0.82	1.076	0.291
Total	99.61	99.61	99.62	99.64	99.64	99.64	99.68	99.66	99.67		
(ppm)											
Sc_2O_3	3.1	3.2	6.1	20.0	18.5	21.5	4.6	3.1	3.1	9.2	8.2
V_2O_3	79.4	75.7	72.8	84.0	87.2	76.7	80.9	80.5	92.9	81.1	6.2
Cr_2O_3	22.3	19.5	17.4	54.2	47.0	42.5	16.1	17.8	22.0	28.7	14.8
CoO	51.8	41.8	49.1	47.1	35.8	34.4	59.7	52.8	57.3	47.8	8.9
NiO	20.7	19.6	17.6	33.1	32.0	29.3	2.5	5.2	7.6	18.6	11.6
CuO	12.8	12.9	16.1	1.3	1.3	2.5	7.5	6.3	3.8	7.2	5.6
ZnO	50.7	48.6	45.6	37.4	40.0	36.2	42.3	34.1	61.1	44.0	8.5
Ga_2O_3	28.8	29.0	28.0	32.3	33.8	31.0	28.2	27.2	18.9	28.6	4.2
Rb_2O	286.3	286.8	274.0	317.6	317.6	293.8	260.2	260.4	241.0	282.0	26.0
SrO	468.6	471.9	461.4	394.4	398.1	404.2	435.0	448.2	375.6	428.6	36.2
Y_2O_3	13.5	10.6	10.2	13.3	8.9	8.9	5.9	6.0	4.4	9.1	3.2
ZrO_2	216.0	214.0	184.6	247.5	236.2	245.1	160.7	266.9	239.5	223.4	33.5
Nb_2O_3	6.4	6.5	7.5	12.6	12.6	12.6	11.3	7.7	8.8	9.6	2.7
BaO	2462.5	2509.1	2433.3	2085.2	2075.8	2106.1	1901.7	2079.4	1996.7	2183.3	223.2
U_2O_3	1.1	1.1	1.1	7.7	8.9	7.7	1.1	1.1	1.1	3.4	3.5
Th_2O_3	5.6	3.4	3.3	7.7	6.7	7.7	3.3	3.4	3.3	4.9	2.0
PbO	46.1	46.5	44.8	69.0	70.4	69.1	29.1	29.5	36.7	49.0	16.7
HfO_2	14.4	4.9	4.7	11.8	11.9	11.8	3.5	8.4	3.5	8.3	4.3
Ta_2O_3	3.5	2.3	3.4	3.4	3.4	3.4	2.3	2.3	2.3	2.9	0.6
La_2O_3	41.8	39.8	38.3	49.3	57.8	54.1	41.0	34.5	20.0	41.8	11.2
Ce_2O_3	40.6	38.5	34.8	49.3	56.5	57.5	39.8	39.2	45.8	44.7	8.2
Pr_2O_3	4.8	3.6	4.6	8.2	9.4	8.2	5.8	4.7	2.3	5.8	2.4
Nd_2O_3	16.6	13.2	15.0	21.0	19.9	19.9	14.0	15.4	5.8	15.7	4.6
Sm_2O_3	2.4	2.4	2.3	7.0	4.7	7.0	3.5	2.3	2.3	3.8	2.0

Table 4.2b Whole rock analyses of zone D (corundum-biotite-plagioclase gneiss)

Sample No.	RU 9805 AL	RU 9805 AM	RU 9805 AN	RU 9805 L	RU 9805 M	RU 9805 N	average	1s
SiO_2 %	60.25	60.82	60.77	57.05	55.57	56.18	58.44	2.436
Al_2O_3 %	24.33	23.64	23.72	27.18	28.50	27.70	25.84	2.189
Fe_2O_3 %	0.34	0.26	0.26	0.30	0.42	0.43	0.33	0.075
MnO %	0.00	0.00	0.00	0.00	0.00	0.01	0.00	0.004
MgO %	0.40	0.45	0.41	0.48	0.63	0.70	0.51	0.123
CaO %	2.37	2.34	2.33	5.53	5.42	5.46	3.91	1.714
Na_2O %	6.61	6.68	6.71	6.75	6.52	6.59	6.64	0.084
K_2O %	3.84	4.02	3.82	1.20	1.25	1.21	2.56	1.468
TiO_2 %	0.09	0.06	0.01	0.10	0.13	0.12	0.08	0.044
P_2O_5 %	0.02	0.02	0.02	0.02	0.02	0.02	0.02	0.000
LOI %	1.42	1.37	1.61	1.04	1.17	1.18	1.30	0.206
Total	99.66	99.65	99.66	99.64	99.63	99.61		
(ppm)								
Sc_2O_3	3.1	4.6	1.5	4.6	4.6	7.6	4.3	2.0
V_2O_3	7.3	5.9	7.3	8.8	13.2	11.7	9.0	2.8
Cr_2O_3	2.9	2.9	2.9	2.9	2.9	4.4	3.2	0.6
CoO	126.9	139.6	185.4	153.4	208.0	205.0	169.7	34.5
NiO	3.8	1.3	1.3	5.1	5.1	3.8	3.4	1.7
[illegible] Zn								
Ga_2O_3	30.9	29.5	29.5	28.1	29.5	28.1	29.3	1.0
Rb_2O	60.0	63.3	68.8	50.2	55.6	54.4	58.7	6.7
SrO	777.8	793.3	787.7	1096.5	1055.8	1057.1	928.0	156.1
Y_2O_3	30.9	26.5	27.9	32.3	33.8	33.7	30.8	3.1
ZrO_2	84.9	80.9	87.7	113.1	124.0	135.8	104.4	23.0
Nb_2O_3	12.6	7.5	7.5	10.0	13.8	13.8	10.9	2.9
BaO	2038.1	2134.3	2045.9	1781.0	1841.1	1996.0	1972.7	134.4
U_2O_3	13.2	9.9	9.9	48.3	73.6	69.0	37.3	30.1
Th_2O_3	18.7	16.5	16.5	30.8	46.2	45.0	29.0	14.0
PbO	58.1	60.2	57.0	89.1	89.2	89.0	73.8	16.8
HfO_2	4.7	5.9	3.5	5.9	5.9	8.2	5.7	1.6
Ta_2O_3	3.4	3.4	3.4	4.5	4.5	4.5	4.0	0.6
La_2O_3	22.2	22.2	22.3	33.9	33.9	33.9	28.1	6.4
Ce_2O_3	28.1	18.7	23.4	54.9	47.9	50.1	37.2	15.6
Pr_2O_3	5.8	4.7	3.5	7.0	5.8	5.8	5.4	1.2
Nd_2O_3	21.0	15.1	17.5	24.4	25.6	26.7	21.7	4.7
Sm_2O_3	3.5	2.3	2.3	5.8	6.9	4.6	4.2	1.9

Table 4.2c Whole rock analyses of (Zone C) (corundum-plagioclase-biotite-bearing gneiss)

Sample No.	RU 9806 CL	RU 9806 CM	RU 9806 CN	Average	1s
SiO_2 %	24.41	24.05	24.39	24.28	0.162
Al_2O_3 %	56.92	57.44	56.94	57.10	0.241
Fe_2O_3 %	0.57	0.53	0.50	0.54	0.029
MnO %	0.01	0.01	0.01	0.01	0.000
MgO %	4.47	4.44	4.26	4.39	0.093
CaO %	5.21	5.19	5.37	5.26	0.081
Na_2O %	0.64	0.63	0.68	0.65	0.023
K_2O %	2.70	2.64	2.58	2.64	0.052
TiO_2 %	0.39	0.38	0.37	0.38	0.009
P_2O_5 %	0.03	0.04	0.03	0.03	0.005
LOI %	4.25	4.25	4.47	4.32	0.104
Total	99.60	99.60	99.59		
(ppm)					
Sc_2O_3	12.3	10.8	12.3	11.8	0.7
V_2O_3	47.3	44.5	44.2	45.3	1.4
Cr_2O_3	22.0	13.3	20.5	18.6	3.8
CoO	316.7	236.1	359.3	304.0	51.1
NiO	5.1	3.9	6.4	5.1	1.0
CuO	7.5	6.3	8.8	7.5	1.0
ZnO	28.8	35.2	32.4	32.1	2.6
Ga_2O_3	40.2	41.4	42.1	41.2	0.8
Rb_2O	180.1	177.6	172.0	176.6	3.4
SrO	668.7	668.2	716.9	684.6	22.8
Y_2O_3	34.0	41.6	36.9	37.5	3.1
ZrO_2	177.7	203.1	204.4	195.1	12.3
Nb_2O_3	32.9	33.0	34.0	33.3	0.5
BaO	1973.7	1984.9	1945.4	1968.0	16.6
U_2O_3	48.6	66.6	56.3	57.2	7.4
Th_2O_3	46.5	57.9	47.5	50.7	5.1
PbO	16.2	17.4	16.2	16.6	0.6
HfO_2	4.7	7.1	5.9	5.9	1.0
Ta_2O_3	8.0	6.9	10.2	8.3	1.4
La_2O_3	84.8	91.1	82.3	86.1	3.7
Ce_2O_3	122.3	131.2	125.6	126.4	3.6
Pr_2O_3	15.3	17.7	14.1	15.7	1.5
Nd_2O_3	46.9	51.8	46.7	48.5	2.3
Sm_2O_3	11.6	7.0	11.6	10.1	2.2

Table 4.2d Whole rock analyses of Zone A (phlogopite-spinel-sapphirine-bearing gneiss)

Sample No.	RU 9806 SL	RU 9806 SM	RU 9806 SN	Average	1s
SiO_2 %	16.87	16.86	17.18	16.969	0.147
Al_2O_3 %	52.15	51.62	52.35	52.042	0.309
Fe_2O_3 %	1.02	1.10	1.08	1.066	0.030
MnO %	0.02	0.02	0.02	0.020	0.000
MgO %	21.11	21.47	20.20	20.927	0.534
CaO %	1.33	1.29	1.56	1.391	0.119
Na_2O %	0.39	0.32	0.33	0.349	0.031
K_2O %	3.24	3.28	3.18	3.234	0.044
TiO_2 %	0.35	0.35	0.36	0.355	0.005
P_2O_5 %	0.33	0.33	0.30	0.322	0.014
LOI %	2.81	2.97	3.07	2.949	0.104
Total	99.63	99.62	99.62		
(ppm)					
Sc_2O_3	6.2	3.1	7.7	5.7	1.9
V_2O_3	81.3	84.4	81.3	82.3	1.5
Cr_2O_3	13.2	11.8	13.2	12.7	0.7
CoO	90.7	124.2	111.2	108.7	13.8
NiO	8.9	7.7	7.7	8.1	0.6
CuO	7.5	7.6	10.1	8.4	1.2
ZnO	949.1	998.7	908.3	952.0	37.0
Ga_2O_3	101.5	105.7	99.5	102.2	2.6
Rb_2O	251.6	256.5	250.6	252.9	2.6
SrO	211.5	219.1	246.0	225.5	14.8
Y_2O_3	37.0	38.5	38.5	38.0	0.7
ZrO_2	267.3	252.9	255.2	258.5	6.3
Nb_2O_3	31.6	30.4	32.9	31.6	1.0
BaO	1340.4	1347.6	1381.4	1356.5	17.9
U_2O_3	64.1	63.2	62.0	63.1	0.9
Th_2O_3	37.7	36.7	34.4	36.2	1.4
PbO	8.7	8.7	8.7	8.7	0.0
HfO_2	8.3	8.3	9.5	8.7	0.6
Ta_2O_3	5.7	6.8	6.8	6.5	0.5
La_2O_3	54.2	49.6	54.2	52.7	2.2
Ce_2O_3	88.3	89.6	91.8	89.9	1.5
Pr_2O_3	12.9	13.0	10.6	12.2	1.1
Nd_2O_3	35.2	35.2	35.2	35.2	0.0
Sm_2O_3	7.0	4.7	4.7	5.4	1.1

Table 4.3a. complete list of all possible Isocon compatible element combinations obtained from overlapping cone method (siliceous granulite to zone D alteration) The element combination 65 has taken as best fit-isocon (Baumgartner and olsen 1995)

	Si	Al	Ti	Fe	Mn	Mg	Ca	K	Na	P	LOI	Sc	V	Cr	Co	Ni	Cu	Zn	Ga	Rb	Sr	Y	Zr	Nb	Ba	U	Th	Pb	Hf	Ta	La	Ce	Pr	Nd	Sm
1					X																											X				
2																										X	X								
3				X	X																											X				
4												X					X				X															
5																						X				X	X								
6				X	X									X			X															X				
7												X					X				X															X
8												X					X				X					X										
9												X					X					X				X										
10															X							X				X										
11															X							X				X	X									
12				X	X									X																	X	X				
13				X									X	X																	X	X				
14														X		X		X													X	X				
15												X					X				X							X								
16												X					X				X	X				X										
17												X			X		X					X				X										
18															X		X					X				X	X									
19				X	X								X	X																	X	X				
20				X									X	X		X															X	X				
21				X										X		X		X													X	X				
22			X											X		X		X													X	X				
23			X											X		X				X											X	X				
24			X					X				X				X															X	X				
25			X					X				X				X							X								X					
26								X				X				X							X						X		X					
27							X					X					X					X						X			X	X				X
28				X									X	X		X		X													X	X				
29														X		X		X		X											X	X				
30			X									X		X		X				X											X	X				
31			X									X				X				X											X	X				
32			X					X				X				X							X													
33			X					X				X				X							X						X		X					
34			X					X				X				X	X						X						X		X					
35						X		X				X					X						X						X		X					
36						X		X				X					X												X		X					X
37							X		X			X					X											X						X	X	X
38							X					X					X				X							X						X	X	X
39			X					X				X		X		X				X												X				
40						X		X				X				X	X							X					X		X					
41						X		X				X					X							X					X				X			X
42						X		X				X																	X			X	X			X
43							X		X			X					X											X		X				X	X	X
44							X		X								X				X							X							X	X
45						X	X	X				X					X												X		X		X			X
46							X		X			X					X								X			X		X				X	X	X
47						X	X		X			X					X								X			X		X			X			X
48							X		X		X	X					X								X			X		X				X	X	X
49						X	X	X				X					X								X	X			X		X		X			X
50						X	X					X					X		X						X	X			X		X		X			X
51							X				X	X					X		X						X				X		X		X	X	X	X
52							X				X	X					X								X			X	X	X			X	X	X	X
53							X		X		X	X					X								X			X		X			X	X	X	X
54						X	X	X				X					X		X						X	X			X		X		X			X
55	X					X	X					X					X		X						X	X			X		X		X			X
56	X						X				X	X					X		X						X	X			X		X		X			X
57							X				X	X					X		X						X	X			X		X		X	X	X	X
58							X				X	X					X		X						X			X	X		X		X	X	X	X
59							X				X	X					X		X						X			X	X	X			X	X	X	X
60		X					X				X	X					X								X			X	X	X			X	X	X	X
61		X					X		X		X	X					X								X			X		X			X	X	X	X
62	X					X	X				X	X					X		X						X	X			X		X		X			X
63	X						X				X	X					X		X						X	X			X		X		X	X	X	X
64							X				X	X					X		X						X			X	X	X	X		X	X	X	X
65		X					Y		X		Y	Y					Y								Y			Y	Y	Y			Y	Y	Y	Y

Table 4.3b. complete list of all possible Isocon compatible element combinations obtained from overlapping cone method (after Baumgartner and Olsen 1995) (Siliceous granulite to zone C alteration) The element combination 61 has taken as best fit-isocon

	Si	Al	Ti	Fe	Mn	Mg	Ca	K	Na	P	LOI	Sc	V	Cr	Co	Ni	Cu	Zn	Ga	Rb	Sr	Y	Zr	Nb	Ba	La	Ce	Pr	Nd	Sm
1				X					X								X													
2				X													X													
3																	X								X					
4																														
5				X					X								X													
6								X									X								X					
7						X						X				X														
8												X				X									X					
9												X													X					
10	X							X								X									X					
11								X						X		X									X					
12						X						X			X							X								
13						X						X			X										X					
14												X			X										X					
15	X							X						X		X									X					
16								X						X		X									X					
17								X		X				X		X														
18			X									X		X				X												
19							X					X						X								X				X
20						X					X	X										X								X
21						X						X			X							X								X
22								X		X				X		X									X					
23								X		X			X	X		X														
24			X							X		X		X				X												
25			X				X					X		X				X												
26			X				X					X						X		X										
27			X				X					X						X		X		X								
28			X				X					X						X								X				X
29							X					X						X								X		X		X
30						X					X	X										X		X						X
31						X					X	X			X							X								X
32								X		X			X	X		X				X										
33							X			X		X		X				X	X											
34			X							X		X		X				X					X							
35			X				X					X		X				X		X										
36			X				X					X						X		X	X									
37			X				X					X						X		X	X					X				
38			X				X					X									X					X				X
39							X					X															X	X		X		X
40											X	X										X		X					X		X
41						X					X	X										X		X							X
42								X		X			X	X		X				X											
43								X		X				X		X	X			X											
44								X		X		X		X		X	X														
45			X					X		X		X		X			X														
46			X							X		X		X									X		X						
47			X				X					X								X		X									X
48							X					X															X	X		X	X	X
49												X															X	X	X	X	X	X
50												X												X				X	X	X	X	X
51											X	X										X		X					X	X	X
52						X					X	X										X		X					X		X
53								X		X			X	X		X	X	X		X											
54								X		X		X		X		X	X	X		X											
55			X					X		X		X		X			X	X						X							
56			X							X		X		X			X	X					X		X						
57							X					X						X									X	X	X	X	X	X
58												X						X						X			X	X	X	X	X	X
59		X										X						X						X			X		X	X	X	X
60											X	X						X				X		X			X			X	X	X
61		**X**						**X**		**X**		**X**		**X**				**X**	**X**				**X**		**X**			**X**				
62		X										X						X				X		X			X		X	X	X	X
63											X	X						X				X		X			X		X	X	X	X
64		X									X	X						X				X		X			X		X	X	X	X

le 4.3C. complete list of all possible Isocon compatible element combinations obtained from overlapping cone method (after Baumgartner and Olsen 199

iceous granulite to zone C alteration) The element combination 61has taken as best fit-isocon

Si	Al	Ti	Fe	Mn	Mg	Ca	K	Na	P	LOI	Sc	V	Cr	Co	Ni	Cu	Zn	Ga	Rb	Sr	Y	Zr	Nb	Ba	U	Th	Pb	Hf	Ta	La	Ce	Pr	Nd	Sm
			X																								X							
									X																	X								
																									X	X								
																	X								X									
					X																				X									
X			X																								X							
X			X												X																			
			X								X				X																			
											X					X					X													
									X												X					X								
									X																X	X								
					X												X								X									
X			X												X												X							
X			X								X				X																			
			X								X		X		X																			
											X					X					X		X											
									X		X					X					X													
									X							X					X					X								
X	X		X			X					X		X		X																			
						X	X				X		X		X																			
											X					X		X			X		X											
									X		X					X					X					X								
			X			X	X				X		X		X																			
						X	X				X		X		X					X														
						X	X				X		X		X									X										
		X									X					X												X		X				X
											X					X												X		X		X		X
											X					X												X			X	X		X
										X	X					X		X			X		X											
						X	X				X		X		X					X				X										
						X	X				X		X		X	X								X										
		X					X				X		X		X	X												X						
		X									X					X						X						X		X				X
		X									X					X												X		X		X		X
											X					X												X		X	X	X		X
											X					X												X			X	X	X	X
										X	X					X							X									X	X	X
										X	X					X		X			X		X									X		
						X	X				X		X		X	X								X				X						
		X				X	X				X		X		X	X												X						
		X					X				X		X		X	X			X									X						
		X					X				X				X	X			X															X
		X									X				X	X						X						X		X				X
											X					X												X	X		X	X	X	X
											X			X		X													X		X	X	X	X
										X	X			X		X													X			X	X	X
	X									X	X					X							X									X	X	X
										X	X					X					X		X									X	X	X
										X	X					X		X			X		X									X	X	
		X				X	X				X		X	X	X	X								X				X						
		X					X				X		X		X	X			X									X						X
		X					X				X	X			X	X			X									X						X
		X					X				X	X			X	X												X		X				X
		X									X	X			X	X						X						X		X				X
											X			X		X												X	X		X	X	X	X
										X	X			X		X													X		X	X	X	X
										X	X			X		X							X						X			X	X	X
	X									X	X			X		X							X									X	X	X
										X	X					X		X			X		X									X	X	X
		X					X				X	X			X	X			X									X			X			X
		X					**X**				**X**	**X**			**X**	**X**						**X**						**X**			**X**			**X**
	X									X	X			X		X							X						X			X	X	X

Table 4.4 Gibbs free energies and log K values of mineral and aqueous species calculated for the ion exchange reaction; $KFe_3[AlSi_3O_{10}](OH)_2 + 2HCl = KFe_3[AlSi_3O_{10}](Cl)_2 + 2H_2O$

Mineral/Aqueous Species	ΔG (850°C/9kbar) ($Jmol^{-1}$)	Reference
Cl- annite $[KFe_3(AlSi_3O_{10})Cl_2]$	-5093652.10	Zhu and Sverjensky (1991, 1992
Annite $[KFe_3(AlSi_3O_{10})OH_2]$	-5301270.00	Zhu and Sverjensky (1991, 1992)
$HCl_{(aq)}$	-186614.13	Sverjensky et al. (1991)
H_2O	-319351.89	Berman (1988)
$\Delta G^{reaction}$	-57857.62	
Log K	2.6906	

Table 4.5 Average values of $\log(X_{Cl}/X_{OH})$ and X_{Mg} in biotites and the calculated activity of HCl of the respective aqueous fluids

Rock type	$\log(X_{Cl}/X_{OH})$	X_{Mg}	$\log a_{HCl}$
ultramafic rocks	-1.720 ± 0.062	0.991 ± 0.001	-3.50
ultramafic rocks neighbour to physical contact)	-1.650 ± 0.032	0.991 ± 0.001	-3.51
siliceous granulites	-1.551 ± 0.043	0.634 ± 0.009	-3.56

FIGURE CAPTIONS

Fig. 4.1 Simplified Geological map of Sri Lanka (after Cooray 1994; Kröner et al. 1991) and location map of the area. Ultramafic-siliceous granulitic rock units are exposed at the '*Garandu Kandura'* at Rupaha.

Fig. 4.2 Cross section showing the lithological bands along the lines A-B-C in Fig. 4.1. Note the repetition of the ultramafic-siliceous granulite contact, which consist zoning in many places.

Fig. 4.3 (a) Schematic diagram showing the complete sequence of reaction bands formed between the siliceous granulites and the ultramafic rocks. This section is based on the samples RU 9805 and RU 9806. Zone A- phlogopite-spinel-sapphirine gneiss; Zone B-corundum-sapphirine-spinel gneiss; Zone C-corundum-biotite-plagioclase gneiss (30% Crn); Zone D-corundum-biotite-plagioclase gneiss (5%Crn); See text for further details; (b) a hand specimen showing the reaction zones (9805-9806).

Fig. 4.4. Photomicrographs show the mineral assemblages of complete profile 9805-9806: (a). forsterite-diopside-enstatite in ultramafic rock, (b). forsterite-spinel at the contact of ultramafic rock and the reaction zones. Note the formation of phlogopite from spinel and forsterite, (c). phlogopite-spinel-sapphirine gneiss in zone A, (d). corundum-sapphirine-spinel gneiss in zone B, (e). corundum biotite plagioclase gneiss (zone C), (f) sillimanite, biotite, quartz and plagioclase in sillimanite-biotite gneiss.

Fig. 4.5 Chemical potential (μMgO)-temperature diagram for the system Al_2O_3-SiO_2-MgO at 9kbar and X_{CO2} = 0, computed with the thermodynamic data of Holland and Powell (1998). The light shaded area is the stability limit of sapphirine. The dark shaded area demonstrates the increase of the spinel-sapphirine-corundum stability field toward the lower temperatures at 725^{o}C, for a X_{CO2} of 0.5.

Fig 4.6 Quantitative chemical potential diagram of μ_{SiO2} Vs μ_{MgO} for the system SiO_2-MgO-Al_2O_3 at 850^oC and 9kbar and X_{CO2}=0. Phase field boundaries were constructed by balancing the mineral reactions with Al_2O_3 using thermodynamic data of Holland and Powell (1998). The dark line represents the shift of chemical potential from siliceous granulites to ultramafic rock through the reaction zones as inferred by co-existing minerals. Along this path, an increase in μ_{MgO} involves the reduction of μ_{SiO2} towards the ultramafic zone.

Fig 4.7 Double-logarithmic 'isocon diagrams' showing Major, minor and LREE element transfer during the alteration of siliceous granulite to: (a). corundum biotite gneiss (zone D), (b). corundum-biotite-plagioclase gneiss (zone C), (c). phlogopite-spinel-sapphirine gneiss (zone A). Elements bolded are considered as immobile components, which are aligned on the isocon line. See text for details on isocon method.

Fig. 4.8 Histograms summarise the: (a). Major (b) minor element enrichment and depletion during the alteration to reaction bands with respect to siliceous granulites.

Fig. 4.9 Cation distribution of biotite from siliceous granulites to ultramafic rocks through reaction zones: (a). distribution of Si, (b). distribution of Al, (c). distribution of X_{Mg} [Mg/(Fe+Mg)], (d). distribution of Fe and Mg, (e). distribution of Ti, (f). distribution of Cl and F. All cations per formula unit in biotite were calculated on the basis of 22 oxygens. Average values and standard deviation of 1σ for each analytical point were also calculated.

Fig. 4.10 The chemical data for biotites from the siliceous granulites, reaction zones and ultramafic rocks at Rupaha. The lines are calculations of the gradient for 850^oC. The biotites from zone D are partly equilibrated from the siliceous granulites while some biotite analyses from zone A are equivalent with ultramafic rocks.

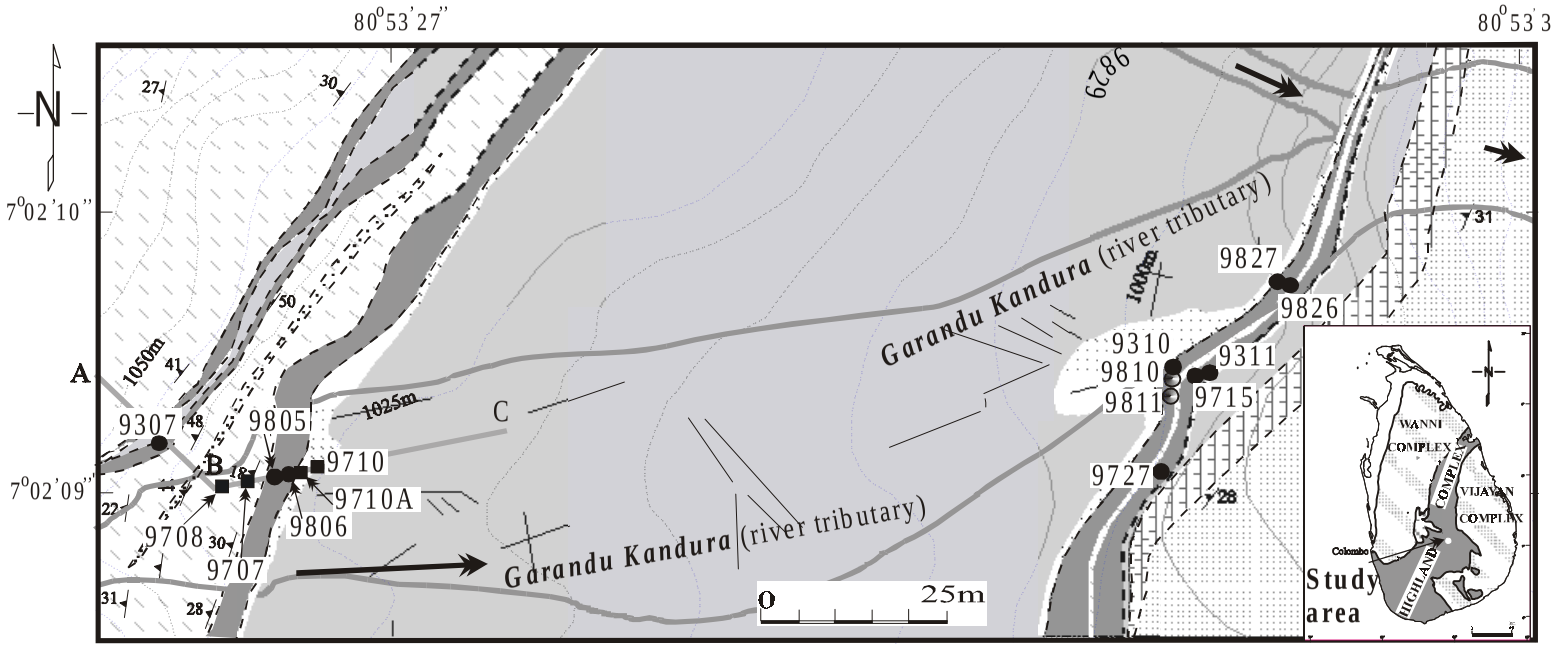

Ultramafic rocks

- ultramafic rocks
- ultramafic rocks with lineated phlogopite

Reaction zone

- corundum-sapphirine-spinel-bearing rocks

Granulites

- charnockite and charnockitic gneisses
- garnet-biotite gneiss and some migmatized rocks
- impure limestones or calc silicate gneiss.

Structural Symbols

- Strike and dip of foliation
- Infered geological boundary
- Minor ductile shear zones
- Rivers & Tributaries
- Contours

Observed mineral assemblages

- Spr +Crn + Phl + Sp
- Crn + Pl + Bt

Fig. 4.1

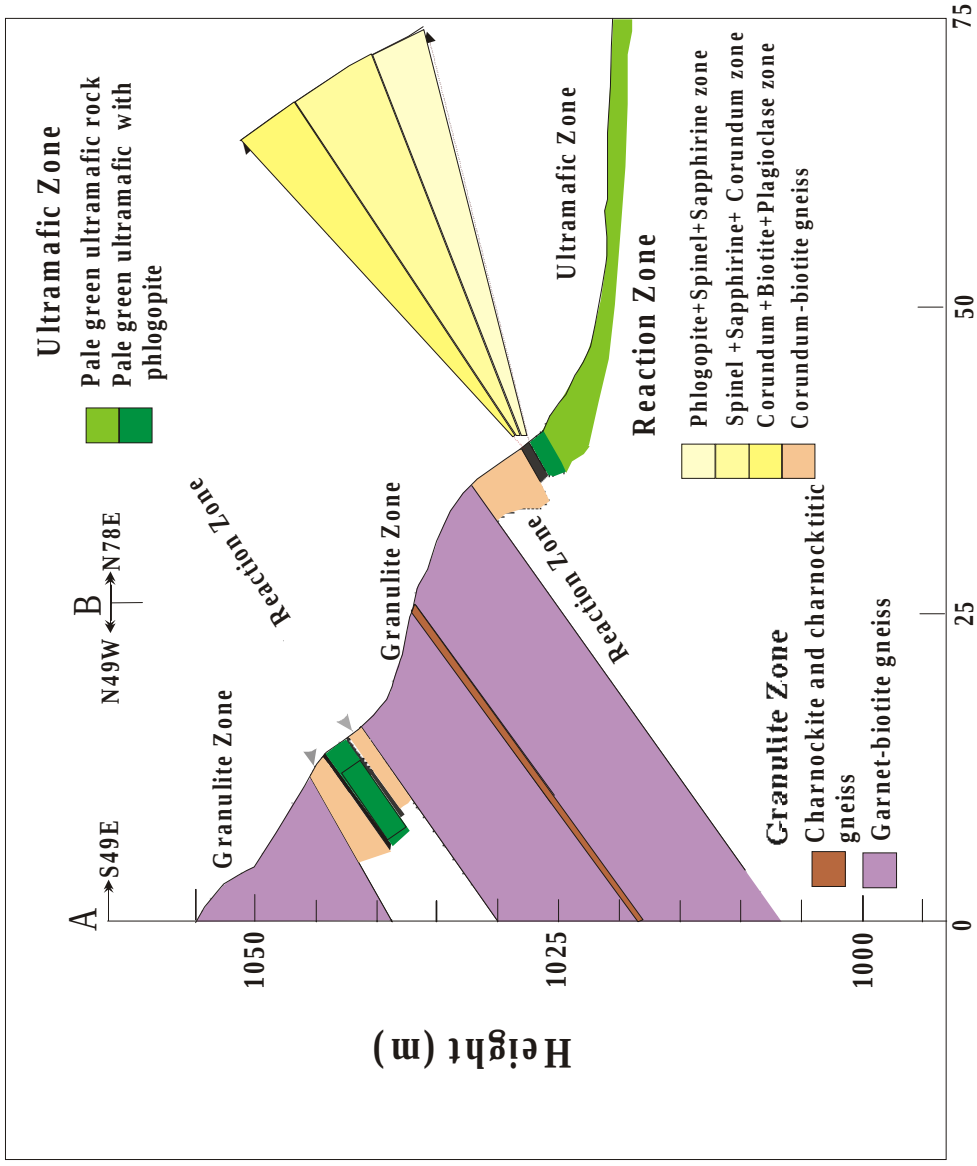
Ultramafic Zone
Pale green ultramafic rock
Pale green ultramafic with phlogopite
Granulite Zone
Charnockite and charnockitic gneiss
Garnet-biotite gneiss
Reaction Zone
Phlogopite+Spinel+Sapphirine zone
Spinel +Sapphirine+ Corundum zone
Corundum+Biotite+Plagioclase zone
Corundum-biotite gneiss
Ultramafic Zone
Reaction Zone
Granulite Zone
Granulite Zone
Reaction Zone
A
S49E
B
N49W
N78E
Height (m)
1050
1025
1000
0
25
50
75
Distance (m)

Fig. 4.2

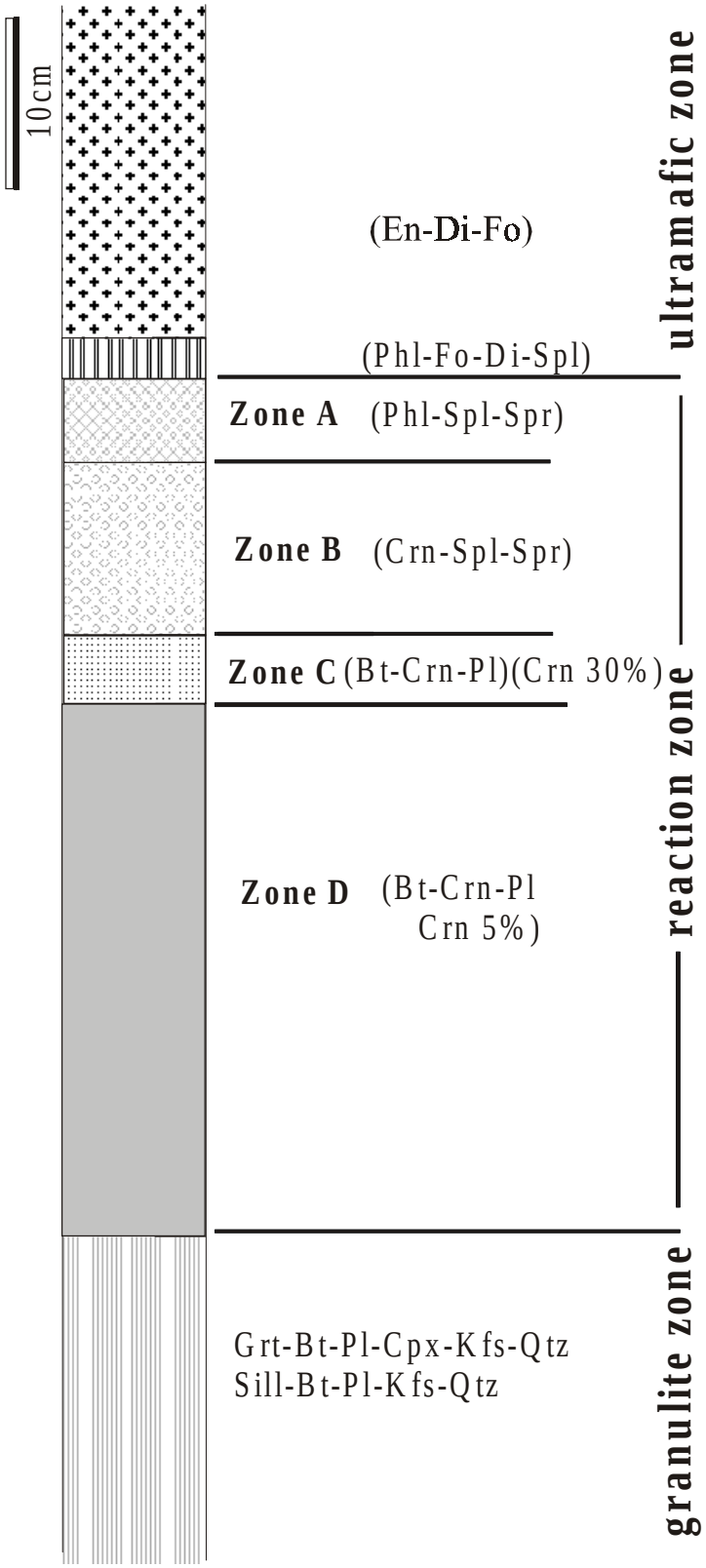
10cm
(En-Di-Fo)
(Phl-Fo-Di-Spl)
Zone A (Phl-Spl-Spr)
Zone B (Crn-Spl-Spr)
Zone C (Bt-Crn-Pl)(Crn 30%)
Zone D (Bt-Crn-Pl
Crn 5%)
Grt-Bt-Pl-Cpx-Kfs-Qtz
Sill-Bt-Pl-Kfs-Qtz
ultramafic zone
reaction zone
granulite zone

Fig. 4.3a

Fig.4.3(b)

Fig. 4.3b

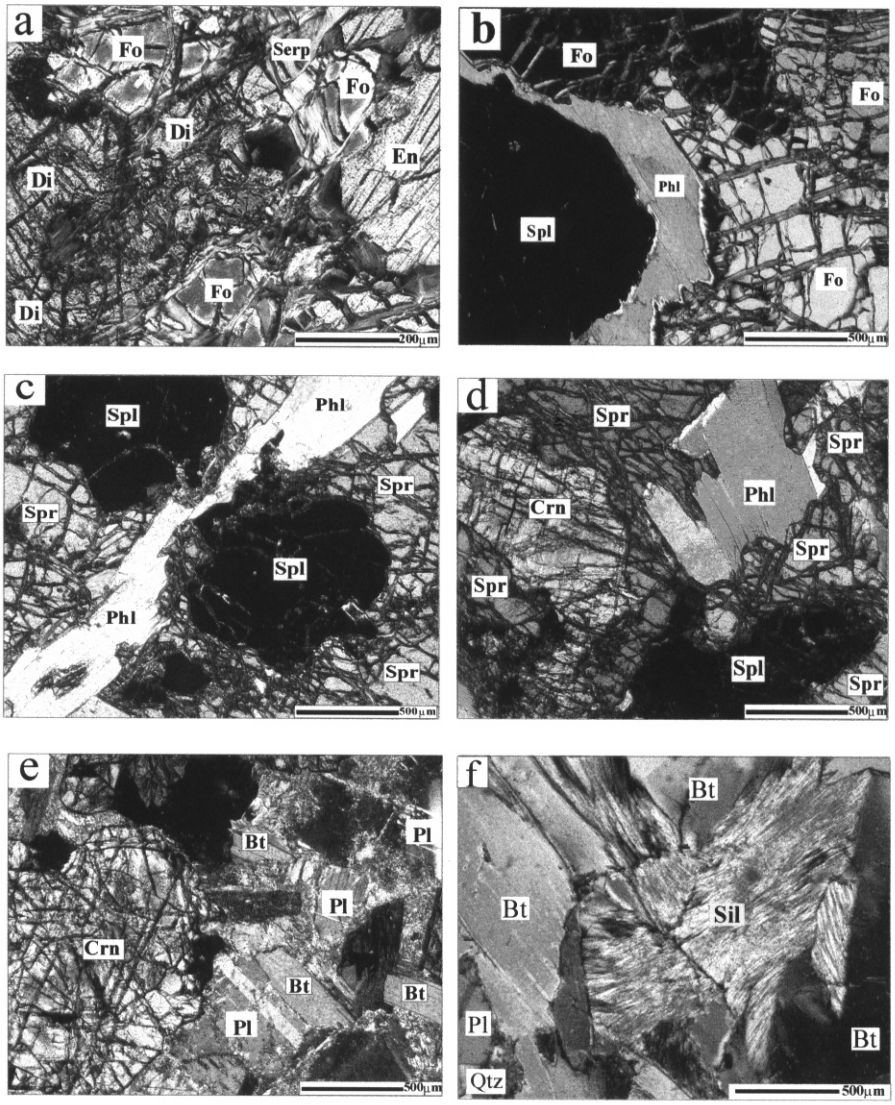
a
Fo
Serp
Fo
Di
En
Di
Fo
Di
200µm
b
Fo
Fo
Phl
Spl
Fo
500µm
c
Spl
Phl
Spr
Spr
Spl
Phl
Spr
500µm
d
Spr
Spr
Phl
Crn
Spr
Spr
Spl
Spr
500µm
e
Bt
Pl
Pl
Crn
Bt
Bt
Pl
500µm
f
Bt
Bt
Sil
Pl
Bt
Qtz
500µm

Fig. 4.4

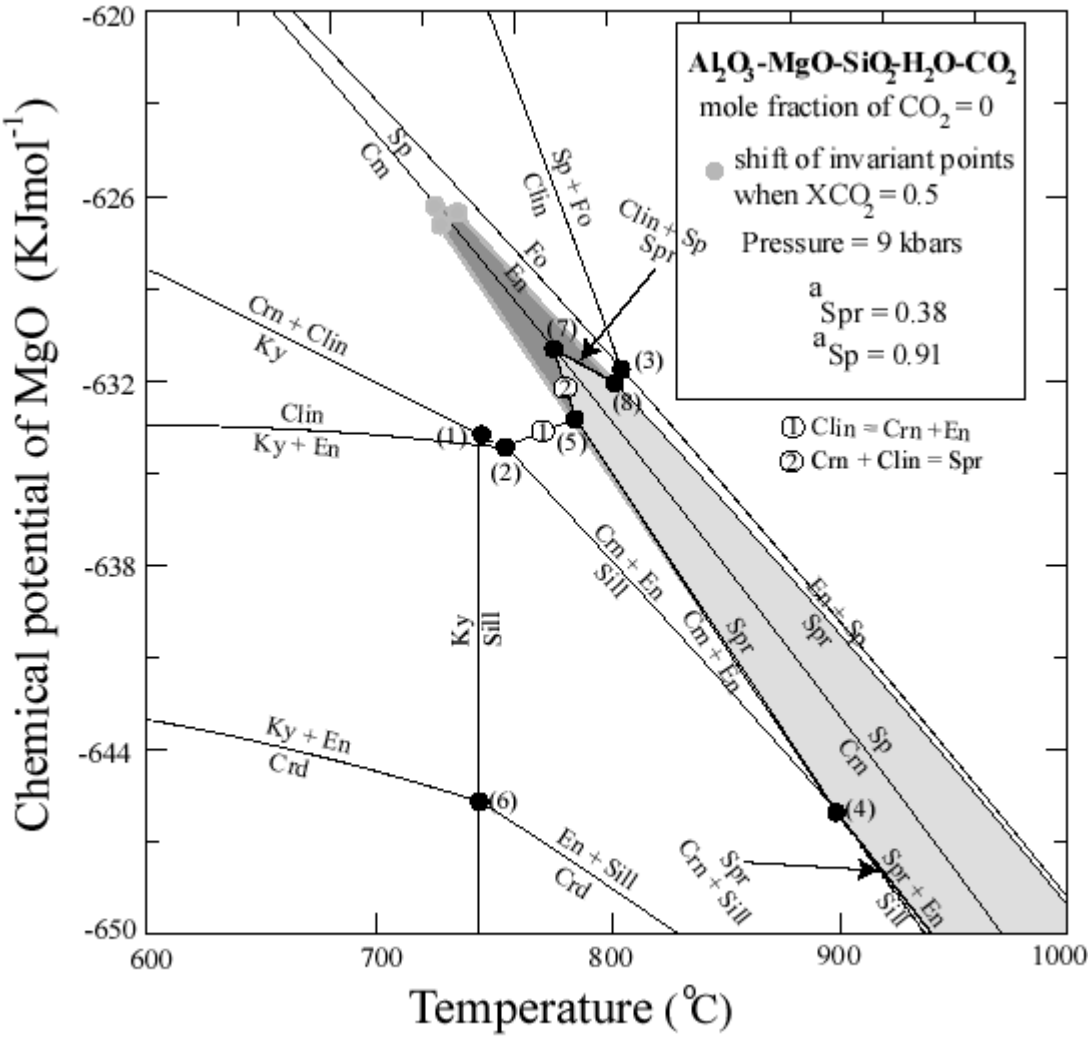
Al2O3-MgO-SiO2-H2O-CO2
mole fraction of CO2 = 0
shift of invariant points when XCO2 = 0.5
Pressure = 9 kbars
aSpr = 0.38
aSp = 0.91
① Clin = Crn + En
② Crn + Clin = Spr
Chemical potential of MgO (KJmol-1)
Temperature (℃)
-620
-626
-632
-638
-644
-650
600
700
800
900
1000
Sp
Crn
Clin
Sp + Fo
Fo
En
Clin + Spr
Sp
Crn + Clin
Ky
Clin
Ky + En
Ky
Sill
Crn + En
Sill
Spr
Spr
En + Sp
Sp
Crn
Ky + En
Crd
En + Sill
Crd
Crn + Sill
Spr
Sill
Spr + En
(1)
(2)
(3)
(4)
(5)
(6)
(7)
(8)

Fig. 4.5

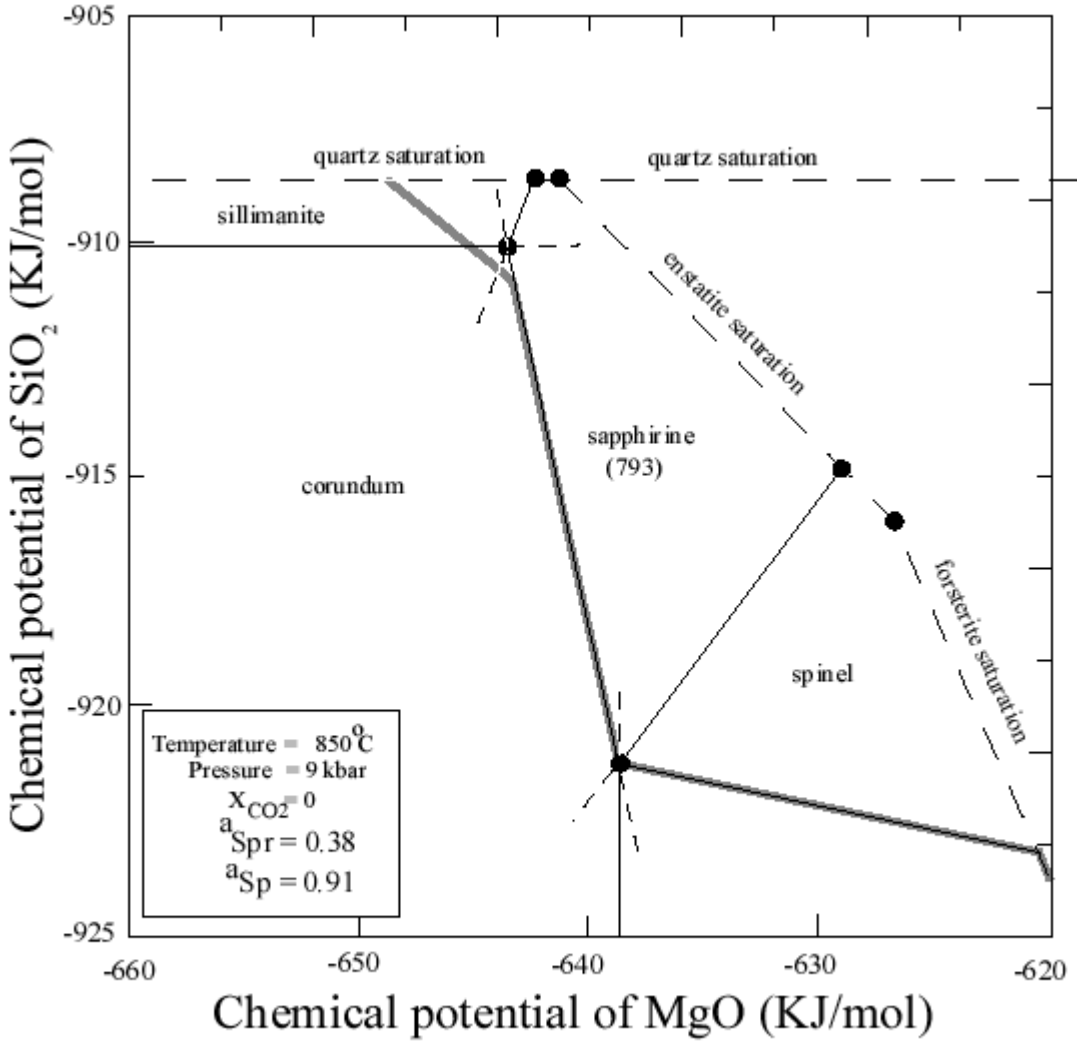
-905
-910
-915
-920
-925
-660
-650
-640
-630
-620
quartz saturation
quartz saturation
sillimanite
enstatite saturation
sapphirine
(793)
corundum
spinel
forsterite saturation
Temperature = 850°C
Pressure = 9 kbar
X_{CO2} = 0
a_{Spr} = 0.38
a_{Sp} = 0.91
Chemical potential of SiO_2 (KJ/mol)
Chemical potential of MgO (KJ/mol)

Fig .4.6

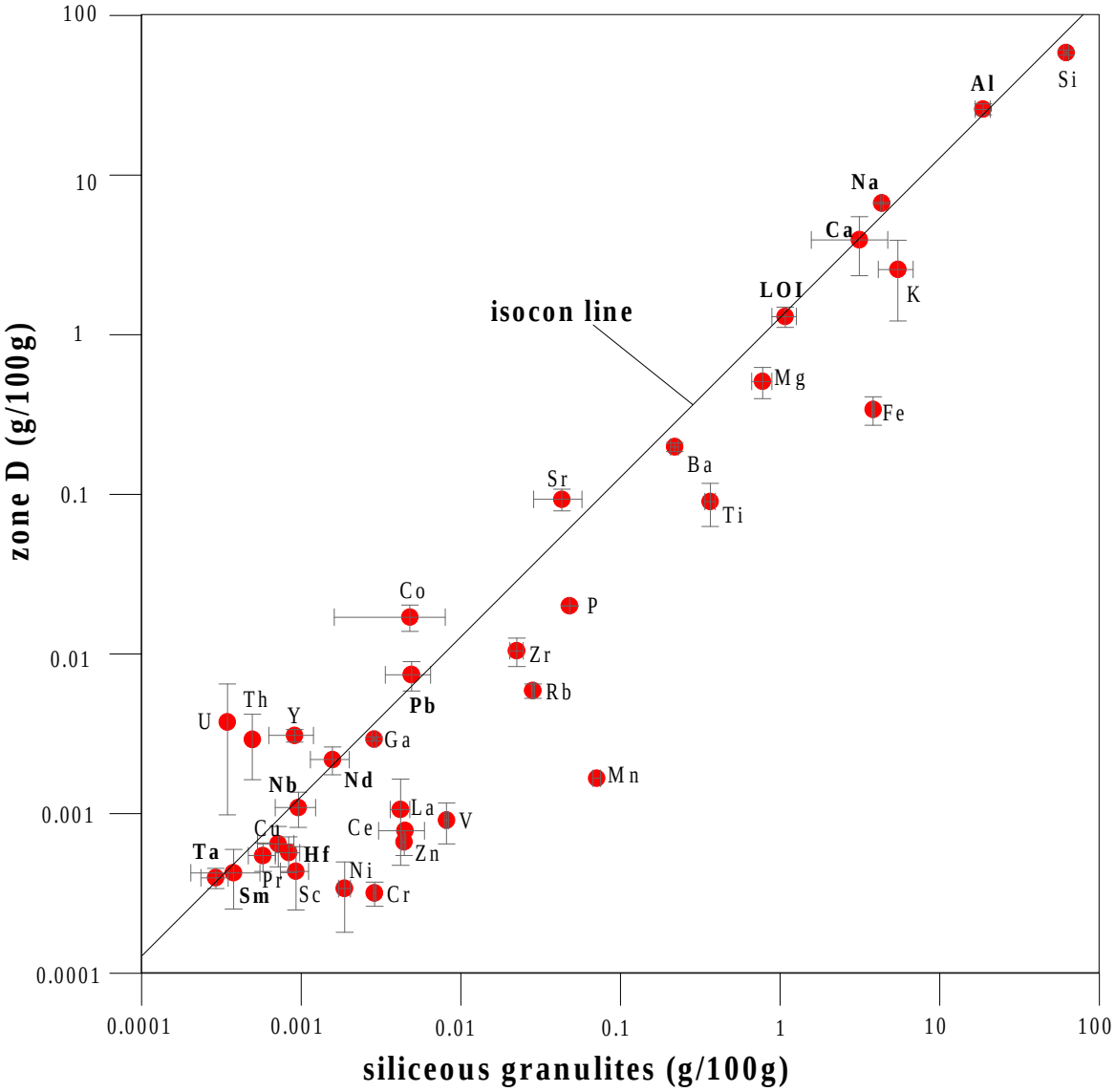
zone D (g/100g)
siliceous granulites (g/100g)
isocon line
100
10
1
0.1
0.01
0.001
0.0001
0.0001
0.001
0.01
0.1
1
10
100
Si
Al
Na
Ca
K
LOI
Mg
Fe
Ba
Ti
Sr
P
Zr
Rb
Mn
Co
Pb
Th
U
Y
Ga
Nd
Nb
La
V
Ce
Zn
Cu
Ta
Hf
Pr
Sm
Sc
Ni
Cr

Fig. 4.7(a)

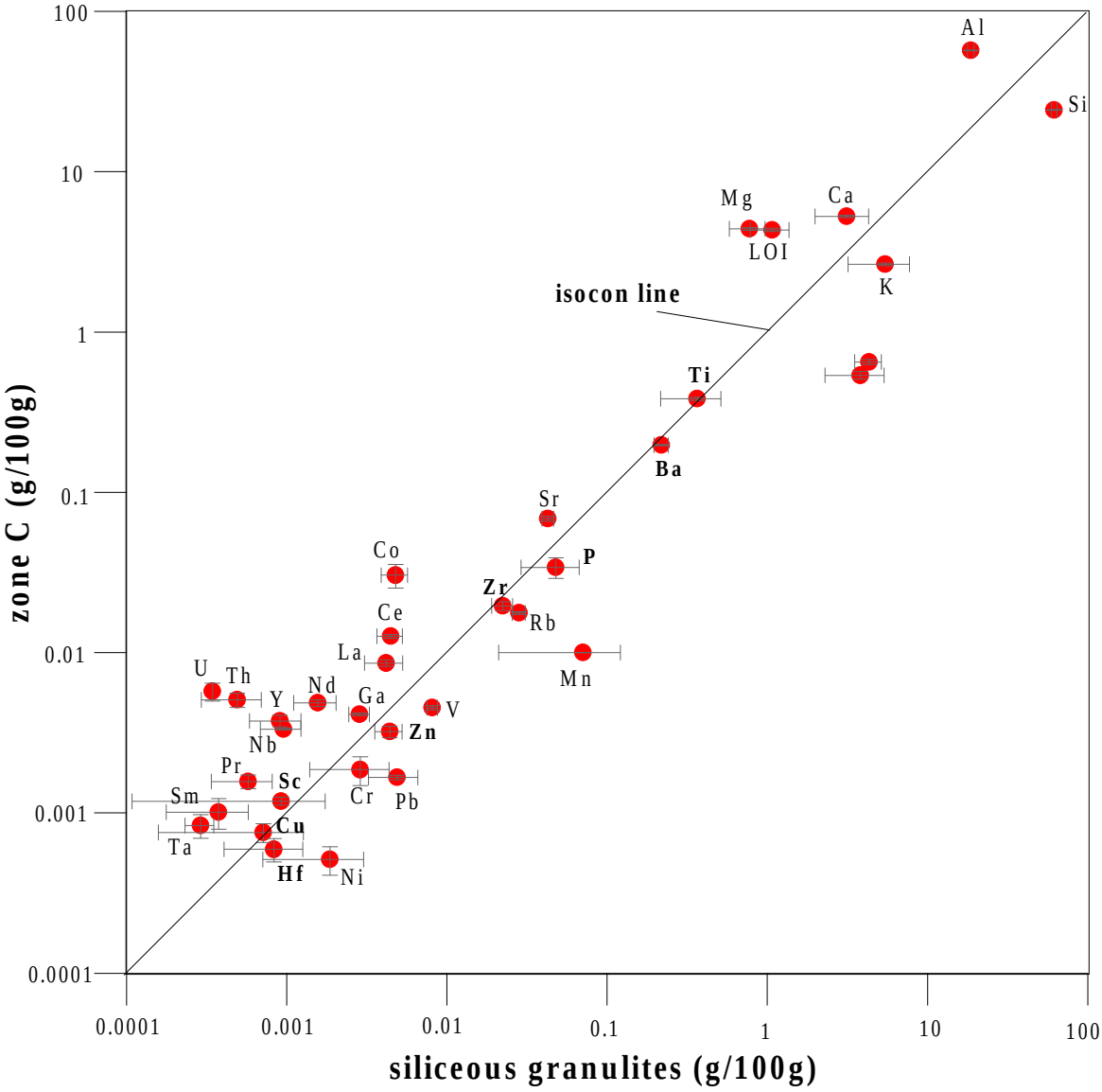
100
10
1
0.1
0.01
0.001
0.0001
zone C (g/100g)
0.0001
0.001
0.01
0.1
1
10
100
siliceous granulites (g/100g)
isocon line
Al
Si
Mg
Ca
LOI
K
Ti
Ba
Sr
P
Zr
Rb
Mn
Co
Ce
La
U
Th
Y
Nd
Ga
V
Zn
Nb
Pr
Sc
Sm
Cr
Pb
Cu
Ta
Hf
Ni

Fig. 4.7(b)

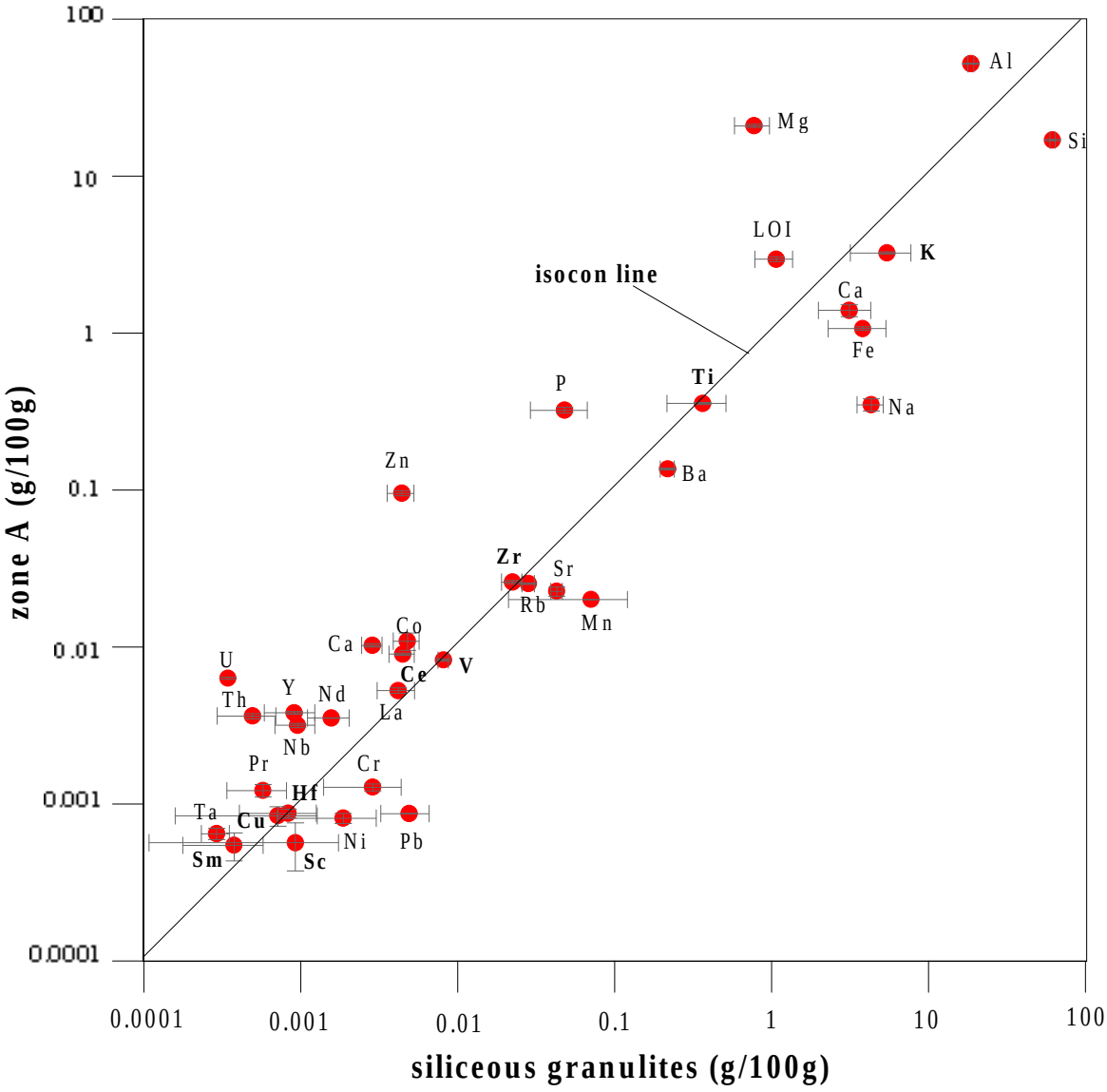
100
10
1
0.1
0.01
0.001
0.0001
zone A (g/100g)
0.0001
0.001
0.01
0.1
1
10
100
siliceous granulites (g/100g)
isocon line
Al
Mg
Si
LOI
K
Ca
Fe
P
Ti
Na
Zn
Ba
Zr
Sr
Rb
Mn
Co
Ca
V
Ce
La
U
Th
Y
Nd
Nb
Pr
Cr
Hf
Ta
Cu
Ni
Pb
Sm
Sc

Fig. 4.7(c)

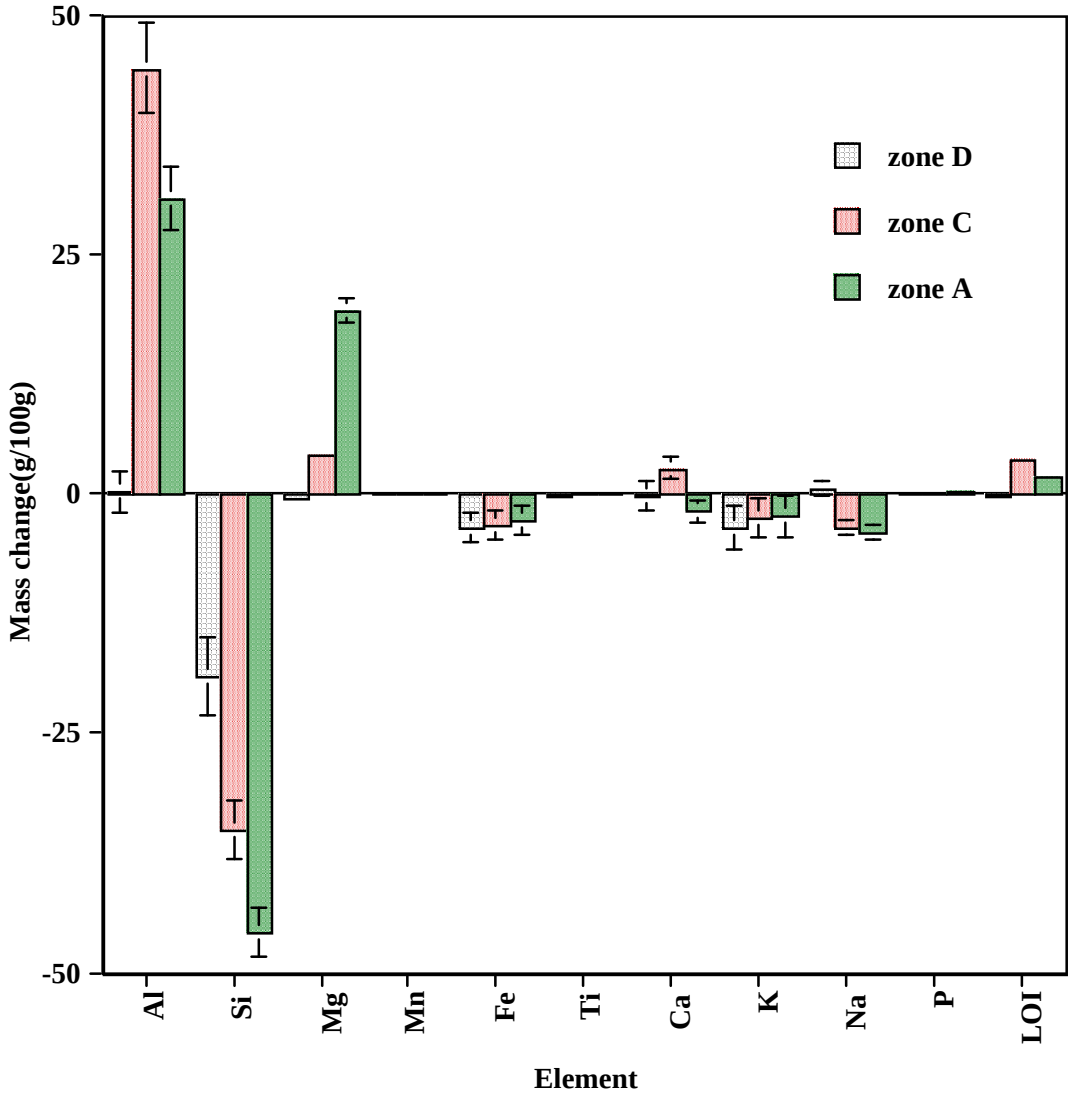
50
25
0
-25
-50
Mass change(g/100g)
zone D
zone C
zone A
Al
Si
Mg
Mn
Fe
Ti
Ca
K
Na
P
LOI
Element

Fig. 4.8a

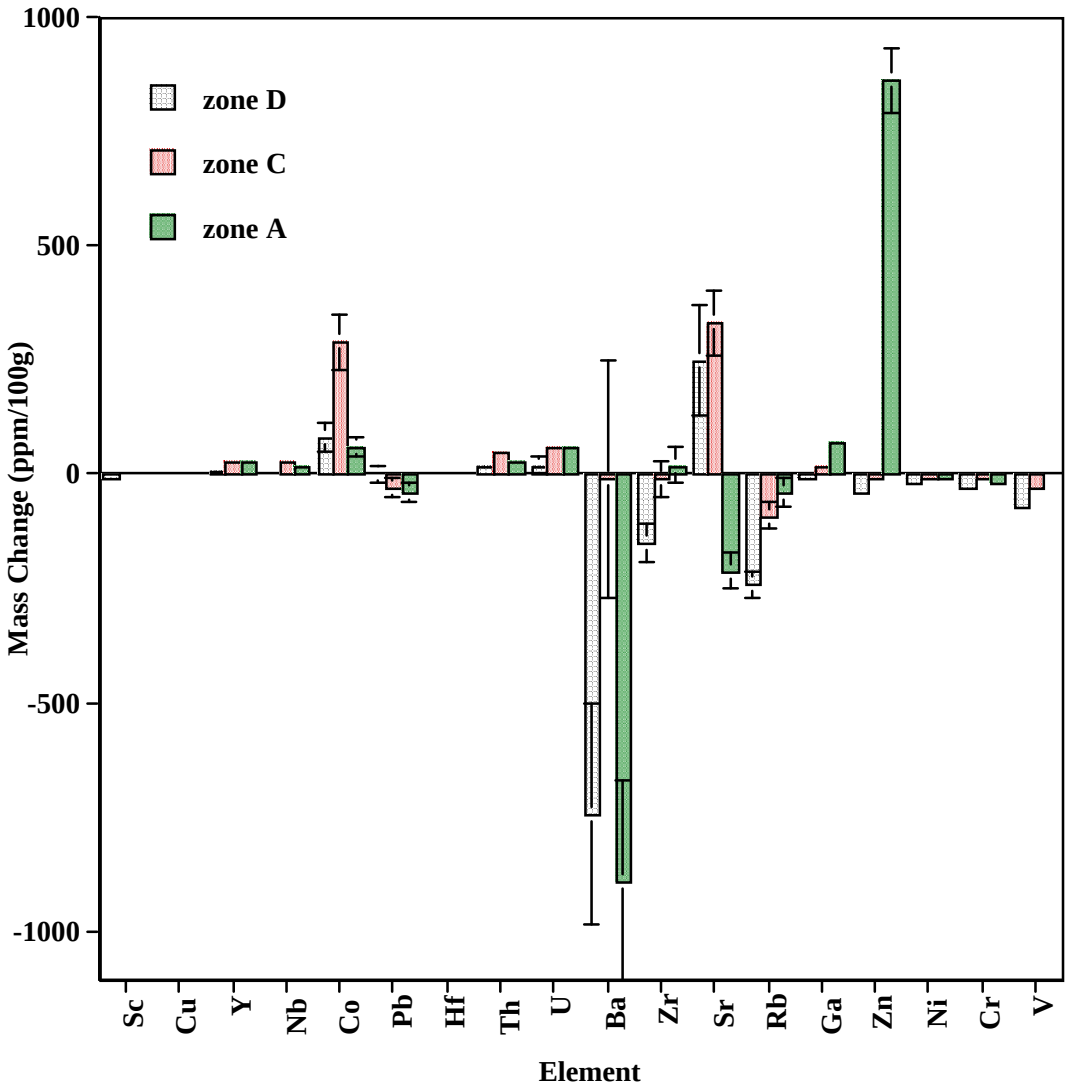
1000
500
0
-500
-1000
Mass Change (ppm/100g)
zone D
zone C
zone A
Sc
Cu
Y
Nb
Co
Pb
Hf
Th
U
Ba
Zr
Sr
Rb
Ga
Zn
Ni
Cr
V
Element

Fig. 4.8b

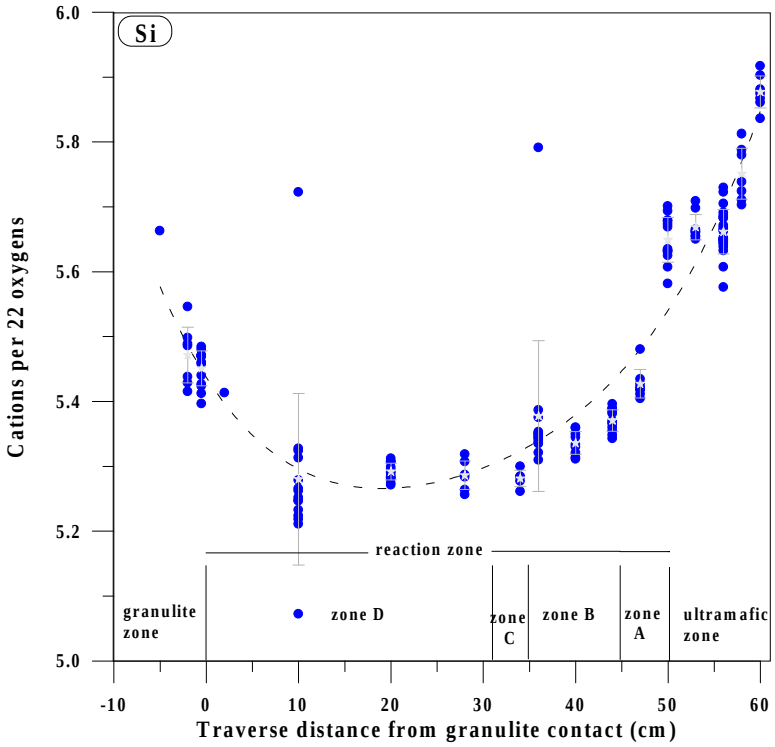

Fig. 4.9a

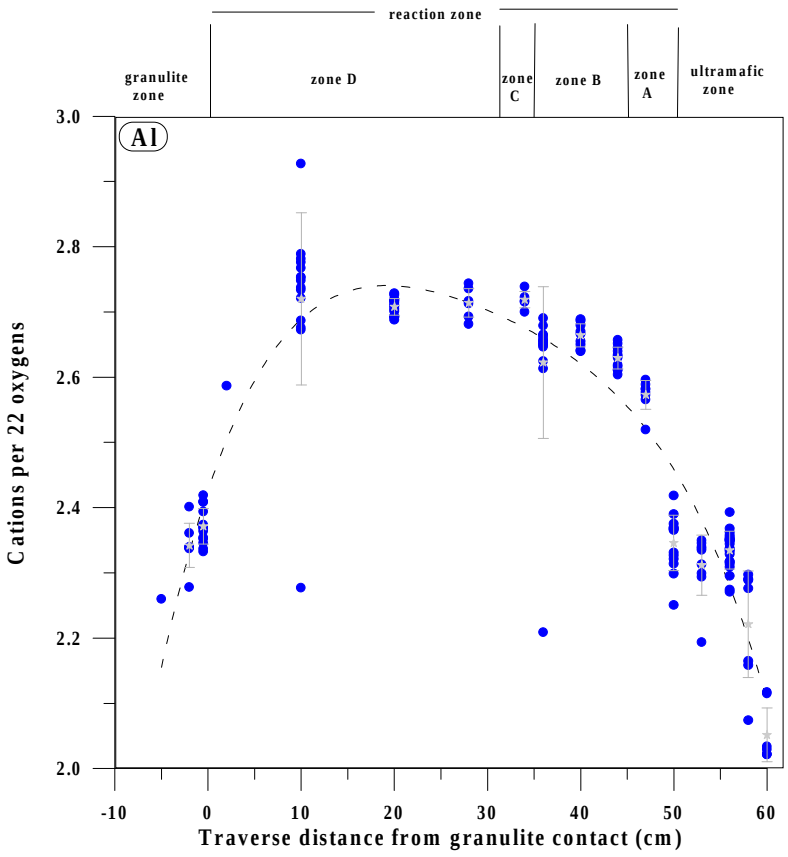

Fig. 4.9b

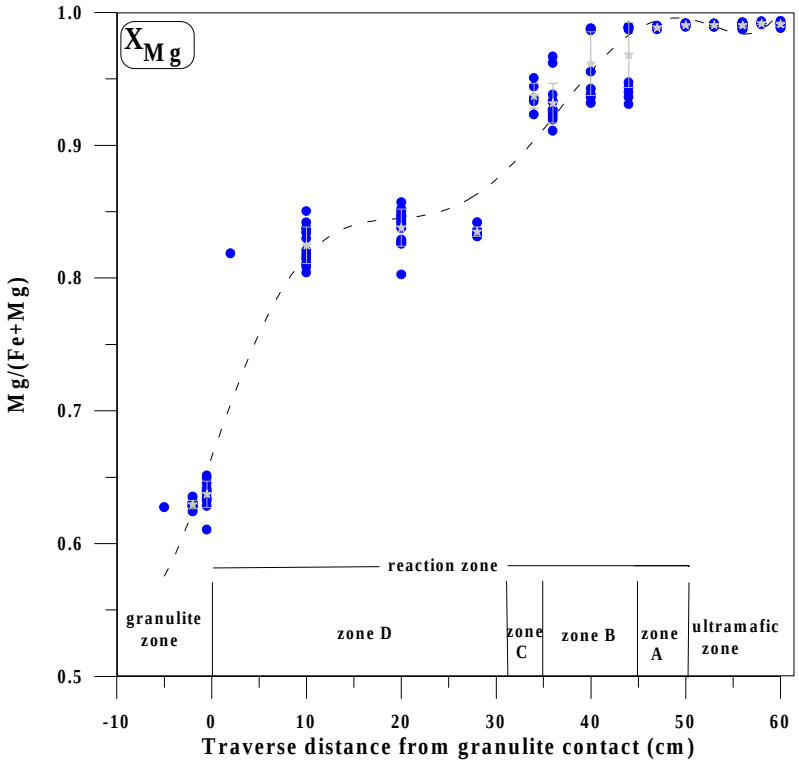

Fig. 4.9c

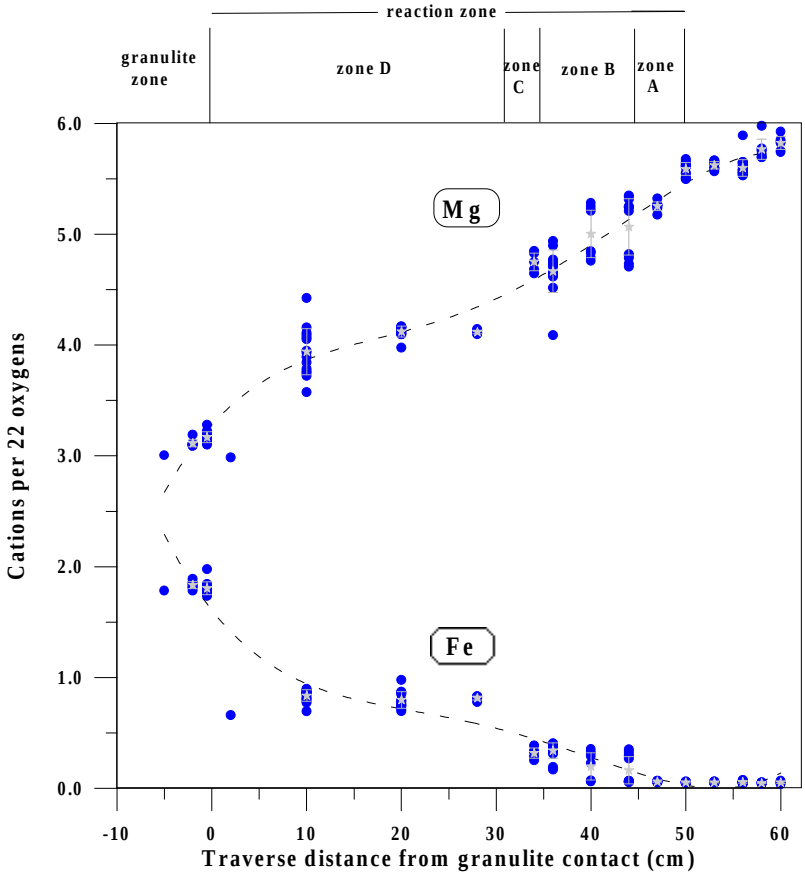

Fig.4.9d

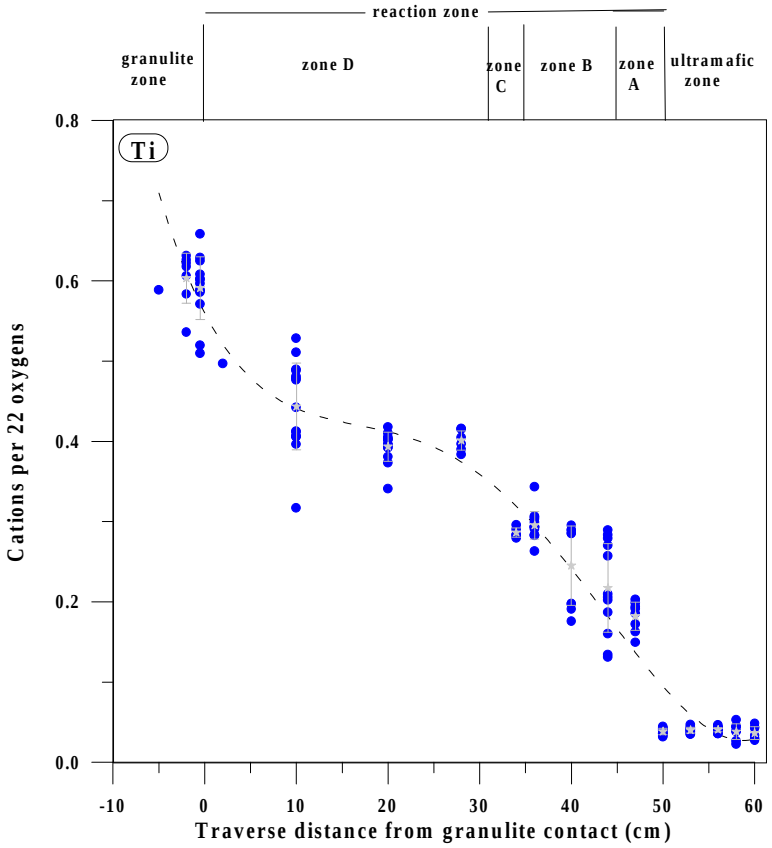

Fig. 4.9e

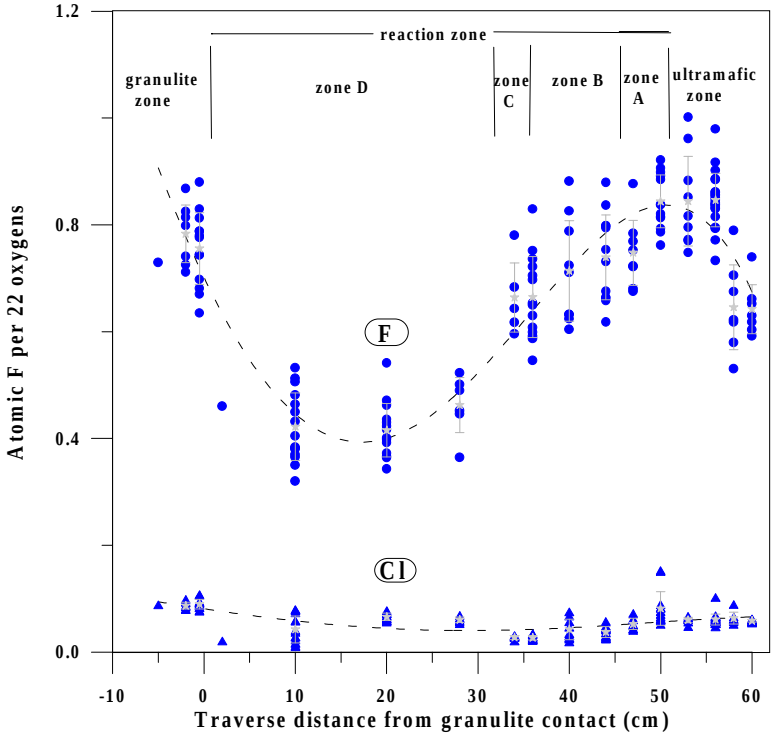

Fig. 4.9f

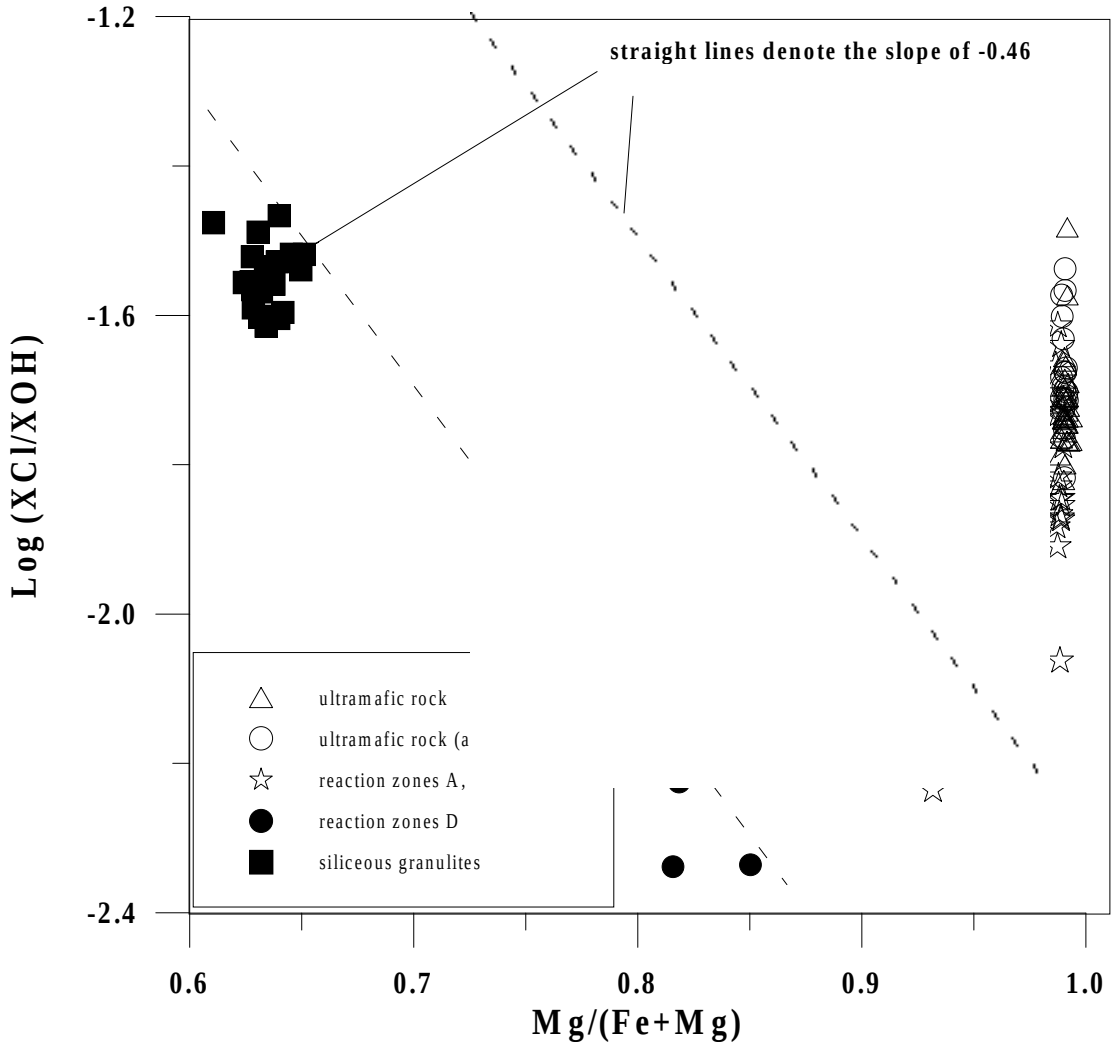
straight lines denote the slope of -0.46
-1.2
-1.6
-2.0
-2.4
Log (XCl/XOH)
0.6
0.7
0.8
0.9
1.0
Mg/(Fe+Mg)
ultramafic rock
ultramafic rock (a
reaction zones A,
reaction zones D
siliceous granulites

Fig. 4.10

Appendix

Appendix A - List of abbreviations

A.1 Minerals and phases after Kretz (1983)

Ab	albite	En	enstatite	Pl	plagioclase
Alm	almandine	Fo	forsterite	Prp	pyrope
Ann	annite	Fs	ferrosilite	Qtz	quartz
An	anorthite	Grt	garnet	San	sanidine
Atg	antigorite	Grs	grossular	Sil	sillimanite
Ap	apatite	Hed	hedenbergite	Spr	sapphirine
Bt	biotite	Ilm	ilmenite	Spl	spinel
Cal	calcite	Kfs	K-feldspar	Srp	serpentine
Chl	chlorite	Ol	olivine	Tlc	talc
Crn	corundum	Opx	orthopyroxene	Tr	tremolite
Di	diopside	Per	periclase		
Dol	dolomite	Phl	phlogopite		

A.2 Thermodynamic and mathematical symbols

For chemical elements and compounds, the standard symbols are used (H_2O, CO_2 etc.)

R	universal gas constant (1.987 cal K^{-1} mol^{-1})
P	pressure
T	temperature
t	time
a	activity
ΔG	Gibbs free energy
ln	natural logarithm (base e)
log	logarithm to the base 10
σ	standard deviation
exp	exponent

Appendix B – Analytical procedures

(1) X-Ray Fluorescence Spectroscopy

Overview

In X-Ray fluorescence (XRF) spectroscopy a continuous spectrum of X-Rays is used to cause emission of characteristic X-Rays (secondary fluorescence) in a sample by excitation of inner shell electrons. Intensity and wavelength of the emitted X-Rays are characteristic for the elements and their concentration present in the sample. The spectrum is then diffracted by suitable monochromator crystals, and characteristic element peaks are measured at source-sample-detector angles given for a specific wavelength by Bragg equation $n\lambda = 2d \sin\theta$. The X-Ray source is an evacuated tube where electrons, emitted from a heated W cathode are accelerated towards a metal anode by as much as 100kV, producing a continuous spectrum of X-Rays by collision with the metal. The characteristic X-Rays of the metal anode are superimposed on the continuous spectrum. Analytical work is performed in the Institute of Geosciences at the University of Mainz using fully automated Philips PW-1404 wavelength dispersive X–Ray fluorescence spectrometer operating with Rh-tube (see table B1 for standard operating conditions) with automated sample changer (72 positions). All major and trace element concentrations are determined by comparing the fluorescence intensities of the sample with calibration curve obtained from international standards, which closely match the sample matrix in overall composition. Remote control and data processing, including matrix correction procedures, was done with Philips software running on 486 PC.

Preparation methods

Major and trace element analysis performed in XRF spectrometer require different techniques of rock powder preparation.

(a) Major elements (Si, Ti, Al, Fe, Mn, Mg, Ca, Na, K, P, Cr, Ni) are diluted with an excess of a substance that absorbs X-Rays only weakly (i.e. has a low atomic number) and are fused to a glass tablet. This reduces matrix effects and makes them essentially constant in both, the unknown sample and the reference standards (Skoog and Leary 1992). Additionally, better homogeneity of the sample improves the quality in analysing the light elements (Na, Mg), which can significantly suffer from surface effects.

(b) Trace elements (Sc, Y, Rb, Sr, Ba, Zn, Cu, Ni, Co, Cr, V, Ga, Nb, Zr, Pb, Th, U, Hf, Ta) and light rare earth elements (La, Ce, Pr, Nd, Sm) are ` nalysed on pressed powder pellets.

Glass tablet preparation

Rock powder (< 63μm) was dried for 24h at 105^{o}C to adhesive water. The glass tablet was produced by thoroughly mixing of 0.8g of the sample with a 4.80g charge of lithium tetraborate (Merck Spectromelt A10) in a platinum crucible and subsequent melting at 1100^{o}C using a semi-automated melting apparatus. The molten mixture was shaken carefully for 10 minutes and then automatically poured into platinum mold.

Powder Pellet Preparation

Pressed powder pellets were produced by homogenizing of 6g of sample powder and two-component SCANDIPLEX epoxy resin and hardener (ratio 3:2) in a agate mortar and subsequent compression of the mixture at pressures of 7.0 metric ton/cm^2 for 40 seconds. The pellets were then dried at 60^{o}C for 4-5 hours.

Determination of Loss of Ignition (LOI)

The amount of volatile elements in the samples (H_2O, CO_2, S, F, Cl etc.) was determined by heating if 1g rock powder, dried at 105^{o}C, in a muffle furnace to more than 1000^{o}C for about 4 hours. The weight loss reported in percent (of the original weight) as loss of ignition (LOI). The LOI is an essential term for the correction of the major element analysis because it considers the loss of volatiles during glass tablet preparation. However, errors can be introduced if ferrous ion is oxidized to a different extent in the furnace compared to fusion of the glass tablet, which takes significantly less time.

Analyses of ferrous/ ferric ion contents

The amount of ferrous and ferric ion present in a sample cannot be distinguished by XRF analyses. Thus, the iron content is reported as total ferric ion (Fe_2O_3).

International Standards

The following international standards were used for analysing of major, minor and LREE elements. The different standards were used for different rock types.

Standards for basaltic and ultramafic rocks:

AN-G, BCR-1, BE-N, BHVO-1, BIR-1, BM, BR, DNC-1, DR-N, DZE-2, GSS-4, GSS-5, GSS-6, JA-2, JB-1, JB-3, JGB-1, JP-1, MRG-1, NBS688, NIM-D, NIM-N, NIM-P, PACS-1, S-18, SDU-1, W-1, W-2

Standards for granitic rocks:

G-2, GA, GH, GM, GSD-02, GSD-08, GSD-09, GSD-12, GSP-1, GSR-1, GSR-4, GSS-3, JA-1, JF-1, JF-2, JG-1, JG-1a, JR-2, MA-N, NBS278, NBS2704, NIM-G, RGM-1, SDC-1, STM-1, SY-2, T-1, TB, TS,

Standards for carbonate rocks:

BCS368, BCS393, GSR-6, KH-2, NBS88A

Standards for trace elements (Routine):

AGV-1, AN-G, BCR-1, BE-N, BHVO-1, BIR-1, BR, DNC-1, DR-N, DZE-2, G-2, GSD-02, GSD-06, GSD-08, GSD-09, GSD-12, GSN, GSP-1, GSR-1, GSR-6, GSS-2, GSS-3, GSS-4, GSS-5, JB-2, JG-2, MAG-1, MY-4, NIM-G, NIM-S, QLO-1, RGM-1, SCO-1, SDC-1, SDU-1, SGR-1, SO-4, STM-1, SY-2, W-1, W-2 ,

Discussion of analytical quality

The major element analyses sum up to 99 and 100.2 wt% with all Fe calculated as Fe_2O_3. In order to determine the precision of the measurements, ten replicate analyses of the same glass and powder tablets were performed in sequence (Tables B2 and B3). The resulting standard deviations (1σ error) from the mean are less than 0.6% for the major elements except for Na, where it is > 0.6% and for Mn with 0.88%. The smaller precision of Mn is due to its low concentration.

Table B1. Operating condition for major- and trace elements analyses with a Philips PW 1404 XRF spectrometer using Rh-anode at Institute of Geosciences, University of Mainz

Element Line		Accl. kV	Current mA	Collimator	Crystal	Detector
TRACE ELEMENTS						
Sc	Kα	40	60	Fine	LIF200	FL
V	Kα	40	60	Fine	LIF220	FL
Cr	Kα	40	60	Fine	LIF220	FL
Co	Kα	60	40	Fine	LIF220	FS
Ni	Kα	60	40	Fine	LIF220	FS
Cu	Kα	60	40	Fine	LIF220	FS
Zn	Kα	80	30	Fine	LIF220	FS
Ga	Kα	80	30	Fine	LIF200	FS
As	Kα	80	35	Fine	LIF200	FS
Rb	Kα	80	30	Fine	LIF220	SC
Sr	Kα	80	30	Fine	LIF220	SC
Y	Kα	80	30	Fine	LIF220	SC
Zr	Kα	80	30	Fine	LIF220	SC
Nb	Kα	80	30	Fine	LIF220	SC
Cd	Kα*	80	35	Coarse	LIF200	SC
Sn	Kα	80	35	Coarse	LIF200	SC
Sb	Kα	80	35	Coarse	LIF200	SC
Ba	Lα	40	60	Fine	LIF200	FL
La	Lα	40	70	Coarse	LIF220	FL
Ce	Lα	40	70	Coarse	LIF220	FL
Pr	Lα	40	70	Coarse	LIF220	FL
Nd	Lα	40	70	Coarse	LIF220	FL
Sm	Lα	40	70	Coarse	LIF220	FL
Hf	Lα	60	40	Fine	LIF200	FS
Ta	Lα	60	40	Fine	LIF200	FS
Pb	Lβ	80	30	Fine	LIF200	SC
Th	Lα	80	30	Fine	LIF200	SC
U	Lα	80	30	Fine	LIF200	SC
Rh	Compton	80	30	Fine	LIF220	SC
MAJOR ELEMENTS						
Na	Kα	40	60	Coarse	PX1	FL
Mg	Kα	40	60	Coarse	PX1	FL
Al	Kα	40	60	Coarse	PE	FL
Si	Kα	40	60	Coarse	PE	FL
P	Kα	40	60	Coarse	GE	FL
K	Kα	40	60	Fine	LIF200	FL
Ca	Kα	40	60	Fine	LIF200	FL
Ti	Kα	40	60	Fine	LIF200	FL
Cr	Kα	40	60	Fine	LIF200	FL
Mn	Kα	60	40	Fine	LIF220	FL
Fe	Kα	60	40	Fine	LIF220	FS
Ni Kα		60	40	Fine	LIF200	FS

* with Messing-Filte

LIF lithium fluoride PE pentaerythrite PX1 multilayer crystal GE germanium

Table B2. Reproducibility of major elements

Reproducibility of major elements from 10 replicate analyses of same glass tablets			
Oxide	**Average (Wt%)**	**Standard Deviation (s)**	**s (% rel)**
SiO_2	44.2	0.060	0.13
TiO_2	2.17	0.003	0.16
Al_2O_3	12.33	0.031	0.25
Fe_2O_3	12.27	0.014	0.11
MnO	0.19	0.002	0.88
MgO	12.23	0.029	0.23
CaO	10.06	0.016	0.16
Na_2O	2.70	0.016	0.61
K_2O	1.08	0.005	0.45
P_2O_5	0.62	0.003	0.48
Cr_2O_3	0.063	0.000	0.54
NiO	0.043	0.000	0.56

For the trace elements, precision is better than 3%, except for Co (3.9%), Cu (3.7%), Ga (3.9%), Pr (4.9%), Nd (5.1%), Sm (6.9%), Hf (5.0%), Ta (4.3%), Th (3.1%), U (6.0%). The large standard deviation (1σ error) of these elements is caused by their low concentration, which is close to the detection limit.

Accuracy of all major elements, determined from re lative deviations to USGS standards, measured together with samples, is less that 1% (Table B2). Trace element analyses generally have accuracy within 6% (Table B3) of the working value of the measured standard (Govindaraju 1989).

Table B3. Reproducibility and detection limits of minor elements

Reproducibility of major elements from 10 replicate analyses of same glass tablets				
Element	**average (ppm)**	**Standard deviation (s)**	**s (%rel)**	**Detection limit (ppm)**
V	220	1.8	0.8	1.1
Cr	435	5.1	1.2	2.1
Co	57	2.3	3.9	1.9
Ni	345	2.9	0.8	1.1
Cu	60	2.2	3.7	0.4
Zn	105	1.5	1.3	1.8
Ga	18	0.7	3.9	1.4
Rb	44	1.0	2.4	1.3
Sr	755	2.5	0.3	1.4
Y	26	0.6	2.4	1.6
Zr	223	1.5	0.7	1.1
Nb	77	0.3	0.4	1.0
Ba	585	3.6	0.6	6.6
La	278	1.9	0.7	3.6
Ce	406	3.7	0.9	9.1
Pr	39	1.9	4.9	2.5
Nd	109	2.1	2.0	5.1
Sm	8	1.8	2.2	6.9
Hf	24	1.2	5.0	2.5
Ta	23	1.0	4.3	3.2
Pb	30	0.6	2.0	2.0
Th	13	0.4	3.1	1.0
U	5	0.3	6.0	1.6

(2) Electron Probe Microanalyser (EPMA)

Overview

The electron microprobe (EMP) is used for the quantitative chemical analysis of small areas (typically 1-10μm in diameter) on a polished surface (e.g. polished thin sections). The concentration of elements from Be to U can be measured in minerals and glasses at levels as low as 100ppm, and their lateral distribution can be determined by mapping. When an electron beam is focussed on a sample surface, emission of characteristic X-Rays is one of the numerous effects caused by interaction of energetic electrons (normally 10 to 30 keV) with sample material. Wavelength and intensity of the characteristic X-Rays reflect the specific elements and their concentration in the excited area. All emitted X-Rays are diffracted by suitable monochromator crystals arranged together with the detector and the sample in a setting (configuration) to satisfy the Bragg equation $n\lambda = 2d \sin\theta$.

All mineral compositions were analysed using the electron microprobe in the Institute for Geosciences, University of Mainz. The EMP in Mainz is fully automated JEOL JXA 8900 RL with five wavelength dispersive defractometers, which is operated from a windows-based menu running on a HP-UX workstation (software from JEOL). Spectrometers with fixed monochromator crystals allow off-peak measurement of the background. Mean atomic number and background correction are then iteratively calculated in combination with ZAF X-Ray absorption correction (Amstrong 1988, 1989).

Standard operating conditions listed in Table B4 was used. The following Table B5 contain information on the spectrometer configuration and standards used for electron microprobe analyses at the University of Mainz, Germany. X-Ray intensities were automatically corrected for probe current drift, dead time, background and matrix effects by the built-in software.

Discussion of Analytical quality

Accurate determination of mineral compositions is indispensable for accurate estimates of metamorphic temperatures, pressures and some other applications as well. He quality of microprobe data was evaluated on the basis of stoichiometry of minerals. It can be generally concluded that for element oxides with concentrations greater than 5% wt the standard deviation is smaller than 2%, and that for concentrations between 5 and 0.5 wt%

it is smaller than 10%. Accuracy is better than 1% of the working value from major elements (Govindraju 1989).

Table B4. Normal operating conditions for the electron probe microanalyser in Institute for Geosciences, University of Mainz

Acceleration voltage	15 kV
Probe current	12 nA (Ba 8nA)
Probe diameter	2μm
Take off angle	40^{o}
Absorption correction	ZAF
Background correction	Off-peak

Table B5. Spectrometer configuration and standards used for calibration in electron microprobe analyses in Institute for Geosciences, University of Mainz

Element peak	X-Ray line	Spectro meter	Crystal	Standard	element concen- (wt%)		peak-counting time (s) intensity (cps)
Na	**Kα**	**2**	**TAP**	**albite**	**11.7409**	**15**	**694.6**
K	**Kα**	**3**	**PET**	**orthoclase**	**14.6721**	**15**	**36.0**
Fe	**Kα**	**5**	**LIF**	**Fe_2O_3**	**89.9765**	**15**	**4417.6**
Si	**Kα**	**1**	**TAP**	**wollastonite**	**51.5118**	**15**	**6917.7**
Mg	**Kα**	**2**	**TAP**	**MgO**	**99.9874**	**15**	**10834.1**
Ca	**Kα**	**3**	**PET**	**wollastonite**	**47.7408**	**15**	**2968.2**
Ti	**Kα**	**4**	**PET**	**TiO_2**	**100.0001**	**15**	**5758.5**
Mn	**Kα**	**5**	**LIF**	**rhodocrosite**	**43.4885**	**15**	**1990.3**
Al	**Kα**	**1**	**TAP**	**Al_2O_3**	**99.9949**	**15**	**14128.6**
Cr	**Kα**	**4**	**PET**	**Cr_2O_3**	**99.9985**	**30**	**7172.6**
Ba	**Lα**	**2**	**LIF**	**$BaSO_4$**	**65.6948**	**15**	**745.1**
Cl	**Kα**	**5**	**PET**	**tugtupit**	**7.5800**	**15**	**564.5**
F	**Kα**	**1**	**TAP**	**F-phlogopite**	**9.2000**	**15**	**36.0**

TAP thallium acide phtalate **LIF lithium fluoride**

PET pentaerythrite

References

Amstrong JT (1988). Quantitative analyses of silicate and oxide minerals: comparisions of Monte Carlo, ZAF and Phi-rho-z procedures. In: *Newbury DE* (eds) Microbeam analysis-1988. San Francisco Press, San Francisco, 239-246

Amstrong JT (1989). CITZAF: combined ZAF and phi-rho (Z) electron beam correction programs. California Institute of Technology, Pasadena, CA

Govindraju K (1989). Compiltatoin of working values and sample descriptions for 272 geostandards. Special Issue of Geostandards Newsletter (sp. Issue), 1-113

Kretz R (1983). Symbols for rock forming minerals. Am. Mineral. 68: 277-279

Skoog DA, Leary JJ (1992). Principles of instrumental analysis, Saunders College publishing

Appendix C- Mineral Chemistry

The following tables contain detailed list of mineral analyses referenced in this dissertation.

Table C1 Chemistry of orthopyroxene used for Opx-Cpx ion exchange thermometry

Sample No.	RU 9817A	RU 9817A	RU 9817A	RU 9817A	RU 9817A	RU 9817A
Analysis No.	63	65	84	108	119	60
Mineral pair	1	2	3	4	5	6
SiO_2	48.83	48.33	48.56	48.28	49.17	49.22
TiO_2	0.10	0.08	0.05	0.10	0.07	0.06
Al_2O_3	0.70	0.68	0.54	0.52	0.54	0.77
FeO	37.61	38.03	38.40	38.02	37.99	38.03
Cr_2O_3	0.02	0.05	0.04	0.01	0.00	0.00
MnO	0.90	0.89	0.87	0.89	0.89	0.83
MgO	10.78	10.66	10.95	11.20	11.27	10.64
CaO	0.96	0.87	0.89	0.87	0.87	0.92
Na_2O	0.06	0.01	0.00	0.04	0.00	0.03
K_2O	0.02	0.00	0.00	0.01	0.00	0.01
Total	99.97	99.61	100.31	99.93	100.80	100.51
formula			formula for 6 oxygens			
Si	1.974	1.967	1.964	1.959	1.971	1.978
Ti	0.003	0.002	0.001	0.003	0.002	0.002
Al	0.033	0.033	0.026	0.025	0.026	0.036
Fe	1.271	1.294	1.299	1.290	1.274	1.278
Cr	0.001	0.002	0.001	0.000	0.000	0.000
Mn	0.031	0.031	0.030	0.030	0.030	0.028
Mg	0.650	0.647	0.660	0.678	0.674	0.638
Ca	0.041	0.038	0.039	0.038	0.037	0.040
Na	0.005	0.001	0.000	0.003	0.000	0.002
K	0.001	0.000	0.000	0.001	0.000	0.000
Total cations	4.010	4.015	4.020	4.027	4.014	4.002

$Fe^{[3]}$ as total iron

mineral pairs concerned: 63-64, 65-66, 84-87, 106-108, 119-121, 60-122

Table C1 Chemistry of clinopyroxene used for Opx-Cpx ion exchange thermometry

Sample No.	RU 9817A	RU 9817A	RU 9817A	RU 9817A	RU 9817A	RU 9817A
Analysis No.	64	66	87	106	121	122
Mineral pair	1	2	3	4	5	6
SiO_2	49.73	50.65	50.58	49.58	49.69	49.93
TiO_2	0.13	0.09	0.10	0.19	0.19	0.15
Al_2O_3	1.57	1.22	1.28	1.49	1.91	1.88
FeO	18.15	18.44	18.17	18.22	19.46	18.91
Cr_2O_3	0.03	0.05	0.11	0.04	0.04	0.07
MnO	0.44	0.38	0.45	0.38	0.45	0.38
MgO	8.20	8.45	8.55	8.42	7.97	8.03
CaO	20.99	20.75	20.68	20.39	19.91	20.41
Na_2O	0.63	0.51	0.55	0.58	0.72	0.64
K_2O	0.00	0.00	0.01	0.00	0.03	0.00
Total	99.87	100.55	100.48	99.28	100.37	100.40
formula			formula for 6 oxygens			
Si	1.946	1.964	1.961	1.949	1.940	1.944
Ti	0.004	0.003	0.003	0.005	0.006	0.004
Al	0.072	0.056	0.059	0.069	0.088	0.086
Fe	0.594	0.598	0.589	0.599	0.635	0.616
Cr	0.001	0.002	0.003	0.001	0.001	0.002
Mn	0.015	0.012	0.015	0.013	0.015	0.013
Mg	0.478	0.488	0.494	0.493	0.464	0.466
Ca	0.880	0.862	0.859	0.859	0.833	0.852
Na	0.048	0.038	0.041	0.044	0.054	0.048
K	0.000	0.000	0.000	0.000	0.002	0.000
Total cations	4.038	4.023	4.024	4.032	4.038	4.031

$Fe^{[3]}$ as total iron

Temperature pressure estimates

Combined Opx-Cpx / GADS

Brey and Köhler (1990) and Eckert et al. (1991)

Analysis No.	Pair No.	Temperature(°C)	Pressure(kbar)
63-64	1	873	8.7
65-66	2	870	8.6
84-87	3	872	8.6
106-108	4	875	8.1
119-121	5	882	9.1
60-122	6	871	9.0
	Average	874 ± 4	8.7 ± 0.4

Table C2. Chemistry of garnet used for Grt-Cpx ion exchange thermom

Sample No.	RU 9708	RU 9708	RU 9708	RU 9708	RU 9708	RU 9708	RU 9708
Analysis No	64	66	68	70	74	76	78
Mineral pair	1	2	3	4	5	6	7
SiO_2	38.79	38.46	38.22	38.58	38.92	38.63	38.65
TiO_2	0.05	0.02	0.05	0.05	0.08	0.07	0.08
Al_2O_3	20.99	21.23	20.94	21.03	21.37	21.03	21.15
FeO	22.74	23.02	23.24	22.94	22.31	22.94	23.30
Cr_2O_3	0.09	0.08	0.03	0.08	0.02	0.14	0.10
MnO	6.39	6.35	6.50	6.42	7.12	6.39	6.25
MgO	5.71	5.50	5.42	5.55	5.10	5.41	5.44
CaO	5.95	6.03	6.06	6.01	6.19	5.93	6.05
Na_2O	0.16	0.02	0.09	0.05	0.07	0.05	0.19
K_2O	0.00	0.00	0.00	0.00	0.00	0.00	0.00
Total	100.87	100.72	100.55	100.72	101.17	100.59	101.21
			formula for 24 oxygens				
Si	6.012	5.981	5.959	5.999	6.034	6.020	5.978
Al	3.831	3.889	3.845	3.852	3.902	3.860	3.853
Ti	0.006	0.003	0.006	0.006	0.009	0.009	0.009
Fe	2.947	2.994	3.030	2.983	2.892	2.990	3.014
Cr	0.011	0.010	0.004	0.010	0.002	0.017	0.012
Mg	1.319	1.275	1.260	1.287	1.179	1.257	1.254
Mn	0.839	0.836	0.858	0.846	0.935	0.844	0.819
Ca	0.988	1.005	1.012	1.001	1.028	0.990	1.003
Na	0.048	0.007	0.026	0.016	0.020	0.014	0.058
K	0.000	0.000	0.000	0.000	0.000	0.000	0.000
total cations	16.001	16.000	16.000	16.000	16.001	16.001	16.000

Fe^{tot} as total iron

mineral pairs concerned: 64-106, 66-88, 68-90, 70-82, 74-98, 76-93, 78-79

Table C2. Chemistry of clinopyroxene used for Grt-Cpx ion exchange thermome

Sample No	RU 9708	RU 9708	RU 9708	RU 9708	RU 9708	RU 9708
Analysis N	106	88	90	82	98	93
Mineral pa	1	2	3	4	5	6
SiO_2	52.29	51.97	51.35	52.40	51.90	52.07
TiO_2	0.24	0.23	0.20	0.18	0.24	0.19
Al_2O_3	1.92	1.87	1.88	1.65	2.10	1.83
FeO	9.99	9.70	9.85	9.83	10.11	9.78
Cr_2O_3	0.06	0.05	0.05	0.03	0.06	0.06
MnO	1.14	1.05	1.08	1.04	1.04	1.17
MgO	13.35	13.20	13.68	13.53	13.38	13.13
CaO	20.92	20.62	20.54	21.24	19.54	21.07
Na_2O	0.52	0.51	0.49	0.46	0.48	0.57
K_2O	0.04	0.04	0.05	0.01	0.16	0.03
Total	100.46	99.24	99.17	100.37	99.01	99.90
			formula for 6 oxygens			
Si	1.946	1.958	1.932	1.951	1.959	1.949
Al	0.085	0.082	0.083	0.072	0.094	0.080
Ti	0.007	0.007	0.006	0.005	0.007	0.005
Fe	0.312	0.306	0.310	0.307	0.318	0.307
Cr	0.002	0.002	0.002	0.001	0.002	0.002
Mg	0.741	0.741	0.767	0.751	0.753	0.733
Mn	0.036	0.034	0.034	0.033	0.033	0.037
Ca	0.834	0.832	0.828	0.847	0.790	0.845
Na	0.037	0.037	0.036	0.033	0.035	0.041
K	0.002	0.002	0.002	0.000	0.008	0.002
total cations	4.002	4.001	4.000	4.000	3.999	4.001

Fe^{tot} as total iron

Temperature pressure estimates

Combined Grt-Cpx / GADS

Sengupta et al. (1989) and Eckert et al. (1991)

Analysis No	Pair No	Temperature(°C)	Pressure(kbar)
64-106	1	738	7.24
66-88	2	728	7.14
68-90	3	714	7.08
70-82	4	724	7.10
74-98	5	728	7.14
76-93	6	727	7.13
78-79	7	706	6.91
	Average	724 ± 10	7.1 ± 0.1

Table C3. Chemistry of garnet used for Grt-Bt ion exchange thermometry

Sample No.	9708	9708	9708	9708	9708	9708	9708	9708	9708	9708	9708	9708	9708
Analysis No.	32	33	34	36	40	41	42	44	46	54	55	71	56
Mineral pair	12C	13A	14C	15A	16A	17A	18A	19C	20A	21A	21B	22C	21C
SiO_2	38.40	38.64	38.95	38.54	38.84	38.99	38.37	38.52	38.73	38.47	38.52	38.24	38.48
TiO_2	0.13	0.03	0.08	0.02	0.07	0.09	0.02	0.08	0.06	0.08	0.09	0.06	0.04
Al_2O_3	21.22	21.26	21.15	21.14	21.65	21.58	21.14	20.85	21.06	21.33	21.32	21.43	21.37
Cr_2O_3	0.10	0.08	0.06	0.02	0.07	0.05	0.10	0.00	0.08	0.12	0.10	0.05	0.08
FeO	23.78	23.52	23.65	23.59	23.54	23.63	23.65	23.72	23.51	23.58	23.72	23.61	23.60
MnO	5.90	5.74	6.08	5.96	6.01	5.64	5.78	5.88	5.69	5.81	5.89	5.91	5.82
MgO	5.45	5.52	5.32	5.49	5.75	5.81	5.28	5.28	5.45	5.60	5.49	5.48	5.38
CaO	6.08	6.18	6.08	6.08	5.96	5.68	6.16	6.15	6.11	5.86	6.05	5.92	6.14
Na_2O	0.04	0.02	0.04	0.09	0.00	0.04	0.06	0.06	0.04	0.07	0.06	0.07	0.05
F	0.00	0.10	0.00	0.00	0.00	0.13	0.03	0.00	0.00	0.02	0.08	0.00	0.00
Cl	0.01	0.01	0.02	0.05	0.01	0.00	0.02	0.02	0.04	0.03	0.01	0.01	0.01
Total	101.00	101.01	101.37	100.96	101.83	101.59	100.51	100.56	100.68	100.85	101.23	100.73	100.88
O F Cl	0.00	0.04	0.01	0.01	0.00	0.05	0.02	0.00	0.01	0.01	0.04	0.00	0.00
C Total	101.00	100.97	101.37	100.95	101.83	101.53	100.49	100.56	100.67	100.84	101.19	100.72	100.88
						formula for 24 oxygens							
Si	5.956	5.992	6.026	5.981	5.965	6.006	5.982	6.011	6.025	5.967	5.962	5.943	5.972
Al	3.876	3.883	3.853	3.863	3.916	3.915	3.882	3.832	3.858	3.896	3.886	3.922	3.906
Ti	0.015	0.003	0.009	0.002	0.008	0.010	0.002	0.010	0.007	0.010	0.010	0.007	0.004
Cr	0.012	0.010	0.008	0.002	0.008	0.006	0.012	0.000	0.010	0.015	0.012	0.006	0.010
Fe	3.085	3.050	3.060	3.061	3.024	3.044	3.084	3.095	3.058	3.059	3.070	3.069	3.063
Mg	1.260	1.276	1.227	1.270	1.317	1.334	1.227	1.228	1.264	1.295	1.267	1.270	1.245
Mn	0.775	0.754	0.797	0.783	0.782	0.736	0.763	0.777	0.750	0.763	0.772	0.778	0.765
Ca	1.010	1.027	1.008	1.011	0.981	0.937	1.029	1.028	1.018	0.974	1.003	0.986	1.021
Na	0.011	0.005	0.013	0.026	0.000	0.013	0.019	0.019	0.011	0.021	0.017	0.020	0.014
Total cations	16.000	16.000	16.001	15.999	16.001	16.001	16.000	16.000	16.001	16.000	15.999	16.001	16.000
F	0	0.048	0	0	0	0.06	0.012	0	0	0	0	0	0
Cl	0.003	0.002	0.005	0.013	0.002	0	0.005	0.005	0.009	0.009	0.009	0.009	0.009

$Fe^{[2]}$ as total iron

Suffix A and B of mineral pairs are the analyses from the garnet core while suffix C denote the analyses from the rim of garnet touching biotite

Table C3 contd…….

Sample No.	9708	9708	9708	9708	9708	9708	9708	9708	9708	9708	9708	9708	9708	9708
Analysis No.	72	73	75	76	77	79	80	81	83	84	85	86	169	84
Mineral pair	22B	22A	23C	23B	23A	24C	24B	24A	25C	25B	26A	26B	27C	27A
SiO_2	37.92	37.95	38.49	38.31	38.69	38.12	38.40	38.30	38.41	38.07	38.47	37.99	38.57	38.59
TiO_2	0.10	0.08	0.06	0.06	0.07	0.07	0.06	0.08	0.06	0.08	0.10	0.10	0.097	0.057
Al_2O_3	21.45	21.21	21.34	21.49	21.32	21.49	21.42	21.63	21.49	21.44	21.14	21.07	21.75	21.74
Cr_2O_3	0.07	0.06	0.03	0.09	0.06	0.19	0.07	0.06	0.05	0.06	0.05	0.00	0.064	0.042
FeO	23.01	22.98	24.06	23.36	23.78	23.52	23.39	23.62	22.68	23.08	22.99	22.69	24.72	23.63
MnO	5.94	5.81	5.76	5.75	5.80	6.12	5.90	5.63	6.55	6.46	6.35	6.45	6.5	5.68
MgO	5.71	5.66	5.50	5.61	5.68	5.32	5.58	5.86	5.38	5.74	5.74	5.66	4.14	5.6
CaO	6.09	5.96	6.09	6.03	5.98	6.12	5.96	5.93	6.16	6.11	6.05	5.96	5.99	5.97
Na_2O	0.05	0.11	0.09	0.05	0.03	0.02	0.07	0.06	0.01	0.01	0.02	0.06	0	0.13
F	0.00	0.09	0.00	0.00	0.00	0.00	0.00	0.04	0.00	0.06	0.00	0.00	0	0
Cl	0.00	0.03	0.00	0.00	0.00	0.02	0.01	0.01	0.01	0.01	0.02	0.00	0	0
Total	100.27	99.88	101.38	100.66	101.35	100.79	100.79	101.16	100.75	101.06	100.88	99.98	101.831	101.439
O F Cl	0.00	0.04	0.00	0.00	0.00	0.00	0.00	0.02	0.00	0.03	0.00	0.00	0	0
C Total	100.27	99.83	101.38	100.66	101.35	100.79	100.79	101.14	100.75	101.04	100.87	99.98	101.831	101.439
						formula for 24 oxygens								
Si	5.907	5.941	5.945	5.948	5.974	5.921	5.958	5.915	5.969	5.895	5.966	5.944	5.987	5.967
Al	3.935	3.910	3.882	3.929	3.877	3.932	3.914	3.934	3.933	3.910	3.861	3.883	3.979	3.962
Ti	0.011	0.010	0.007	0.007	0.008	0.008	0.007	0.009	0.007	0.010	0.011	0.012	0.011	0.007
Cr	0.009	0.008	0.004	0.010	0.007	0.023	0.008	0.007	0.007	0.007	0.007	0.000	0.008	0.005
Fe	2.997	3.008	3.108	3.033	3.071	3.055	3.035	3.051	2.948	2.989	2.982	2.969	3.209	3.055
Mg	1.326	1.321	1.266	1.298	1.307	1.232	1.291	1.349	1.246	1.325	1.327	1.320	0.958	1.291
Mn	0.784	0.770	0.754	0.756	0.759	0.805	0.775	0.736	0.862	0.847	0.834	0.855	0.855	0.744
Ca	1.016	1.000	1.008	1.003	0.989	1.019	0.991	0.981	1.026	1.014	1.005	0.999	0.996	0.989
Na	0.015	0.032	0.026	0.015	0.008	0.005	0.021	0.018	0.003	0.003	0.007	0.018	0.000	0.039
Total cations	16.000	16.000	16.000	15.999	16.000	16.000	16.000	16.000	16.001	16.000	16.000	16.000	16.002	16.059
F	0	0	0	0	0	0.000	0.000	0.000	0.000	0.000	0.000	0.000	0	0
Cl	0.009	0.009	0.009	0.009	0.009	0.009	0.009	0.009	0.009	0.009	0.009	0.009	0	0

$Fe^{[2]}$ as total iron

Suffix A and B of mineral pairs are the analyses from the garnet core while suffix C denote the analyses from the rim of garnet touching biotite

Table C3. Chemistry of biotite used for Grt-Bt ion exchange thermometry

Sample No.	9708	9708	9708	9708	9708	9708	9708	9708	9708	9708	9708	9708	9708	9708	9708	9708
Analysis No	28	30	31	35	37	39	43	45	47	57	70	74	78	88	82	171
Mineral Pair	12	13	14	15	16	17	18	19	20	21	22	23	24	26	25	27
SiO_2	36.76	37.48	37.62	37.92	36.84	37.23	36.28	37.67	37.52	36.68	38.07	37.28	37.51	36.29	37.18	36.43
TiO_2	5.1	4.65	4.74	5.4	5.4	5.73	5.36	5.57	5.47	5.37	5.51	5.49	3.89	5.41	5.67	5.28
Al_2O_3	13.65	14.03	13.77	13.8	13.97	14.1	13.24	13.87	13.75	13.26	13.76	13.51	13.73	12.84	13.18	13.34
Cr_2O_3	0.058	0.102	0.059	0.083	0.105	0.028	0.059	0.056	0.046	0.068	0.067	0.073	0.076	0.052	0.096	0.054
FeO	13.93	14.54	14.42	14.81	14.69	14.89	15.82	14.98	15.08	14.99	14.55	14.67	13.55	14.01	14.63	14.49
MnO	0.19	0.134	0.207	0.121	0.159	0.128	0.181	0.118	0.182	0.122	0.201	0.135	0.106	0.163	0.207	0.197
MgO	14.48	14.84	15.1	14.76	14.49	14.45	13.91	14.43	14.3	14.12	13.67	14.47	16	13.89	14.12	13.92
CaO	0.038	0.09	0	0	0	0.026	0.058	0	0	0.067	0.027	0	0	0.03	0.051	0.049
Na_2O	0.225	0.14	0.228	0.292	0.172	0.177	0.377	0.198	0.132	0.229	0.183	0.097	0.108	0.216	0.21	0.169
K_2O	9.23	9.43	9.51	9.52	9.39	9.55	9.04	9.44	9.36	8.53	9.43	9.29	9.44	8.99	9.08	9.21
BaO	0.247	0.384	0.451	0.393	0.302	0.431	0.301	0.37	0.303	0.215	0.296	0.256	0.281	0.104	0.305	0
F	1.58	1.91	1.71	1.71	1.6	1.81	1.44	1.52	1.45	1.52	1.416	1.76	1.87	1.51	1.63	1.51
Cl	0.363	0.372	0.383	0.435	0.352	0.366	0.424	0.353	0.337	0.342	0.332	0.336	0.355	0.308	0.305	0.308
Total	95.851	98.102	98.198	99.244	97.47	98.916	96.49	98.575	97.93	95.513	97.512	97.367	96.916	93.813	96.664	94.957
O F Cl	0.747	0.888	0.806	0.818	0.753	0.845	0.702	0.72	0.687	0.717	0.671	0.817	0.867	0.705	0.755	0.705
CTotal	95.104	97.214	97.392	98.426	96.717	98.071	95.788	97.855	97.243	94.796	96.841	96.55	96.049	93.108	95.909	94.252
						formula for 22 oxygens										
Si	5.576	5.583	5.592	5.581	5.516	5.512	5.522	5.569	5.58	5.585	5.663	5.584	5.623	5.62	5.605	5.582
Ti	0.582	0.521	0.53	0.598	0.608	0.638	0.614	0.619	0.612	0.615	0.617	0.619	0.439	0.63	0.643	0.609
Al	2.438	2.461	2.411	2.392	2.463	2.458	2.373	2.415	2.408	2.378	2.411	2.383	2.424	2.342	2.34	2.409
Fe	1.767	1.811	1.793	1.823	1.84	1.843	2.014	1.852	1.875	1.909	1.81	1.838	1.699	1.814	1.844	1.857
Cr	0.007	0.012	0.007	0.01	0.012	0.003	0.007	0.007	0.005	0.008	0.008	0.009	0.009	0.006	0.011	0.007
Mn	0.024	0.017	0.026	0.015	0.02	0.016	0.023	0.015	0.023	0.016	0.025	0.017	0.013	0.021	0.026	0.026
Mg	3.274	3.296	3.346	3.239	3.234	3.189	3.156	3.18	3.17	3.205	3.031	3.231	3.576	3.207	3.173	3.180
Ba	0.015	0.022	0.026	0.023	0.018	0.025	0.018	0.021	0.018	0.013	0.017	0.015	0.017	0.006	0.018	0
Ca	0.006	0.014	0	0	0	0.004	0.009	0	0	0.011	0.004	0	0	0.005	0.008	0.008
Na	0.066	0.04	0.066	0.083	0.05	0.051	0.111	0.057	0.038	0.068	0.053	0.028	0.031	0.065	0.061	0.050
K	1.786	1.792	1.803	1.788	1.794	1.804	1.755	1.78	1.776	1.657	1.79	1.775	1.805	1.776	1.746	1.800
Total cations	15.541	15.569	15.6	15.552	15.555	15.543	15.602	15.515	15.505	15.465	15.429	15.499	15.636	15.492	15.475	15.527
F	1.516	1.8	1.608	1.592	1.515	1.695	1.386	1.421	1.364	1.464	1.332	1.667	1.773	1.479	1.554	0
Cl	0.187	0.188	0.193	0.217	0.179	0.184	0.219	0.177	0.17	0.177	0.167	0.171	0.18	0.162	0.156	0

$Fe^{[2]}$ as total iron

Table C3.Temperature-pressure estimates

From combined Grt-Bt / GADS
Dasgupta et al. (1990) and Eckert et al. (1991)

	for garnet core/biotite				**for garnet rim/biotite**		
Analysis No.	Pair No	T	P	Analysis No.	Pair No	T	P
33-30	13A	807	7.96	32-28	12C	780	7.68
36-35	15A	803	7.92	34-31	14C	783	7.71
40-37	16A	826	8.16	44-45	19C	793	7.82
41-39	17A	823	8.13	56-57	21C	814	8.04
42-43	18A	834	8.25	71-70	22C	804	7.93
46-47	20A	819	8.09	75-74	23C	794	7.83
54-57	21A	829	8.19	79-78	24C	757	7.44
55-57	21B	820	8.10	83-82	25C	821	8.11
73-70	22A	834	8.25	169-171	27C	685	6.17
72-70	22B	839	8.30		average	781	7.6
77-74	23A	812	8.02		standard	41	0.6
76-74	23B	817	8.07		deviation		
81-78	24A	787	7.76				
80-78	24B	774	7.62				
84-82	25B	840	8.31				
85-88	26A	832	8.22				
86-88	26B	833	8.24				
85-171	27A	818	7.52				
	average	819	8.1				
	standard	18	0.2				
	deviation						

Table C4 Representative mineral pairs used for Grt-Cpx-Pl-Qtz barometry (Eckert et al. 1991)

	Garnet			Quartz			Clinopyroxene			Plagioclase	
Sample No	9708	9708	Sample No	9708	9708	Sample No	9708	9708	Sample No	9708	9708
Analysis No.	62	66	Analysis No.	136	137	Analysis No.	63	67	Analysis No.	64	68
Pair No.	1	2	Pair No.	1	2	Pair No.	1	2	Pair No.	1	2
SiO_2	38.52	39.12	SiO_2	99.69	100.05	SiO_2	51.49	52.04	SiO_2	38.44	60.51
TiO_2	0.042	0.064	TiO_2	0.00	0.00	TiO_2	0.217	0.219	TiO_2	0.08	0.00
Al_2O_3	21.32	21.72	Al_2O_3	0.00	0.06	Al_2O_3	2.12	2	Al_2O_3	21.22	23.54
Cr_2O_3	0.045	0.063	Cr_2O_3	0.02	0.00	FeO	9.82	10.2	Cr_2O_3	0.10	0.02
FeO	23.5	22.58	FeO	0.02	0.00	Cr_2O_3	0	0.061	FeO	23.25	0.09
MnO	6.27	6.24	MnO	0.03	0.00	MnO	1.126	1.225	MnO	6.10	0.01
MgO	5.59	5.22	MgO	0.00	0.00	MgO	12.86	13.14	MgO	5.54	0.01
CaO	5.99	6.11	CaO	0.01	0.03	CaO	20.92	21.09	CaO	6.00	6.19
Na_2O	0.011	0.093	Na_2O	0.04	0.09	Na_2O	0.527	0.515	Na_2O	0.01	8.37
F	0	0	K_2O	0.05	0.10	K_2O	0.011	0.017	K_2O	0.03	0.21
Cl	0.016	0.033	BaO	0.00	0.01	Total	99.091	100.507	BaO	0.00	0.00
Total	101.26	101.18	F	0.00	0.00	formula for 6 oxygens			F	0.00	0.12
formula for 24 oxygens			Cl	0.03	0.07				Cl	0.02	0.01
Si	5.959	6.049	Total	99.89	100.41				Total	100.78	99.09
Al	3.884	3.955	formula for 2 oxygens						formula for 32 oxygens		
Cr	0.005	0.009	Si	0.999	0.998	Si	1.951	1.948	Si	7.990	10.888
Ti	0.005	0.007	Al	0.000	0.001	Al	0.095	0.088	Al	5.198	4.992
Fe	3.040	2.920	Cr	0.000	0.000	Fe	0.311	0.319	Cr	0.016	0.003
Mg	1.289	1.203	Ti	0.000	0.000	Ti	0.006	0.006	Ti	0.012	0.000
Mn	0.822	0.817	Fe	0.000	0.000	Cr	0	0.002	Fe	4.041	0.013
Ca	0.993	1.012	Mg	0.000	0.000	Mg	0.727	0.733	Mg	1.717	0.004
Na	0.003	0.028	Mn	0.000	0.000	Mn	0.036	0.039	Mn	1.074	0.002
Total Cation	16.000	16.000	Ca	0.000	0.000	Ca	0.849	0.846	Ca	1.336	1.193
			Na	0.001	0.002	Na	0.039	0.037	Na	0.003	2.920
F	0	0	K	0.001	0.001	K	0.001	0.001	K	0.007	0.049
Cl	0.004	0.009	Ba	0.000	0.000	Total Cation	4.015	4.019	Ba	0.000	0.000
			Total Cations	1.001	1.002				Total Cations	21.392	20.063
			F	0.000	0.000				F	0.000	0.069
			Cl	0.001	0.001				Cl	0.008	0.003

Table C5. Chemical composition of garnet along the drawn line AB in Fig.2.3

part 1

Analyse	1	2	3	4	5	6	7	8	9	10	11	12	13	14	15	16	17	18	19	20	21	22	23	24	25	26	27	28
distance (micro meter)	0.00	3.97	7.94	11.90	15.87	19.84	23.81	27.78	31.75	35.71	39.68	43.65	47.62	51.59	55.56	59.52	63.49	67.46	71.43	75.40	79.37	83.33	87.30	91.27	95.24	99.21	103.17	107.14
SiO_2	38.44	38.35	38.77	38.65	38.43	38.50	38.68	38.77	38.58	38.38	38.69	38.67	37.80	38.26	38.68	38.76	38.73	38.57	38.66	38.66	38.30	38.34	38.45	38.32	38.34	38.49	38.61	38.22
TiO_2	0.14	0.07	0.11	0.05	0.05	0.05	0.01	0.11	0.05	0.02	0.08	0.05	0.07	0.06	0.08	0.02	0.07	0.06	0.07	0.04	0.11	0.12	0.04	0.04	0.05	0.05	0.07	0.05
Al_2O_3	21.81	21.49	21.63	21.72	21.63	21.90	21.83	21.95	21.76	21.89	22.00	21.86	21.45	21.64	21.75	21.89	21.79	21.69	21.85	21.98	21.68	21.58	21.71	21.74	21.84	21.96	22.04	22.05
FeO	24.62	24.11	23.88	23.74	24.03	24.07	23.82	23.78	23.63	24.11	23.51	23.57	22.87	23.42	23.70	23.65	23.59	23.42	23.36	23.60	23.29	23.37	23.18	23.67	23.55	23.48	23.49	23.53
Cr_2O_3	0.06	0.13	0.05	0.04	0.02	0.09	0.03	0.04	0.08	0.11	0.05	0.05	0.05	0.07	0.07	0.07	0.06	0.13	0.08	0.00	0.08	0.07	0.10	0.12	0.09	0.10	0.03	0.02
MnO	6.31	6.22	5.92	5.85	6.18	5.95	5.99	5.89	5.81	5.84	6.06	5.86	5.60	5.81	6.05	5.95	5.95	5.77	5.88	5.77	5.81	5.79	5.88	5.86	5.71	5.81	5.82	5.84
MgO	4.44	4.70	4.82	5.10	5.03	5.11	5.21	5.25	5.12	5.36	5.35	5.43	5.23	5.37	5.39	5.37	5.51	5.48	5.50	5.45	5.45	5.48	5.56	5.43	5.51	5.67	5.61	5.60
CaO	6.04	6.02	6.14	6.12	6.00	6.02	5.97	6.02	6.10	6.05	6.10	6.02	5.99	5.99	6.09	5.83	5.99	5.93	6.03	6.01	6.08	5.88	5.97	5.99	5.98	5.89	6.00	5.85
Na_2O	0.00	0.05	0.02	0.03	0.05	0.08	0.04	0.00	0.02	0.02	0.03	0.07	1.22	0.16	0.04	0.04	0.05	0.04	0.16	0.04	0.32	0.07	0.07	0.12	0.03	0.00	0.05	0.03
K_2O	0.04	0.00	0.04	0.01	0.02	0.01	0.00	0.01	0.03	0.02	0.00	0.01	0.37	0.03	0.02	0.01	0.03	0.01	0.05	0.02	0.24	0.03	0.00	0.03	0.02	0.02	0.00	0.02
Total	101.90	101.25	101.37	101.32	101.44	101.78	101.58	101.82	101.18	101.80	101.87	101.59	100.65	100.81	101.87	101.58	101.77	101.11	101.64	101.57	101.36	100.73	100.96	101.33	101.12	101.47	101.72	101.20
Si	5.961	5.981	6.011	5.991	5.969	5.953	5.982	5.976	5.986	5.934	5.961	5.972	5.922	5.961	5.967	5.985	5.973	5.981	5.966	5.968	5.943	5.972	5.970	5.946	5.949	5.947	5.950	5.926
Ti	0.016	0.008	0.013	0.006	0.006	0.006	0.001	0.012	0.006	0.003	0.009	0.006	0.008	0.007	0.010	0.002	0.008	0.007	0.008	0.005	0.013	0.014	0.005	0.005	0.006	0.005	0.008	0.006
Al	3.986	3.950	3.952	3.968	3.959	3.991	3.978	3.987	3.979	3.988	3.994	3.978	3.961	3.973	3.954	3.983	3.960	3.964	3.974	3.999	3.964	3.961	3.972	3.975	3.994	3.999	4.003	4.029
Fe	3.193	3.144	3.096	3.077	3.121	3.112	3.080	3.065	3.066	3.117	3.029	3.044	2.996	3.051	3.057	3.053	3.042	3.037	3.015	3.046	3.022	3.044	3.009	3.071	3.056	3.034	3.027	3.051
Cr	0.007	0.016	0.006	0.005	0.003	0.011	0.004	0.005	0.010	0.014	0.006	0.006	0.006	0.008	0.009	0.008	0.007	0.016	0.010	0.000	0.010	0.009	0.012	0.015	0.011	0.012	0.003	0.002
Mn	0.829	0.822	0.777	0.768	0.813	0.779	0.785	0.769	0.763	0.765	0.791	0.766	0.743	0.767	0.790	0.778	0.777	0.758	0.769	0.754	0.763	0.764	0.773	0.770	0.750	0.760	0.760	0.767
Mg	1.026	1.093	1.114	1.179	1.165	1.178	1.201	1.206	1.184	1.235	1.229	1.250	1.222	1.247	1.240	1.236	1.267	1.267	1.265	1.254	1.261	1.272	1.287	1.256	1.275	1.306	1.289	1.294
Ca	1.003	1.006	1.020	1.016	0.998	0.997	0.989	0.994	1.014	1.002	1.007	0.996	1.005	1.000	1.007	0.964	0.990	0.985	0.997	0.994	1.011	0.981	0.993	0.996	0.994	0.975	0.991	0.972
Na	0.000	0.016	0.007	0.010	0.015	0.022	0.012	0.000	0.005	0.007	0.009	0.022	0.372	0.050	0.011	0.011	0.016	0.013	0.047	0.011	0.095	0.022	0.022	0.037	0.010	0.000	0.015	0.008
K	0.009	0.000	0.007	0.003	0.004	0.003	0.000	0.002	0.006	0.004	0.000	0.002	0.075	0.006	0.004	0.002	0.006	0.003	0.010	0.005	0.048	0.006	0.000	0.007	0.003	0.004	0.000	0.005
$Fe^{[3]}$ as total iron																												
formula for 24 oxygens																												

part2

Analyse	30	31	32	33	34	35	36	37	38	39	40	41	42	43	44	45	46	47	48	49	50	51	52	53	54	55	56	57
distance (micro meter)	115.08	119.05	123.02	126.98	130.95	134.92	138.89	142.86	146.83	150.79	154.76	158.73	162.70	166.67	170.63	174.60	178.57	182.54	186.51	190.48	194.44	198.41	202.38	206.35	210.32	214.29	218.25	222.22
SiO_2	38.52	38.34	38.51	38.69	38.73	38.61	38.79	38.99	38.62	38.61	38.89	38.67	38.90	38.50	38.83	38.69	38.62	38.96	38.66	38.77	38.74	38.93	38.49	38.74	38.84	38.83	38.57	38.66
TiO_2	0.06	0.06	0.06	0.05	0.13	0.12	0.07	0.07	0.10	0.07	0.06	0.07	0.10	0.05	0.13	0.06	0.09	0.08	0.05	0.10	0.11	0.02	0.03	0.07	0.06	0.01	0.07	0.13
Al_2O_3	21.72	21.96	21.94	21.82	21.87	21.84	21.73	21.81	21.72	21.59	21.77	21.73	21.76	22.10	21.83	21.80	22.03	21.81	22.06	21.83	21.75	22.05	21.93	21.77	22.02	21.84	21.82	21.87
FeO	23.48	23.29	23.58	23.39	23.45	23.38	23.66	23.79	23.42	23.31	23.64	23.41	23.80	23.59	23.75	23.35	23.68	23.74	23.34	23.40	23.53	23.26	23.38	23.39	23.60	23.15	23.45	23.57
Cr_2O_3	0.11	0.01	0.09	0.04	0.13	0.08	0.07	0.09	0.12	0.13	0.04	0.05	0.08	0.06	0.09	0.07	0.11	0.04	0.02	0.15	0.01	0.08	0.02	0.07	0.07	0.10	0.07	0.04
MnO	5.82	5.88	5.83	5.74	5.77	5.75	5.93	5.83	5.83	5.74	5.83	5.93	6.01	5.77	5.83	5.73	5.86	5.74	5.67	5.80	5.87	5.71	5.80	5.82	5.70	5.75	5.71	5.64
MgO	5.54	5.51	5.60	5.61	5.77	5.60	5.73	5.52	5.53	5.62	5.65	5.58	5.67	5.54	5.60	5.54	5.72	5.55	5.57	5.59	5.68	5.64	5.60	5.67	5.72	5.70	5.63	5.77
CaO	6.00	5.86	5.97	6.02	5.91	5.97	5.82	5.89	5.96	5.95	5.78	6.00	5.84	5.99	5.86	5.94	6.06	5.90	5.77	6.03	5.91	5.87	5.94	5.81	5.83	5.97	5.88	6.04
Na_2O	0.01	0.05	0.00	0.05	0.01	0.04	0.03	0.07	0.08	0.04	0.04	0.06	0.02	0.00	0.00	0.03	0.07	0.07	0.00	0.07	0.05	0.05	0.07	0.03	0.01	0.05	0.07	0.04
K_2O	0.00	0.01	0.00	0.00	0.01	0.01	0.00	0.00	0.05	0.03	0.01	0.04	0.01	0.04	0.02	0.00	0.00	0.00	0.00	0.02	0.03	0.01	0.07	0.05	0.03	0.00	0.03	0.00
Total	101.26	100.97	101.58	101.40	101.77	101.40	101.83	102.06	101.41	101.10	101.71	101.55	102.19	101.65	101.93	101.20	102.24	101.89	101.14	101.77	101.67	101.62	101.33	101.42	101.89	101.40	101.30	101.76
Si	5.968	5.952	5.948	5.977	5.962	5.966	5.976	5.992	5.973	5.985	5.992	5.974	5.976	5.941	5.975	5.986	5.930	5.993	5.977	5.972	5.975	5.989	5.956	5.984	5.970	5.990	5.967	5.955
Ti	0.007	0.006	0.007	0.005	0.015	0.014	0.008	0.008	0.011	0.009	0.007	0.008	0.011	0.006	0.015	0.006	0.011	0.009	0.006	0.012	0.012	0.002	0.003	0.008	0.007	0.001	0.008	0.015
Al	3.966	4.018	3.993	3.973	3.968	3.977	3.945	3.950	3.959	3.944	3.953	3.956	3.939	4.019	3.959	3.975	3.986	3.954	4.020	3.963	3.953	3.998	3.999	3.963	3.989	3.971	3.979	3.970
Fe	3.042	3.023	3.045	3.022	3.019	3.021	3.048	3.057	3.029	3.022	3.046	3.024	3.057	3.044	3.056	3.021	3.040	3.054	3.018	3.014	3.035	2.992	3.025	3.021	3.033	2.986	3.034	3.036
Cr	0.013	0.002	0.011	0.005	0.016	0.010	0.008	0.011	0.014	0.016	0.004	0.007	0.010	0.007	0.010	0.009	0.014	0.005	0.003	0.018	0.001	0.010	0.002	0.009	0.008	0.013	0.008	0.005
Mn	0.764	0.773	0.763	0.751	0.752	0.753	0.774	0.759	0.764	0.754	0.761	0.776	0.782	0.754	0.760	0.751	0.762	0.748	0.742	0.757	0.767	0.744	0.760	0.761	0.742	0.751	0.748	0.736
Mg	1.280	1.275	1.289	1.292	1.324	1.290	1.316	1.265	1.275	1.299	1.298	1.285	1.298	1.274	1.285	1.278	1.309	1.273	1.284	1.284	1.306	1.294	1.292	1.306	1.311	1.311	1.299	1.325
Ca	0.996	0.975	0.988	0.996	0.975	0.988	0.961	0.970	0.988	0.988	0.954	0.993	0.961	0.990	0.966	0.985	0.997	0.972	0.956	0.995	0.977	0.967	0.985	0.961	0.960	0.987	0.975	0.997
Na	0.004	0.015	0.000	0.015	0.002	0.011	0.008	0.021	0.023	0.012	0.013	0.018	0.005	0.000	0.000	0.007	0.019	0.021	0.000	0.022	0.014	0.014	0.022	0.010	0.004	0.014	0.020	0.012
K	0.000	0.002	0.000	0.000	0.002	0.003	0.000	0.000	0.009	0.007	0.003	0.008	0.002	0.008	0.003	0.000	0.000	0.000	0.000	0.005	0.006	0.003	0.014	0.010	0.007	0.000	0.005	0.000

Table C5. contd...

part3

Analyse	59	60	61	62	63	64	65	66	67	68	69	70	71	72	73	74	75	76	77	78	79	80	81	82	83	84	85	86	87
distance	230,16	234,13	238,10	242,06	246,03	250,00	253,97	257,94	261,90	265,87	269,84	273,81	277,78	281,75	285,71	289,68	293,65	297,62	301,59	305,56	309,52	313,49	317,46	321,43	325,40	329,37	333,33	337,30	341,27
(micro meter)																													
SiO_2	38,56	38,66	38,51	38,79	38,64	38,59	38,38	38,70	38,63	38,50	39,01	38,56	38,49	38,83	37,33	38,95	38,88	38,85	38,63	38,48	38,77	38,82	38,85	39,03	38,55	38,59	38,48	38,63	38,08
TiO_2	0,11	0,05	0,06	0,07	0,06	0,05	0,14	0,03	0,07	0,07	0,09	0,06	0,12	0,08	0,08	0,04	0,03	0,12	0,01	0,08	0,07	0,07	0,14	0,06	0,11	0,06	0,06	0,11	0,04
Al_2O_3	21,98	21,83	21,83	21,77	22,06	21,83	21,90	21,74	21,95	21,85	22,14	21,86	21,94	21,85	17,09	21,96	21,73	22,13	21,86	21,86	21,83	21,93	22,03	21,81	21,82	21,74	21,79	21,79	21,83
FeO	23,35	23,53	23,84	23,92	23,29	23,70	23,45	23,28	23,77	23,48	23,58	23,35	23,48	23,63	23,78	23,87	23,48	23,52	23,28	23,52	23,30	23,26	23,45	23,35	23,42	23,63	23,68	24,03	24,35
Cr_2O_3	0,11	0,06	0,01	0,12	0,04	0,07	0,09	0,10	0,04	0,09	0,03	0,09	0,03	0,07	0,07	0,09	0,05	0,05	0,02	0,02	0,13	0,06	0,11	0,03	0,05	0,04	0,08	0,09	0,04
MnO	5,75	5,69	5,85	5,74	5,89	5,82	5,80	5,80	5,77	5,84	5,94	5,70	5,72	5,71	4,09	5,64	5,67	5,58	5,87	5,78	5,74	5,67	5,62	5,73	5,86	5,68	5,79	5,72	5,74
MgO	5,51	5,74	5,58	5,61	5,66	5,80	5,64	5,68	5,64	5,68	5,71	5,71	5,55	5,64	7,76	5,74	5,51	5,71	5,74	5,63	5,69	5,51	5,55	5,56	5,41	5,60	5,60	5,34	5,08
CaO	5,97	5,79	5,96	5,92	6,00	5,88	5,80	5,85	6,08	6,01	5,92	6,11	5,95	5,92	4,47	6,02	5,96	6,00	6,04	6,03	6,02	6,03	6,02	5,81	5,87	5,97	5,90	5,94	5,98
Na_2O	0,02	0,00	0,00	0,00	0,02	0,06	0,14	0,05	0,03	0,04	0,01	0,02	0,04	0,03	0,00	0,05	0,01	0,03	0,11	0,05	0,05	0,06	0,05	0,02	0,20	0,13	0,04	0,07	0,12
K_2O	0,00	0,00	0,00	0,01	0,03	0,03	0,06	0,03	0,02	0,01	0,01	0,00	0,00	0,00	0,16	0,00	0,00	0,03	0,01	0,00	0,02	0,00	0,00	0,01	0,06	0,04	0,01	0,04	0,05
Total	101,36	101,35	101,64	101,95	101,69	101,83	101,39	101,25	101,99	101,57	102,44	101,47	101,32	101,76	94,83	102,36	101,32	102,02	101,57	101,45	101,61	101,40	101,83	101,41	101,35	101,48	101,43	101,75	101,30
Si	5,959	5,974	5,951	5,972	5,953	5,948	5,939	5,986	5,946	5,947	5,965	5,955	5,954	5,979	6,184	5,966	6,008	5,960	5,961	5,950	5,975	5,989	5,972	6,018	5,968	5,967	5,955	5,966	5,927
Ti	0,012	0,005	0,007	0,008	0,007	0,006	0,016	0,003	0,008	0,009	0,011	0,007	0,014	0,010	0,010	0,005	0,003	0,013	0,001	0,010	0,008	0,008	0,017	0,007	0,013	0,007	0,007	0,012	0,004
Al	4,003	3,976	3,976	3,950	4,005	3,966	3,994	3,963	3,981	3,978	3,990	3,979	4,000	3,965	3,336	3,964	3,957	4,001	3,976	3,983	3,965	3,987	3,991	3,963	3,981	3,962	3,974	3,966	4,004
Fe	3,018	3,040	3,081	3,080	3,000	3,055	3,034	3,011	3,059	3,033	3,015	3,015	3,037	3,043	3,294	3,057	3,034	3,017	3,004	3,041	3,003	3,001	3,014	3,010	3,032	3,055	3,064	3,103	3,169
Cr	0,013	0,008	0,001	0,015	0,005	0,009	0,010	0,012	0,005	0,011	0,003	0,011	0,004	0,008	0,009	0,011	0,006	0,006	0,002	0,002	0,016	0,007	0,013	0,003	0,006	0,005	0,010	0,011	0,005
Mn	0,753	0,745	0,766	0,748	0,769	0,760	0,760	0,760	0,752	0,764	0,769	0,746	0,749	0,745	0,574	0,732	0,742	0,725	0,767	0,757	0,749	0,741	0,732	0,748	0,768	0,744	0,759	0,748	0,757
Mg	1,270	1,322	1,286	1,288	1,300	1,333	1,301	1,310	1,294	1,308	1,302	1,315	1,280	1,295	1,916	1,311	1,269	1,306	1,321	1,298	1,307	1,267	1,272	1,278	1,249	1,291	1,292	1,229	1,179
Ca	0,988	0,959	0,987	0,976	0,990	0,971	0,962	0,969	1,003	0,995	0,970	1,011	0,986	0,977	0,793	0,988	0,987	0,986	0,999	0,999	0,994	0,997	0,991	0,960	0,974	0,989	0,978	0,983	0,997
Na	0,007	0,000	0,000	0,000	0,006	0,019	0,041	0,014	0,008	0,012	0,003	0,007	0,011	0,009	0,000	0,014	0,002	0,010	0,033	0,015	0,015	0,017	0,015	0,007	0,059	0,039	0,013	0,020	0,035
K	0,000	0,000	0,000	0,002	0,006	0,005	0,011	0,006	0,003	0,002	0,002	0,000	0,000	0,000	0,033	0,000	0,000	0,006	0,003	0,000	0,004	0,000	0,000	0,002	0,011	0,007	0,003	0,008	0,010
Fe^{2+} as total iron																													
formula for 24 oxygens																													

part4

Analyse	88	89	90	91	92	93	94	95	96	97	98	99	100	101	102	103	104	105	106	107	108	109	110	111	112	113	114	115	116
distance	345,24	349,21	353,17	357,14	361,11	365,08	369,05	373,02	376,98	380,95	384,92	388,89	392,86	396,83	400,79	404,76	408,73	412,70	416,67	420,63	424,60	428,57	432,54	436,51	440,48	444,44	448,41	452,38	456,35
(micro meter)																													
SiO_2	36,77	38,44	38,78	38,97	38,85	38,37	38,78	38,85	38,73	39,10	38,54	38,78	38,58	38,58	38,70	38,78	38,73	38,88	38,74	38,67	38,94	38,55	38,68	38,58	38,46	38,60	38,63	38,77	38,62
TiO_2	3,10	1,04	0,08	0,05	0,05	0,13	0,00	0,09	0,00	0,14	0,06	0,11	0,02	0,04	0,16	0,03	0,04	0,03	0,05	0,05	0,10	0,06	0,03	0,04	0,05	0,05	0,05	0,11	0,06
Al_2O_3	18,34	20,61	21,75	21,59	21,90	21,64	21,94	21,93	21,71	21,47	21,62	21,68	22,00	21,72	21,85	21,85	21,83	22,19	22,07	21,60	21,89	21,88	21,85	21,90	21,73	22,05	21,87	21,86	21,96
FeO	20,29	23,27	24,30	23,88	23,83	24,08	23,68	23,37	23,64	23,79	23,12	23,54	23,43	23,67	23,78	23,51	23,70	23,37	23,61	23,28	23,45	23,43	23,78	23,51	23,46	23,71	23,57	23,71	23,36
Cr_2O_3	0,10	0,05	0,09	0,05	0,02	0,11	0,09	0,11	0,07	0,08	0,15	0,03	0,06	0,08	0,08	0,05	0,07	0,14	0,10	0,09	0,09	0,11	0,07	0,00	0,00	0,00	0,08	0,07	0,04
MnO	3,78	5,17	5,70	5,87	6,03	5,85	5,93	5,75	5,79	5,63	5,73	5,69	5,90	5,85	5,69	5,72	5,90	5,78	5,80	5,70	5,58	5,72	5,80	5,78	5,70	5,87	5,78	5,83	5,86
MgO	8,56	6,03	5,38	5,28	5,50	5,51	5,55	5,43	5,55	5,53	5,51	5,48	5,50	5,52	5,62	5,53	5,70	5,57	5,60	5,56	5,57	5,65	5,52	5,67	5,63	5,59	5,54	5,53	5,62
CaO	3,65	5,21	5,91	5,78	5,92	5,92	5,97	5,95	5,98	6,19	6,02	6,13	6,01	6,03	5,96	6,07	6,09	6,03	6,06	6,15	6,00	5,97	6,02	5,97	5,92	5,94	5,92	5,98	6,11
Na_2O	0,19	0,09	0,02	0,02	0,05	0,04	0,03	0,04	0,02	0,02	0,22	0,00	0,04	0,00	0,06	0,04	0,04	0,04	0,00	0,00	0,00	0,03	0,06	0,05	0,01	0,03	0,01	0,00	0,02
K_2O	3,72	1,27	0,03	0,01	0,04	0,00	0,00	0,00	0,02	0,01	0,05	0,00	0,00	0,00	0,02	0,00	0,01	0,02	0,00	0,01	0,00	0,03	0,03	0,02	0,01	0,02	0,01	0,02	0,02
Total	98,51	101,18	102,03	101,51	102,19	101,65	101,96	101,53	101,51	101,96	101,01	101,44	101,55	101,49	101,92	101,57	102,10	102,05	102,03	101,11	101,62	101,43	101,84	101,52	100,97	101,86	101,45	101,88	101,67
Si	5,878	5,981	5,975	6,023	5,971	5,941	5,967	5,990	5,985	6,015	5,981	5,992	5,957	5,968	5,958	5,983	5,956	5,964	5,953	5,992	5,995	5,957	5,963	5,958	5,970	5,947	5,970	5,970	5,955
Ti	0,373	0,121	0,009	0,006	0,005	0,016	0,000	0,010	0,000	0,016	0,006	0,013	0,003	0,005	0,018	0,003	0,004	0,004	0,006	0,005	0,011	0,007	0,004	0,005	0,006	0,005	0,005	0,012	0,007
Al	3,455	3,779	3,949	3,933	3,967	3,949	3,979	3,985	3,954	3,892	3,954	3,948	4,004	3,960	3,964	3,973	3,956	4,012	3,997	3,945	3,971	3,985	3,970	3,986	3,975	4,003	3,983	3,967	3,990
Fe	2,712	3,028	3,131	3,086	3,062	3,118	3,047	3,013	3,055	3,060	3,000	3,041	3,025	3,062	3,061	3,033	3,048	2,998	3,034	3,017	3,019	3,028	3,066	3,036	3,045	3,054	3,046	3,053	3,012
Cr	0,013	0,006	0,010	0,006	0,003	0,013	0,010	0,014	0,008	0,009	0,018	0,004	0,007	0,010	0,010	0,006	0,008	0,017	0,012	0,011	0,011	0,014	0,009	0,000	0,000	0,000	0,009	0,009	0,005
Mn	0,512	0,681	0,744	0,768	0,785	0,767	0,773	0,751	0,758	0,733	0,753	0,745	0,772	0,766	0,742	0,747	0,768	0,751	0,755	0,748	0,728	0,749	0,757	0,756	0,749	0,766	0,756	0,760	0,765
Mg	2,040	1,399	1,236	1,217	1,260	1,272	1,273	1,248	1,279	1,268	1,275	1,262	1,266	1,273	1,290	1,272	1,307	1,274	1,283	1,284	1,278	1,302	1,269	1,306	1,303	1,284	1,276	1,270	1,292
Ca	0,625	0,868	0,976	0,957	0,975	0,982	0,984	0,983	0,990	1,020	1,001	1,015	0,994	0,999	0,983	1,003	1,003	0,991	0,998	1,021	0,990	0,988	0,994	0,988	0,985	0,980	0,980	0,987	1,009
Na	0,059	0,028	0,005	0,006	0,014	0,011	0,009	0,012	0,007	0,006	0,066	0,000	0,013	0,000	0,016	0,011	0,011	0,011	0,000	0,000	0,000	0,009	0,018	0,014	0,002	0,009	0,003	0,000	0,006
K	0,758	0,252	0,006	0,003	0,007	0,000	0,000	0,000	0,004	0,002	0,010	0,000	0,000	0,000	0,005	0,000	0,003	0,005	0,000	0,002	0,000	0,006	0,006	0,003	0,001	0,004	0,002	0,005	0,005
Fe^{2+} as total iron																													
formula for 24 oxygens																													

Table C5. contd....

part5

Analyse	117	118	119	120	121	122	123	124	125	126	127	128	129	130	131	132	133	134	135	136	137	138	139	140	141	142	143	144	145
distance (micro meter)	460.32	464.29	468.25	472.22	476.19	480.16	484.13	488.10	492.06	496.03	500.00	503.97	507.94	511.90	515.87	519.84	523.81	527.78	531.75	535.71	539.68	543.65	547.62	551.59	555.56	559.52	563.49	567.46	571.43
SiO_2	38.51	38.49	38.76	38.74	38.55	38.66	38.51	38.54	38.79	38.74	38.56	38.66	38.93	38.69	38.81	38.76	38.95	38.72	38.73	38.83	38.59	38.85	39.01	38.78	39.17	38.77	38.75	38.65	38.72
TiO_2	0.10	0.16	0.02	0.01	0.07	0.05	0.05	0.05	0.09	0.07	0.07	0.05	0.11	0.06	0.10	0.07	0.07	0.10	0.05	0.09	0.08	0.08	0.07	0.05	0.09	0.05	0.04	0.09	0.08
Al_2O_3	21.68	21.83	22.05	21.89	21.82	21.92	21.83	21.82	21.82	21.99	21.84	21.86	21.90	21.57	21.94	21.93	21.82	21.98	21.71	22.06	21.70	21.91	21.95	22.01	21.74	21.75	22.13	21.68	21.70
FeO	23.42	23.52	23.59	23.62	23.53	23.40	23.66	23.84	23.49	23.51	23.67	23.77	23.92	23.25	23.56	23.65	23.66	23.81	23.68	23.29	23.69	23.63	23.73	23.75	23.35	23.36	23.63	23.36	23.45
Cr_2O_3	0.13	0.07	0.07	0.06	0.08	0.10	0.06	0.06	0.07	0.07	0.04	0.11	0.08	0.02	0.09	0.11	0.09	0.11	0.01	0.03	0.07	0.08	0.05	0.00	0.02	0.03	0.07	0.07	0.12
MnO	5.81	5.73	5.93	5.88	5.72	5.74	5.66	5.92	5.68	5.83	5.80	5.64	5.97	5.83	5.74	5.68	5.95	5.77	5.90	5.68	5.76	5.98	5.66	5.91	5.86	5.84	5.86	5.78	5.80
MgO	5.59	5.68	5.59	5.51	5.53	5.61	5.50	5.65	5.51	5.61	5.65	5.55	5.58	5.56	5.44	5.66	5.59	5.63	5.58	5.54	5.46	5.62	5.50	5.46	5.39	5.50	5.39	5.40	5.69
CaO	6.08	6.05	6.09	6.07	5.96	5.98	5.93	6.11	6.18	5.99	6.04	6.05	6.01	6.12	6.01	6.08	6.02	5.94	6.05	5.90	6.02	6.05	5.99	5.88	6.03	6.03	6.06	5.98	5.94
Na_2O	0.07	0.05	0.02	0.00	0.01	0.03	0.05	0.04	0.03	0.06	0.06	0.00	0.00	0.04	0.02	0.03	0.04	0.08	0.05	0.03	0.03	0.00	0.04	0.04	0.03	0.03	0.04	0.00	0.03
K_2O	0.00	0.03	0.04	0.01	0.01	0.00	0.00	0.01	0.00	0.00	0.04	0.02	0.01	0.00	0.00	0.01	0.02	0.03	0.02	0.00	0.02	0.03	0.00	0.02	0.00	0.00	0.02	0.04	0.02
Total	101.38	101.61	102.17	101.79	101.28	101.49	101.25	102.04	101.66	101.88	101.77	101.71	102.52	101.15	101.70	101.99	102.20	102.18	101.79	101.45	101.42	102.23	102.00	101.91	101.68	101.36	101.98	101.04	101.56
Si	5.960	5.943	5.953	5.971	5.968	5.967	5.965	5.939	5.980	5.961	5.949	5.963	5.964	5.995	5.979	5.959	5.980	5.948	5.974	5.984	5.973	5.964	5.991	5.970	6.028	5.993	5.959	5.994	5.977
Ti	0.011	0.018	0.002	0.001	0.008	0.005	0.006	0.005	0.011	0.008	0.008	0.006	0.013	0.007	0.011	0.008	0.008	0.012	0.006	0.011	0.009	0.009	0.009	0.006	0.010	0.006	0.004	0.010	0.009
Al	3.955	3.972	3.991	3.976	3.981	3.987	3.985	3.962	3.964	3.987	3.971	3.974	3.954	3.939	3.984	3.974	3.948	3.979	3.947	4.007	3.958	3.964	3.972	3.993	3.943	3.962	4.011	3.963	3.948
Fe	3.031	3.037	3.029	3.044	3.046	3.020	3.065	3.072	3.028	3.025	3.054	3.066	3.064	3.012	3.035	3.041	3.037	3.058	3.054	3.001	3.066	3.033	3.047	3.057	3.005	3.019	3.039	3.029	3.027
Cr	0.016	0.009	0.009	0.007	0.009	0.012	0.007	0.007	0.008	0.009	0.005	0.014	0.010	0.003	0.011	0.013	0.011	0.014	0.002	0.004	0.009	0.009	0.006	0.000	0.002	0.003	0.008	0.008	0.015
Mn	0.762	0.749	0.771	0.768	0.750	0.750	0.743	0.773	0.742	0.760	0.758	0.737	0.775	0.765	0.749	0.740	0.774	0.751	0.771	0.741	0.755	0.777	0.736	0.770	0.764	0.765	0.763	0.759	0.758
Mg	1.290	1.308	1.280	1.266	1.276	1.291	1.270	1.298	1.266	1.287	1.300	1.276	1.274	1.284	1.249	1.297	1.279	1.289	1.283	1.273	1.260	1.286	1.259	1.253	1.237	1.267	1.236	1.249	1.309
Ca	1.008	1.001	1.002	1.002	0.988	0.989	0.984	1.009	1.021	0.987	0.998	1.000	0.986	1.016	0.992	1.001	0.990	0.978	1.000	0.974	0.998	0.995	0.985	0.970	0.994	0.999	0.998	0.994	0.982
Na	0.020	0.016	0.007	0.000	0.002	0.010	0.016	0.010	0.009	0.018	0.017	0.000	0.000	0.013	0.005	0.010	0.011	0.025	0.013	0.010	0.008	0.000	0.012	0.013	0.010	0.010	0.011	0.000	0.009
K	0.000	0.006	0.008	0.003	0.002	0.000	0.000	0.002	0.000	0.000	0.008	0.004	0.002	0.000	0.000	0.003	0.003	0.005	0.005	0.000	0.004	0.005	0.000	0.004	0.000	0.000	0.004	0.007	0.004
$Fe^{[2]}$ as total iron																													
formula for 24 oxygens																													

part6

Analyse	146	147	148	149	150	151	152	153	154	155	156	157	158	159	160	161	162	163	164	165	166	167	168	169
distance (micro meter)	575.40	579.37	583.33	587.30	591.27	595.24	599.21	603.17	607.14	611.11	615.08	619.05	623.02	626.98	630.95	634.92	638.89	642.86	646.83	650.79	654.76	658.73	662.70	666.67
SiO_2	38.61	38.68	38.59	38.65	38.59	38.81	38.47	38.62	38.66	38.89	38.52	38.94	38.90	38.55	38.89	38.77	38.71	38.59	38.60	38.78	38.83	38.93	38.65	38.57
TiO_2	0.07	0.03	0.04	0.08	0.01	0.06	0.02	0.11	0.00	0.04	0.07	0.04	0.06	0.04	0.10	0.06	0.05	0.10	0.05	0.07	0.02	0.06	0.08	0.10
Al_2O_3	21.72	21.94	21.81	21.94	22.05	22.00	21.95	21.90	21.67	21.90	21.76	21.91	21.82	21.74	21.86	21.81	21.73	21.60	21.76	21.73	21.51	21.47	21.64	21.75
FeO	23.66	23.53	23.48	23.56	23.75	23.48	23.61	23.57	23.67	23.65	23.61	23.16	23.50	23.36	23.80	24.02	23.96	23.55	24.01	23.88	24.20	24.34	24.60	24.72
Cr_2O_3	0.07	0.05	0.05	0.08	0.05	0.07	0.00	0.08	0.02	0.05	0.02	0.02	0.08	0.10	0.07	0.07	0.11	0.03	0.08	0.08	0.04	0.04	0.08	0.06
MnO	5.90	6.02	5.93	5.86	5.90	5.95	6.04	6.01	5.79	6.06	5.87	5.98	5.75	6.09	6.05	5.91	6.08	5.90	6.08	6.10	6.26	6.27	6.30	6.50
MgO	5.59	5.44	5.48	5.58	5.46	5.48	5.46	5.35	5.33	5.38	5.19	5.41	5.34	5.22	5.34	5.15	5.22	5.04	5.17	4.93	4.78	4.72	4.43	4.14
CaO	5.98	6.00	6.03	6.02	6.09	5.96	5.98	5.87	5.98	5.97	6.15	6.16	6.15	6.03	6.05	6.01	6.04	6.18	6.16	6.17	6.06	6.28	6.09	5.99
Na_2O	0.05	0.08	0.00	0.10	0.03	0.00	0.07	0.00	0.07	0.00	0.05	0.11	0.06	0.05	0.03	0.01	0.04	0.05	0.05	0.01	0.06	0.00	0.08	0.00
K_2O	0.01	0.02	0.02	0.03	0.00	0.01	0.02	0.00	0.03	0.02	0.02	0.02	0.01	0.03	0.04	0.04	0.01	0.02	0.04	0.01	0.01	0.01	0.00	0.06
Total	101.66	101.79	101.43	101.89	101.94	101.82	101.61	101.51	101.22	101.95	101.25	101.74	101.66	101.21	102.23	101.85	101.94	101.06	102.01	101.76	101.77	102.12	101.95	101.89
Si	5.964	5.964	5.969	5.953	5.945	5.974	5.947	5.969	5.994	5.985	5.975	5.995	5.997	5.980	5.976	5.983	5.974	5.997	5.960	5.994	6.013	6.013	5.989	5.987
Ti	0.008	0.004	0.005	0.009	0.001	0.007	0.002	0.013	0.000	0.005	0.008	0.004	0.007	0.005	0.012	0.007	0.006	0.011	0.006	0.008	0.002	0.007	0.009	0.011
Al	3.954	3.987	3.976	3.982	4.003	3.991	3.999	3.989	3.960	3.972	3.978	3.975	3.964	3.974	3.959	3.967	3.952	3.956	3.959	3.958	3.926	3.908	3.952	3.979
Fe	3.056	3.034	3.037	3.034	3.059	3.022	3.052	3.046	3.069	3.044	3.062	2.981	3.029	3.030	3.058	3.100	3.092	3.060	3.100	3.086	3.134	3.144	3.188	3.209
Cr	0.009	0.006	0.006	0.009	0.007	0.008	0.000	0.010	0.003	0.006	0.002	0.002	0.009	0.012	0.008	0.008	0.013	0.004	0.010	0.009	0.005	0.005	0.010	0.008
Mn	0.772	0.786	0.777	0.764	0.770	0.776	0.791	0.787	0.760	0.790	0.771	0.780	0.751	0.800	0.787	0.772	0.795	0.777	0.795	0.798	0.821	0.820	0.827	0.855
Mg	1.287	1.251	1.264	1.281	1.254	1.258	1.258	1.233	1.232	1.234	1.200	1.242	1.227	1.207	1.223	1.185	1.201	1.168	1.190	1.136	1.104	1.087	1.023	0.958
Ca	0.990	0.991	0.999	0.993	1.005	0.983	0.990	0.972	0.993	0.984	1.022	1.016	1.016	1.002	0.996	0.994	0.999	1.029	1.019	1.022	1.005	1.039	1.011	0.996
Na	0.013	0.023	0.000	0.029	0.009	0.000	0.021	0.000	0.020	0.000	0.015	0.032	0.018	0.016	0.009	0.004	0.012	0.014	0.016	0.004	0.017	0.000	0.024	0.000
K	0.002	0.005	0.003	0.005	0.000	0.001	0.004	0.000	0.006	0.004	0.004	0.003	0.002	0.006	0.007	0.008	0.002	0.005	0.009	0.002	0.002	0.001	0.000	0.012
$Fe^{[2]}$ as total iron																								
formula for 24 oxygens																								

Table C6. Chemistry of biotite in ultramafic rocks (distance is referred to as from physical boundary between granulite and zone D)

sample No.	9710(1	9710(1	9710(1	9710(1	9710(1	9710(1	9710(1	9710(1	9710(1	9710(1	9710(1	9710(1	9710	9710	9710(1	9710(1	9710(1
analysis No.	3	4	9	16	19	20	28	1	2	21	26	42	33	4	65	66	68
zone	UM	UM	UM	UM	UM	UM	UM	UM	UM	UM	UM	UM	UM	UM	UM	UM	UM
distance (cm)	60	60	60	60	60	60	60	58	58	58	58	58	58	58	56	56	56
SiO_2	42.66	42.69	42.94	42.53	42.43	42.12	43.13	41.44	41.72	42.39	41.70	41.75	41.95	41.61	40.94	40.52	40.74
TiO_2	0.32	0.28	0.26	0.42	0.41	0.47	0.29	0.26	0.22	0.37	0.37	0.51	0.43	0.43	0.42	0.39	0.42
Al_2O_3	13.05	12.51	12.48	12.48	13.06	12.33	12.50	14.21	14.31	13.43	14.12	13.25	12.70	14.21	14.75	14.77	14.46
FeO	0.59	0.40	0.44	0.55	0.33	0.42	0.43	0.34	0.41	0.41	0.42	0.46	0.45	0.41	0.46	0.47	0.48
Cr_2O_3	0.05	0.00	0.00	0.06	0.06	0.01	0.04	0.05	0.03	0.00	0.05	0.06	0.07	0.02	0.05	0.00	0.01
MnO	0.04	0.00	0.04	0.00	0.03	0.04	0.00	0.00	0.00	0.00	0.02	0.03	0.04	0.00	0.02	0.00	0.02
MgO	28.00	28.49	28.55	28.27	28.05	28.56	28.47	28.14	28.03	28.35	27.76	27.83	28.94	27.76	27.01	26.65	26.65
CaO	0.00	0.01	0.00	0.00	0.00	0.00	0.01	0.02	0.00	0.00	0.00	0.00	0.00	0.02	0.00	0.01	0.00
Na_2O	0.20	0.17	0.19	0.21	0.18	0.12	0.18	0.18	0.19	0.18	0.17	0.23	0.12	0.23	0.45	0.51	0.54
K_2O	9.68	9.43	9.33	9.31	10.02	9.09	9.60	10.11	10.14	9.94	10.07	9.61	9.14	10.12	9.91	9.64	9.65
BaO	0.00	0.12	0.03	0.12	0.00	0.09	0.10	0.22	0.10	0.06	0.20	0.16	0.08	0.16	0.20	0.09	0.14
F	1.39	1.70	1.50	1.44	1.52	1.41	1.36	1.43	1.63	1.83	1.42	1.54	1.21	1.33	1.96	1.90	2.05
Cl	0.23	0.26	0.25	0.24	0.26	0.26	0.25	0.24	0.25	0.27	0.26	0.22	0.28	0.38	0.24	0.24	0.28
Total	96.21	96.06	96.01	95.63	96.34	94.92	96.36	96.62	97.03	97.23	96.56	95.65	95.42	96.68	96.40	95.19	95.43
							formula on the basis of 22 oxygens										
Si	5.867	5.875	5.903	5.881	5.836	5.861	5.917	5.703	5.711	5.780	5.739	5.788	5.813	5.724	5.649	5.651	5.671
Ti	0.033	0.029	0.027	0.044	0.043	0.049	0.030	0.026	0.023	0.038	0.039	0.053	0.044	0.044	0.043	0.041	0.044
Al	2.115	2.029	2.022	2.034	2.117	2.022	2.021	2.305	2.309	2.158	2.290	2.165	2.074	2.304	2.398	2.427	2.372
$Al^{[4]}$	2.115	2.029	2.022	2.034	2.117	2.022	2.021	2.297	2.289	2.158	2.290	2.165	2.074	2.276	2.351	2.349	2.329
$Al^{[6]}$	0	0	0	0	0	0	0	0.008	0.020	0	0	0	0	0.028	0.047	0.078	0.044
Fe	0.068	0.046	0.051	0.064	0.037	0.049	0.049	0.039	0.047	0.047	0.048	0.053	0.052	0.047	0.053	0.055	0.056
Cr	0.005	0.000	0.000	0.006	0.006	0.001	0.004	0.005	0.003	0.000	0.005	0.006	0.008	0.003	0.006	0.000	0.001
Mn	0.005	0.000	0.004	0.000	0.003	0.004	0.000	0.000	0.000	0.000	0.003	0.003	0.005	0.000	0.003	0.000	0.002
Mg	5.741	5.845	5.851	5.828	5.752	5.924	5.823	5.773	5.720	5.763	5.695	5.752	5.978	5.693	5.556	5.541	5.531
Ca	0.000	0.001	0.000	0.000	0.000	0.000	0.002	0.002	0.000	0.000	0.000	0.000	0.000	0.003	0.000	0.001	0.000
Na	0.053	0.045	0.051	0.056	0.049	0.033	0.049	0.047	0.050	0.047	0.045	0.063	0.033	0.060	0.119	0.138	0.145
K	1.698	1.655	1.636	1.642	1.758	1.613	1.680	1.775	1.771	1.729	1.768	1.699	1.616	1.776	1.744	1.715	1.714
Ba	0.000	0.006	0.001	0.007	0.000	0.005	0.005	0.012	0.006	0.003	0.011	0.009	0.004	0.008	0.011	0.005	0.008
F	0.603	0.740	0.652	0.630	0.661	0.618	0.592	0.622	0.706	0.789	0.618	0.675	0.530	0.579	0.855	0.838	0.902
Cl	0.055	0.061	0.059	0.057	0.060	0.062	0.057	0.057	0.058	0.061	0.061	0.052	0.066	0.089	0.057	0.057	0.066
OH	3.342	3.200	3.289	3.313	3.279	3.320	3.351	3.321	3.236	3.149	3.321	3.273	3.404	3.332	3.088	3.105	3.032
X_{Mg}	0.988	0.992	0.991	0.989	0.994	0.992	0.992	0.993	0.992	0.992	0.992	0.991	0.991	0.992	0.991	0.990	0.990
X_{Fe}	0.012	0.008	0.009	0.011	0.006	0.008	0.008	0.007	0.008	0.008	0.008	0.009	0.009	0.008	0.009	0.010	0.010
X_{Cl}	0.014	0.015	0.015	0.014	0.015	0.016	0.014	0.014	0.015	0.015	0.015	0.013	0.016	0.022	0.014	0.014	0.017
X_F	0.151	0.185	0.163	0.157	0.165	0.155	0.148	0.156	0.176	0.197	0.154	0.169	0.133	0.145	0.214	0.209	0.226
X_{OH}	0.836	0.800	0.822	0.828	0.820	0.830	0.838	0.830	0.809	0.787	0.830	0.818	0.851	0.833	0.772	0.776	0.758
all iron as Fe																	
OH calculated by stoichiometry																	

Table C6 contd....

sample No.	9710(1	9710(1	9710(1	9710(1	9710(1	9710(1	9710(1	9710(1	9710(1	9710(1	9710(1	9710(1	9710(1	9710(1	9710(1	9710(1
analysis No.	72	73	74	75	76	77	78	79	57	58	59	60	61	62	63	64
zone	UM	UM	UM	UM	UM	UM	UM	UM	UM	UM	UM	UM	UM	UM	UM	UM
distance (cm)	56	56	56	56	56	56	56	56	56	56	56	56	56	56	56	56
SiO_2	40.55	41.20	41.61	41.03	41.01	41.44	40.00	41.85	41.08	40.86	41.16	40.84	40.68	40.76	40.99	40.48
TiO_2	0.39	0.41	0.38	0.40	0.42	0.35	0.38	0.42	0.37	0.38	0.41	0.35	0.34	0.41	0.39	0.44
Al_2O_3	14.71	14.84	14.03	14.43	14.80	14.85	14.27	14.09	14.85	14.22	14.43	14.59	14.66	14.46	14.54	14.47
FeO	0.50	0.48	0.47	0.39	0.40	0.48	0.62	0.46	0.36	0.45	0.49	0.49	0.49	0.41	0.50	0.63
Cr_2O_3	0.04	0.04	0.00	0.04	0.04	0.02	0.06	0.00	0.05	0.00	0.00	0.01	0.07	0.00	0.00	0.01
MnO	0.04	0.00	0.00	0.00	0.00	0.03	0.09	0.00	0.00	0.00	0.00	0.03	0.00	0.06	0.03	0.03
MgO	27.39	27.20	27.37	27.27	26.95	27.07	28.34	27.61	27.14	26.75	27.12	26.95	27.27	26.69	26.98	26.88
CaO	0.00	0.00	0.00	0.01	0.00	0.00	0.00	0.03	0.00	0.00	0.00	0.05	0.03	0.00	0.00	0.00
Na_2O	0.51	0.53	0.49	0.55	0.73	0.45	0.46	0.48	0.47	0.49	0.49	0.58	0.47	0.53	0.46	0.46
K_2O	9.83	9.66	9.86	9.70	9.77	9.68	8.76	9.60	9.50	9.55	9.84	9.57	9.27	9.86	9.86	9.61
BaO	0.21	0.23	0.07	0.03	0.23	0.05	0.14	0.13	0.21	0.09	0.21	0.00	0.36	0.09	0.15	0.21
F	1.91	2.04	1.98	1.97	1.82	1.95	1.75	1.92	1.87	1.94	1.92	2.24	1.92	1.66	2.10	1.93
Cl	0.24	0.26	0.29	0.27	0.44	0.20	0.28	0.24	0.23	0.27	0.24	0.26	0.26	0.26	0.25	0.23
Total	96.32	96.88	96.56	96.08	96.60	96.56	95.15	96.83	96.14	94.99	96.30	95.94	95.82	95.19	96.25	95.39
								formula on the basis of 22 oxygens								
Si	5.607	5.649	5.723	5.667	5.652	5.686	5.576	5.729	5.665	5.705	5.683	5.648	5.638	5.691	5.662	5.645
Ti	0.041	0.042	0.039	0.041	0.043	0.036	0.040	0.044	0.038	0.040	0.042	0.036	0.036	0.043	0.041	0.046
Al	2.397	2.398	2.274	2.349	2.404	2.401	2.344	2.273	2.413	2.340	2.348	2.378	2.395	2.379	2.367	2.378
$Al^{[4]}$	2.393	2.351	2.274	2.333	2.348	2.314	2.344	2.271	2.335	2.295	2.317	2.352	2.362	2.309	2.338	2.355
$Al^{[6]}$	0.005	0.047	0	0.016	0.055	0.088	0	0.003	0.078	0.045	0.031	0.025	0.033	0.071	0.029	0.024
Fe	0.057	0.055	0.054	0.045	0.046	0.055	0.073	0.052	0.042	0.052	0.056	0.057	0.057	0.048	0.058	0.074
Cr	0.004	0.004	0.000	0.004	0.004	0.002	0.007	0.000	0.006	0.000	0.000	0.001	0.007	0.000	0.000	0.002
Mn	0.005	0.000	0.000	0.000	0.000	0.003	0.010	0.000	0.000	0.000	0.000	0.003	0.000	0.008	0.003	0.004
Mg	5.647	5.560	5.612	5.615	5.537	5.537	5.890	5.635	5.579	5.568	5.582	5.556	5.635	5.556	5.556	5.589
Ca	0.000	0.000	0.000	0.002	0.000	0.000	0.000	0.004	0.000	0.000	0.000	0.007	0.004	0.000	0.000	0.000
Na	0.137	0.141	0.132	0.148	0.195	0.120	0.125	0.127	0.126	0.132	0.132	0.155	0.127	0.144	0.123	0.123
K	1.734	1.690	1.730	1.709	1.717	1.694	1.558	1.676	1.671	1.701	1.733	1.688	1.639	1.756	1.737	1.710
Ba	0.011	0.012	0.004	0.002	0.012	0.003	0.008	0.007	0.011	0.005	0.011	0.000	0.020	0.005	0.008	0.012
F	0.835	0.884	0.861	0.860	0.793	0.846	0.771	0.831	0.815	0.856	0.838	0.980	0.841	0.733	0.917	0.851
Cl	0.057	0.060	0.068	0.063	0.102	0.047	0.065	0.057	0.053	0.064	0.055	0.060	0.061	0.062	0.058	0.053
OH	3.108	3.056	3.071	3.077	3.105	3.107	3.163	3.112	3.131	3.080	3.107	2.961	3.098	3.205	3.025	3.096
X_{Mg}	0.990	0.990	0.990	0.992	0.992	0.990	0.988	0.991	0.993	0.991	0.990	0.990	0.990	0.992	0.990	0.987
X_{Fe}	0.010	0.010	0.010	0.008	0.008	0.010	0.012	0.009	0.007	0.009	0.010	0.010	0.010	0.008	0.010	0.013
X_{Cl}	0.014	0.015	0.017	0.016	0.026	0.012	0.016	0.014	0.013	0.016	0.014	0.015	0.015	0.016	0.015	0.013
X_F	0.209	0.221	0.215	0.215	0.198	0.212	0.193	0.208	0.204	0.214	0.210	0.245	0.210	0.183	0.229	0.213
X_{OH}	0.777	0.764	0.768	0.769	0.776	0.777	0.791	0.778	0.783	0.770	0.777	0.740	0.774	0.801	0.756	0.774

all iron as Fe

OH calculated by stoichiometry

Table C7. Chemistry of biotite in zone A (distance is referred to as from the physical boundary between granulite and zone

sample No.	9806	9806	9806	9806	9806	9806	9806	9806
analysis No.	47	49	55	56	61	62	63	64
zone	A	A	A	A	A	A	A	A
distance (cm)	47	47	47	47	47	47	47	47
SiO_2	39.00	38.06	37.98	38.85	38.47	39.03	38.79	38.91
TiO_2	1.65	1.52	1.89	1.89	1.83	1.83	1.76	1.41
Al_2O_3	16.54	16.69	16.14	16.73	16.70	16.70	16.39	16.56
FeO	0.55	0.55	0.46	0.58	0.55	0.51	0.45	0.49
Cr_2O_3	0.00	0.06	0.06	0.00	0.03	0.00	0.01	0.02
MnO	0.05	0.01	0.00	0.00	0.01	0.00	0.00	0.00
MgO	25.69	24.72	24.76	25.27	25.09	25.41	25.14	24.64
CaO	0.00	0.00	0.04	0.01	0.00	0.01	0.00	0.00
Na_2O	0.47	0.65	0.51	0.47	0.44	0.51	0.48	0.52
K_2O	9.90	9.62	9.56	9.72	9.55	9.48	9.42	9.65
BaO	0.33	0.28	0.39	0.28	0.44	0.42	0.45	0.31
F	1.75	1.61	1.60	1.53	1.53	1.71	1.98	1.76
Cl	0.18	0.26	0.25	0.17	0.20	0.18	0.22	0.30
Total	96.11	94.02	93.63	95.49	94.84	95.79	95.09	94.57
			formula on the basis of 22 oxygens					
Si	5.419	5.404	5.418	5.423	5.411	5.427	5.434	5.480
Ti	0.172	0.163	0.203	0.198	0.194	0.191	0.185	0.149
Al	2.708	2.793	2.713	2.752	2.768	2.737	2.706	2.749
$Al^{[4]}$	2.581	2.596	2.582	2.577	2.589	2.573	2.566	2.520
$Al^{[6]}$	0.127	0.197	0.131	0.175	0.180	0.164	0.141	0.229
Fe	0.064	0.065	0.054	0.067	0.065	0.059	0.053	0.058
Cr	0.000	0.007	0.006	0.000	0.003	0.000	0.001	0.002
Mn	0.006	0.001	0.000	0.000	0.001	0.000	0.000	0.000
Mg	5.321	5.233	5.266	5.259	5.261	5.268	5.251	5.174
Ca	0.000	0.000	0.006	0.001	0.000	0.001	0.000	0.000
Na	0.127	0.178	0.141	0.127	0.121	0.137	0.129	0.141
K	1.755	1.742	1.740	1.731	1.714	1.682	1.683	1.734
Ba	0.018	0.015	0.022	0.015	0.024	0.023	0.025	0.017
F	0.769	0.723	0.722	0.675	0.681	0.752	0.877	0.784
Cl	0.043	0.062	0.060	0.040	0.049	0.043	0.052	0.072
OH	3.188	3.215	3.218	3.284	3.271	3.205	3.071	3.144
X_{Mg}	0.988	0.988	0.990	0.987	0.988	0.989	0.990	0.989
X_{Fe}	0.012	0.012	0.010	0.013	0.012	0.011	0.010	0.011
X_{Cl}	0.011	0.016	0.015	0.010	0.012	0.011	0.013	0.018
X_F	0.192	0.181	0.180	0.169	0.170	0.188	0.219	0.196
X_{OH}	0.797	0.804	0.805	0.821	0.818	0.801	0.768	0.786

all iron as Fe

OH calculated by stoichiometry

Table C8. Chemistry of biotite in zone B (distance is referred to as from the physical boundary between granulite and zone D)

sample No.	9806	9806	9806	9806	9806	9806	9806	9806	9806	9806	9806	9806	9806	9806	9806	9806	9806	9806
analysis No.	85	86	51	50	52	53	59	22	23	24	29	30	31	34	36	37	39	79
zone	B	B	B	B	B	B	B	B	B	B	B	B	B	B	B	B	B	B
distance (cm	44	44	44	44	44	44	44	44	44	44	44	44	40	40	40	40	40	40
SiO_2	38.52	38.28	38.65	39.11	38.88	38.51	38.46	37.78	37.75	37.75	38.49	38.09	37.79	37.22	37.51	37.51	37.58	36.60
TiO_2	1.29	1.24	1.93	1.55	1.79	1.96	2.00	2.40	2.62	2.72	2.69	2.55	2.72	2.65	2.69	2.77	2.68	1.80
Al_2O_3	17.09	17.00	17.07	17.31	16.71	16.95	17.18	17.35	17.34	17.15	17.54	17.82	17.52	17.17	17.25	17.41	17.26	16.43
FeO	0.52	0.50	0.59	0.50	0.57	0.49	0.52	2.94	2.43	2.77	2.58	2.26	2.45	2.65	1.89	2.77	2.99	0.58
Cr_2O_3	0.02	0.03	0.04	0.00	0.00	0.06	0.00	0.02	0.00	0.08	0.00	0.00	0.07	0.05	0.00	0.04	0.00	0.01
MnO	0.04	0.01	0.00	0.00	0.04	0.07	0.04	0.05	0.01	0.01	0.04	0.03	0.00	0.05	0.03	0.00	0.07	0.05
MgO	25.81	25.52	25.25	25.53	25.67	25.27	25.07	22.17	22.78	22.84	22.67	22.78	22.54	22.67	22.74	22.66	22.92	23.97
CaO	0.00	0.00	0.00	0.00	0.00	0.00	0.00	0.00	0.00	0.01	0.00	0.00	0.02	0.00	0.03	0.00	0.01	0.01
Na_2O	0.48	0.53	0.36	0.50	0.59	0.50	0.55	0.08	0.12	0.12	0.17	0.09	0.10	0.10	0.14	0.07	0.12	0.57
K_2O	9.72	9.70	9.53	9.74	9.40	9.55	9.69	9.82	10.12	9.91	9.94	9.79	9.99	9.80	9.79	10.05	9.90	9.52
BaO	0.34	0.22	0.44	0.36	0.39	0.27	0.48	0.62	0.46	0.42	0.39	0.39	0.50	0.39	0.50	0.49	0.40	0.40
F	2.00	1.80	1.66	1.92	1.81	1.81	1.71	1.50	1.48	1.47	1.50	1.39	1.41	1.33	1.38	1.41	1.62	1.71
Cl	0.18	0.24	0.18	0.19	0.21	0.19	0.12	0.10	0.11	0.15	0.11	0.13	0.13	0.14	0.11	0.10	0.08	0.27
Total	96.00	95.08	95.70	96.71	96.05	95.62	95.82	94.83	95.22	95.40	96.11	95.32	95.24	94.23	94.06	95.29	95.63	91.93
							formula on the basis of 22 oxygens											
Si	5.355	5.370	5.384	5.389	5.396	5.368	5.360	5.381	5.348	5.343	5.389	5.366	5.350	5.330	5.360	5.321	5.311	5.334
Ti	0.134	0.131	0.202	0.160	0.187	0.205	0.210	0.257	0.279	0.290	0.283	0.270	0.290	0.285	0.289	0.296	0.285	0.197
Al	2.800	2.810	2.802	2.811	2.733	2.784	2.822	2.912	2.895	2.861	2.894	2.958	2.923	2.898	2.905	2.910	2.875	2.822
$Al^{[4]}$	2.645	2.630	2.616	2.611	2.604	2.632	2.640	2.619	2.652	2.657	2.611	2.634	2.650	2.670	2.640	2.679	2.689	2.666
$Al^{[6]}$	0.155	0.180	0.186	0.200	0.129	0.152	0.182	0.294	0.244	0.203	0.283	0.324	0.273	0.228	0.265	0.231	0.186	0.156
Fe	0.060	0.059	0.069	0.057	0.066	0.057	0.061	0.350	0.288	0.328	0.302	0.266	0.290	0.317	0.226	0.329	0.353	0.071
Cr	0.002	0.003	0.004	0.000	0.000	0.006	0.000	0.002	0.000	0.009	0.000	0.000	0.007	0.005	0.000	0.005	0.000	0.001
Mn	0.005	0.001	0.000	0.000	0.005	0.008	0.005	0.006	0.001	0.001	0.004	0.004	0.000	0.007	0.004	0.000	0.008	0.006
Mg	5.349	5.337	5.244	5.245	5.311	5.251	5.209	4.708	4.812	4.819	4.732	4.784	4.757	4.840	4.844	4.792	4.829	5.208
Ca	0.000	0.000	0.000	0.000	0.000	0.000	0.000	0.000	0.000	0.001	0.000	0.000	0.003	0.000	0.005	0.000	0.002	0.002
Na	0.130	0.144	0.097	0.134	0.158	0.134	0.149	0.023	0.032	0.034	0.045	0.024	0.028	0.029	0.039	0.020	0.033	0.162
K	1.724	1.736	1.693	1.712	1.664	1.698	1.723	1.784	1.829	1.789	1.775	1.759	1.804	1.790	1.784	1.818	1.785	1.770
Ba	0.019	0.012	0.024	0.020	0.021	0.014	0.026	0.035	0.026	0.023	0.021	0.022	0.027	0.022	0.028	0.027	0.022	0.023
F	0.879	0.798	0.731	0.837	0.794	0.798	0.754	0.676	0.663	0.658	0.664	0.618	0.632	0.604	0.624	0.632	0.724	0.788
Cl	0.041	0.058	0.042	0.045	0.048	0.044	0.028	0.024	0.027	0.036	0.025	0.030	0.030	0.035	0.027	0.024	0.019	0.068
OH	3.080	3.144	3.227	3.119	3.157	3.158	3.219	3.300	3.310	3.306	3.311	3.352	3.338	3.361	3.349	3.343	3.257	3.144
X_{Mg}	0.989	0.989	0.987	0.989	0.988	0.989	0.988	0.931	0.944	0.936	0.940	0.947	0.943	0.938	0.955	0.936	0.932	0.987
X_{Fe}	0.011	0.011	0.013	0.011	0.012	0.011	0.012	0.069	0.056	0.064	0.060	0.053	0.057	0.062	0.045	0.064	0.068	0.013
X_{Cl}	0.010	0.014	0.011	0.011	0.012	0.011	0.007	0.006	0.007	0.009	0.006	0.008	0.008	0.009	0.007	0.006	0.005	0.017
X_F	0.220	0.200	0.183	0.209	0.199	0.199	0.188	0.169	0.166	0.164	0.166	0.154	0.158	0.151	0.156	0.158	0.181	0.197
X_{OH}	0.770	0.786	0.807	0.780	0.789	0.790	0.805	0.825	0.827	0.826	0.828	0.838	0.834	0.840	0.837	0.836	0.814	0.786
all iron as Fe																		
OH calculated by stoichiometry																		

Table C8 contd....

sample No.	9806	9806	9806	9806	9806	9806	9806	9806	9806	9806	9806	9806	9806	9806	9806	9806
analysis No.	81	84	5	6	7	8	9	10	11	12	13	14	16	18	19	20
zone	B	B	B	B	B	B	B	B	B	B	B	B	B	B	B	B
distance (cm	40	40	36	36	36	36	36	36	36	36	36	36	36	36	36	36
SiO_2	38.35	37.91	37.80	41.06	38.33	38.01	37.43	38.20	37.83	37.95	37.40	37.09	37.24	37.25	37.29	37.23
TiO_2	1.82	1.65	2.73	2.48	2.85	2.65	2.81	2.79	2.66	2.78	2.73	2.71	3.18	2.85	2.63	2.84
Al_2O_3	17.13	17.12	17.77	16.56	17.56	17.95	17.18	17.65	17.33	17.57	17.40	17.40	16.90	17.37	17.34	17.18
FeO	0.56	0.54	2.82	3.39	3.31	3.25	3.16	1.65	1.43	2.94	3.16	2.59	2.82	3.15	3.39	3.06
Cr_2O_3	0.00	0.01	0.08	0.01	0.04	0.01	0.05	0.05	0.00	0.02	0.05	0.05	0.00	0.07	0.09	0.03
MnO	0.02	0.06	0.06	0.01	0.07	0.04	0.07	0.00	0.05	0.05	0.04	0.05	0.00	0.06	0.03	0.00
MgO	25.12	24.91	22.05	19.45	22.19	21.37	21.67	23.45	23.43	22.82	22.13	22.07	22.10	22.37	21.69	21.71
CaO	0.00	0.00	0.01	0.03	0.00	0.03	0.00	0.08	0.02	0.01	0.00	0.00	0.00	0.00	0.00	0.00
Na_2O	0.49	0.52	0.10	0.20	0.12	0.12	0.13	0.11	0.24	0.06	0.12	0.18	0.07	0.09	0.13	0.17
K_2O	9.74	9.59	9.80	9.24	9.98	9.60	9.98	9.99	9.70	9.87	9.90	9.78	9.81	9.86	9.66	9.80
BaO	0.36	0.31	0.50	0.37	0.35	0.50	0.43	0.25	0.46	0.62	0.43	0.44	0.50	0.55	0.42	0.45
F	2.00	1.59	1.41	1.65	1.88	1.45	1.20	1.34	1.56	1.59	1.35	1.32	1.44	1.30	1.66	1.59
Cl	0.24	0.19	0.09	0.15	0.12	0.14	0.12	0.11	0.11	0.12	0.10	0.14	0.09	0.10	0.09	0.10
Total	95.83	94.40	95.21	94.60	96.79	95.11	94.23	95.66	94.82	96.40	94.80	93.80	94.15	95.02	94.42	94.16
					formula on the basis of 22 oxygens											
Si	5.345	5.359	5.353	5.791	5.350	5.387	5.376	5.351	5.347	5.321	5.336	5.335	5.344	5.310	5.340	5.344
Ti	0.191	0.176	0.291	0.263	0.299	0.282	0.304	0.294	0.283	0.293	0.293	0.293	0.343	0.306	0.283	0.307
Al	2.814	2.852	2.966	2.753	2.888	2.998	2.908	2.914	2.887	2.903	2.926	2.949	2.858	2.918	2.926	2.906
$Al^{[4]}$	2.655	2.641	2.647	2.209	2.650	2.613	2.624	2.649	2.653	2.679	2.664	2.665	2.656	2.690	2.660	2.656
$Al^{[6]}$	0.159	0.211	0.319	0.544	0.238	0.385	0.283	0.265	0.234	0.224	0.261	0.284	0.202	0.227	0.266	0.251
Fe	0.065	0.063	0.334	0.400	0.386	0.385	0.379	0.193	0.169	0.345	0.377	0.311	0.338	0.375	0.406	0.367
Cr	0.000	0.001	0.009	0.002	0.005	0.001	0.006	0.006	0.000	0.002	0.005	0.005	0.000	0.008	0.010	0.004
Mn	0.003	0.007	0.007	0.001	0.008	0.005	0.008	0.000	0.006	0.006	0.005	0.006	0.000	0.007	0.003	0.000
Mg	5.219	5.250	4.655	4.090	4.617	4.515	4.640	4.897	4.937	4.770	4.707	4.732	4.728	4.754	4.630	4.646
Ca	0.000	0.000	0.002	0.004	0.000	0.005	0.000	0.012	0.002	0.002	0.000	0.000	0.000	0.000	0.000	0.000
Na	0.132	0.142	0.026	0.055	0.031	0.033	0.037	0.029	0.065	0.016	0.034	0.050	0.020	0.025	0.037	0.048
K	1.732	1.729	1.770	1.662	1.777	1.735	1.828	1.785	1.749	1.765	1.802	1.794	1.796	1.793	1.764	1.795
Ba	0.019	0.017	0.027	0.020	0.019	0.028	0.024	0.014	0.026	0.034	0.024	0.025	0.028	0.031	0.023	0.025
F	0.881	0.711	0.630	0.736	0.830	0.650	0.546	0.592	0.697	0.705	0.608	0.599	0.653	0.587	0.752	0.722
Cl	0.057	0.046	0.022	0.035	0.029	0.033	0.028	0.025	0.027	0.028	0.023	0.033	0.022	0.024	0.023	0.024
OH	3.062	3.243	3.349	3.229	3.142	3.318	3.426	3.383	3.275	3.267	3.369	3.368	3.325	3.389	3.226	3.254
X_{Mg}	0.988	0.988	0.933	0.911	0.923	0.921	0.924	0.962	0.967	0.933	0.926	0.938	0.933	0.927	0.919	0.927
X_{Fe}	0.012	0.012	0.067	0.089	0.077	0.079	0.076	0.038	0.033	0.067	0.074	0.062	0.067	0.073	0.081	0.073
X_{Cl}	0.014	0.012	0.005	0.009	0.007	0.008	0.007	0.006	0.007	0.007	0.006	0.008	0.005	0.006	0.006	0.006
X_F	0.220	0.178	0.157	0.184	0.207	0.162	0.136	0.148	0.174	0.176	0.152	0.150	0.163	0.147	0.188	0.180
X_{OH}	0.765	0.811	0.837	0.807	0.785	0.829	0.857	0.846	0.819	0.817	0.842	0.842	0.831	0.847	0.806	0.814
all iron as Fe																
OH calculated by stoichiometry																

Table C9. Chemistry of biotite in zone C (distance is referred to as from the physical boundary between granulite and zone I

sample No.	9806	9806	9806	9806	9806
analysis No.	60	62	70	71	77
zone	C	C	C	C	C
distance (cm)	34	34	34	34	34
SiO_2	37.33	36.53	37.50	38.27	37.26
TiO_2	2.66	2.67	2.68	2.84	2.62
Al_2O_3	17.99	17.89	18.11	17.95	17.85
FeO	2.77	2.78	2.44	2.18	3.26
Cr_2O_3	0.00	0.05	0.05	0.01	0.00
MnO	0.01	0.00	0.01	0.02	0.05
MgO	22.50	21.74	23.08	23.48	21.98
CaO	0.01	0.00	0.00	0.00	0.01
Na_2O	0.13	0.10	0.12	0.09	0.10
K_2O	10.17	9.97	10.30	10.36	10.25
BaO	0.39	0.45	0.43	0.52	0.33
F	1.38	1.30	1.45	1.56	1.74
Cl	0.13	0.12	0.12	0.12	0.09
Total	95.47	93.60	96.28	97.40	95.54
	formula on the basis of 22 oxygens				
Si	5.285	5.277	5.261	5.300	5.283
Ti	0.283	0.290	0.283	0.296	0.279
Al	3.001	3.046	2.994	2.929	2.983
$Al^{[4]}$	2.715	2.723	2.739	2.700	2.717
$Al^{[6]}$	0.286	0.323	0.256	0.229	0.266
Fe	0.328	0.336	0.286	0.252	0.387
Cr	0.000	0.005	0.005	0.002	0.000
Mn	0.001	0.000	0.001	0.002	0.006
Mg	4.749	4.682	4.828	4.848	4.646
Ca	0.002	0.000	0.000	0.000	0.002
Na	0.037	0.027	0.032	0.024	0.028
K	1.837	1.837	1.843	1.830	1.854
Ba	0.022	0.025	0.024	0.028	0.019
F	0.617	0.596	0.643	0.683	0.780
Cl	0.031	0.030	0.029	0.027	0.021
OH	3.352	3.374	3.328	3.290	3.199
X_{Mg}	0.935	0.933	0.944	0.951	0.923
X_{Fe}	0.065	0.067	0.056	0.049	0.077
X_{Cl}	0.008	0.007	0.007	0.007	0.005
X_F	0.154	0.149	0.161	0.171	0.195
X_{OH}	0.838	0.844	0.832	0.822	0.800
all iron as Fe					
OH calculated by stoichiometry					

Table C10 Chemistry of biotite in Zone D (distance is referred to as from the physical boundary between granulite and zone D)

sample No.	9805	9805	9805	9805	9805	9805	9805	9805	9805	9805	9805	9805	9805	9805	9805	9805	9805	9805
analysis No.	113	114	115	116	117	118	120	121	122	123	124	125	126	127	128	129	130	131
zone	D	D	D	D	D	D	D	D	D	D	D	D	D	D	D	D	D	D
distance (cm)	28	28	28	28	28	28	20	20	20	20	20	20	20	20	20	20	20	20
SiO_2	37.00	37.02	36.71	36.47	37.14	36.69	36.47	36.67	36.99	36.34	36.98	36.62	36.42	36.87	36.75	36.55	36.63	36.96
TiO_2	3.75	3.57	3.68	3.83	3.86	3.60	3.41	3.72	3.82	3.67	3.66	3.62	3.83	3.66	3.72	3.64	3.50	3.76
Al_2O_3	17.45	17.82	17.77	17.58	17.61	17.67	17.40	17.74	18.07	17.70	17.87	17.87	17.56	17.61	17.79	17.49	17.42	17.81
FeO	6.89	6.92	6.76	6.90	6.50	6.76	8.04	6.56	5.81	5.84	6.21	6.11	6.55	6.33	6.44	7.14	7.20	6.26
Cr_2O_3	0.00	0.03	0.00	0.01	0.00	0.01	0.01	0.04	0.00	0.00	0.05	0.04	0.02	0.03	0.03	0.02	0.02	0.00
MnO	0.04	0.07	0.10	0.06	0.02	0.03	0.06	0.05	0.08	0.05	0.03	0.04	0.08	0.05	0.03	0.05	0.08	0.08
MgO	19.20	19.30	19.32	19.07	19.41	19.17	18.33	19.45	19.54	18.87	19.24	19.39	18.94	19.45	19.39	18.98	19.15	19.46
CaO	0.00	0.00	0.00	0.00	0.02	0.00	0.00	0.00	0.00	0.00	0.00	0.01	0.00	0.00	0.03	0.01	0.02	0.00
Na_2O	0.17	0.12	0.19	0.10	0.18	0.26	0.14	0.16	0.12	0.20	0.10	0.13	0.26	0.15	0.15	0.08	0.11	0.16
K_2O	9.62	9.90	9.65	9.72	9.55	9.75	9.82	9.25	9.72	9.43	9.66	9.73	9.47	9.66	9.54	9.55	9.67	9.68
BaO	0.66	0.64	0.62	0.70	0.62	0.64	0.40	0.67	0.84	1.03	0.76	0.84	0.81	0.52	0.82	0.64	0.77	0.61
F	1.08	0.99	1.11	1.15	0.80	0.99	0.91	1.02	0.94	0.79	0.86	0.96	0.81	1.19	0.88	0.94	0.80	0.89
Cl	0.24	0.28	0.23	0.26	0.26	0.22	0.30	0.29	0.24	0.25	0.24	0.23	0.31	0.25	0.28	0.26	0.29	0.24
Total	96.10	96.66	96.13	95.84	95.98	95.80	95.28	95.62	96.17	94.17	95.66	95.59	95.05	95.77	95.84	95.35	95.66	95.91
							formula on the basis of 22 oxygens											
Si	5.307	5.287	5.264	5.256	5.318	5.283	5.307	5.271	5.282	5.308	5.312	5.274	5.286	5.290	5.281	5.292	5.299	5.296
Ti	0.405	0.383	0.397	0.415	0.416	0.390	0.373	0.402	0.410	0.403	0.395	0.392	0.418	0.395	0.402	0.396	0.381	0.405
Al	2.950	2.999	3.003	2.986	2.972	2.999	2.984	3.005	3.041	3.047	3.025	3.033	3.003	2.977	3.013	2.984	2.970	3.007
$Al^{[4]}$	2.693	2.713	2.736	2.744	2.682	2.717	2.693	2.729	2.718	2.692	2.688	2.726	2.714	2.710	2.719	2.708	2.701	2.704
$Al^{[6]}$	0.257	0.286	0.267	0.243	0.290	0.282	0.291	0.277	0.323	0.355	0.338	0.307	0.289	0.267	0.294	0.276	0.269	0.303
Fe	0.826	0.826	0.811	0.832	0.778	0.814	0.978	0.789	0.694	0.713	0.746	0.736	0.795	0.759	0.774	0.864	0.871	0.750
Cr	0.000	0.003	0.000	0.001	0.000	0.001	0.001	0.005	0.000	0.000	0.006	0.005	0.002	0.003	0.004	0.002	0.002	0.000
Mn	0.005	0.009	0.012	0.007	0.002	0.004	0.007	0.007	0.009	0.006	0.004	0.005	0.009	0.006	0.003	0.006	0.009	0.009
Mg	4.106	4.109	4.130	4.098	4.144	4.115	3.977	4.168	4.160	4.109	4.121	4.163	4.098	4.160	4.154	4.097	4.130	4.157
Ca	0.000	0.000	0.000	0.000	0.003	0.000	0.000	0.000	0.000	0.000	0.000	0.002	0.000	0.000	0.004	0.002	0.003	0.000
Na	0.047	0.033	0.053	0.027	0.051	0.073	0.041	0.043	0.034	0.057	0.028	0.035	0.073	0.041	0.042	0.022	0.031	0.046
K	1.760	1.804	1.765	1.787	1.744	1.791	1.823	1.696	1.771	1.757	1.770	1.788	1.753	1.768	1.749	1.764	1.784	1.769
Ba	0.037	0.036	0.035	0.040	0.035	0.036	0.023	0.038	0.047	0.059	0.043	0.048	0.046	0.029	0.046	0.037	0.043	0.034
F	0.490	0.446	0.501	0.523	0.364	0.452	0.416	0.462	0.423	0.364	0.392	0.436	0.372	0.541	0.398	0.430	0.366	0.401
Cl	0.059	0.069	0.056	0.063	0.063	0.053	0.073	0.072	0.059	0.062	0.058	0.056	0.075	0.062	0.067	0.063	0.072	0.059
OH	3.451	3.486	3.443	3.415	3.573	3.495	3.511	3.467	3.518	3.574	3.550	3.508	3.553	3.397	3.535	3.507	3.562	3.540
X_{Mg}	0.832	0.833	0.836	0.831	0.842	0.835	0.803	0.841	0.857	0.852	0.847	0.850	0.838	0.846	0.843	0.826	0.826	0.847
X_{Fe}	0.168	0.167	0.164	0.169	0.158	0.165	0.197	0.159	0.143	0.148	0.153	0.150	0.162	0.154	0.157	0.174	0.174	0.153
X_{Cl}	0.015	0.017	0.014	0.016	0.016	0.013	0.018	0.018	0.015	0.016	0.015	0.014	0.019	0.015	0.017	0.016	0.018	0.015
X_F	0.122	0.111	0.125	0.131	0.091	0.113	0.104	0.115	0.106	0.091	0.098	0.109	0.093	0.135	0.100	0.107	0.091	0.100
X_{OH}	0.863	0.871	0.861	0.854	0.893	0.874	0.878	0.867	0.880	0.893	0.887	0.877	0.888	0.849	0.884	0.877	0.891	0.885
all iron as Fe																		
OH calculated by stoichiometry																		

Table C10 contd.....

sample No.	9805	9805	9805	9805	9805	9805	9805	9805	9805	9805	9805	9805	9805	9805	9805	9805	9805	9805
analysis No.	132	133	98	99	100	103	104	105	107	111	112	106	107	112	114	122	123	108
zone	D	D	D	D	D	D	D	D	D	D	D	D	D	D	D	D	D	D
distance (cm)	20	20	10	10	10	10	10	10	10	10	10	10	10	10	10	10	10	2
SiO_2	36.15	36.66	37.00	36.45	36.62	36.22	39.65	36.75	36.67	36.67	36.31	36.09	36.46	36.72	34.43	34.26	36.43	38.10
TiO_2	3.57	3.13	4.94	4.52	4.74	4.00	3.74	4.37	4.44	3.72	3.73	4.40	4.54	3.83	2.86	3.60	3.67	4.65
Al_2O_3	17.58	17.80	18.23	18.72	18.54	17.34	16.40	17.38	17.70	17.61	17.76	18.80	18.90	18.21	18.66	17.02	18.08	21.37
FeO	7.03	6.99	5.84	7.22	7.13	7.30	7.22	7.08	7.19	6.88	6.69	7.34	7.18	6.58	7.14	6.06	6.72	5.57
Cr_2O_3	0.06	0.01	0.00	0.07	0.00	0.00	0.00	0.00	0.00	0.00	0.01	0.02	0.02	0.07	0.00	0.02	0.00	0.05
MnO	0.03	0.07	0.06	0.05	0.06	0.06	0.04	0.06	0.09	0.03	0.03	0.08	0.00	0.05	0.04	0.11	0.04	0.10
MgO	18.90	18.98	18.61	17.33	17.72	17.53	16.61	18.19	18.13	18.84	18.93	17.38	17.66	19.01	20.14	18.08	19.42	14.10
CaO	0.03	0.01	0.00	0.01	0.00	0.02	0.05	0.00	0.00	0.02	0.02	0.00	0.01	0.00	0.01	0.00	0.00	0.02
Na_2O	0.11	0.14	0.39	0.24	0.17	0.45	0.49	0.34	0.20	0.21	0.15	0.25	0.18	0.12	0.19	0.17	0.24	0.20
K_2O	9.18	9.44	9.66	9.68	9.73	9.08	8.80	9.39	9.51	9.60	9.40	9.65	10.02	9.98	8.03	9.16	9.62	9.36
BaO	0.63	0.51	0.60	0.45	0.48	0.49	0.47	0.33	0.44	0.49	0.77	0.57	0.48	0.42	0.50	0.70	0.63	0.44
F	0.74	1.03	0.96	0.80	0.84	1.10	0.77	0.84	1.17	0.70	0.98	0.81	1.03	1.12	0.87	1.00	0.84	1.02
Cl	0.28	0.32	0.07	0.05	0.07	0.11	0.17	0.12	0.15	0.30	0.24	0.09	0.04	0.24	0.32	0.30	0.33	0.09
Total	94.28	95.08	96.35	95.59	96.10	93.70	94.40	94.85	95.68	95.07	95.02	95.48	96.51	96.35	93.18	29.41	96.01	95.07
							formula on the basis of 22 oxygens											
Si	5.283	5.307	5.263	5.252	5.248	5.324	5.723	5.327	5.279	5.313	5.266	5.218	5.211	5.247	5.073	5.224	5.233	5.413
Ti	0.392	0.341	0.528	0.490	0.511	0.442	0.406	0.476	0.481	0.405	0.407	0.479	0.488	0.412	0.317	0.413	0.396	0.497
Al	3.028	3.037	3.056	3.179	3.131	3.004	2.790	2.969	3.003	3.007	3.035	3.204	3.183	3.066	3.240	3.058	3.061	3.578
$Al^{[4]}$	2.717	2.693	2.737	2.748	2.752	2.676	2.277	2.673	2.721	2.687	2.734	2.782	2.789	2.753	2.927	2.776	2.767	2.587
$Al^{[6]}$	0.311	0.344	0.318	0.431	0.379	0.328	0.513	0.297	0.282	0.321	0.301	0.422	0.395	0.313	0.312	0.282	0.294	0.992
Fe	0.859	0.846	0.695	0.870	0.854	0.897	0.871	0.858	0.865	0.834	0.811	0.887	0.858	0.786	0.880	0.773	0.807	0.662
Cr	0.007	0.002	0.000	0.008	0.000	0.000	0.000	0.000	0.000	0.000	0.001	0.002	0.002	0.007	0.000	0.003	0.000	0.005
Mn	0.004	0.008	0.007	0.006	0.007	0.007	0.005	0.008	0.011	0.004	0.004	0.009	0.000	0.006	0.005	0.015	0.005	0.012
Mg	4.118	4.096	3.946	3.723	3.786	3.841	3.574	3.931	3.891	4.070	4.093	3.747	3.763	4.049	4.424	4.110	4.159	2.987
Ca	0.005	0.001	0.000	0.001	0.000	0.003	0.007	0.000	0.000	0.003	0.003	0.000	0.001	0.000	0.002	0.000	0.000	0.003
Na	0.032	0.039	0.106	0.067	0.048	0.127	0.136	0.096	0.054	0.060	0.042	0.071	0.049	0.033	0.053	0.051	0.066	0.055
K	1.711	1.743	1.753	1.779	1.779	1.702	1.620	1.736	1.746	1.774	1.739	1.780	1.827	1.819	1.509	1.782	1.763	1.696
Ba	0.036	0.029	0.033	0.026	0.027	0.028	0.027	0.019	0.025	0.028	0.044	0.032	0.027	0.024	0.029	0.042	0.036	0.025
F	0.343	0.471	0.431	0.365	0.382	0.512	0.350	0.383	0.532	0.320	0.449	0.370	0.464	0.506	0.404	0.481	0.380	0.460
Cl	0.068	0.078	0.016	0.012	0.017	0.028	0.040	0.029	0.037	0.073	0.058	0.023	0.010	0.058	0.079	0.077	0.079	0.021
OH	3.589	3.451	3.552	3.623	3.601	3.460	3.610	3.588	3.431	3.607	3.493	3.607	3.526	3.436	3.516	3.442	3.541	3.519
X_{Mg}	0.827	0.829	0.850	0.811	0.816	0.811	0.804	0.821	0.818	0.830	0.835	0.808	0.814	0.837	0.834	0.842	0.837	0.819
X_{Fe}	0.173	0.171	0.150	0.189	0.184	0.189	0.196	0.179	0.182	0.170	0.165	0.192	0.186	0.163	0.166	0.158	0.163	0.181
X_{Cl}	0.017	0.019	0.004	0.003	0.004	0.007	0.010	0.007	0.009	0.018	0.015	0.006	0.002	0.015	0.020	0.019	0.020	0.005
X_F	0.086	0.118	0.108	0.091	0.095	0.128	0.087	0.096	0.133	0.080	0.112	0.092	0.116	0.127	0.101	0.120	0.095	0.115
X_{OH}	0.897	0.863	0.888	0.906	0.900	0.865	0.903	0.897	0.858	0.902	0.873	0.902	0.881	0.859	0.879	0.860	0.885	0.880

all iron as Fe

OH calculated by stoichiometry

Table C11. Chemistry of biotite in siliceous granulites (distance is referred to as from the physical contact of granulite)

sample No.	9708	9708	9708	9708	9708	9708	9708	9708	9708	9708	9708	9708	9708	9708	9708	9708	9708	9708
analysis No.	28	30	31	35	37	39	43	45	47	85	87	89	92	97	99	101	103	107
zone	granulite	granulite	granulite	granulite	granulite	granulite	granulite	granulite	granulite	granulite	granulite	granulite	granulite	granulite	granulite	granulite	granulite	granulit
distance (cm)	-0.5	-0.5	-0.5	-0.5	-0.5	-0.5	-0.5	-0.5	-0.5	-0.5	-0.5	-0.5	-0.5	-2	-2	-2	-2	-2
SiO_2	36.76	37.48	37.62	37.92	36.84	37.23	36.28	37.67	37.52	36.21	37.14	37.46	37.04	37.39	37.09	38.06	37.56	37.17
TiO_2	5.10	4.65	4.74	5.40	5.40	5.73	5.36	5.57	5.47	5.18	5.99	5.74	5.32	5.23	5.54	5.77	5.52	5.76
Al_2O_3	13.65	14.03	13.77	13.80	13.97	14.10	13.24	13.87	13.75	13.21	13.57	13.71	13.69	13.03	13.39	13.76	13.58	13.75
FeO	13.93	14.54	14.42	14.81	14.69	14.89	15.82	14.98	15.08	14.11	14.76	14.64	14.63	14.62	14.40	15.03	15.00	15.26
Cr_2O_3	0.06	0.10	0.06	0.08	0.11	0.03	0.06	0.06	0.05	0.03	0.05	0.02	0.10	0.06	0.02	0.02	0.08	0.04
MnO	0.19	0.13	0.21	0.12	0.16	0.13	0.18	0.12	0.18	0.18	0.23	0.15	0.20	0.18	0.17	0.14	0.19	0.19
MgO	14.48	14.84	15.10	14.76	14.49	14.45	13.91	14.43	14.30	14.01	14.34	14.70	14.57	13.99	14.07	14.43	14.23	14.22
CaO	0.04	0.09	0.00	0.00	0.00	0.03	0.06	0.00	0.00	0.07	0.01	0.00	0.05	0.18	0.00	0.00	0.02	0.00
Na_2O	0.23	0.14	0.23	0.29	0.17	0.18	0.38	0.20	0.13	0.27	0.37	0.17	0.13	0.21	0.20	0.18	0.24	0.18
K_2O	9.23	9.43	9.51	9.52	9.39	9.55	9.04	9.44	9.36	9.17	9.36	9.61	9.30	8.79	9.37	9.67	9.57	9.60
BaO	0.25	0.38	0.45	0.39	0.30	0.43	0.30	0.37	0.30	0.21	0.15	0.36	0.32	0.18	0.28	0.31	0.14	0.31
F	1.58	1.91	1.71	1.71	1.60	1.81	1.44	1.52	1.45	1.65	1.68	1.38	1.75	1.85	1.58	1.56	1.57	1.79
Cl	0.36	0.37	0.38	0.44	0.35	0.37	0.42	0.35	0.34	0.36	0.31	0.34	0.31	0.39	0.32	0.33	0.35	0.35
Total	95.85	98.10	98.20	99.24	97.47	98.92	96.49	98.58	97.93	94.65	97.95	98.27	97.41	96.10	96.42	99.25	98.04	98.61
							formula on the basis of 22 oxygens											
Si	5.470	5.460	5.480	5.469	5.412	5.397	5.424	5.470	5.484	5.471	5.427	5.458	5.440	5.546	5.498	5.489	5.486	5.415
Ti	0.571	0.510	0.519	0.586	0.597	0.625	0.603	0.608	0.601	0.589	0.658	0.629	0.588	0.583	0.618	0.626	0.606	0.631
Al	2.394	2.409	2.364	2.346	2.419	2.409	2.333	2.374	2.369	2.352	2.337	2.354	2.370	2.278	2.339	2.339	2.338	2.361
$Al^{[4]}$	2.394	2.409	2.364	2.346	2.419	2.409	2.333	2.374	2.369	2.352	2.337	2.354	2.370	2.278	2.339	2.339	2.338	2.361
$Al^{[6]}$	0	0	0	0	0	0	0	0	0	0	0	0	0	0	0	0	0	0
Fe	1.733	1.771	1.757	1.786	1.805	1.805	1.978	1.819	1.843	1.783	1.803	1.784	1.797	1.813	1.785	1.812	1.832	1.859
Cr	0.007	0.012	0.007	0.009	0.012	0.003	0.007	0.006	0.005	0.003	0.006	0.003	0.012	0.007	0.002	0.002	0.009	0.004
Mn	0.024	0.017	0.026	0.015	0.020	0.016	0.023	0.015	0.023	0.023	0.028	0.018	0.025	0.023	0.021	0.016	0.023	0.023
Mg	3.212	3.223	3.279	3.174	3.174	3.123	3.100	3.124	3.116	3.156	3.124	3.193	3.190	3.094	3.109	3.102	3.099	3.088
Ca	0.006	0.014	0.000	0.000	0.000	0.004	0.009	0.000	0.000	0.011	0.002	0.000	0.008	0.028	0.000	0.000	0.003	0.000
Na	0.065	0.040	0.064	0.082	0.049	0.050	0.109	0.056	0.037	0.078	0.105	0.047	0.036	0.060	0.056	0.051	0.067	0.050
K	1.752	1.752	1.767	1.752	1.760	1.766	1.724	1.749	1.745	1.767	1.745	1.786	1.742	1.663	1.772	1.779	1.783	1.784
Ba	0.014	0.022	0.026	0.022	0.017	0.024	0.018	0.021	0.017	0.012	0.008	0.021	0.018	0.010	0.016	0.018	0.008	0.018
F	0.743	0.880	0.788	0.780	0.743	0.830	0.681	0.698	0.670	0.788	0.776	0.635	0.813	0.868	0.741	0.711	0.725	0.825
Cl	0.092	0.092	0.095	0.106	0.088	0.090	0.107	0.087	0.083	0.092	0.077	0.083	0.077	0.099	0.080	0.080	0.087	0.086
OH	3.165	3.028	3.118	3.114	3.169	3.080	3.212	3.215	3.246	3.119	3.147	3.282	3.110	3.034	3.180	3.208	3.188	3.089
X_{Mg}	0.650	0.645	0.651	0.640	0.637	0.634	0.611	0.632	0.628	0.639	0.634	0.642	0.640	0.630	0.635	0.631	0.628	0.624
X_{Fe}	0.350	0.355	0.349	0.360	0.363	0.366	0.389	0.368	0.372	0.361	0.366	0.358	0.360	0.370	0.365	0.369	0.372	0.376
X_{Cl}	0.023	0.023	0.024	0.027	0.022	0.022	0.027	0.022	0.021	0.023	0.019	0.021	0.019	0.025	0.020	0.020	0.022	0.021
X_F	0.186	0.220	0.197	0.195	0.186	0.207	0.170	0.174	0.168	0.197	0.194	0.159	0.203	0.217	0.185	0.178	0.181	0.206
X_{OH}	0.791	0.757	0.779	0.778	0.792	0.770	0.803	0.804	0.812	0.780	0.787	0.820	0.777	0.758	0.795	0.802	0.797	0.772
all iron as Fe																		
OH calculated by stoichiometry																		

Appendix D -Sample List

The following table contains a list of sample numbers and the rocks type referenced in this dissertation. The suffix RU, which is originally labelled in the samples, was not added to the sample numbers in this thesis.

Sample No.	Rock Type	Category
RU 9316	Carbonatized vein	Ultramafic rock
RU 9317	Carbonatized vein	Ultramafic rock
RU 9318	Carbonatized vein	Ultramafic rock
RU 9319	Pale green rock	Ultramafic rock
RU 9319A	Pale green rock	Ultramafic rock
RU 9320 S	Dark green rock	Ultramafic rock
RU 9320	Dark green rock	Ultramafic rock
RU 9327	Blackwall zone	Ultramafic rock
RU 9328	Blackwall zone	Ultramafic rock
RU 9703 A	Dark green rock	Ultramafic rock
RU 9703 B	Dark green rock	Ultramafic rock
RU 9710	Pale green rock	Ultramafic rock
RU 9710 A	Blackwall zone	Ultramafic rock
RU 9710 B	Blackwall zone	Ultramafic rock
RU 9712	Blackwall zone	Ultramafic rock
RU 9716	Dark green rock	Ultramafic rock
RU 9717	Dark green rock	Ultramafic rock
RU 9718	Dark green rock	Ultramafic rock
RU 9725	Blackwall zone	Ultramafic rock
RU 9725A	Dark green rock	Ultramafic Rock
RU 9725B	Dark green rock	Ultramafic Rock
RU 9725C	Dark green rock	Ultramafic Rock
RU 9728	Dark green rock	Ultramafic Rock
RU 9740 L	Pale green rock	Ultramafic rock
RU 9740 M	Pale green rock	Ultramafic rock
RU 9740 N	Pale green rock	Ultramafic rock
RU 9741	Pale green rock	Ultramafic rock
RU 9743	Pale green rock	Ultramafic rock
RU 9744 L	Pale green rock	Ultramafic rock
RU 9744 M	Pale green rock	Ultramafic rock
RU 9744 N	Pale green rock	Ultramafic rock
RU 9803	Dark green rock	Ultramafic rock
RU 9807	Blackwall zone	Ultramafic rock
RU 9821	Pale green rock	Ultramafic rock
RU 9822	Dark green rock	Ultramafic rock
RU 9824	Dark green rock	Ultramafic rock
RU 9829	Blackwall zone	Ultramafic rock
RU 9830	Blackwall zone	Ultramafic rock

Sample No.	Rock Type	Category
RU 9307 A	Zone A, B	Metasomatic reaction zones
RU 9307 B	Zone C	Metasomatic reaction zones
RU 9310	Zone C	Metasomatic reaction zones
RU 9310A	Zone C	Metasomatic reaction zones
RU 9311A	Zone A, B	Metasomatic reaction zones
RU 9311B	Zone C	Metasomatic reaction zones
RU 9312 A	Zone A, B	Metasomatic reaction zones
RU 9312 B	Zone C	Metasomatic reaction zones
RU 9713	Zone C	Metasomatic reaction zones
RU 9806	Zone A, B	Metasomatic reaction zones
RU 9806 SL	Zone A, B	Metasomatic reaction zones
RU 9806 SM	Zone A, B	Metasomatic reaction zones
RU 9806 SN	Zone A, B	Metasomatic reaction zones
RU 9806 CL	Zone C	Metasomatic reaction zones
RU 9806 CM	Zone C	Metasomatic reaction zones
RU 9806 CN	Zone C	Metasomatic reaction zones
RU 9809	Zone A, B, C	Metasomatic reaction zones
RU 9827	Zone A, B, C	Metasomatic reaction zones
RU 9828	Zone A, B, C	Metasomatic reaction zones
RU 9828A	Zone A, B, C	Metasomatic reaction zones
RU 9301	Zone D	Metasomatic reaction zones
RU 9302	Zone D	Metasomatic reaction zones
RU 9303	Zone D	Metasomatic reaction zones
RU 9322	Zone D	Metasomatic reaction zones
RU 9323	Zone D	Metasomatic reaction zones
RU 9324	Zone D	Metasomatic reaction zones
RU 9350	Zone D	Metasomatic reaction zones
RU 9706	Zone D	Metasomatic reaction zones
RU 9727	Zone D	Metasomatic reaction zones
RU 9701	Zone D	Metasomatic reaction zones
RU 9702	Zone D	Metasomatic reaction zones
RU 9801	Zone D	Metasomatic reaction zones
RU 9805 L	Zone D	Metasomatic reaction zones
RU 9805 M	Zone D	Metasomatic reaction zones
RU 9805 N	Zone D	Metasomatic reaction zones
RU 9805 AL	Zone D	Metasomatic reaction zones
RU 9805 AM	Zone D	Metasomatic reaction zones
RU 9805 AN	Zone D	Metasomatic reaction zones
RU 9810	Zone D	Metasomatic reaction zones
RU 9811	Zone D	Metasomatic reaction zones
RU 9813	Zone D	Metasomatic reaction zones
RU 9821	Zone D	Metasomatic reaction zones
RU 9825	Zone D	Metasomatic reaction zones
RU 9826	Zone D	Metasomatic reaction zones
RU 9827	Zone D	Metasomatic reaction zones

Sample No.	Rock Type	Category
RU 9703	Metabasite	Granulite
RU 9707 L	Metabasite	Granulite
RU 9707 M	Metabasite	Granulite
RU 9707 N	Metabasite	Granulite
RU 9708B	Charnockite	Granulite
RU 9708 C	Metabasite	Granulite
RU 9708 A	Garnet-biotite gneiss	Granulite
RU 9708 L	Garnet-biotite gneiss	Granulite
RU 9708 M	Garnet-biotite gneiss	Granulite
RU 9708 N	Garnet-biotite gneiss	Granulite
RU 9715	sillimanite-biotite gneiss	Granulite
RU 9721	Charnockite	Granulite
RU 9723	Charnockite	Granulite
RU 9722	Garnet-biotite gneiss	Granulite
RU 9801	Charnockite	Granulite
RU 9802	Charnockite	Granulite
RU 9804	Charnockite	Granulite
RU 9804 A	Charnockite	Granulite
RU 9814	Charnockite	Granulite
RU 9815	Migmatitzed garnet-Bt gneiss	Migmatite
RU 9816	Charnockite	Granulite
RU 9817 A	Charnockite	Granulite
RU 9817 B	Charnockite	Granulite
RU 167	Calc Silicate Gneiss	Marble
RU 9314	Calc Silicate Gneiss	Marble
RU 9329	Calc Silicate Gneiss	Marble
RU 9701	Calc Silicate Gneiss	Marble
RU 9714	Calc Silicate Gneiss	Marble
RU 9724	Calc Silicate Gneiss	Marble
RU 9724A	Calc Silicate Gneiss	Marble
RU 9724B	Calc Silicate Gneiss	Marble
RU 9725A	Scapolite-plagioclase-scheelite	Retrograded overprints
RU 9726	Calc Silicate Gneiss	Marble
RU 9726 A	Scapolite-plagioclase-scheelite	Retrograded overprints
RU 9825 A	Scapolite-plagioclase-scheelite	Retrograded overprints
RU 9823	Quartz-feldspar gneiss	Pegmatite